UC Berkeley
UC Berkeley Electronic Theses and Dissertations

Title

The Role of Ferroxidases in Mammalian Iron Absorption and Metabolism

Permalink

https://escholarship.org/uc/item/7zk8h1xr

Author

Fuqua, Brie Katherine

Publication Date

2012

Peer reviewed|Thesis/dissertation

eScholarship.org Powered by the California Digital Library
University of California

The Role of Ferroxidases in Mammalian Iron Absorption and Metabolism

by

Brie Katherine Fuqua

A dissertation submitted in partial satisfaction of the

requirements for a degree of

Doctor of Philosophy

in

Metabolic Biology

in the Graduate Division

of the

University of California, Berkeley

Committee in charge:

Associate Professor Chris D. Vulpe, Chair
Assistant Professor Danica Chen
Associate Professor Arash Komeili
Associate Professor Andreas Stahl

Fall 2012

The Role of Ferroxidases in Mammalian Iron Absorption and Metabolism

© 2012

by Brie Katherine Fuqua

Abstract

The Role of Ferroxidases in Mammalian Iron Absorption and Metabolism

by

Brie Katherine Fuqua

Doctor of Philosophy in Metabolic Biology

University of California, Berkeley

Associate Professor Chris D. Vulpe, Chair

Everyday, billions of iron atoms from the diet must cross the intestine and enter the blood in order for the body to maintain iron balance. The vertebrate multicopper ferroxidase (MCF) hephaestin (HP) is hypothesized to play an important role in iron release from intestinal enterocytes by oxidizing ferrous iron from the only known enterocyte iron exporter ferroportin for delivery to the ferric iron carrier transferrin in the blood. Mutation of the gene encoding HP in the sex-linked anemia (*sla*) mouse leads to a partial block in iron export from enterocytes, resulting in iron deficiency. However, *sla* mice still retain some hephaestin ferroxidase activity, and they survive, breed, and their anemia improves with age.

In order to clarify whether or not HP, the only MCF known to be expressed in enterocytes, is essential for intestinal iron absorption, the cre-lox system was used to generate knockout mouse models with whole body ($Hp^{-/-}$) and intestine-specific ($Hp^{int/int}$) ablation of HP. Both types of mice were viable and able to absorb iron, indicating that HP is not absolutely required for intestinal iron absorption or survival. To determine whether the systemic MCF of the plasma, ceruloplasmin (CP), can compensate for loss of HP, a cross was then made between $Hp^{-/-}$ and $Cp^{-/-}$ mice to generate double knockout $Hp^{-/-}$ $Cp^{-/-}$ mice. In order to differentiate between phenotypes due to ablation in the intestine versus other tissues, mice were also generated with whole body knockout of CP but deletion of HP only in the intestine ($Hp^{int/int}$ $Cp^{-/-}$ mice). Studies of these models indicate that, while HP and CP are not essential for intestinal iron absorption, expression of both proteins is critical for normal intestinal iron absorption and trafficking. They also point to important extra-intestinal roles for HP in maintaining whole body iron homeostasis, and suggest that another mechanism for iron oxidation in the intestine may exist. Double knockout mouse models with HP were also generated for two newly discovered ferroxidases, amyloid precursor protein (APP) and zyklopen (ZP), and preliminary results are discussed.

DEDICATION

For my father and mother, Mark and Suzanne, and my brother Jeff, who are always in my heart

TABLE OF CONTENTS

CHAPTER 3. THE ROLE OF OTHER FERROXIDASES IN INTESTINAL IRON ABSORPTION AND METABOLISM

LIST OF FIGURES

LIST OF TABLES

LIST OF ABBREVIATIONS

A	absorbance
AICD	anemia of inflammation and chronic disease
AIN-93G	American Institute of Nutrition 1993 purified rodent diet formula
ANOVA	analysis of variance
APP	amyloid precursor protein
BLAST	Basic Local Alignment Search Tool
ARE	antioxidant response element
bp	base pair
BSA	bovine serum albumin
CP	ceruloplasmin
cDNA	complementary DNA
DMT1	divalent metal ion transporter 1
DTA	diphtheria toxin A
ECL	enhanced chemiluminescence
EDTA	ethylenediaminetetraacetic acid
ES	embryonic stem
FTN	ferritin
FTN-H	ferritin H
FTN-L	ferritin L
FPN1	ferroportin 1
FXN	frataxin
GI	gastrointestinal
GPI	glycophosphatidylinositol
HCl	hydrochloric acid
HP or *Heph*	hephaestin
HIF	hypoxia inducible factor
HRP	horseradish peroxidase
IP	intraperitoneal
IRP	iron regulatory protein
IRE	iron responsive element
kD	kilodalton
MCF	multicopper ferroxidase
mFTN	mitochondrial ferritin
mRNA	messenger RNA
NCBI	National Center for Biotechnology Information
Neo	neomycin
NIH	National Institutes of Health

NTBI	non-transferrin bound iron
PAGE	polyacrylamide gel electrophoresis
PBS	phosphate buffered saline
PCR	polymerase chain reaction
PHZ	phenylhydrazine hydrochloride
QIMR	Queensland Institute of Medical Research, Brisbane
RT-qPCR	real-time quantitative polymerase chain reaction
SDS	sodium dodecyl sulfate
SEM	standard error of the mean
sla	sex-linked anemia
TBS	tris-buffered saline
TF	transferrin
TFR1 or *Tfrc*	transferrin receptor 1
TIBC	total iron binding capacity
Tris	tris(hydroxymethyl)aminomethane
UCB	University of California, Berkeley
UPAGE	urea polyacrylamide gel electrophoresis
UTR	untranslated region
XO	xanthine oxidase
ZP or *Hephl1*	zyklopen

ACKNOWLEDGEMENTS

Many people have contributed over the years to make this work possible, and it is difficult to even begin to describe how much this has meant to me. I would first like to thank my research advisors, Professors Chris Vulpe and Greg Anderson, for their unyielding support and encouragement, and for all of the time they have spent working with me to make me a better scientist. I am continually amazed and inspired by their generosity, enthusiasm for exploring the world, incredible depth of knowledge, various other superpowers, and the obvious joy they both get from providing opportunities and teaching others what they do so well. They both truly exemplify what a great mentor can be.

I am also grateful to my labmates, both in Australia and the USA, who have made the laboratories fun and innovative environments, and have, each in their own way, contributed to this work. Korry Hintze, Xiaofeng Liu, and Takehiko Tosha were extremely helpful to me during my beginning years at the Children's Hospital Oakland Research Institute. Over the past few years, I have learned so much from working with Deepak Darshan, and I am indebted to him for making the work presented here possible. David Frazer and Sarah Wilkins have also shared many great ideas and provided important technical assistance, and it has been a pleasure to also get to work with Linda Dunn, Daphne Belcher, Alison Smith, Rebecca Watts, Haiza Ahmed, Cornel Mirciov, and Elizabeth Czislowski. Undergraduates Catherine Yu, Austin Bell, Joanne Hsu, Erica Lachenauer, Chiffonia Lam, Julie Luong, Michelle Nguyen, Anna Nguyen, and Shawn Pan, as well as research assistant Candace Clark, greatly assisted with the mouse colony management at UC Berkeley and also made important contributions to experiments. It was also great getting to work with and also spend some fun time outside the lab with Tamara Lawson, Giuliano Bellapadrona, Suranjana Haldar, Rubayet Hasan, Ramune Leipuviene, Stela Masle, Mani Tagmount, Leona Scanlan, Vanessa de la Rosa, and Brandon Gaytan.

I am very grateful to my dissertation committee members Professors Arash Komeili, Andreas Stahl, and Danica Chen for their guidance, support, and very helpful advice. Additionally, visiting Professors Huijun Chen and Zouhair Attieh provided much helpful discussion and technical expertise regarding working with multicopper ferroxidases. I am also thankful for the fortune of getting to collaborate with Professors Josh Dunaief, James Duce, James Collins, and with fellow graduate student Yan Lu. It has been very fun to find two people in particular, Yan Lu and Annyk Wong, who enjoy talking about ferroxidases as much as I do. I am also grateful to Melissa Kazantzis (Stahl Laboratory, UCB) for assisting with the energy expenditure experiments, and Lindsey Jennings (OLAC

veterinary technician, UCB) for great suggestions for working with mouse models. I would also like to thank Glynn Rees of the Histotechnology Facility at QIMR for the beautiful and informative Perls' stained tissue sections, and Madeleine Flynn at QIMR for her graphic design expertise. I must also warmly acknowledge Professors James Boggs, Delia Brownson, Kent Chapman, Su Dharmawardhane, Edward Marcotte, and David Thurnham for amazing pre-graduate school research opportunities and experiences that were important in my decision to pursue graduate studies in Metabolic Biology.

A very special thanks goes out to Shirley Huang and Michael Hoffman, who have both been role models and great friends since our days as undergraduates at UT Austin. They strongly encouraged me to apply for the National Science Foundation Graduate Research Fellowship that greatly helped to support my graduate studies. Shirley, Maryam Ahmadian, and Kasuen Mauldin were invaluable in helping me to prepare for talks, and their friendship has been extremely important to me. I also treasure the memories of beautiful late night walks around Berkeley talking about science and life and so many other interesting things with Yassi Hafezi, Victor Brar, Jason Wolfe, Gautam Agarwal, Erin Oakman, and Amanda Merchant.

My parents, Mark and Suzanne, have been incredibly and unconditionally loving and supportive throughout my life through all the ups and downs, and I would not be where I am without them. By example they taught me to work hard and persevere and have always encouraged me to follow my heart. I do not know how to thank them enough. My grandparents and my stepmother Melissa have also given me immensely helpful advice and encouragement. My brother Jeff, although no longer here, is still always in my thoughts. I know that everything I am and do will forever be entwined with him, because he was so important in shaping who I am. I still get inspiration out of thinking what he would do or say in certain situations. Working in the lab and seeing the commitment of so many other scientists takes on a whole new meaning when I think of him, as I know that someday science will find a cure to help others like him. Finally, I would like to thank my best friend and boyfriend Victor for always, no matter how far away we are or what the timezone difference is, being there for me. He has provided support on so many levels. His kindness and creative spirit bring so much joy to my life.

CHAPTER 1.

INTRODUCTION

I. Iron in biology

Virtually all organisms require iron for life (Posey and Gherardini 2000; Collins and Anderson 2012). The powerful ability of iron to gain and donate electrons, and thus transfer energy and reversibly bind ligands, has been elegantly harnessed by biology to perform a myriad of functions, ranging from DNA synthesis to nitrogen fixation. Life is believed to have arisen in an anaerobic world rich in available iron, where iron became a crucial part of biological systems. The advent of photosynthesis however led to the creation of the aerobic world that exists today, where oxygen is abundant and rapidly reacts with iron to form insoluble iron oxides and hydroxides. Although iron is the fourth most abundant element in earth's crust, most of the iron in the environment is now in the form of minerals that are not readily accessible by biology. Organisms have thus evolved diverse mechanisms to obtain and use iron from their surroundings (Ilbert and Bonnefoy 2012). These include the release of siderophores to tightly bind available iron in a form that can be actively taken up by cells, the lowering of pH to make iron more soluble, the expression of high affinity iron transporters, and the oxidation/reduction of iron to facilitate transport (De Luca and Wood 2000; Barbeau, Rue et al. 2001; Zheng 2010; Collins and Anderson 2012). Still, iron is often the limiting factor in the expansion of organisms, from phytoplankton in several of the world's oceans to viruses, bacteria, and other pathogens that have invaded the body (Behrenfeld and Kolber 1999; Drakesmith and Prentice 2008).

Under physiological conditions, iron typically exists in three oxidation states: ferrous (Fe^{2+}), ferric (Fe^{3+}), and ferryl (Fe^{4+}). Iron interconverts between these states via powerful electron transfer reactions. Organisms use several mechanisms to keep iron in a usable and controlled form, as the solubility of ferric iron at physiological pH is extremely low ([aqueous Fe^{3+}] < 10^{-17} M), and rapid reactions of incompletely liganded iron with oxygen species form toxic free radicals that can damage nearly all components of cells (Aisen, Enns et al. 2001; Crichton 2001). Most iron in cells is liganded to proteins directly or associated in the form of heme and iron-sulfur clusters via interactions with oxygen, nitrogen, and sulfur groups. In addition, iron is stored bound to small molecules in vacuoles or as an iron oxide mineral inside the protein ferritin. In mammals as

well as many other organisms, iron is essential for oxygen transport and storage (via hemoglobin and myoglobin), for DNA synthesis (via ribonucleotide reductase), for energy production (via multiple heme and iron-sulfur containing proteins in the electron transport chain), and for detoxification by the cytochrome p450 enzymes (Collins and Anderson 2012). The ability of iron to facilitate the production of reactive oxygen species has even been exploited by macrophages to kill pathogens (Collins 2003). Iron is also found as a mineral in the magnetotactic magnetosomes of some bacteria and as a mineral strengthener in the teeth of chitons (Komeili, Li et al. 2006; Shaw, Macey et al. 2010).

II. Intestinal iron absorption

1. Overview and clinical importance

Typical adult males and females contain approximately 50 mg/kg and 40 mg/kg of iron, respectively (Bothwell, Charlton et al. 1979). Under normal physiological conditions, all of this iron must come from two sources: the placenta during fetal life and from absorption across the intestine in postnatal life. As there are currently no known regulated mechanisms for the excretion of iron from the body, it is critical that iron absorption is tightly regulated throughout life to precisely match the body's needs (Collins and Anderson 2012).

While every cell in the body requires iron, nearly two-thirds of this iron is found in red blood cells in hemoglobin (Figure 1.1). Other tissues that normally contain significant levels of iron include the liver (where iron is stored) and the muscles (rich in myoglobin and mitochondria). In healthy adults, most of the body's daily iron needs are met by the recycling of iron from red blood cells, which have a lifespan of approximately 120 days. Damaged or aging red cells are phagocytosed and broken down to release their iron by reticuloendothelial macrophages (mainly in the spleen and liver), and then this iron (20-30 mg/day) is exported to the iron carrier protein transferrin (TF) in the blood for trafficking to the rest of the body (Sharp 2010).

In addition to recycled erythrocyte iron, healthy adults need to absorb approximately 1-2 mg of iron from the diet per day to make up for iron lost through the shedding of epithelial cells, menstruation, and several other minor routes. Iron absorption also needs to be adapted to the increased iron and red cell requirements of children and adults during periods of growth, pregnancy, hypoxia, and after blood loss. Circulating levels of the hormone hepcidin, primarily produced by the liver, increase in response to iron loading and other stimuil and systemically inhibit intestinal iron absorption and recycling. Conversely, hepcidin levels decrease when iron requirements increase, leading to greater iron uptake and recycling. If iron needs are not met from the diet, iron is mobilized first from iron stores in the liver, and then depleted from other tissues (Collins and Anderson 2012). The body prioritizes the delivery of iron to the bone

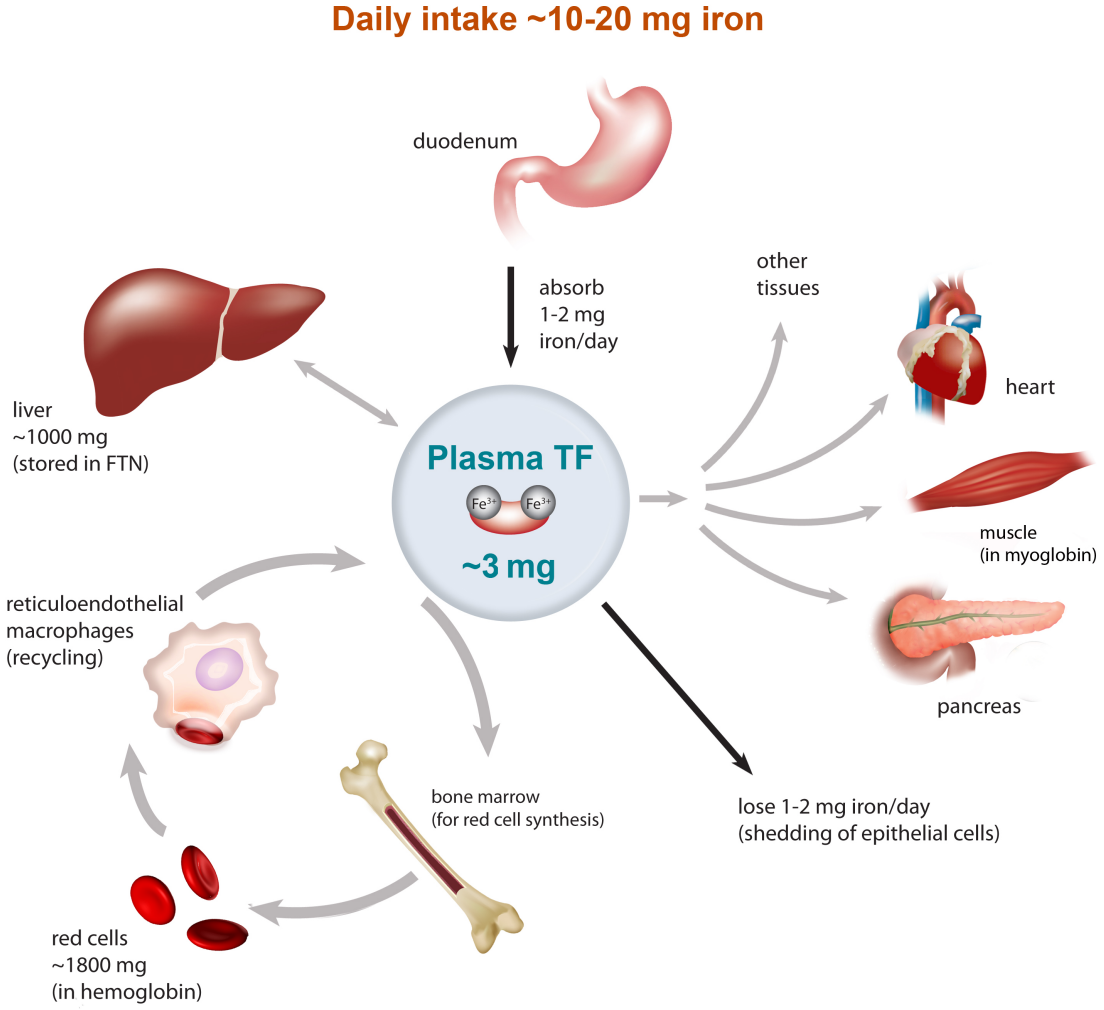

Figure 1.1. Mammalian iron metabolism. Dietary iron is primarily absorbed by the duodenum and is then exported into the blood, where it circulates bound to the protein transferrin (TF). TF delivers iron to all tissues, but most iron is taken up by developing red cells in the bone marrow. When red cells senescence, they are phagocytosed and degraded by reticuloendothelial macrophages that then recycle this iron back to TF in the circulation. Iron is also stored in the liver and released to the circulation as needed. Humans typically need to absorb approximately 1-2 mg of iron per day in order to make up for iron lost primarily by the shedding of epithelial cells. Graphic design by Madeleine Flynn at QIMR.

marrow for the production of red blood cells. Only after other tissues have become low in iron do defects in red cell synthesis occur, resulting eventually in anemia (Conrad and Barton 1981).

There is a critical need to discover and understand the detailed mechanisms by which the body acquires and handles iron, as iron overload, iron deficiency, and disorders of iron distribution afflict many people worldwide. If too much iron is absorbed, as in the cases of genetic diseases like hemochromatosis, one of the most common genetic disorders in individuals of European ancestry, iron will eventually be deposited in large quantities in various tissues (Anderson 2001). Because iron is redox active, excessive iron can lead to oxidative stress, resulting in organ damage and failure. In addition, uncontrolled excess iron can promote the survival and expansion of pathogens, with iron status affecting parasitic and infectious disease progression and outcome (Sazawal, Black et al. 2006; Boelaert, Vandecasteele et al. 2007; McDermid, van der Loeff et al. 2009).

On the other hand, anemia due to iron deficiency is estimated to affect approximately 1/8 of the world's population, with costs to health and productivity in the billions of dollars (Horton and Ross 2003; de Benoist, McLean et al. 2008). Iron deficiency causes fatigue and immune suppression, and in severe cases leads to growth defects and irreversible cognitive impairment. The causes of iron deficiency anemia are complex and multifactorial, but insufficient dietary iron is a leading cause. Not surprisingly, women and children are disproportionally affected due to their increased dietary iron needs to support growth, pregnancy, and menstruation (Stoltzfus 2011).

Disease and infection can also greatly exacerbate iron deficiency. Over one billion people worldwide are infected with helminths that can cause chronic blood loss (Imhoff-Kunsch and Briggs 2012). In addition, chronic diseases including malaria, HIV/AIDS, schistosomiasis, and tuberculosis are also very important contributors to iron deficiency, particularly in the developing world (Shaw and Friedman 2011). These diseases and others such as cancer, kidney disease, rheumatoid arthritis, and heart failure can lead to the anemia of inflammation and chronic disease (AICD) (Weiss and Goodnough 2005; Roy 2012). The innate immune system normally rapidly shuts down the recycling and absorption of iron during illness in an attempt to limit the availability of iron to pathogens. If an underlying condition is not or cannot be successfully treated, chronic reduced iron uptake and recycling can lead to AICD and iron-deficiency and further exacerbate the disease. Efforts to decrease anemia in ill or disease-prone populations by iron supplementation have had mixed results, with supplementation improving prognosis in some studies but leading to increased morbidity in others (Sazawal, Black et al. 2006; Macdougall 2011; Shaw and Friedman 2011; Harding and Neufeld 2012). Defining the factors affecting the fine balance between when iron supplementation is warranted and when it is not, and what forms of supplementation are most advantageous, will be aided by a

better understanding of how iron is absorbed and trafficked in the body (Stoltzfus 2008). The hope is that findings in this area will give scientists and physicians the insight to develop new recommendations and treatments to solve both current and future disorders of iron metabolism, with significant implications for improved quality of life.

2. Forms of iron in the diet

Dietary iron comes in many forms but is typically classified as either heme or non-heme iron (Sharp 2010). Heme iron, found in highest abundance in the diet in meat as part of the hemoproteins hemoglobin and myoglobin, consists of an iron atom coordinated at the center of an organic, hydrophobic porphyrin ring. The low pH of the stomach, coupled with proteolytic enzymes in the stomach and small intestine, help to release heme from hemoproteins. Heme itself has very limited solubility, but it forms soluble complexes with other dietary components in the gut lumen (Conrad, Cortell et al. 1966).

Non-heme iron encompasses many diverse forms of iron, and is naturally found in the diet in both plant and animal foods, This iron is associated with a range of proteins, including the iron storage protein ferritin, and is also found in vacuoles in plant cells (Jeong 2009; Sharp 2010). It also may be given as a supplement, either in an inorganic form (ferrous or ferric salts, nanoparticulate iron oxides/sulfides) or bound to various carbon-containing compounds (carbonyl iron, iron dextran, iron gluconate). While the low pH of stomach acid can stabilize iron in the reduced Fe (II) or ferrous form, dietary iron is most often in the oxidized Fe (III) or ferric form, which has low solubility and bioavailability. During the digestion process, however, non-heme iron likely exists in many different complexes with other digestion products in the intestinal tract, which can improve or impair absorption. For example, phytates and tannins, two classes of indigestible iron chelators found in many plant foods, can sequester some forms of non-heme iron and greatly decrease their absorption, whereas ascorbic acid and compounds from meats can increase absorption (Hurrell, B. et al. 2006; Armah, Sharp et al. 2008; Sharp 2010). Several studies have indicated that the absorption of ferritin iron, found at high levels in legumes and liver, is not as strongly affected by indigestible iron chelators. This has been hypothesized to be due to shielding of iron inside ferritin by the ferritin protein shell, which has been shown to be relatively resistant to both proteases and denaturation at low pH (Theil 2004; Lonnerdal 2009). Similarly, heme iron absorption is little affected by dietary iron chelators or enhancers (West and Oates 2008).

3. Mechanisms of iron absorption

3.1 Iron uptake into enterocytes

Most iron absorption occurs in the upper part of the intestine, the duodenum and proximal jejunum, by polarized intestinal epithelial cells called enterocytes

(Conrad, Weintraub et al. 1966; Wheby 1970; Wheby, Suttle et al. 1970). These cells are characterized by an apical side (brush border) in contact with the gut lumen and dietary contents, and a basolateral side in contact with the blood. Enterocytes emerge from dividing stem cells in the crypts, which are located between fingerlike projections called villi. The villi increase the surface area of the intestine (Figure 1.2). The cells mature as they migrate up to the tip of each villus, where they are eventually sloughed off. The intestinal epithelium is continually being renewed, with the life cycle of an enterocyte being only 3-4 days in adult humans (Lipkin 1985). Physical properties of the gastrointestinal tract, such as the surface area of the intestine and the pH in the stomach, influence iron uptake. In rats and mice, the length of the villi and thus the available absorptive surface area of the duodenum increases under conditions when iron absorption is elevated (O'Riordan, Sharp et al. 1995). Impairment in gastric acid production also leads to a reduction in iron absorption, presumably due to the higher pH and thus lower solubilization of iron (Skikne, Lynch et al. 1981).

Differentiated duodenal enterocytes express high levels of proteins involved in iron absorption from the diet (Figure 1.3). On the brush border, the major iron import protein is the ferrous iron transporter divalent metal ion transporter 1 (DMT1) (Gunshin, Mackenzie et al. 1997; Collins and Anderson 2012). Mice with intestine-specific ablation of *Dmt1* die shortly after birth of a severe anemia, testifying to the importance of this transporter in iron absorption (Gunshin, Mackenzie et al. 1997; Gunshin, Fujiwara et al. 2005). A ferric reductase activity on the brush border facilitates the reduction of dietary ferric iron to the ferrous form, the substrate for DMT1 (Collins and Anderson 2012). Duodenal cytochrome B (DCYTB) provides some of this reductase activity, but other reductases, such as STEAP2, could also play a role (Ohgami, Campagna et al. 2006; McKie 2008). The integrin/mobilferrin pathway and the paraferritin complex (mobilferrin, beta-integrin, flavin monooxygenase, and beta-2 microglobulin) may also aid in ferric iron uptake (Umbreit, Conrad et al. 2001).

The absorption of heme and dietary ferritin iron is less well understood. There is evidence that heme is taken up by receptor-mediated endocytosis (Wyllie and Kaufman 1982; Worthington, Cohn et al. 2001), but a high-affinity receptor for heme in enterocytes has yet to be identified. Heme carrier protein-1/proton coupled folate transporter (HCP1/PCFT) was identified as an apical heme transporter, however, the protein appears to play a more important role in the absorption of folate and has a much lower affinity for heme (Shayeghi, Latunde-Dada et al. 2005; Qiu, Jansen et al. 2006). Disruption of this protein by mutation

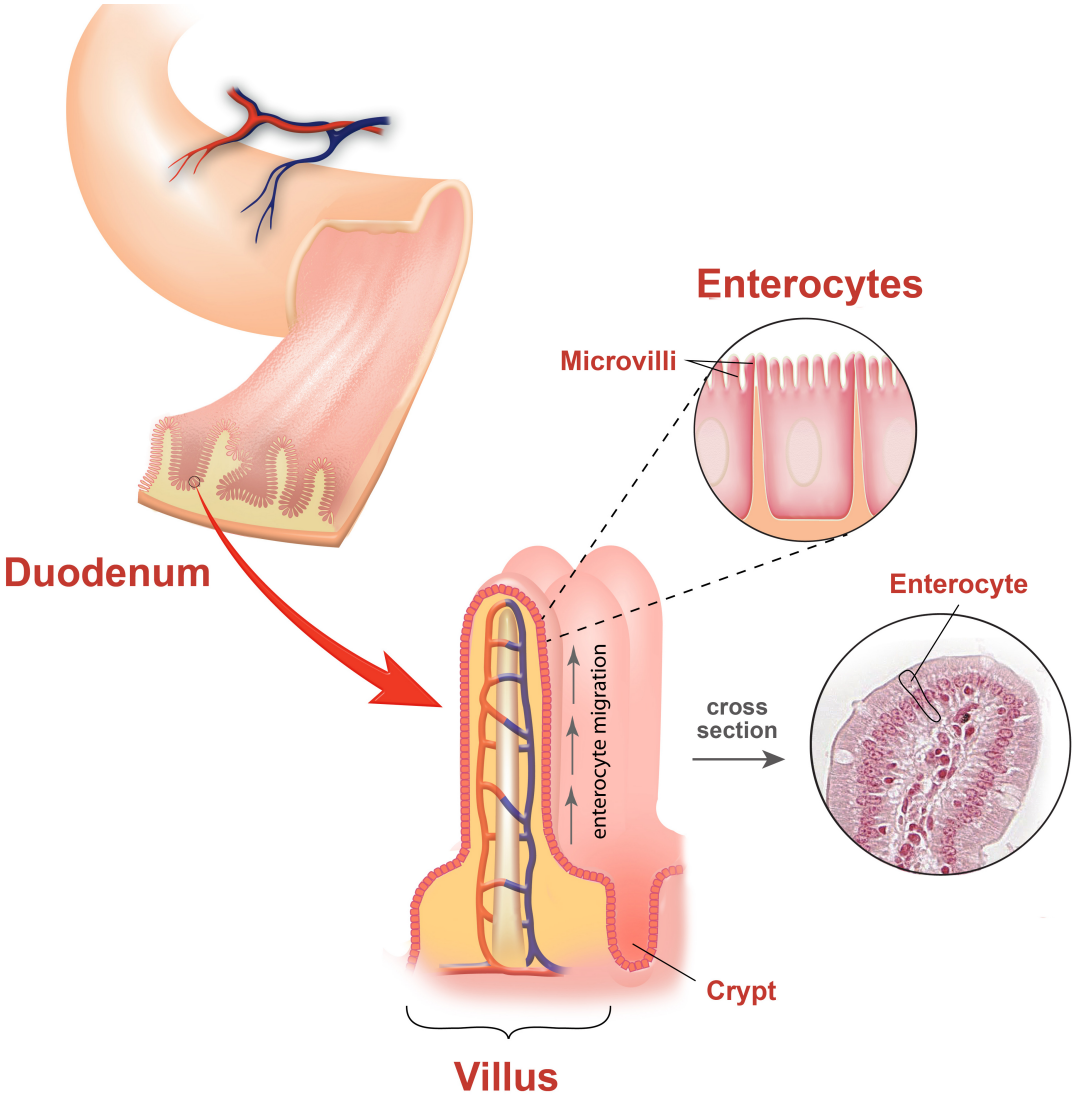

Figure 1.2. Structure of the proximal small intestine. Partially digested food from the stomach enters the small intestine at the duodenum, where the pH is raised and additional digestive enzymes are released. The folds of the duodenum contain small finger-like projections called villi that are lined with cells, most of which are absorptive epithelial cells called enterocytes. Enterocytes originate in the crypts at the base of the villi and migrate to the villus tips. During this migration the cells differentiate and acquire the characteristics necessary for maximal absorption of dietary iron. The intestinal epithelium is continually renewed, with the total lifespan of enterocytes from crypt to sloughing off at the villus tip generally lasting only 3-4 days in human adults. Graphic design by Madeleine Flynn at QIMR.

in human patients results in folate but not iron deficiency, suggesting that its role in heme iron absorption may be limited (Qiu, Jansen et al. 2006). There are thus likely other, as yet unknown, mechanisms by which heme iron can be absorbed. The absorption of iron from dietary ferritin has been shown to have some differences from the absorption of iron salts, and this form of iron may be taken up into enterocytes by endocytosis (San Martin, Garri et al. 2008; Kalgaonkar and Lonnerdal 2009; Theil, Chen et al. 2012).

3.2 Transit of iron across enterocytes and its delivery to tissues

Once iron has been taken up into intestinal enterocytes, it can either be stored inside endogenous ferritin (FTN) or exported into the blood for transport to other tissues in the body. Ingested heme iron is broken down in enterocytes, likely by heme oxygenase-1 (HO1) and/or heme oxygenase-2 (HO2), to release free ferrous iron, and ingested ferritin iron has also been shown to be released from ferritin (Raffin, Woo et al. 1974; San Martin, Garri et al. 2008; West and Oates 2008; Theil, Chen et al. 2012). The stages at which different forms of dietary iron converge, if they do, into a common cellular iron pool in enterocytes are not yet known, however, and more studies are needed to determine precisely how iron is trafficked in the cell. Promising leads include poly (rC)-binding proteins 1 and 2 (PCBP1 and PCBP2), which were recently discovered to serve as cytosolic chaperones that deliver iron to endogenous FTN, asparaginyl hydroxylase (FIH1), and hypoxia inducible factor (HIF) prolyl hydroxylases (PHDs) (Shi, Bencze et al. 2008; Nandal, Ruiz et al. 2011). Transcytosis of iron in vesicles has also been proposed (Ma, Yeh et al. 2006).

Ferroportin (FPN1), a multipass transmembrane protein found on the basolateral membrane of enterocytes, is the only known mammalian iron export protein. It is also expressed throughout the body where it exports iron from cells and thus aids in iron recycling (Abboud and Haile 2000; Donovan, Brownlie et al. 2000; McKie, Marciani et al. 2000). Tamoxifen-inducible deletion of *Fpn1* in intestinal cells of mice results in a near complete block in intestinal iron absorption and a corresponding accumulation of iron in intestinal enterocytes. Whole body and intestinal knockout of FPN1 (using the villin promoter driven cre) results in embryonic lethality, likely due to an extraembryonic requirement for FPN1 in cells that express villin in the latter case (Donovan, Lima et al. 2005).

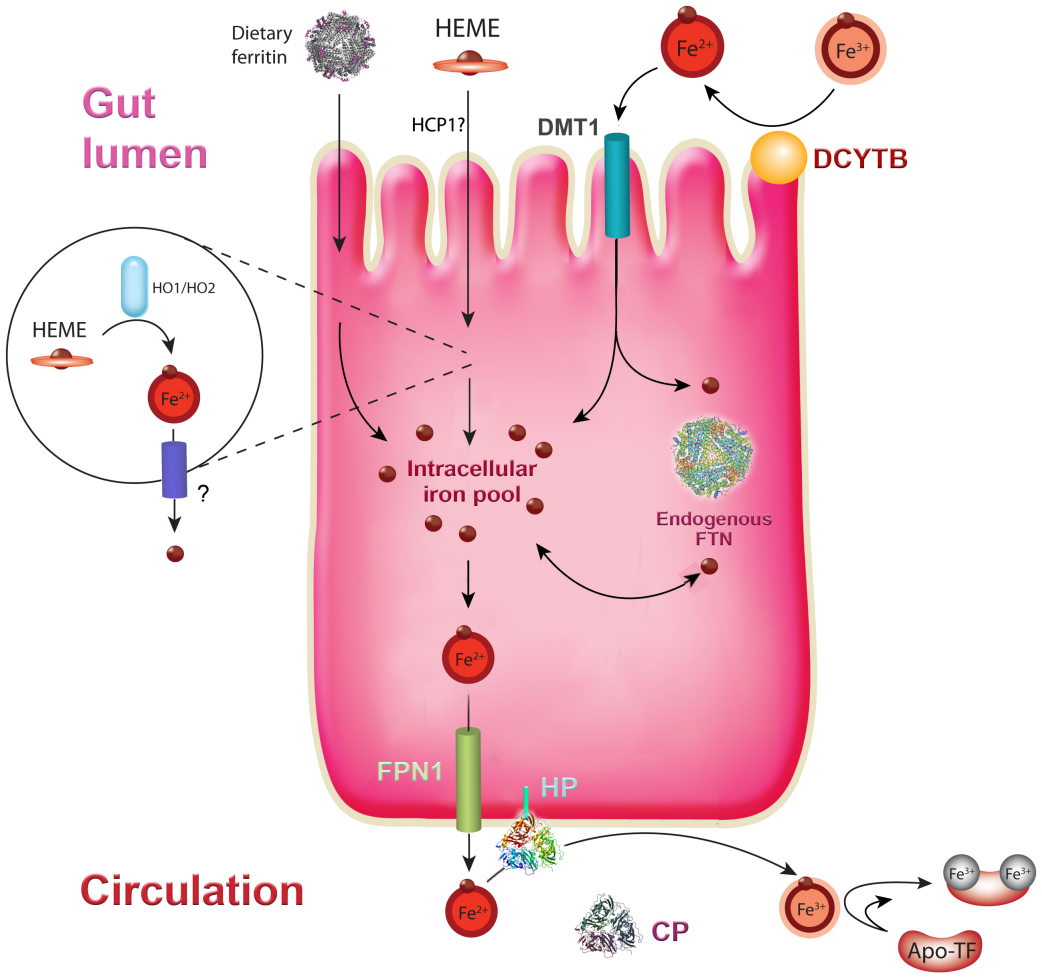

Figure 1.3. Intestinal iron absorption. Dietary iron is absorbed into intestinal enterocytes at the apical brush border membrane. The ferric reductase duodenal cytochrome B (DCYTB) reduces ferric iron to the ferrous form, which can then be transported into the cell by divalent metal transporter 1 (DMT1). Heme iron is taken up by unknown mechanisms, but the transporter heme carrier protein 1 (HCP1) may be involved. Iron can be released from heme by heme oxygenases 1 and 2 (HO1/HO2) and can then join the intracellular iron pool. Dietary ferritin iron can be taken up by clathrin-mediated endocytosis and released into the intracellular iron pool. Ferroportin (FPN) exports ferrous iron from the basolateral membrane of enterocytes into the blood, and the multicopper ferroxidase hephaestin (HP) oxidizes this iron to the ferric form that is then bound to transferrin (TF). The circulating paralog of HP, ceruloplasmin (CP), may also help to oxidize iron from FPN. Iron that is not released from the enterocyte is stored in endogenous ferritin (FTN). Graphic design by Madeleine Flynn at QIMR.

FPN1 likely transports iron in the ferrous form, but plasma TF, the circulating iron transport protein primarily originating in the liver, only binds iron in the ferric form. Ferroxidases are believed to play an important role in oxidizing iron from FPN1 so that it can bind to TF. Studies in glioma cells have shown that FPN1 requires a ferroxidase in order to release iron, and without a ferroxidase FPN1 is internalized and degraded (De Domenico, Ward et al. 2007; Kono, Yoshida et al. 2010). Kinetic studies also suggest that the rate of iron oxidation without an enzyme catalyst is not sufficient to provide adequate iron to TF to meet the body's iron needs (Osaki, Johnson et al. 1966). While many cell types in the body utilize the circulating or GPI-linked multicopper ferroxidase ceruloplasmin (CP) as a ferroxidase for FPN1, disruption of *Cp* does not seem to affect iron absorption except under extreme situations of iron need (Cherukuri, Potla et al. 2005). Instead, a membrane-bound paralog of CP called hephaestin (HP) that is highly expressed in the intestine is involved in iron export from enterocytes. HP is mutated in the sex-linked anemia (*sla*) mouse, resulting in iron accumulation in intestinal enterocytes and systemic anemia (Vulpe, Kuo et al. 1999). A variety of colocalization and immunoprecipitation studies have also indicated that HP and FPN1 may interact (Han and Kim 2007; Yeh, Yeh et al. 2009). Recently, amyloid precursor protein (APP) has been discovered to possess ferroxidase activity and to interact with FPN1 (Duce, Tsatsanis et al. 2010). There is some evidence that APP is expressed in intestinal enterocytes, and it could thus potentially play a role in intestinal iron absorption as well (Galloway, Jian et al. 2007).

TF-bound iron released from enterocytes enters the hepatic portal vein and passes through the liver before joining the general circulation. Most tissues in the body express transferrin receptor 1 (TFR1), encoded by the *TFRC* gene, which recognizes and binds to iron-bound TF. The level of expression of TFR1 is proportional to the iron needs of the cell, and TFR1 has greatest affinity for iron-saturated diferric TF. The TFR1/TF complex is internalized by endocytosis into an endosome, which becomes acidified by the action of V-type proton ATPase. The low pH leads to the release of iron from TF into the vesicle, and then the iron is reduced and exported out of the vesicle and into the cell for use. The iron-free TF (apo-TF) recycles back to the cell surface where it is released into the circulation (Anderson and Vulpe 2009). Under normal circumstances most iron released from the intestine as well as reticuloendothelial macrophages involved in iron recycling is bound to TF. However, iron can still be exported out of intestinal enterocytes even if no TF is available to bind the iron, as has been demonstrated in people and animals either lacking TF due to mutation, or in people and animals with iron-saturated TF (Craven, Alexander et al. 1987; Buys, Martin et al. 1991; Trenor, Campagna et al. 2000; Shamsian, Rezaei et al. 2009). Non-transferrin bound iron (NTBI) is taken up by cells in the body, especially the liver, but it does not appear to be properly trafficked to or utilized by the tissues that need it most, such as the bone marrow. NTBI also may have a greater

potential to cause oxidative damage than TF-bound iron (Breuer, Hershko et al. 2000).

4. Regulation of iron absorption

The regulation of intestinal iron absorption is mediated through the complex interaction of both systemic and local influences.

4.1 Systemic regulation

The absorption of iron from intestinal enterocytes, as well as the efflux of recycled iron from macrophages and other cell types, is systemically controlled by the 25 amino acid peptide hormone hepcidin (Nemeth and Ganz 2009). Hepcidin, which is primarily produced by hepatocytes in the liver, circulates in the blood and binds to the iron exporter FPN1 on cell surfaces, including the enterocyte basolateral membrane. This binding leads to the internalization and degradation of FPN1, and thus iron release into the blood is decreased (Nemeth, Tuttle et al. 2004). Mutations in FPN1 that disrupt the binding of hepcidin result in the iron overload disease type IV hemochromatosis in humans (De Domenico, Ward et al. 2005). The regulation of hepcidin production is complex, but levels are known to increase as iron stores increase and during infection and inflammation, and to decrease during hypoxia, iron deficiency and when erythropoietic needs increase (Collins, Wessling-Resnick et al. 2008). Animal models and human diseases that lead to inappropriate iron intake have helped in the elucidation of hepcidin regulatory mechanisms, although these mechanisms remain incompletely understood.

The BMP6/SMAD pathway is central to the multiple mechanisms that regulate hepcidin expression, and it appears to be particularly important in modulating the hepcidin response to changes in iron stores (Ramos, Kautz et al. 2011). Several members of the bone morphogenic protein (BMP) family, notably BMPs 2, 6, and 9, have been shown to modulate hepcidin expression. However, BMP6 appears to be the most important physiologically, as knockout of the gene encoding this protein in mice leads to significantly reduced hepcidin expression and subsequent systemic iron overload (Andriopoulos, Corradini et al. 2009; Meynard, Kautz et al. 2009). BMP6 is a transforming growth factor beta family cytokine produced and secreted by hepatocytes in proportion to their iron load. It may also be produced by other cells in the body and be trafficked to the liver via the circulation. BMP6 binds to a BMP receptor I/II complex on hepatocytes, leading to the phosphorylation of receptor-regulated son of mothers against decapentaplegic proteins (SMADs) 1, 5, and 8. Phosphorylation allows these proteins to interact with SMAD 4, and the resulting heteromeric complexes are trafficked to the nucleus where they stimulate transcription of the gene encoding hepcidin, *HAMP* (Viatte and Vaulont 2009). The BMP6 receptor complex includes a co-receptor called hemojuvelin (HJV) that is critical for this pathway to function

(Ramos, Kautz et al. 2011). Individuals with a congenital defect preventing HJV synthesis have very low hepcidin levels and develop the severe iron loading disease juvenile hemochromatosis. HJV is normally found bound to the plasma membrane of cells, but a soluble form can be produced by the action of the protease furin. Soluble HJV can compete with membrane-bound HJV for BMP binding and thus is able to decrease BMP/SMAD signaling. Furin synthesis is upregulated by iron deficiency and hypoxia, and thus generation of soluble HJV may be a mechanism by which BMP6 signaling can be reduced when iron needs are increased (Collins and Anderson 2012). TMPRSS6, a cell surface serine protease that degrades HJV, is also able to dampen BMP signaling (Finberg, Whittlesey et al. 2010). Hepcidin expression can also be increased by inflammation and infection through the induction of inflammatory cytokines such as interleukin-6 (IL-6) and the Janus kinase/signal transducer and activator of transcription (JAK-STAT) signaling pathway (Nemeth, Rivera et al. 2004; Wrighting and Andrews 2006; Verga Falzacappa, Vujic Spasic et al. 2007) (Figure 1.4).

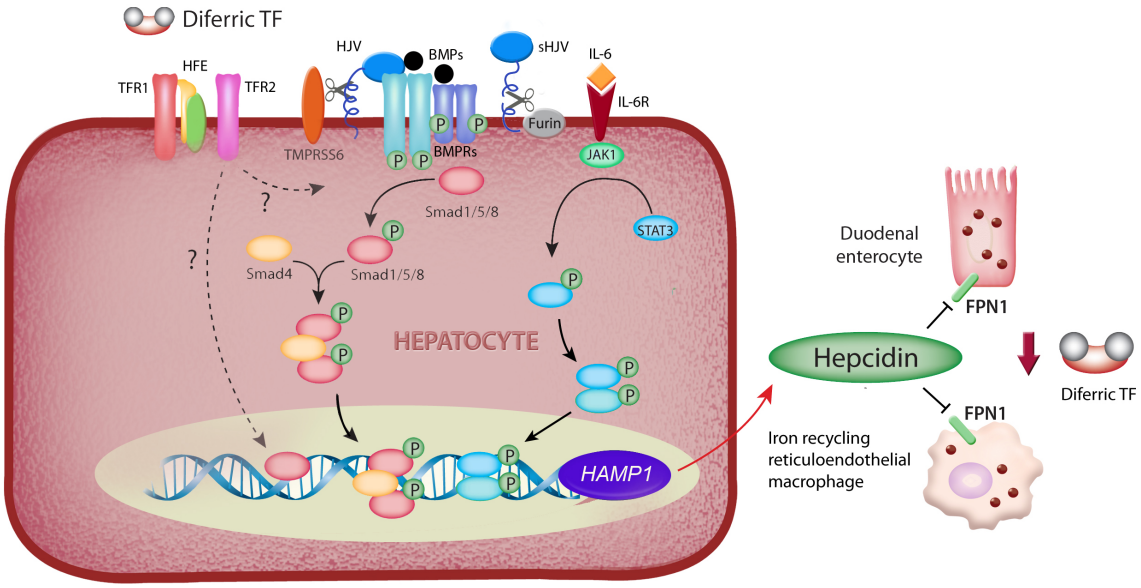

Figure 1.4. Systemic regulation of intestinal iron absorption. The expression of the peptide hormone hepcidin, which systemically inhibits the release of iron from cells and reduces both intestinal iron absorption and recycling of iron from reticuloendothelial macrophages, is increased in hepatocytes in response to various stimuli including iron overloading and infection. The major known pathways involved in the regulation of hepcidin expression in hepatocytes are the BMP/SMAD pathway and the IL-6/JAK-STAT pathway. The proteins HFE and TRF2 are also known to be involved in hepcidin regulation, but their mechanism of action is unclear. Graphic design by Madeleine Flynn at QIMR.

How body iron levels are relayed to the liver to regulate hepcidin levels is incompletely understood, but it is likely to involve both the iron-dependent regulation of BMP6 and the degree of saturation of TF with iron (Nemeth and Ganz 2009).The membrane proteins transferrin receptor 2 (TFR2) and the hemochromatosis protein (HFE) may both be involved in sensing TF saturation. Mutation of either protein can lead to a reduction in basal hepcidin production, increased iron absorption, and subsequent iron overload disease (Darshan, Frazer et al. 2010). TFR2 is a paralog of TFR1, but, unlike TFR1, it is primarily expressed in the liver and is upregulated by increased diferric TF levels. HFE is homologous to the major histocompatibility complex (MHC) class I proteins and, like them, interacts with beta-2 microglobulin. HFE can bind to TFR1 at the same site as diferric TF, and it can also bind to TFR2 and increase TFR2 stability. One hypothesized mechanism by which HFE and TFR2 could sense circulating iron levels is that high levels of diferric TF could limit the binding of HFE to TFR1, thus leading to increased binding of HFE to TFR2 and stimulation of a signaling cascade that activates hepcidin (Goswami and Andrews 2006; Schmidt, Toran et al. 2008; Gao, Chen et al. 2009). However, this has yet to be proven and mice lacking both of these proteins have a more severe phenotype than single knockouts of either gene, suggesting that these proteins may have independent roles as well (Wallace, Summerville et al. 2009).

4.2 Local regulation

Iron absorption is also regulated at the local level in intestinal enterocytes by cellular iron levels and hypoxia. One major player in this regulation is the iron responsive element (IRE)/iron regulatory protein (IRP) system, which operates by affecting the half-life and translation of mRNA sequences encoding proteins involved in iron metabolism (Rouault 2012). There are two homologous IRP proteins in the cytosol of mammalian cells, IRP1 and IRP2. IRP1 exists in two forms in cells: as a soluble cytosolic aconitase containing an iron-sulfur cluster cofactor when iron levels are sufficient, or, when cellular iron levels are low, as an iron-free form that binds to IREs. IRP2 does not bind iron, but it is degraded when cellular iron levels are sufficient. *TFRC* and two isoforms of *DMT1* mRNA have IRE stem loop structures in their 3' untranslated regions (UTRs) that bind iron-free IRP1 or IRP2. IRP binding increases the half-life of the mRNA and thus increases the amount of protein translated when iron levels are low. Conversely, *FTN*, *APP*, and one isoform of *FPN1* have IREs in their 5' UTR. In this location, IRP binding blocks translation. The major splice form of *FPN1* in intestinal cells, however, lacks the 5'IRE and thus FPN1 protein levels can still be maintained even if iron levels in the cell are low. This allows the body to absorb iron from the diet when there is systemic iron deficiency or when dietary iron levels are minimal (Zhang, Hughes et al. 2009).

Endogenous enterocyte FTN, which stores most of the iron in enterocytes that is not in the labile iron pool, also appears to be important for regulating iron uptake

as intestine-specific knockout in mice of the ferroxidase-active subunit of cytosolic FTN, ferritin H (FTN-H), leads to inappropriately increased iron absorption. While enterocyte *Dmt1*, *DcytB*, and *Fpn1* mRNA levels are suppressed in these mice, FPN1 protein levels are increased despite increased hepcidin expression (Vanoaica, Darshan et al. 2010). This suggests that increased iron in the labile iron pool in enterocytes may be able to partially override systemic regulatory signals. Whether FTN plays an active role in modulating enterocyte iron flux under normal physiological conditions, however, remains to be determined.

Hypoxia is a strong stimulus for iron absorption and hence several proteins involved in absorption are regulated at the transcriptional level by iron and oxygen status by hypoxia inducible factor 2α (HIF2α). HIF2α is a part of a transcription factor complex that binds to promoters containing HIF responsive elements (HREs) and induces transcription. Iron metabolism genes that contain HREs include *DCYTB*, *DMT1*, and *FPN1* (Shah, Matsubara et al. 2009; Taylor, Qu et al. 2011). HIF2α is made constitutively by cells but is rapidly ubiquitinated and degraded in proteosomes after hydroxylation by the iron- and oxygen-dependent PHDs. HIF2α levels, and thus the transcription of target genes, rise when oxygen and iron levels decrease and thus limit the activity of PHDs. Overexpression of HIF2α by intestinal knockout of the E3 ubiquitin ligase Von Hippel-Lindau tumor suppressor (pVHL) in mice leads to increased *Dmt1* and *DcytB* expression and increased iron absorption, whereas intestinal knockout of HIF2α leads to low levels of *Dmt1*, *DcytB*, and *Fpn1* expression and subsequent systemic iron deficiency despite low levels of hepcidin (Mastrogiannaki, Matak et al. 2009; Shah, Matsubara et al. 2009; Taylor, Qu et al. 2011). Together this indicates a very important role for HIF2α in the local regulation of iron absorption. HIF1α, another related HIF protein also regulated by PHDs, is expressed in enterocytes but appears to not play as significant of a role in iron gene regulation, as evidenced by lack of an iron-related phenotype when this gene is disrupted in mouse enterocytes (Mastrogiannaki, Matak et al. 2009).

III. Ferroxidases

1. Overview

Ferroxidases are enzymes that oxidize iron from the ferrous (Fe^{2+}) to the ferric (Fe^{3+}) form by removing an electron and shuttling it to an electron acceptor. There are two major classes of mammalian ferroxidases: ferritin ferroxidases and multicopper ferroxidases. Both families of proteins are found in eukaryotes and prokaryotes, and both types of ferroxidases typically use oxygen as their electron acceptor (Theil, Matzapetakis et al. 2006; Kosman 2010). Ferroxidases are important for the rapid and controlled oxidation of iron to a form that can be stored and trafficked by biology, and the controlled reduction of oxygen to safe

forms. Because free iron can react with oxygen species to produce toxic hydroxyl radicals and superoxide as well as insoluble iron oxides, controlled iron oxidation is important for both preventing oxidative damage and for keeping iron available for use. Ferroxidases not only increase the kinetics of iron oxidation but may also help to channel iron specifically to the next iron acceptor (Kosman 2010).

2. Multicopper ferroxidases

Multicopper ferroxidases (MCFs) are members of a family of proteins called blue copper oxidases that use the redox activity of copper to oxidize a variety of substrates, including iron (Kosman 2010). Mammalian MCFs include the paralogous proteins CP, found primarily in the blood, HP found predominately in the intestine, and zyklopen (ZP), a newly discovered MCF first identified in the placenta (Chen, Attieh et al. 2010). In humans one MCF pseudogene exists as well (CPHL1P) (Flicek, Amode et al. 2012). Mammalian MCFs are evolutionarily related to several other proteins: laccases, found in fungi and plants and involved in the oxidation of phenols and diamines; plastocyanins, small proteins involved in the transfer of electrons in photosynthesis; ascorbate oxidase, found in plants; Fet3 and Fet5, multicopper ferroxidases found in yeast that oxidize iron and facilitate its movement across membranes; and domain A of the mammalian blood coagulation factors V and VIII (David and Patel 2000).

2.1 Genes and expression

The genes encoding CP (*CP*), HP (*HEPH*), and ZP (*HEPHL1*) contain 19-22 exons and are located on unique chromosomes in both humans and mice, with *HEPH* located on the X chromosome, *CP* on chromosome 3, and *HEPHL1* on chromosome 11 in humans and chromosome 9 in mice. According to Ensembl (www.ensembl.org), there are currently eight predicted protein-coding transcripts in mice for *Cp*, three for *Heph*, and one for *Hephl1*. Mouse *Hephl1* shares approximately 59.4 % and 56% identity with *Heph* and *Cp* at the nucleotide level, respectively (Chen, Attieh et al. 2010).

The full-length nascent human CP protein is made up of a single chain of approximately 1065 amino acids, while human HP and ZP are predicted to be single chains of approximately 1158 and 1159 amino acids, respectively. The predicted full-length mouse proteins are similar in amino acid length. The extra residues in HP and ZP can be attributed to an elongated C-terminus encoding a transmembrane domain, which suggests that HP and ZP are membrane bound type 1 transmembrane proteins (Chen, Attieh et al. 2010). CP lacks this domain, but a splice variant is found attached to membranes via a glycophosphatidylinositol anchor (GPI-anchor) in some cell types including astrocytes, macrophages, and Sertoli cells (Patel and David 1997; Fortna, Watson et al. 1999; Marques, Auriac et al. 2012). Mouse HP is 49% identical to ZP at the protein level, and CP shares approximately 50% and 46% identity with

HP and ZP, respectively. Comparison between the mouse and human proteins for each MCF reveals over 83% sequence identity, indicating that these proteins are highly conserved (Chen, Attieh et al. 2010; Flicek, Amode et al. 2012).

CP, and likely HP and ZP as well, is synthesized in the endoplasmic reticulum (ER) and traffics through the Golgi apparatus, and is believed to acquire its copper atoms required for function at the late Golgi stage (Terada, Kawarada et al. 1995; Syed, Beaumont et al. 2002). A copper transporting ATPase (ATP7B in the liver, and perhaps ATP7A in some other tissues) is required for proper loading of copper into CP (Lutsenko, Barnes et al. 2007). If adequate copper is not available an apo version of CP is released that has a shorter half-life (5 hours) than holo-CP (5.5 days). Based on their amino-acid sequences alone, the predicted molecular weights of the MCFs are lower than observed, and this is likely due in part to glycosylation. HP and CP have been shown to be N-glycosylated, and ZP has several predicted glycosylation sites (Hellman and Gitlin 2002; Nittis and Gitlin 2004; Chen, Attieh et al. 2010).

The three mammalian MCFs exhibit unique expression patterns with some overlap at the cellular and tissue level. More studies however are still needed to specify the precise expression pattern in particular cell types, and to determine if any species-specific differences exist. CP has been detected in many tissues and cell types in the body including the liver, brain, eye, macrophages, spleen, lung, and pancreas. *CP* mRNA has not been detected in mouse or human duodenal enterocytes, however in one study CP protein was present in mouse enterocytes (Cherukuri, Potla et al. 2005). CP is found at high levels circulating in the blood (270-370 mg/L in normal human adults), and most of this protein is believed to be secreted from the liver (Kratz, Ferraro et al. 2004). CP is considered an acute phase protein, with serum levels increasing 2-3 fold in response to infection, inflammation, and trauma, although the role of CP in the acute phase response is not clear (Hellman and Gitlin 2002). *CP* expression may be regulated at the transcriptional level by iron, oxygen and copper via HIF1α and activator protein-1 (AP-1) (Mukhopadhyay, Mazumder et al. 2000; Martin, Linden et al. 2005; Das, Tapryal et al. 2007).

HP is highly expressed along the length of the intestinal tract, and lower levels of expression are reported in a variety of tissues including the central nervous system, lungs, heart, and exocrine pancreas. Unlike CP, no HP expression has been detected in the liver or serum (Vulpe, Kuo et al. 1999; Frazer, Vulpe et al. 2001; Qian, Chang et al. 2007; Hudson, Curtis et al. 2009; Schulz, Vulpe et al. 2011). Most studies of HP expression have examined whether expression is affected by iron status or stimuli that affect the regulation of iron metabolism. Duodenal *HEPH* mRNA expression was not increased in rats during pregnancy or in humans with hepatic hemosiderosis or untreated hemochromatosis despite increased iron absorption in these conditions (Stuart, Anderson et al. 2003; Millard, Frazer et al. 2004; Stuart, Anderson et al. 2004). Duodenal *Heph* mRNA

and protein expression were also not affected when rats were switched to an iron-deficient diet for two weeks, after the induction of an acute phase response, or after an oral dose of iron (Anderson, Frazer et al. 2002; Frazer, Wilkins et al. 2003). However *HEPH* mRNA and protein levels were increased in duodenal samples from patients with chronic iron deficiency anemia as compared to controls in two studies (Zoller, Theurl et al. 2003; Dostalikova-Cimburova, Kratka et al. 2012). In addition, duodenal *Heph* expression was shown to be hampered by a high fat diet in mice (Sonnweber, Ress et al. 2012). The mechanisms by which HP expression can be regulated have not been well studied, but there is a report that the iron-regulated homeobox transcription factor caudal type homeobox 2 (CDX2) can directly upregulate *HEPH* transcription in intestinal cells (Hinoi, Gesina et al. 2005). Like CP, levels of HP protein are decreased by copper deficiency due to decreased stability and increased protein turnover (Prohaska 2011). HP activity may be primarily regulated not by the level of expression but by cellular relocalization. In support of this, HP protein has been observed in cell models and rat enterocytes to redistribute from the supranuclear region to a proximal basolateral compartment upon iron treatment (Yeh, Yeh et al. 2009; Lee, Attieh et al. 2012).

ZP was first discovered in the human placental cell line BeWo when a ferroxidase activity that could not be ascribed to HP was noted, followed by a search of the annotated human genome sequence for new putative MCFs. The protein is expressed in mouse mammary gland, placenta, embryo, heart, kidney, eye, testes, brown fat, bladder and brain, but has not been detected in mouse intestine or liver. Little is currently known about the regulation of ZP. ZP protein levels are decreased in copper-deficient cells (Chen, Attieh et al. 2010). Phosphorylated tyrosine residues on the protein have also been detected in lung, colon, and leukemia cancers by mass spectrometry-based global phosphorylation screens. These residues are conserved in mice and humans and thus may affect ZP function. Mono-methylation has also been observed in human T-cell leukemia at Lys258 (Hornbeck, Kornhauser et al. 2012).

2.2 Structure and enzymatic activity

Much of what we know about the structure and function of MCFs is based on studies of ancestrally related multicopper oxidases in other organisms and of CP, which, as noted above, shares a high degree of sequence similarity with HP and ZP. CP has been modeled based on X-ray crystallography data to contain six domains that are each made up of a plastocyanin-like fold and beta-barrel strands organized like those found in the cupredoxin family of metalloreductases (Bento, Peixoto et al. 2007) (Figure 1.5). Based on sequence similarity and molecular modeling, HP and ZP likely share a similar 3D structure as CP (Syed, Beaumont et al. 2002; Chen, Attieh et al. 2010). All three proteins are believed to contain six integral copper atoms in their functional form, three in type I (blue)

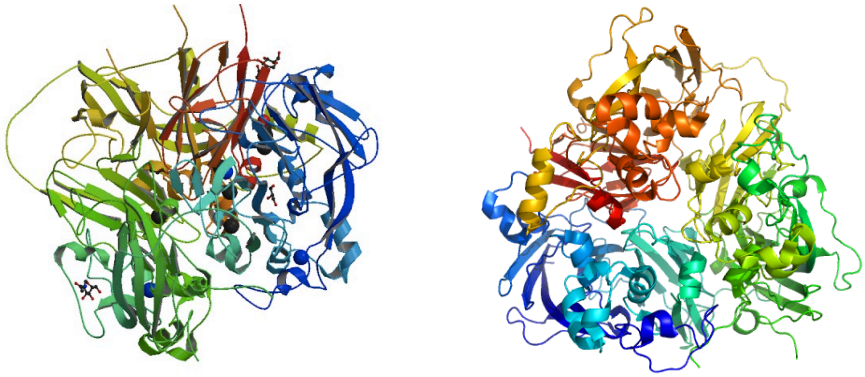

Figure 1.5. X-ray crystal structure of human serum ceruloplasmin. The data for this structure is located online in the RCSB Protein Data Bank (www.pdb.org) under PDB ID 2J5W and was originally obtained by Bento et al. (Berman, Westbrook et al. 2000; Bento, Peixoto et al. 2007). The view on the left is available on the PDB website and the image at right was created using MacPyMol (MacPyMOL 2006).

copper sites located in domains 2, 4, and 6, and three copper atoms in a type II/type III trinuclear cluster at the interface of domains 1 and 6. Type I, II, and III copper sites have different spectroscopic properties and multicopper oxidases in general are defined as proteins possessing all three types of sites. Type I copper sites exhibit a strong absorbance centered around 610 nm, giving these proteins a characteristic intense sky-blue color. Based on sequence alignment, all of the residues involved in copper binding and disulfide bond formation (5 bridges) in CP are conserved in HP and ZP (Chen, Attieh et al. 2010).

Labile iron holding and binding sites have been detected in domains 4 and 6 of CP by crystal soaking studies. Ferrous iron is suspected to dock at an iron-binding site on the protein and deliver an electron to the nearest Type I copper site. This is associated with the transfer of the oxidized iron to an adjacent ferric iron holding site. Based on the crystal structure model of CP, all Type I sites are located within 18 Å of each other, well within electron transfer range and with clear paths for electron transfer to the Type I copper site in domain 6, located closest to the Type II/Type III trinuclear cluster. Electrons can thus be moved through the protein to the Type II/Type III site, where molecular oxygen binds. The Type II/Type III site can then sequentially transfer a total of 4 electrons originally donated from different ferrous iron atoms to dioxygen to make water (Lindley 2001). This reaction consumes four protons as well:

$$4Fe^{2+} + O_2 + 4H^+ \rightarrow 4Fe^{3+} + 2H_2O$$

The presence of only one active Type I copper site can be sufficient for ferroxidase activity in MCFs, as MCFs in other organisms such as yeast only

have one Type I site (de Silva, Davis-Kaplan et al. 1997). CP interestingly has a non-typical, permanently-reduced type I copper site in domain 2 that is believed to be non functional, while all three Type I copper sites are predicted to be functional in HP and ZP (Chen, Attieh et al. 2010). A functional Type II/Type III site is critical for MCF activity, however, and sodium azide, which binds to this site, is a potent MCF inhibitor (Zaitsev, Zaitseva et al. 1999).

CP has also been shown to oxidize aromatic amines and phenols including the synthetic aromatic amines *p*-phenylene diamine (pPD) and *o*-dianisidine and biogenic amines in the epinephrine and 5'hydroxyindole series including dopamine, norepinephrine, and serotonin (Rydén 1984; Lindley 2001). The K_m for these molecules ranges from 20 μM to 0.3 M, while the K_m for iron is only 0.3 μM. The site for binding of biogenic amines to CP has been determined by X-ray crystallography to be close to the iron-binding site in domain 6. On the other hand, the binding site for pPD has been determined to be in a different region unique to domain 4 (Zaitsev, Zaitseva et al. 1999). Reactions with synthetic aromatic amines have been utilized to demonstrate CP, HP, and ZP activity *in vitro*, but the importance of any of the MCFs in biogenic amine catabolism is not yet known.

2.3 Biological role

The MCFs CP and HP have both been shown to play particularly important roles in iron metabolism. CP was the first of the mammalian MCFs to be discovered and characterized. Over 95% of the copper in plasma is bound by CP, which originally suggested that CP may be particularly important for copper trafficking in the blood. However, mice with genetic ablation of *Cp* and human patients that lack CP (aceruloplasminemia) due to mutation do not appear to have any clear defects in copper metabolism beyond two to four-fold higher hepatic copper levels than normal (Morita, Ikeda et al. 1995; Meyer, Durley et al. 2001). Aceruloplasminemia patients however develop iron loading in the liver, pancreas, retina, and brain, leading to diabetes, retinal degeneration, and dementia later in life (Morita, Ikeda et al. 1995; Xu, Pin et al. 2004). Mice null for CP exhibit a mild anemia, iron loading in the liver and reticuloendothelial macrophages, and iron deficiency in some regions of the brain (Harris, Durley et al. 1999; Cherukuri, Tripoulas et al. 2004; Texel, Camandola et al. 2012). These phenotypes, as well as further studies with CP null mouse models and cells, have revealed that CP plays an important role in iron efflux from some cell types, including hepatocytes, astrocytes, and macrophages (Young, Fahmy et al. 1997; Sarkar, Seshadri et al. 2003). CP interacts with the iron export protein FPN1 and has been shown in astrocytes and glioma cells to be required for FPN1-mediated iron export and maintenance of FPN1 cell surface localization (Jeong and David 2003; De Domenico, Ward et al. 2007). Interestingly, there is a precedent for this role in yeast, with the Saccharomyces cerevisiae MCF Fet3p oxidizing iron for transport by the iron permease Ftr1p via a mechanism that involves direct interactions

between the proteins (Kwok, Severance et al. 2006). CP does not appear to normally play a role in intestinal iron absorption (Harris, Durley et al. 1999). In addition, although iron recycling appears to be somewhat impaired by CP ablation, there are clearly other iron recycling mechanisms that can function independently of CP.

An important role of HP in iron metabolism was first revealed when HP was discovered to be the protein mutated in the *sla* mouse (Vulpe, Kuo et al. 1999). The requirement for a copper-rich protein for iron export from intestinal enterocytes to the blood agrees with early evidence showing that copper deficient pigs accumulate iron in enterocytes and that iron absorption is reduced in copper deficiency (Lee, Nacht et al. 1968). Mice with the *sla* mutation have also been shown to load iron in oligodendrocytes in the brain, leading to defects in motor coordination and indicating an important role for HP in this cell type as well (Schulz, Vulpe et al. 2011). HP also plays a role in the retina, as mouse models on a CP null background with either the *sla* mutation or HP ablation develop retinal iron overload and symptoms consistent with age-related macular degeneration (Hahn 2004, Wolkow 2012). Those studies also suggest that CP and HP may partially compensate for each other in some tissues. There is evidence from colocalization and immunoprecipitation studies that HP and FPN1 interact (Yeh, Yeh et al. 2009). Although HP and CP have been hypothesized to directly channel ferric iron to TF, no protein-protein interactions have been yet detected between HP and TF and only a weak interaction was reported *in vitro* for CP and TF (Hudson, Krisinger et al. 2008; Ha-Duong, Eid et al. 2010). CP however has been shown to interact with lactoferrin, a TF paralog (Sabatucci, Vachette et al. 2007).

Currently no cases of HP mutation or dysfunction have been reported in humans, which could be due to either a mild or compensable phenotype in individuals with a mutation, a role in conditions with no known etiology (including the many diseases correlated with iron loading in certain cell types, particularly in the brain), or an absolutely essential role for HP for survival. Recently a single nucleotide polymorphism in the 5'UTR of HP was correlated with migraine in a genome-wide association study (Maher, Lea et al. 2012). Interestingly, iron loading in certain regions of the brain has also been associated with migraine (Lakhan, Avramut et al. 2012). The role of ZP in iron metabolism has not yet been studied.

The mammalian MCFs may have other important functions not directly related to iron homeostasis. CP in macrophages has also been recently been shown to be important for managing inflammation in the colon (Bakhautdin, Febbraio et al. 2012). Reduced HP expression has also been correlated with increased disease severity in colorectal carcinomas (Brookes 2006). CP has been reported to scavenge reactive oxygen species, to possess a glutathione-peroxidase activity,

and to oxidize copper and nitric oxide (Cha and Kim 1999; Shiva, Wang et al. 2006; Healy and Tipton 2007).

3. Ferritin ferroxidases

The ferritin ferroxidases include the ferritins, bacterioferritins, and miniferritins (Dps proteins). Ferritins, made up of 24 subunits that come together to form a hollow protein sphere, are found in all kingdoms of life. They are the only type of ferritin ferroxidases expressed in mammals and are particularly important for the storage of iron in a safe and bioavailable form. Ferritins are evolutionarily related to the prokaryotic bacterioferritins and miniferritins. Bacterioferritins are also made up of 24 subunits and contain heme as a cofactor, while miniferritins are made up of only 12 subunits and bind to and protect prokaryotic DNA from oxidative stress. Ferritin proteins are also evolutionarily related to the diiron cofactor oxygenases ribonucleotide reductase, Δ^9 desaturase, and methane monooxygenase (Crichton and Declercq 2010).

Mammals express cytosolic, serum, and mitochondrial ferritins. Cytosolic ferritins are found in nearly every cell type and are made up of a mix of both ferritin H (FTN-H) and ferritin L (FTN-L) subunits, the ratio depending on both the tissue type and conditions in that tissue. Ferritin H and L subunits are similar, yet encoded by different genes, and only ferritin H possesses ferroxidase activity (Harrison and Arosio 1996). Serum ferritin is of debated tissue origin but is mainly made up of FTN-L subunits, and unlike cytosolic ferritins, is highly glycosylated, suggesting active secretion (Wang, Knovich et al. 2010). Ferritins found in the mitochondria are made up exclusively of mitochondrial ferritin subunits, which are encoded by a single intronless nuclear gene different from those that encode FTN-H and FTN-L. mFTN subunits contain a ferroxidase active site (Levi, Corsi et al. 2001).

3.1 Genes and expression

In humans, the genes encoding FTN-L, FTN-H, and mFTN are located on chromosomes 19, 11, and 5 respectively. In mice there are two *Ftn-L* genes located on chromosomes 7 and 5, and the *Ftn-H* and *mFtn* genes are on chromosomes 19 and 18, respectively. There are also numerous ferritin pseudogenes scattered throughout the human and mouse genomes (Flicek, Amode et al. 2012). Human FTN-L and FTN-H protein subunits are made up of 175 and 183 amino acids, respectively, and have molecular weights of approximately 19 kD and 21 kD. In general, mammalian FTN-H and FTN-L subunits are approximately 50% identical at the amino acid level (Harrison and Arosio 1996). Nascent human mFTN is 242 amino acids long but is further processed to a mature 22 kD form by cleavage of the ~57 amino acid mitochondrial transit peptide. Human mFTN is 79% identical to FTN-H and 63% identical to FTN-L at the protein level when overlapping coding regions are

compared, and mouse mFTN is 84% identical to human mFTN (Levi, Corsi et al. 2001).

Cytosolic FTN is expressed in most cells in proportion to their iron status. FTN-H and FTN-L are highly expressed in tissues that contain significant iron stores, especially the liver, spleen, and bone marrow. Serum FTN increases in proportion to iron stores under normal circumstances, and is thus used routinely as a marker of whole body iron status. Serum FTN however also increases dramatically in response to infection, inflammation, and cancer and is considered to be an acute phase protein (Wang, Knovich et al. 2010). Levels of FTN in the serum can also increase due to release of cytosolic FTN from damaged ferritin-rich tissues, although this form of ferritin can be differentiated by its higher iron content and lack of glycosylation (Hubel, Bodnar et al. 2004). mFTN is most highly expressed in the testes, but also is found at low levels in the heart, brain, kidney, and pancreas, but not the liver or spleen (Santambrogio, Biasiotto et al. 2007).

Little is currently known about the regulation of mFTN expression, but FTN-H and FTN-L expression in mammals can be affected by a myriad of stimuli including inflammation, infection, hormones, growth factors, hypoxia, and differentiation (Torti and Torti 2002). Of note, FTN-H and FTN-L subunits are regulated at the transcriptional level by oxidative stress and heme, and at the translational and protein levels by cellular iron status. The promoter region for the genes encoding both FTN-H and FTN-L contains overlapping MAF antioxidant response element (MARE) and antioxidant response element (ARE) motifs that are under the control of the MAF, nuclear factor E2-related factor 2 (NRF2), and Btb And Cnc Homology 1 (BACH1) repressor proteins (Hintze and Theil 2005; Hintze, Katoh et al. 2007). In this system, oxidative stress leads to the release of cytosolic NRF2 from the inhibitor protein kelch-like ECH-associated protein (KEAP1), allowing NRF2 to translocate to the nucleus. There, NRF2 binds to MAFS at MARE/AREs to stimulate the expression of target genes. The repressor BACH1, however, can inhibit NRF2/MAF stimulated transcription. However, when free heme, a potent generator of reactive oxygen species, is present it binds to and inactivates BACH1 (Dhakshinamoorthy, Jain et al. 2005). Thus, when oxidative stress and/or free heme levels in a cell increase, more ferritin is made, presumably to sequester iron and oxygen and prevent further generation of reactive oxygen species. *FTN-H* and *FTN-L* mRNA, but not *mFTN* mRNA, also contain an IRE in the 5' UTR, which is responsible for decreased translation when iron levels are low as it is a target for IRPs 1 and 2. This allows for rapid tuning of ferritin levels to match iron availability in the cell (Hintze and Theil 2006). Furthermore, cytosolic FTN depleted of iron due to increased cellular iron export has been shown to be marked by ubiquitination for degradation by the proteosome, but the exact details of how low-iron FTN is recognized are not yet known (De Domenico, Vaughn et al. 2006).

3.2 Structure and enzymatic activity

Individual FTN-H, FTN-L, and mFTN subunits spontaneously assemble into hollow spherical proteins of 24 subunits (Figure 1.6). mFTN subunits are trafficked first to the mitochondria before assembling into a homopolymer (Levi, Corsi et al. 2001; Theil 2011). Assembled FTN proteins typically are 12 nm in diameter, with the spherical protein shell being approximately 2 nm thick and the hollow core 8 nm in diameter. The proteins exhibit an octahedral 432 symmetry with visible pores at both the eight 3-fold axes and the six 4-fold axes of the protein. Each FTN subunit is primarily organized into a four alpha helix bundle with a fifth short helix. Ferroxidase-active FTN-H and mFTN subunits contain a diiron ferroxidase active site near the center of each subunit. FTN-L subunits lack a ferroxidase active site but contain residues that form nucleation sites that promote ferritin mineral formation. FTN subunits are linked to each other via hydrophobic and hydrophilic interactions, hydrogen and disulfide bonds, and salt bridges (Crichton and Declercq 2010).

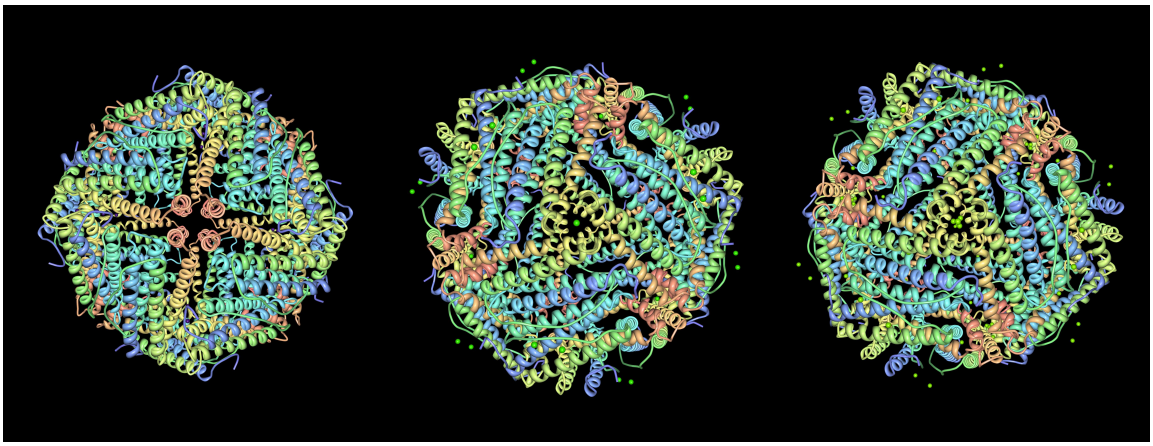

Figure 1.6. X-ray crystal structures of assembled recombinant human ferritin homopolymers. Left: FTN-L image centered on a 4-fold axis pore, PDB ID: 2FG8 (Wang, Li et al. 2006). Center: FTN-H image centered on a 3-fold axis pore, PDB ID: 2FHA (Hempstead, Yewdall et al. 1997). Right: mFTN centered on a 3-fold axis pore, PDB ID: 1R03 (Langlois d'Estaintot, Santambrogio et al. 2004). These structures are available online at the RCSB Protein Data Bank (www.pdb.org)(Berman, Westbrook et al. 2000).

Ferroxidase active subunits greatly accelerate the mineralization of ferritins, while FTN-L subunits are hypothesized to provide structural stability to the protein and influence ferritin mineral structure. Ferritin mineralization is a complex process with many intermediates, many of which are rust-colored due to their absorption of light in 300-350 nm range. Evidence suggests that ferrous iron enters the ferritin protein shell via the 3-fold axis pores. Ferroxidase active sites in

catalytically active subunits coordinate two ferrous irons and facilitate their reaction with dioxygen to form diferric oxo products. The blue (maximum absorbance 650 nm) diferric peroxo (DFP) intermediate, which forms within milliseconds and decays rapidly to a diferric oxo mineral precursor, is the first detectable intermediate in the ferritin ferroxidase reaction. The diferric oxo precursors then are channeled into the ferritin protein core, where they react with other iron and oxygen atoms to build iron oxide mineral. Ferritins are capable of holding up to 4,500 iron atoms that can then be made available to the cell as needed (Chasteen and Harrison 1999; Theil 2011).

mFTN and cytosolic FTN (that contains H subunits) produced by overexpression in *E.coli* or purified from organisms are able to rapidly oxidize and sequester ferrous iron in solution *in vitro* (Bou-Abdallah, Santambrogio et al. 2005). However, the low solubility of iron in solutions at physiological oxygen concentrations and pH suggests that very little ferrous iron exists in a free form *in vivo*. Chaperones of the poly(rC)-binding protein (PCBP) family instead appear to be important for cytosolic FTN iron incorporation *in vivo* (Shi, Bencze et al. 2008). The mechanism by which iron is released from FTN in cells is not known, but cytosolic FTN has been shown to be degraded both by the proteosome following iron depletion, and in lysosomes (De Domenico, Ward et al. 2009). *In vitro*, addition of specific reductant/chelator combinations leads to the release of iron from FTN without degradation of the FTN protein itself. Release of iron from FTN likely involves the pores at the 3-fold axes of the protein. When these pores are opened by mutations in key conserved residues, *in vitro* iron release is greatly accelerated leading to the hypothesis that opening of these pores *in vivo* may play a role in FTN iron release (Jin, Takagi et al. 2001).

3.3 Biological role

FTN clearly plays a primary and essential role in cellular iron storage and detoxification in mammals, although it may have other functions as well. Knockout of *Ftn-H* was reported to be embryonic lethal in mice, while conditional ablation in adult mice led to loss of iron stores and severe tissue damage in mice challenged with a high iron diet (Ferreira, Bucchini et al. 2000; Darshan, Vanoaica et al. 2009). The generation of mice lacking FTN-L has not yet been reported. Although no human patients have been identified that completely lack FTN-H or FTN-L, several different mutations have been identified that disrupt the ratio of H and L subunits and lead to disease. A mutation in the IRE of H ferritin in one family led to decreased FTN-H synthesis, decreased iron uptake into assembled ferritins, and subsequent marked tissue iron overloading (Kato, Fujikawa et al. 2001). Similarly, conditional knockout of *Ftn-H* in the intestine of mice led to increased labile iron in enterocytes, increased intestinal iron absorption, and increased body iron stores, suggesting that increased intestinal iron absorption may be responsible for some of the iron loading seen in patients

with the mutant FTN-H IRE (Vanoaica, Darshan et al. 2010). Mutations in exon 4 of *FTN-L* are responsible for adult-onset neuroferritinopathy. In this disease, iron accumulates in the basal ganglia and is associated with progressive movement defects. The phenotype is believed to be due mainly to disruption of the structure and stability of assembled FTN incorporating the mutant FTN-L subunits as opposed to lack of functional FTN-L (Luscieti, Santambrogio et al. 2010). An IRE-disrupting mutation has also been reported in *FTN-L* in Hereditary Hyperferritinemia-Cataract Syndrome (HHCS) that leads to the upregulation FTN-L protein expression and bilateral nuclear cataracts, but no iron-related pathology (Kroger, Bachli et al. 2011). Given that FTN-H and FTN-L are ubiquitously expressed and regulated by so many different stimuli, any disruption of these genes likely affects many cellular processes, some that may become more apparent with further study (Torti and Torti 2002).

mFTN has been reported in mice to be expressed mainly in tissues with high metabolic activity and oxygen consumption, such as the testes and brain, as opposed to tissues involved in iron storage. This has led to the hypothesis that mFTN may mainly play a role in protecting mitochondria from oxidative damage (Santambrogio, Biasiotto et al. 2007). No human diseases are currently known to be due to defects in mFTN, and ablation of *mFtn* in mice did not lead to any clear defects in iron metabolism or any other disease phenotypes, suggesting that mFTN may only become important in the face of currently unknown stressors (Bartnikas, Campagna et al. 2010).

4. Other proteins with ferroxidase activity

A few other proteins have been reported to possess ferroxidase activity, including xanthine oxidase (XO), TF, frataxin (FXN), and most recently, amyloid precursor protein (APP) (Bates, Workman et al. 1973; Topham, Jackson et al. 1986; O'Neill, Gakh et al. 2005; Duce, Tsatsanis et al. 2010).

4.1 Amyloid precursor protein

APP is most widely known for its pathogenic cleavage product, ß-amyloid (Aß), which forms extracellular plaques in the brain in Alzheimer's disease. Despite extensive study, the normal cellular functions of APP are not currently clear, although APP has been reported to be involved in many processes in neurons including cell adhesion, migration, signaling, synaptogenesis, and axonal transport (Zheng and Koo 2006). The *APP* gene is located on chromosome 21 in humans and chromosome 16 in mice. There are multiple mRNA splice variants in humans, with the major protein products made up of 695, 751, and 770 amino acids. Only a 695 amino acid residue protein product is listed in the www.ensembl.org database for mice (Flicek, Amode et al. 2012). APP is one of three family members present in mammals: APP, APP like protein 1 (APLP1), and APP like protein 2 (APLP2). All three proteins are highly expressed in the

brain in neurons, and APP and APLP2 are also detected in most other tissues (Zheng and Koo 2006). APP, but not APLP1 and APLP2, possesses an IRE in its 5' UTR and has been shown to be regulated at the translational level by iron via the IRE/IRP system. Like ferritin, levels of APP protein increase when iron levels in cells are high (Rogers, Bush et al. 2008).

APP is a multidomain type 1 transmembrane protein with a large extracellular region that is normally proteolytically processed to release a soluble ectodomain containing an E1 and E2 domain. The E1 domain possesses copper and zinc binding sites and a growth factor domain, and the E2 domain contains the putative ferroxidase site of APP (Zheng and Koo 2006; Duce, Tsatsanis et al. 2010). Using a TF iron loading ferroxidase assay, Duce et al. detected ferroxidase activity in the recombinant soluble ectodomain of APP695, referred to as APP695α, which was comparable to that of purified serum CP. They also detected activity at 40% that of APP695α in recombinant E2 domain alone and in a 22 residue synthetic peptide (FD1) within the E2 domain. Addition of the E1 domain, which lacked activity on its own, to a reaction containing the E2 domain enhanced E2 ferroxidase activity. Furthermore, addition of Zn^{2+} inhibited ferroxidase activity, whereas azide did not, consistent with the active site having ferritin-like and not MCF-like properties. Recombinant APLP2 was also tested and did not possess ferroxidase activity (Duce, Tsatsanis et al. 2010). Another group recently reported that they did not detect iron binding or ferroxidase activity in the FD1 peptide and suggested that the ferroxidase activity of APP695α and the E2 domain be revisited using alternative ferroxidase assays, as the TF iron loading assay gives no information as to the stoichiometry of the reaction and is also prone to error by small changes in pH, iron, and zinc concentrations (Ebrahimi, Hagedoorn et al. 2012).

Very little is known at present about the mechanism of iron oxidation by APP. The structure of the active site is also unclear. The putative ferroxidase residues of APP as proposed by Duce et al. are part of an REXXE motif known to coordinate iron in FTN and other proteins (Gutierrez, Yu et al. 1997). When residues in this motif were mutated in the FD1 peptide, ferroxidase activity was lost, suggesting that this motif plays a role in APP ferroxidase activity (Duce, Tsatsanis et al. 2010). As recently highlighted by Ebrahimi et al., REXXE motif residues however are not ligands to the iron in the ferroxidase active site of FTN-H. In addition, the ferroxidase active site of FTN-H is made up of five residues that are liganded to two ferrous irons, while there are only two iron-coordinating residues in the REXXE motif (Ebrahimi, Hagedoorn et al. 2012). This suggests that additional residues must contribute to the APP active site if it is indeed ferritin-like. It has been suggested that APP homodimerization may be required to create a fully-functional active site (James Duce, personal communication). The E2 domain of the protein has been shown to dimerize in several antiparallel orientations *in vitro*, and there is also evidence for dimerization of other APP

protein domains that could in turn affect E2 orientation (Khalifa, Van Hees et al. 2010; Lee, Xue et al. 2011). The E2 domain in general appears to be flexible and capable of adopting many different conformations that can be influenced by metal ion binding (Dahms, Konnig et al. 2012) (Figure 1.7).

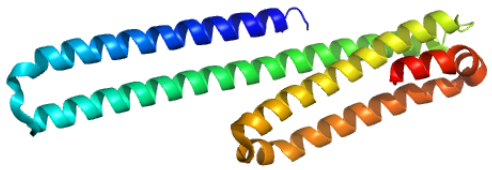

Figure 1.7. X-ray crystal structure of the E2 domain of human APP. The data for this structure, one of several for this domain, is located online in the RCSB Protein Data Bank (www.pdb.org) under PDB ID 3UMK and was originally obtained by Dahms et al. (Berman, Westbrook et al. 2000; Dahms, Konnig et al. 2012). This image was created using MacPyMol (MacPyMOL 2006).

In biological studies APP has shown many properties consistent with it playing an important role in iron metabolism. Duce at al. studied the role of APP in HEK293T cells and cortical neurons, both cell types that do not express CP but do express FPN1. APP suppression by RNAi decreased iron export from HEK293T cells, while the addition of soluble APP695 (but not REXXE mutant APP695) or the E2 domain of APP to the medium increased iron efflux. Decreased iron efflux was also observed in primary cortical neurons from $APP^{-/-}$ mice as compared to WT controls. In animal studies, iron levels in the brain, liver, and kidney of 12 month old $APP^{-/-}$ mice was significantly greater than levels in WT controls. Furthermore, endogenous APP in HEK293T cells and in human and mouse cortical tissue co-immunoprecipitated with endogenous FPN1. The biotinylated soluble ectodomain of APP695 also co-immunoprecipitated with endogenous HEK239T FPN1, providing further support for a mechanism by which APP ferroxidase activity could be biologically relevant for iron efflux from certain cell types (Duce, Tsatsanis et al. 2010). APP has also been reported to be trafficked to the surface of neurons by the microtubule-associated protein TAU, and disruption of TAU in mice led to decreased APP trafficking and iron accumulation in neurons (Lei, Ayton et al. 2012).

4.2 Xanthine oxidase

XO is not generally classed as a ferroxidase, but it has been reported to have ferroxidase activity (Topham, Jackson et al. 1986). XO is generated proteolytically from xanthine dehydrogenase (XDH), the latter of which is typically the more predominant form in cells. XO and XDH are present in endothelial cells, plasma, liver, duodenal enterocytes as well as many other tissues (Linder, Rapola et al. 1999). XO oxidizes multiple substrates including xanthine and hypoxanthine, and in *in vitro* studies XO significantly increased the rate at which ferrous iron was oxidized and bound to TF or loaded into FTN (Hall-Sizemore, Joseph et al. 1994). The molar ferroxidase activity was reported to be 1000 times that of CP. Similarly to MCFs, XO requires oxygen for iron oxidation, functions with a low K_m for O_2 and Fe^{2+} at cellular pH (7.4), and is capable of oxidizing organic substrates. Unlike MCFs, however, XO generates toxic superoxide anion and hydrogen peroxide as a reaction product (MCFs generate water), requires iron, molybdenum, and other cofactors for function, and is not inhibited by azide (Topham, Jackson et al. 1986).

The role of XO ferroxidase activity in cells is unclear. Several human patients have been identified with XO null mutations (xanthinuria type I), and the primary phenotypes are renal failure, urinary tract calculi, and skeletal muscle inflammation that appear to be related to tissue xanthine deposition (Ichida, Amaya et al. 1997). Three different mouse models with disruption of the *Xdh* gene have also been described. The most striking abnormality in all of these mice is severe kidney damage, and defects in lipid metabolism were noted as well (Vorbach, Scriven et al. 2002; Ohtsubo, Rovira et al. 2004; Piret, Esapa et al. 2012). No iron-related parameters or analyses have been reported suggesting that lack of XO does not lead to obvious anemia. Without specific testing however, other potential iron phenotypes are not likely to be readily apparent. XO does not appear to be necessary for normal iron acquisition, as inhibition of XO by molybdenum deficiency did not affect iron absorption in a rat model (Kelley and Amy 1984). There are conflicting reports on the effects on iron metabolism of XO inhibition with the drug allopurinol however (Seelig 1972).

4.3 Transferrin

Apo-TF was reported long ago to promote the oxidation of iron *in vitro* potentially by interacting with ferrous iron to form a complex that is more susceptible to oxidation than ferrous iron in solution alone (Bates, Workman et al. 1973). Harris and Aisen noted however that the increased rate of iron oxidation in the presence of apo-TF was not remarkable and likely even slower than iron oxidation promoted by other ferric binding molecules such as ethylenediaminetetraacetic acid (EDTA) and citrate (Harris and Aisen 1973).

4.4 Frataxin

FXN, a highly evolutionarily conserved protein found in both prokaryotes and eukaryotes, is in mammals a nuclear-encoded protein that is targeted to the mitochondrial matrix. FXN expression is ubiquitous, but levels are particularly high in mitochondria-rich tissues such as the heart, brain, kidney, and liver. Disruption of FXN in Friedreich's ataxia leads to mitochondrial iron overload, oxidative damage, and defects in cellular iron homeostasis that result in neurodegenerative disease and cardiomyopathy. FTX has been shown to be important in the biosynthesis of iron/sulfur clusters and heme, and consequently lack of FTX results in reduced levels of proteins that require these cofactors (Bencze, Kondapalli et al. 2006). Recombinant yeast FTX oligomers have been reported to possess a ferritin-like ferroxidase and mineralization activity (Park, Gakh et al. 2002). However, the ferroxidase activity appears to only be active at low iron concentrations and was reported by another group to be very slow (Bencze, Kondapalli et al. 2006). Further studies are thus needed to determine if mammalian FTX proteins possess this activity and whether it is biologically relevant.

IV. Dissertation research

In the current model of intestinal iron absorption, a MCF is required to oxidize iron from the iron exporter FPN1 in order for dietary iron to be transferred from intestinal cells to the blood (Collins and Anderson 2012). HP, the only known MCF expressed in intestinal enterocytes, is hypothesized to primarily play this role, as the *sla* mutation of HP leads to a partial block in enterocyte iron export in mice (Vulpe, Kuo et al. 1999). *Sla* mice however still absorb adequate iron for survival and reproduction, indicating that either the *SLA* protein still retains some functionality or that another mechanism for iron absorption, ferroxidase-mediated or not, must exist. Previous studies revealed that the *SLA* protein remarkably retains some ferroxidase activity. However, the protein is present at levels 75% lower than normal and is not appropriately trafficked to the basolateral region of enterocytes, where HP may perform some or all of its function (Chen, Attieh et al. 2004; Kuo, Su et al. 2004). My dissertation research has been focused on gaining a better understanding of the role and importance of HP and other ferroxidases in intestinal iron absorption. To this end, I have generated several knockout mouse models lacking ferroxidases and have examined the effect of these deletions on iron absorption and metabolism.

Chapter 2 describes the generation and phenotyping of mouse models with whole body ($Hp^{-/-}$) or intestine-specific ($Hp^{int/int}$) ablation of HP. Both models were viable, indicating for the first time that HP is not essential for iron absorption or survival. Hematology, tissue iron status, and intestinal iron absorption under basal and stressed conditions were studied at several ages in these mice. In addition, the effect of maternal HP expression on pup health was examined, and

comparative studies of $Hp^{-/-}$ and *sla* littermates were performed. Chapter 3 describes efforts to determine if other known ferroxidases are involved in intestinal iron absorption. We reasoned that the circulating MCF CP may partially compensate for loss of HP, since CP plays an analogous role in other tissues, has been reported to aid in intestinal iron absorption during severe iron need, and is the only other MCF known that likely interacts with intestinal cells (Cherukuri, Potla et al. 2005; Chen, Attieh et al. 2010). To test this hypothesis, $Hp^{-/-}$ mice and $Hp^{int/int}$ mice were crossed with CP knockout mice ($Cp^{-/-}$) to generate double knockout models ($Hp^{-/-}$ $Cp^{-/-}$ mice and $Hp^{int/int}$ $Cp^{-/-}$ mice). Both double knockout models were viable, revealing that MCFs are likely not absolutely required for intestinal iron absorption and suggesting that an alternative mechanism for iron oxidation may exist. Characterization of the phenotypes of these mice however revealed new important roles for both CP and HP in ensuring the proper absorption and distribution of iron in the body.

Furthermore, during the course of these studies, the protein APP was reported to have ferroxidase activity and to facilitate iron export from neurons (Duce, Tsatsanis et al. 2010). Because evidence suggested that APP was also present in duodenal enterocytes, an $App^{-/-}$ $Hp^{-/-}$ double knockout model was generated. Finally, a knockout model of the only other known mammalian MCF, ZP, as well as an $Hp^{-/-}$ $Zp^{-/-}$ double knockout model, were also created. Studies are currently underway to further characterize all of these models. The mouse models generated from this work will continue to be important tools for understanding the role of ferroxidases in iron absorption and metabolism. They will also be particularly useful to both characterize and identify the mechanism(s) that allow iron to be absorbed in the absence of the MCFs. In addition, these studies suggest several exciting new areas of research.

CHAPTER 2.

THE ROLE AND IMPORTANCE OF HEPHAESTIN

IN INTESTINAL IRON ABSORPTION

I. Rationale

Every day, billions of iron atoms from the diet must be transferred from intestinal cells to the blood in order to maintain iron balance. The transfer of iron across biological membranes is usually associated with the oxidation or reduction of the iron, and current evidence supports an important role for the vertebrate MCF HP in the export of iron from intestinal enterocytes. HP is hypothesized to oxidize ferrous iron from the only known intestinal iron exporter, FPN1, a multipass membrane protein that has been demonstrated in other cell types to require a ferroxidase to function. This catalyzed oxidation step also ensures that adequate iron is available to bind to its carrier in the blood, TF, which only binds ferric iron. HP is the only known MCF expressed in intestinal enterocytes (Collins and Anderson 2012). While CP, a circulating MCF paralog of HP, has been shown to play an analogous role in iron oxidation and release from other cell types, humans and mice that lack CP do not appear to have defects in iron absorption except, as has been shown in mice, in situations of severe iron need (Cherukuri, Potla et al. 2005).

HP was discovered in 1999 by Vulpe et al., who mapped the mutated gene responsible for the phenotype of the sex-linked anemia (*sla*) mouse (Vulpe, Kuo et al. 1999). The *sla* mouse model arose in the 1950s in an irradiated mouse colony and has a deletion in the gene encoding HP, *Heph*, corresponding to a large internal portion of the protein (Grewal 1962). *Sla* mice have a defect in normal iron absorption. While dietary iron uptake into intestinal enterocytes appears to be normal, iron is not released properly into the body, resulting in iron loading in the intestine and a moderate to severe hypochromic, microcytic anemia. The anemia generally improves with age, as might be expected since iron needs are greatest during the rapid growth that accompanies early life. *Sla* mice still remain iron-deficient throughout life relative to wild-type controls, however (Chen, Attieh et al. 2009).

The phenotype of *sla* mice indicates that HP plays an important role in iron absorption. Subsequent studies revealed, however, that *sla* mice still produce a

mutant HP protein at levels ~25% of wild-type that, remarkably, maintains ferroxidase activity (Chen, Attieh et al. 2004). It thus remained unclear if the *sla* mouse represented a complete null or a hypomorph. If HP is not absolutely required, then either one or more other ferroxidases must be involved, or there must be another mechanism for iron absorption that does not involve an oxidation step. To determine whether or not HP is absolutely required for intestinal iron absorption, we generated both whole body and intestine-specific HP knockout mice ($Hp^{-/-}$ and $Hp^{int/int}$ mice, respectively). The $Hp^{int/int}$ model was designed to enable the study of the specific role of HP in the intestine, since HP is expressed in other tissues as well. We also designed studies to directly compare the phenotypes of $Hp^{-/-}$ and *sla* mice in order to determine potential differences in these models that, if present, could lead to new insight into HP function in future comparative studies.

II. Methods

1. Targeted deletion of *Heph*

We used the cre-lox system to create the $Hp^{-/-}$ and $Hp^{int/int}$ mouse models. The generation of the *Heph* floxed mouse strain (B6-$Heph^{tm1}$, referred to here as $Hp^{fl/fl}$) has been recently described (Wolkow, Song et al. 2012). In these mice, LoxP sites flank exon 4 of the *Heph* gene. We crossed $Hp^{fl/fl}$ mice (kindly provided by Professor Joshua Dunaief at the University of Pennsylvania and previously backcrossed onto the C57BL/6J background) with C57BL/6J transgenic mice bearing the Cre recombinase transgene either driven by the villin promoter, which is only activated in the intestine ("villin-cre" mice, B6SJL-Tg(Vil-Cre)997Gum, The Jackson Laboratory), or the eIIa promoter, which is ubiquitously active ("eIIa-cre" mice, B6.FVB-Tg(EIIa-cre)C5379Lmgd, The Jackson Laboratory), in order to generate the $Hp^{int/int}$ and $Hp^{-/-}$ knockout strains, respectively. Expression of Cre recombinase leads to excision of the region in the DNA between the LoxP sites (exon 4 of *Heph*). Exon 4 is the second protein coding exon in *Heph* and contains residues required for the trinuclear cluster site that is needed for ferroxidase activity. Removal of this exon also causes the remaining protein-coding sequence to be out of frame and introduces an early stop codon. It is important to note that *Heph* is located on the X chromosome, and thus males only carry one allele of *Heph*. For simplicity all mice that are homozygous or hemizygous for a particular *Heph* allele, regardless of sex, are denoted here as "$Hp^{x/x}$", where "x" is the *Heph* allele they carry. For example, a male mouse with a knockout allele of *Heph* will be referred to as "$Hp^{-/-}$", as will a female with two *Heph* knockout alleles. The exceptions to this nomenclature, for simplicity, are wild-type mice, referred to as "WT", and mice homozygous or hemizygous for the *sla* allele of *Heph*, referred to as "*sla*".

We used two breeding schemes in our experiments to generate $Hp^{int/int}$ mice and $Hp^{fl/fl}$ littermate controls: $Hp^{fl/fl}$ females x $Hp^{int/int}$ males or $Hp^{int/int}$ females x $Hp^{fl/fl}$

males. The two different breeding schemes were designed in order to allow differentiation between the effects of maternal intestinal *Heph* ablation and intestinal *Heph* ablation in the pups. In these crosses, all mice and progeny were homozygous or hemizygous for floxed *Heph* alleles, and the $Hp^{int/int}$ breeders and $Hp^{int/int}$ progeny carried only one copy of the villin-cre transgene. Mice that inherited the villin-cre transgene were expected to have recombination and are thus denoted here as "$Hp^{int/int}$"; mice from these crosses that did not inherit the villin-cre transgene are denoted as "$Hp^{fl/fl}$". Litters from both crosses were expected to contain pups that were 50% $Hp^{int/int}$ and 50% $Hp^{fl/fl}$. To generate $Hp^{-/-}$ mice, $Hp^{fl/fl}$ mice were bred with eIIa-cre bearing mice for several generations to achieve germline knockout and then the Cre recombinase transgene was bred out of the line. $Hp^{-/-}$ mice and WT littermate controls were generated by crossing heterozygous $Hp^{+/-}$ females with $Hp^{-/-}$ males. We also crossed $Hp^{-/-}$ mice with *sla* mice to generate females carrying one *sla* allele and one *Heph* knockout allele. We then bred those females with $Hp^{-/-}$ males to produce male $Hp^{-/-}$ and *sla* littermates.

2. Animals

Mice were studied at both the University of California, Berkeley (UCB) (Berkeley, California, USA) and at the Queensland Institute of Medical Research (QIMR) (Herston, Queensland, Australia). Unless otherwise noted, experimental results reported are from studies done at QIMR and with mice on a chow diet. For studies done at UCB, mice were either maintained on a standard rodent chow diet containing ~270 ppm iron (Harlan-Teklad, Indianapolis, IN) or an AIN-93G diet with microcrystalline cellulose as the fiber source and a total iron content of 35 ppm (Dyets, Inc., Bethlehem, PA). At QIMR, mice were maintained on a standard rodent chow diet containing ~160 ppm iron (Norco Stockfeeds, South Lismore, NSW, Australia) or an iron-deficient diet or iron-loaded diet (1% carbonyl iron) made in-house and described previously (Frazer, Vulpe et al. 2001). Mice fed the iron-deficient diet or dosed with ^{59}Fe were provided with iron-free deionized water and housed in grid-bottom cages designed to minimize coprophagia. All mice were allowed unlimited access to food and water. The eIIa-cre and villin-cre mouse strains were obtained from The Jackson Laboratory (Bar Harbor, ME). The CP knockout strain (available at The Jackson Laboratory, Cp^{tm1Hrs}/J, stock # 003582) was obtained from Professor Joshua Dunaief and was originally created by Professor Leah Harris at Vanderbilt University. The *sla* mice were from stocks maintained at QIMR but originally from The Jackson Laboratory (B6.Cg-$Heph^{sla}$/J, stock # 001180). All mice were on the C57BL/6J background unless otherwise noted. All work performed was in accordance with National Institutes of Health (NIH) guidelines and with approval from the Office of Laboratory Animal Care at the University of California, Berkeley, and the Queensland Institute of Medical Research Animal Ethics Committee.

3. Tissue collection

Mice were euthanized by CO_2 gas inhalation or anesthetized by a single intraperitoneal (IP) injection of 44 mg/kg ketamine and 8 mg/kg xylazine in saline. Animals were checked to be unresponsive to paw pinch, and then the abdominal cavity was opened and blood taken from the posterior vena cava and heart. Approximately 250 μL of blood was collected into potassium EDTA tubes (Terumo Corporation, Tokyo, Japan, cat #3T-MQK) for blood analysis, while the rest was allowed to clot and then centrifuged at 4,000 x *g* for 10 minutes to collect serum. Tissues were harvested, trimmed to remove connective tissue, and either immediately snap frozen in liquid nitrogen for future RNA/protein analyses, incubated in 10% phosphate buffered formalin overnight at 25°C for future processing for Perls' Prussian blue staining for iron, or used fresh for ferroxidase assays. Intestinal enterocytes were collected as previously described (Chen, Su et al. 2003). In brief, the duodenal segment was trimmed of connecting tissue and then either cut open longitudinally or everted over a wooden stick. The segment was then washed in ice-cold phosphate buffered saline (PBS), pH 7.4, followed by incubation with agitation in ice-cold PBS containing 1.5 mM EDTA. The EDTA chelates calcium, which disrupts tight junctions and allows the enterocytes to come free from the underlying tissues. The cells were then pelleted by centrifugation at 500 x *g* for 5 minutes at 4°C, and the supernatant was discarded. Blood and other non-enterocyte cells, if present, form a small visible layer on top of the enterocytes after centrifugation. This layer was removed by aspiration if present. Enterocytes were then resuspended in cold PBS by inversion and centrifuged again. The wash and centrifugation steps were repeated twice more, and the cells were then either prepared immediately for ferroxidase assays or snap frozen. Previous analyses have indicated that >95% of the cells collected by this method are enterocytes (Chen, Su et al. 2003).

4. PCR genotyping

Mice were routinely genotyped by polymerase chain reaction (PCR) using DNA obtained from a tail tip or ear punch sample. Other tissues were also genotyped for some experiments. The protocols, primers and annealing temperatures are described in Appendix 1.1.

5. Protein and RNA analyses

A small frozen piece of each tissue was removed from low temperature storage and disrupted by vigorous shaking with 1.4 mm ceramic beads (MO BIO Laboratories, Carlsbad, California, cat. #13113-325) in a Precellys®24 tissue homogenizer (Bertin Technologies, France) in the cold room. For RNA preparation, this homogenization step was performed in ice-cold TRIzol (Invitrogen, Melbourne, VIC, Australia) and RNA was extracted as per the

manufacturer's instructions. Complementary DNA (cDNA) was synthesized using oligo(dT) primers and Moloney Murine Leukemia Virus reverse transcriptase (Invitrogen) as per the manufacturer's instructions. Real-time quantitative PCR (RT-qPCR) was performed using LightCycler (LC) 480 SYBR Green I Master Mix in an LC480 machine (Roche, Basel, Switzerland) as per the manufacturer's instructions, and the data were analyzed by calculating the concentration of each sample from its C_t value using a standard curve made from pooled sample cDNA as described previously (Darshan, Frazer et al. 2010). The results were then normalized to the expression of the housekeeping gene hypoxanthine guanine phosphoribosyl transferase (*Hprt*). All primers (Appendix 1.2) were validated by melt-curve analysis, PCR product size analysis, and in most cases, by PCR product sequencing.

For protein expression analysis by immunoblot, tissue was homogenized as described above in ice-cold lysis buffer containing 25 mM tris(hydroxymethyl)aminomethane (Tris), pH 7.4, 125 mM NaCl, 0.1% sodium dodecyl sulfate (SDS), and 0.2% polysorbate 20 (Tween-20) with protease inhibitors as per the manufacturer's instructions (Complete protease inhibitor cocktail tablets, Roche, cat #11697498001). The homogenized sample was transferred to a new 1.5 mL tube and centrifuged at 13,000 x *g* for 30 minutes at 4°C to pellet debris. The supernatant was then collected and assayed for protein concentration using the Bradford assay (Bio-Rad, cat #500-0002)) with bovine serum albumin (BSA) as a standard. Total protein (30-45 µg) was heated at 95°C for ten minutes in a loading buffer containing a final concentration of 2% SDS and 5% fresh ß-mercaptoethanol, separated on a 6 or 8% Tris-glycine SDS polyacrylamide denaturing gel, and then transferred to an Immobilon-FL polyvinyl difluoride (PDVF) membrane (Merck, Kilsyth, Australia). Membranes were blocked for one hour at room temperature with shaking in blocking buffer. The blocking buffer was 10% non-fat milk in Tris-buffered saline (TBS)/ 0.1% Tween-20 when enhanced chemiluminescence (ECL) was to be used for detection, and Odyssey blocking buffer (LI-COR, Lincoln, NE, cat #927-4000) when the Odyssey Imager (LI-COR) was to be used. Membranes were then incubated overnight at 4°C with shaking in fresh blocking buffer containing 0.1% Tween-20 and the relevant primary antibody [TF (sheep anti-human TF, 1:1000, Silenus Laboratories, Hawthorne, Australia); ACTB (mouse anti-β-actin, 1:1500, Sigma-Aldrich, Castle Hill, NSW, Australia); FTN (rabbit anti-human FTN, 1:5000, cat #650771, ICN Biomedicals, Seven Hills, Australia); HP (rabbit anti-HP C-terminus, 1:1000, cat #HEPH11-A, Alpha Diagnostics, Owings Mills, MD); HP (rabbit anti-HP D4 center, 1:1000, produced in-house (Chen, Attieh et al. 2009))]. The membranes were then washed three times (each for five minutes) with TBS/ 0.1% Tween-20. The blots were incubated for one hour at room temperature with secondary antibody (anti-sheep horseradish peroxidase (HRP) conjugated, 1:5000, Silenus Laboratories; or anti-rabbit HRP, 1:1000, Merck). Blots incubated with infrared (IR) dye-conjugated secondary antibodies for use with the Odyssey

imager (anti-mouse IRdye 680 and anti-rabbit IRdye 800CW, both at 1:10,000, LI-COR) were protected from light starting at this step in order to prevent bleaching. The blots were washed three times (five minutes per wash) with TBS/ 0.1% Tween-20, once for five minutes in TBS, and once for five minutes in water. Blots were imaged using the Odyssey system or on film after incubation with the Western Lightning Plus-ECL Kit (Perkin-Elmer, Glen Waverley, VIC, Australia).

6. Ferroxidase assays

Ferroxidase activity was assayed using both an in-gel and an in-cuvette method. For the in-gel assays, freshly isolated enterocytes were resuspended in 1.5% ice-cold Triton X-100 with protease inhibitors without EDTA (Roche, cat #04693132001) at a final total volume 2-3 times the pellet volume. Cells were lysed by passage through a 27-gauge needle approximately 20 times, and then the lysates were left on ice for 30 minutes. The lysates were then centrifuged at 10,000 x *g* for 30 minutes at 4°C. The supernatant was transferred to a new tube and an aliquot assayed for protein concentration using the Bradford assay as described above. Next, 300 µg of total protein was suspended in native (no SDS or ß-mercaptoethanol) loading dye, loaded onto native 4-12% Tris-glycine gels (Invitrogen, Carlsbad, CA), and separated overnight at 4°C. The gels were then equilibrated in 0.1 M sodium acetate buffer, pH 5.0, for 15 minutes at room temperature with gentle shaking. This solution was then poured off and the gels were incubated in a fresh solution of 0.00784% ferrous ammonium sulfate hexahydrate dissolved in 0.1 M sodium acetate buffer, pH 5.0, for two hours at 37°C with very gentle shaking in the dark. The iron solution was then poured off and 15 mM ferrozine (a ferrous but not ferric iron chelator, Sigma, cat #160601) prepared fresh in water was added. After vigorous shaking by hand, the gel turned a uniform dark purple color as the ferrozine chelated the ferrous iron and changed from a faint yellow to dark purple color. White bands appeared where ferric iron was present due to ferroxidase activity. The gel was placed in a plastic sleeve and scanned immediately.

For the in-cuvette ferroxidase assays, performed by Yan Lu, cytosolic and membrane fractions were prepared as described previously, and all steps were performed at 4°C or on ice (Ranganathan, Lu et al. 2012). In brief, freshly isolated enterocytes were resuspended in ice-cold lysis buffer (0.025 M Tris-HCl (pH 7.4), 0.025 M NaCl, plus protease inhibitors: 1 µg/mL pepstatin A, 100 µM leupeptin, and 1 mM phenylmethylsulfonyl fluoride) and immediately lysed by grinding with a tissue homogenizer (Polytron PT 1200 CL) at setting 4 for two minutes in an ice-water bath. The lysates were then centrifuged at 16,000 x *g* for 15 minutes, and the supernatants were removed and centrifuged at 110,000 x *g* for one hour. The resulting supernatants, or cytosolic fractions, were transferred to new tubes on ice. The pellets were resuspended in lysis buffer with 0.25% (v/v) Tween-20, sonicated twice for five seconds at 5 W in an ice-water slurry with 15 seconds of chilling between sonications, and centrifuged again at 16,000

× *g* for 30 minutes to pellet insoluble material. The supernatants, or membrane fractions, were transferred to new tubes on ice. The concentration of protein in each sample was determined by the 660 Protein Assay Reagent (Thermo-Fisher Scientific Australia, Scoresby, VIC, Australia, cat #PIE22660). The in-cuvette assay is a TF iron loading ferroxidase assay, where ferrous iron is oxidized by ferroxidases in the cytosolic and membrane fractions and can then bind to apo-TF, which has an extremely high affinity for ferric iron. The resulting iron-TF complex has an absorbance maximum at 460 nm that can be monitored spectroscopically. Cytosolic or membrane fractions (100 µg total protein in equal volumes of lysis buffer, 90 µL maximum) were brought up to 120 µL with ice cold deionized water, mixed by pipet, and kept on ice. A blank was also made with just lysis buffer completed to 120 µL with water. To the blank, 40 µL of ice cold 0.125 M sodium acetate buffer, pH 5.0, was added, followed immediately by 20 µL of an ice cold solution containing 40 mg/mL bovine apo-TF (Sigma, cat #T1428), and the blank was mixed by pipet. Then 20 µL of a 1.96 mg/mL solution of ferrous ammonium sulfate dissolved in deionized water was added. The blank was then mixed twice by pipet and transferred in full to a cuvette already placed in a Thermo Biomate 3 spectrometer. The absorbance (A) at 460 nm was recorded by the spectrophotometer and the initial velocities from 15 seconds to two minutes were obtained by calculating the $\Delta A_{460}/\Delta$time. This procedure was then repeated for each sample using a clean cuvette.

7. Tissue iron staining and quantitative tissue iron measurements

Tissue was paraffin processed, cut, and stained for ferric iron using Perls' Prussian blue stain by the Histotechnology Facility at QIMR (Perls 1867). In brief, tissues were submitted to the facility in 70% ethanol after an overnight incubation at room temperature in 10% PBS-buffered formalin. Tissues were dehydrated in ethanol, cleared with xylene, and then embedded in paraffin. Sections 4 µm in thickness were cut, mounted on slides, and then deparaffinized. After rehydration in deionized water, the sections were incubated for 15-30 minutes in an equal volume mixture of 4% hydrochloric acid (HCl) and freshly prepared 4% aqueous potassium ferrocyanide. Sections were washed in distilled water and then counterstained with Nuclear Fast Red for 10 minutes. The slides were then washed, dehydrated, and mounted.

For colorimetric non-heme iron quantification, a modification of the Torrance and Bothwell method was used (Torrance and Bothwell 1968). Tissues were wrapped in aluminum foil and dried in an oven 110°C. A small piece of the dried tissue (15-20 mg) was weighed in a 1.5 mL acid-resistant tube and 1 mL of an acid solution (3 M HCl, 0.6 M trichloroacetic acid) was added. A series of 100 µL final volume standards were also made up containing 0-50 µg iron/mL acid solution. The samples and standards were then incubated for 20 hours in a 65°C water bath. Solutions were then vortexed, centrifuged briefly at maximum speed in a microcentrifuge, and allowed to cool. Freshly prepared chromagen reagent (one

volume 0.1% bathophenanthroline disulfonic acid with 1% w/v thioglycollic acid, five volumes saturated sodium acetate and five volumes iron-free water) was added to wells in a clear plastic 96-well plate (200 µL/well). Sample or standard (4 µL per well) was added and mixed by pipet. The plate was incubated at room temperature for 30 minutes and the absorbance at 535 nm was measured in a plate reader. The concentration of iron in the samples was then calculated based on the constructed standard curve. Each acid-digested tissue sample was analyzed in duplicate by the colorimetric assay.

8. Blood analyses

Blood collected at UCB was analyzed at the University of California, San Francisco (UCSF) Mouse Pathology Core using a HemaVet 850 or 950 blood analyzer (Drew Scientific). Blood samples at QIMR were analyzed on a Coulter® Ac•T diff™ Analyzer using the Veterinary Application Software (Beckman-Coulter, Fullerton, California) or, in some experiments, at the Pathology Department of the Royal Brisbane and Women's Hospital (Brisbane, Australia) using a Sysmex XE-5000 automated hematology analyzer (Roche Diagnostics, Castle Hill, NSW, Australia). Serum iron and total iron binding capacity (TIBC) were measured using the Iron/TIBC Reagent Set (Pointe Scientific, Inc., Canton, MI, cat # 17504). The assays were performed as per the manufacturer's instructions, but were scaled down linearly by a factor of 20 and performed in a 96-well plate, as previously validated in our laboratory. The ratios of apo-, mono ferric-, and diferric-TF were visualized by urea-polyacrylamide gel electrophoresis (urea-PAGE) followed by immunoblot (Appendix 1.3).

9. Iron absorption assays

Whole animal absorption measurements were carried out by giving mice an oral dose of ^{59}Fe followed by whole body counting. Mice were either kept on a chow diet or changed (as indicated) from a chow to an iron-deficient diet and subsequently housed in cages with wire grid bottoms. After a specified period of time on the diet, mice were dosed by gavage with 100 µL of a freshly prepared solution containing 200 µM ferrous sulfate in 10 mM HCl, spiked with ~3 µCi ^{59}Fe radiolabeled iron (Perkin-Elmer, Waltham, MA, cat #NEZ037001MC) per dose. The radiation in each mouse was measured using a RAM DA gamma counter with a PM-11 tube (Rotem Industries, Arava, Israel) at a fixed distance just after dosing and then again five days later. After subtraction of the background counts, the % of the initial dose remaining in the mouse was calculated. Mice were euthanized at the end of the experiment by ketamine/xylazine IP injection as described under "Tissue collection", followed by cervical dislocation once unresponsive to paw pinch. In some experiments, mice were injected IP with the hemolytic agent phenylhydrazine hydrochloride (PHZ) at a dose of 100 mg/kg to stimulate iron absorption.

For experiments where iron distribution was determined, the mice were anesthetized as described above with an IP injection of ketamine/xylazine and, once unresponsive to paw pinch, the body cavity of the mouse was opened. The gastrointestinal tract (GI tract) was first excised and placed in a 10 mL tube. The removed GI tract comprised the lower esophagus just proximal to the stomach down to the anus, and included connective tissue, pancreas and any contents inside the GI tract. Next, the spleen and then liver were excised, connective tissue was removed, and the tissues were wrapped separately in foil. The remainder of the carcass (referred to as "carcass") was wrapped in the small piece of benchcoat it was dissected on and placed in a 50 mL tube. Radiation in the carcass, GI tract, spleen, and liver was then measured at an equal distance from a gamma counter. After background subtraction, the percentage of radiation in each tissue relative to the whole animal was calculated by dividing the counts in each tissue by the sum of counts for all the tissues for that mouse, then multiplying by 100.

10. Statistics

All values are expressed as mean ± standard error of the mean (SEM). Tests for significance were performed in GraphPad Prism version 5a for Mac OS X. For comparisons between two groups, Student's t-test and the F test for equal sample variance were performed. For comparisons among multiple groups, one-way analysis of variance (ANOVA) with Tukey's post test and Bartlett's test for equal sample variance were performed. When the sample variances were determined to be unequal, Welch's correction was applied to t-tests and the Kruskal-Wallis test followed by the Dunn Multiple Comparison post test was performed on data analyzed by one-way ANOVA. Pearson's chi-squared test was used to compare actual versus expected genotype ratios obtained in our breedings. A P value of ≤ 0.05 was considered significant.

III. Results

1. Generation of $Hp^{-/-}$ and $Hp^{int/int}$ mice, and assessment of viability

$Hp^{-/-}$ and $Hp^{int/int}$ mice were successfully generated using the cre-lox system (Methods). Both $Hp^{-/-}$ and $Hp^{int/int}$ mice were viable and the pups appeared grossly normal at birth. Pups born to $Hp^{-/-}$ and $Hp^{int/int}$ mothers were paler in the first week after birth than pups born to $Hp^{+/-}$, WT, or $Hp^{fl/fl}$ mothers.

In a cross between an $Hp^{+/-}$ female and an $Hp^{-/-}$ male, we would expect litters that are 50% $Hp^{-/-}$, 25% WT, and 25% $Hp^{+/-}$. To determine if HP knockout in mice affects viability, 195 weaned pups (95 males, 100 females) from 34 litters born to 8 females bred in such crosses were analyzed (Table 2.1). The genotypes of the weaned mice were 48% $Hp^{-/-}$, 28% WT, and 24% $Hp^{+/-}$. When considering the males and females separately, males were 58% WT and 42% $Hp^{-/-}$, and females were 47% $Hp^{+/-}$ and 53% $Hp^{-/-}$. These values are not significantly different (P =

0.1238 and P = 0.5485, respectively) from the expected percentages. Estimation of average litter size for these breeders is confounded by the fact that five of the 8 females were bred with another female in the cage, so that sometimes litters born to each female could not be distinguished (i.e. large litters could be due to the litter of a single female or that of two females that gave birth near the same time). For the three females that were singly caged with a male, the average litter size was 4.9 ± 2 pups, while for all 8 females in total the average litter size was 5.7 ± 3 pups. Normal litter sizes for wild-type mice on the C57BL/6 background strain are 5.6 on average at The Jackson Laboratory and reported elsewhere to range from 6-10 pups (Verley, Grahn et al. 1967; Casellas and Medrano 2008; The Jackson Laboratory 2009; ARC Australia 2012).

Comparison of expected to observed genotype ratios of pups born to $Hp^{fl/fl}$ females bred with $Hp^{int/int}$ males suggests partial early lethality of $Hp^{int/int}$ mice of both sexes (Table 2.2). From this cross, a total of 309 weaned pups (159 males, 150 females) from 47 litters born to 17 females were examined. The genotypes of the weaned mice were 58% $Hp^{fl/fl}$ and 42% $Hp^{int/int}$, which is significantly different by chi-squared test (P = 0.005) from the expected 50/50 ratio. The genotype ratios determined separately for males and females were the same (58% $Hp^{fl/fl}$ and 42% $Hp^{int/int}$), and still significant different (P values of 0.047 and 0.05, respectively). The average litter size for all litters was 6.5 ± 3.3. Estimation of average litter size over all litters is potentially overestimated due to 14 of the 17 females being bred with another female present. For the three females bred alone, the average litter size was 5.7 ± 2.6.

2. Confirmation of knockout

Knockout at the genomic level was verified by PCR genotyping (37 cycles) in DNA from the liver, kidney, spleen, heart, pancreas, tail tip, and isolated duodenal enterocytes of $Hp^{-/-}$, $Hp^{int/int}$, and $Hp^{fl/fl}$ and WT control littermates (Figure 2.1). As expected, complete knockout of *Heph* was observed in all $Hp^{-/-}$ tissues examined, and only floxed and WT alleles were present in the $Hp^{fl/fl}$ and WT tissues, respectively. In the $Hp^{int/int}$ tissues, knockout of *Heph* was only detected in the enterocytes, and only floxed alleles were present in the other tissues. However, floxed DNA was also detected in the $Hp^{int/int}$ enterocytes. This may be explained by either contamination from other intestinal cell types or by incomplete recombination, as has been reported previously in other intestinal knockout mice generated with this particular Cre transgene (Vujic Spasic, Kiss et al. 2007). Some faint non-specific background bands were present in the $Hp^{-/-}$ tissues in the PCR reactions when tested for WT and/or floxed *Heph* alleles, but these background bands ran at slightly different molecular weights than WT or floxed PCR products.

Table 2.1. Genotypes of weaned pups from $Hp^{+/-}$ female x $Hp^{-/-}$ male matings

	WT males	$Hp^{-/-}$ males	$Hp^{+/-}$ females	$Hp^{-/-}$ females	Total WT	Total $Hp^{+/-}$	Total $Hp^{-/-}$
Actual % (N)	58% (55)	42% (40)	47% (47)	53% (53)	28% (55)	24% (47)	48% (93)
Expected % (N)	50% (47.5)	50% (47.5)	50% (50)	50% (50)	25% (48.75)	25% (48.75)	50% (97.5)

Table 2.2. Genotypes of weaned pups from $Hp^{fl/fl}$ female x $Hp^{int/int}$ male matings

	$Hp^{fl/fl}$ males	$Hp^{int/int}$ males	$Hp^{fl/fl}$ females	$Hp^{int/int}$ females	Total $Hp^{fl/fl}$	Total $Hp^{int/int}$
Actual % (N)	58% (92)	42% (67)	58% (87)	42% (63)	58% (179)	42% (130)
Expected % (N)	50% (79.5)	50% (79.5)	50% (75)	50% (75)	50% (154.5)	50% (154.5)

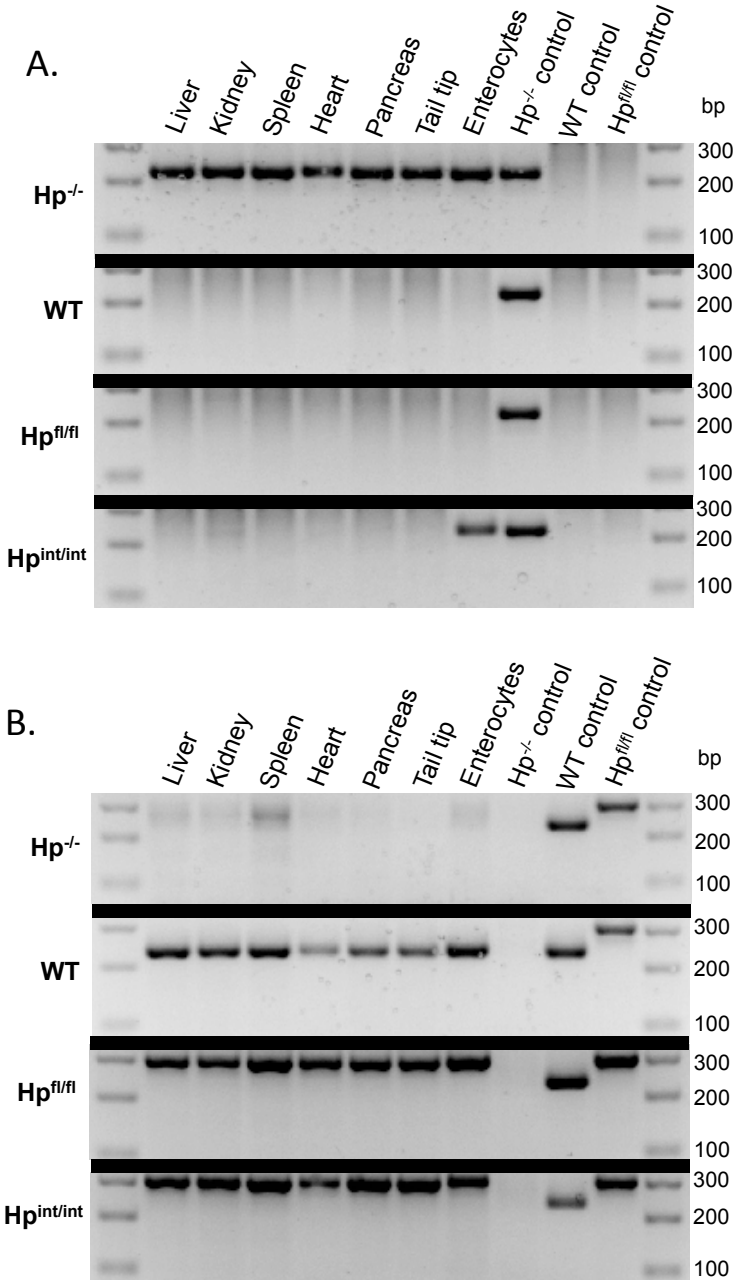

Figure 2.1. Verification of *Heph* knockout at the DNA level. DNA extracted from a panel of homogenized tissues from an $Hp^{-/-}$ mouse and a WT littermate and an $Hp^{int/int}$ mouse and an $Hp^{fl/fl}$ littermate was amplified by PCR. **A.** Results for the "Hp ko" reaction, which yields a strong band at 230 bp if a *Heph* knockout allele is present. **B.** Results for the "Hp wt" reaction, which yields a strong band at 240 bp if wild-type *Heph* DNA is present and a strong band at 300 bp if floxed *Heph* DNA is present.

Messenger RNA (mRNA) levels were examined in duodenal enterocytes from 9-10 week old adult male $Hp^{-/-}$ and WT littermates by RT-qPCR using primers targeting regions proximal, within, and distal to the *Heph* knockout region (Figure 2.2). Equal quantities of cDNA from three mice of each genotype were pooled to make an $Hp^{-/-}$ sample and a WT control sample. Results from five sets of primers targeting different exon-exon junctions both proximal and distal to the knockout region were similar and revealed that *Heph* mRNA was still present in $Hp^{-/-}$ enterocytes at levels approximately half that of WT controls. Two sets of primers were also designed to target the region deleted in $Hp^{-/-}$ mice, spanning the 3-4

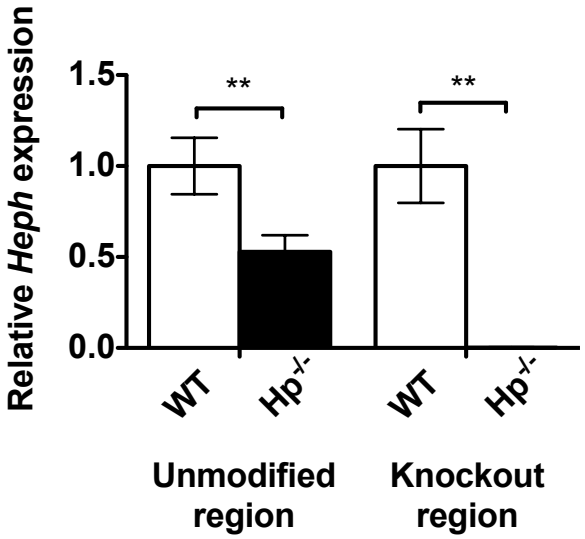

Figure 2.2. Verification of *Heph* knockout at the mRNA level in isolated duodenal enterocytes. *Heph* mRNA expression in enterocytes was analyzed by RT-qPCR in an $Hp^{-/-}$ sample containing an equal pool of cDNA from three $Hp^{-/-}$ mice and a WT sample containing an equal pool of cDNA from three WT littermates. The mean and SEM for results from five sets of primers targeting unmodified regions on either side of the knockout site are shown at the left, and the mean ± SEM for two sets of primers targeting the exon-exon junction regions on either side of the knockout exon target are shown at right. *Heph* mRNA expression results were normalized to expression of the *Hprt* housekeeping gene, and then normalized to *Heph* expression in the WT controls. Significance was determined by t-test using GraphPad Prism. ** $P \leq 0.01$.

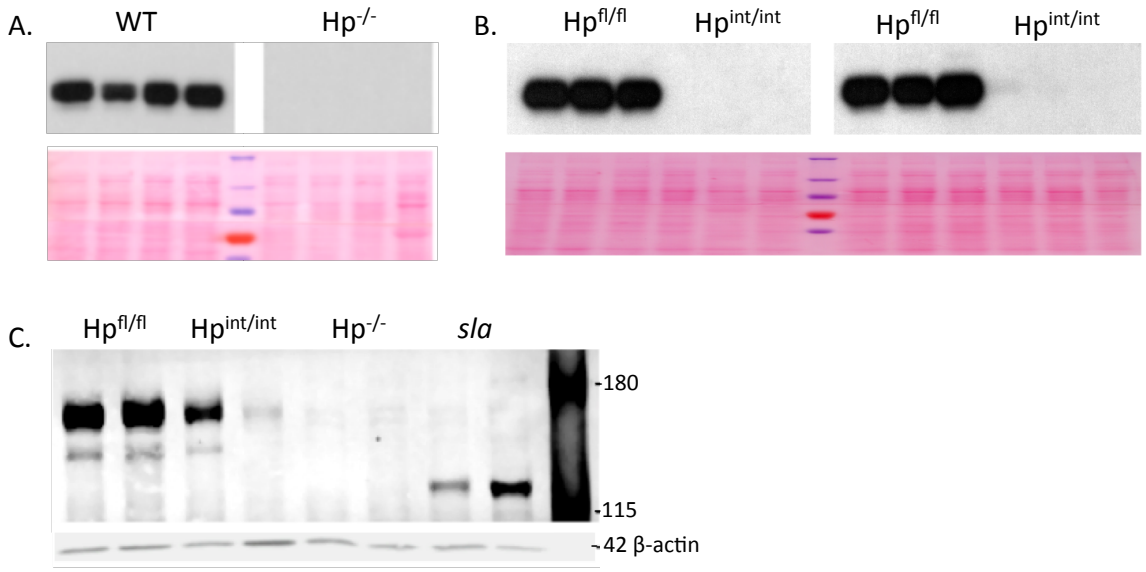

Figure 2.3. Verification of HP knockout at the protein level in isolated duodenal enterocytes. HP protein expression in enterocytes was analyzed by SDS PAGE followed by immunoblotting. The HP protein is ~155 kD and the mutated *SLA* protein is ~130 kD. **A.** Immunoblot of the membrane fraction of enterocyte lysates from male WT and $Hp^{-/-}$ littermates (four per genotype) using an antibody that targets the central region of the protein, with the Ponceau S stained membrane below. **B.** Immunoblot of the membrane fraction of enterocyte lysates from male $Hp^{fl/fl}$ and $Hp^{int/int}$ littermates (six per genotype) using an antibody that targets the central region of the protein, with the Ponceau S stained membrane below. The data in A and B were obtained by visiting collaborator Yan Lu. **C.** Immunoblot of enterocyte lysates from age-matched male mice (two per genotype) showing the expression of HP and the β-actin loading control. This HP antibody targets the C' terminus of the protein and typically detects a smaller unidentified band at ~140 kD in WT mice as is seen here. Of note, HP expression was observed in some $Hp^{int/int}$ enterocyte samples, with the first $Hp^{int/int}$ mouse in immunoblot C representing an extreme.

and 4-5 exon-exon junctions around the deleted exon 4. By regular PCR and analysis by gel electrophoresis, these primers gave the expected size products in cDNA from WT mice, but only non-specific background products in the $Hp^{-/-}$ mice. *Heph* was virtually undetectable (no result or crossing point values above 37 in technical replicates) in the $Hp^{-/-}$ enterocytes by RT-qPCR using these primers, whereas levels in the WT control were similar to those observed for the other primer sets targeting the non-deleted regions.

Knockout of HP was confirmed at the protein level by immunoblotting using two different antibodies that target different regions of the protein (Figure 2.3). No protein was detected in enterocytes from $Hp^{-/-}$ mice even when immunoblots were highly overexposed. Most $Hp^{int/int}$ mice had little to no HP expression in isolated enterocytes, but in some mice there was some expression, reflecting

either lack of complete recombination or contamination from some non-enterocyte cells.

3. General phenotype

All pups born to $Hp^{-/-}$ and $Hp^{int/int}$ mothers on the chow diet or AIN-93G diet at UCB exhibited a striking truncal hair loss beginning at about two weeks of age that generally resolved by the time the mice were six weeks old, but in some animals persisted for months (Figures 2.4 and 2.5). This phenotype was seen in all $Hp^{fl/fl}$ and $Hp^{int/int}$ pups born to $Hp^{int/int}$ mothers, and all $Hp^{-/-}$ and $Hp^{+/-}$ pups born to $Hp^{-/-}$ mothers (because the gene encoding HP is on the X chromosome, it is not possible for an $Hp^{-/-}$ mother to have WT pups). The severity of the phenotype was sometimes variable in a litter but had no clear correlation with pup genotype. The phenotype was not seen in $Hp^{+/-}$ or WT pups born to WT mothers, or in $Hp^{fl/fl}$ or $Hp^{int/int}$ pups born to $Hp^{fl/fl}$ mothers. *Sla* mice born to *sla* mothers sometimes developed truncal hair loss, but it was more variable and in some litters pups had normal hair. $Hp^{+/-}$ mothers sometimes had pups with thin hair, but generally the hair was normal. Surprisingly, the hair loss phenotype was not observed in mice fed the chow diet at QIMR, but in a small study, $Hp^{-/-}$ mothers fed a 30-40 ppm iron diet made in-house had pups with truncal hair loss, while pups born to $Hp^{+/-}$ and $Hp^{fl/fl}$ mothers did not (data not shown). This hair loss phenotype is similar to what has been reported previously in another model of genetic iron deficiency, the Mask or TMPRSS6 knockout mouse (Du, She et al. 2008; Folgueras, de Lara et al. 2008).

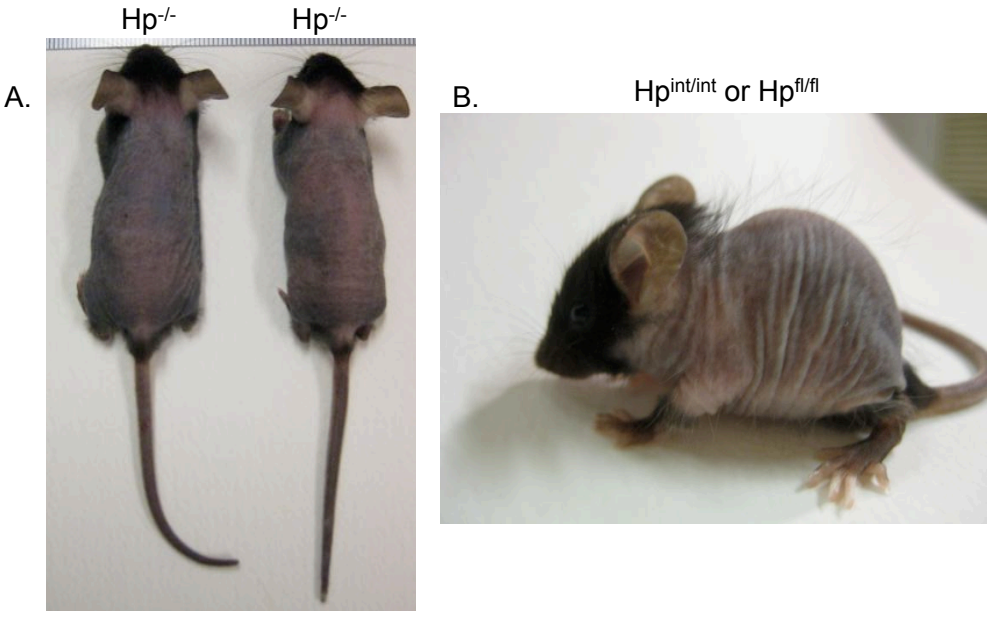

Figure 2.4. Truncal hair loss in weanling mice. Representative photographs of 3-4 week old mice born to **A**. $Hp^{-/-}$ and **B**. $Hp^{int/int}$ mothers at UCB.

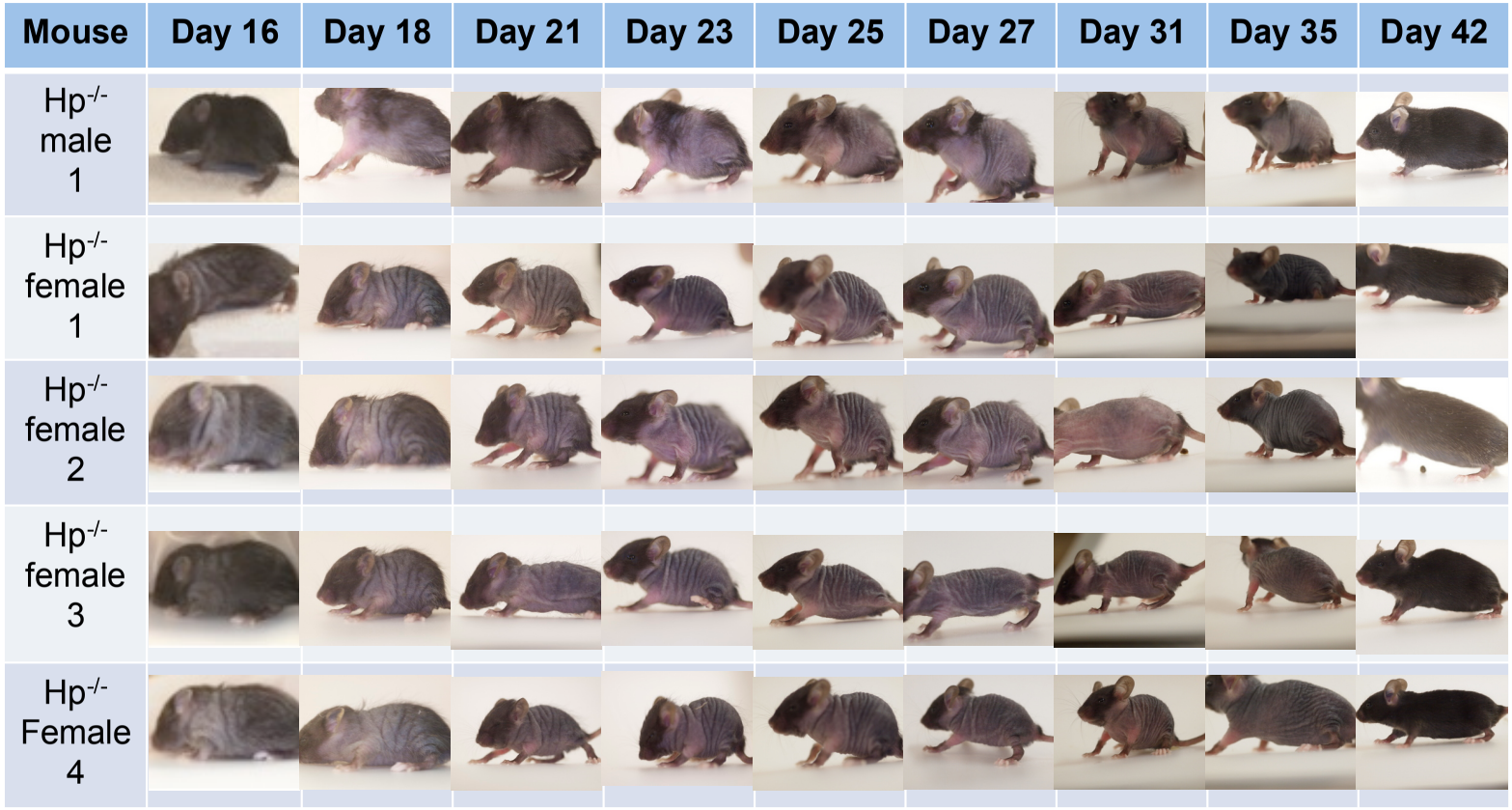

Figure 2.5. Timecourse for hair loss and recovery in $Hp^{-/-}$ littermates born to an $Hp^{-/-}$ mother. Littermates were earpunched for identification and photographed individually starting at an age of 16 days; hair loss began a few days before this time point. All mice were maintained on a chow diet. This data was collected by Erica Lachenauer and Julie Luong at UCB.

No significant weight differences between $Hp^{-/-}$ and WT littermates were detected at single time points (6-7 weeks, 10-12 weeks, 23 weeks, and 76-78 weeks of age) in adult male littermates (data for the first two age groups is shown in Figure 2.6). In addition, $Hp^{-/-}$ mice and WT littermates born to $Hp^{+/-}$ mothers and weighed weekly at both UCB (from 2-6 weeks of age) and QIMR (from 3-6 weeks of age) exhibited no significant differences in body weight (Figure 2.6). $Hp^{-/-}$ mice, however, born to $Hp^{-/-}$ mothers grew significantly less than pups born to $Hp^{+/-}$ or WT mothers when measured every week from 2-6 weeks of age at UCB, suggesting that maternal HP is important for supporting pup growth. At two weeks of age, $Hp^{-/-}$ males and females born to $Hp^{-/-}$ mothers had similar weights to pups born to $Hp^{+/-}$ and WT mothers. However, they failed to grow between 2-3 weeks of age (when pups are still nursing but also beginning to eat solid food) and showed a slower rate of growth from 3-4 weeks of age (weaning age) than the other groups. From 4-6 weeks of age the growth rate in $Hp^{-/-}$ females born to $Hp^{-/-}$ mothers increased and by six weeks of age these mice were not significantly different in weight than $Hp^{-/-}$ mice born to $Hp^{+/-}$ mothers. While growth in the $Hp^{-/-}$ males born to the $Hp^{-/-}$ mothers also increased in this time frame, they still weighed less than the other groups at six weeks of age. The sex differences may be due to males having to support greater growth during this period than females.

Male, but not female, $Hp^{int/int}$ mice born to $Hp^{fl/fl}$ mothers were found to weigh significantly less than $Hp^{fl/fl}$ littermates when examined at ages 4-8 weeks at UCB (Figure 2.7). However, these results may have been confounded by a recently recognized but unidentified mutation in some animals in this strain that leads to a smaller size, shorter tail, and hip dysplasia in both $Hp^{int/int}$ and $Hp^{fl/fl}$ mice. This phenotype has not been observed in $Hp^{-/-}$ mice or any other mice maintained in our colony and is currently being bred out of this strain.

Tissue weights were measured in 6-7 week old $Hp^{-/-}$ and WT male littermates at QIMR. No significant differences were noted between the two groups in total body weight nor the percentage of total body weight in the liver, kidneys or spleen (Figure 2.8). However, the heart was slightly but significantly enlarged in the $Hp^{-/-}$ mice when expressed as a percentage of total body weight. This finding is supported by results from a small concurrent study with $Hp^{-/-}$ and *sla* male littermates, where the heart made up a percentage of total body weight similar to that seen in the $Hp^{-/-}$ mice in the above study. It was also noted in the $Hp^{-/-}$ and *sla* littermate study that the liver was significantly smaller in the *sla* littermates versus the $Hp^{-/-}$ mice, but more animals will need to be examined. No weight differences were observed at 6-7 or 10 weeks of age (data not shown) between $Hp^{-/-}$ and *sla* littermates born to $Hp^{sla/-}$ mothers at QIMR.

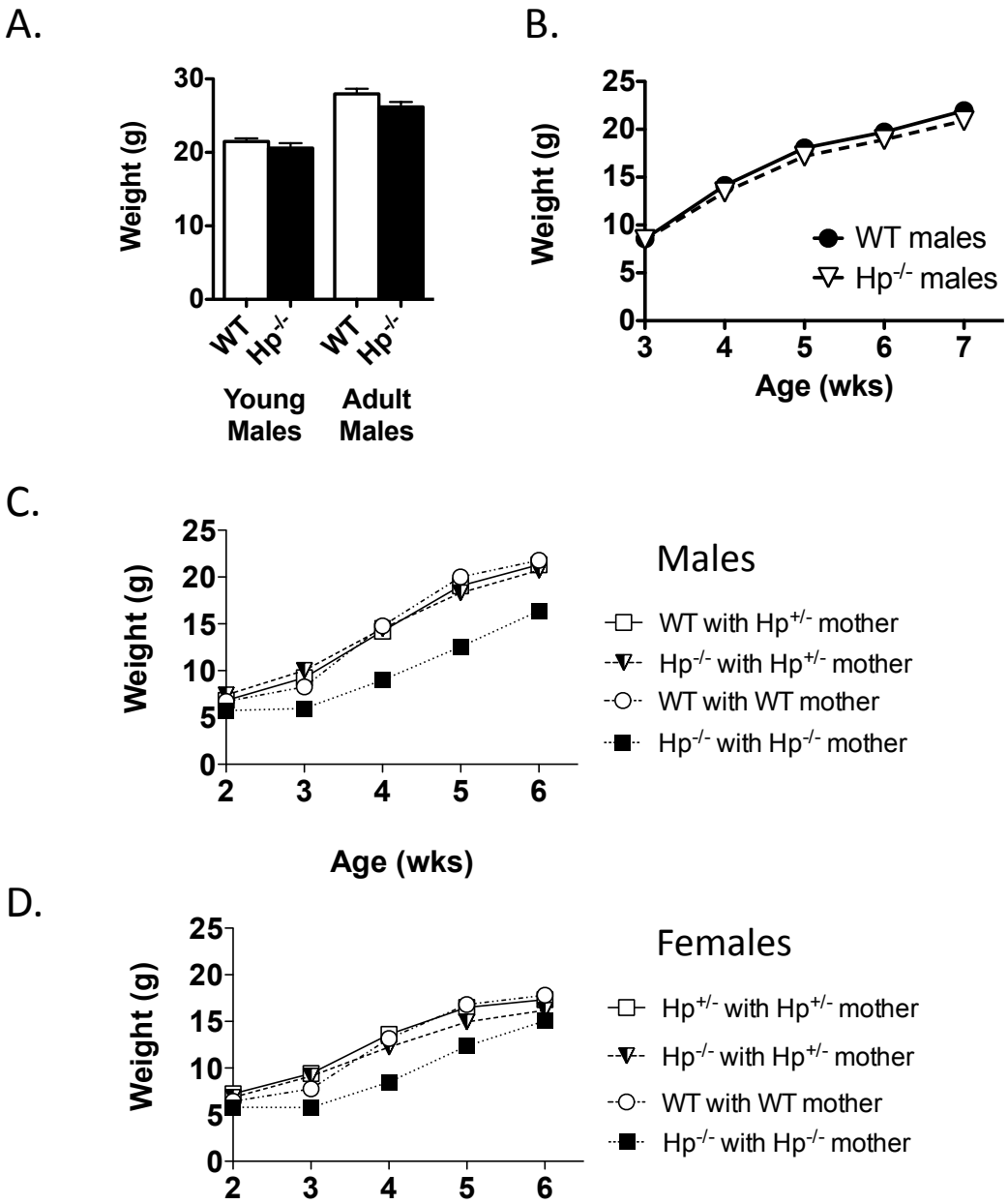

Figure 2.6. Weights of $Hp^{-/-}$ mice and WT littermates. A. Young (6-7 week old) and adult (10-15 week old) male $Hp^{-/-}$ and WT littermates at QIMR, N = 9-14 mice per genotype, all born to $Hp^{+/-}$ mothers. **B**. Weight timecourse for male $Hp^{-/-}$ and WT littermates at QIMR, N = 6-12 mice per age per genotype, all born to $Hp^{+/-}$ mothers. **C.** Weight timecourse for male littermates at UCB, N = 3-10 mice per age per genotype, born to mothers of different genotypes as noted. **D.** Weight timecourse for female littermates at UCB, N = 5-17 per age per genotype, born to mothers of different genotypes as noted. Mice in all experiments were fed a chow diet, and the numbers of mice examined per genotype at each age were similar. Mean ± SEM. Data in C. and D. were collected by Erica Lachenauer and Julie Luong at UCB.

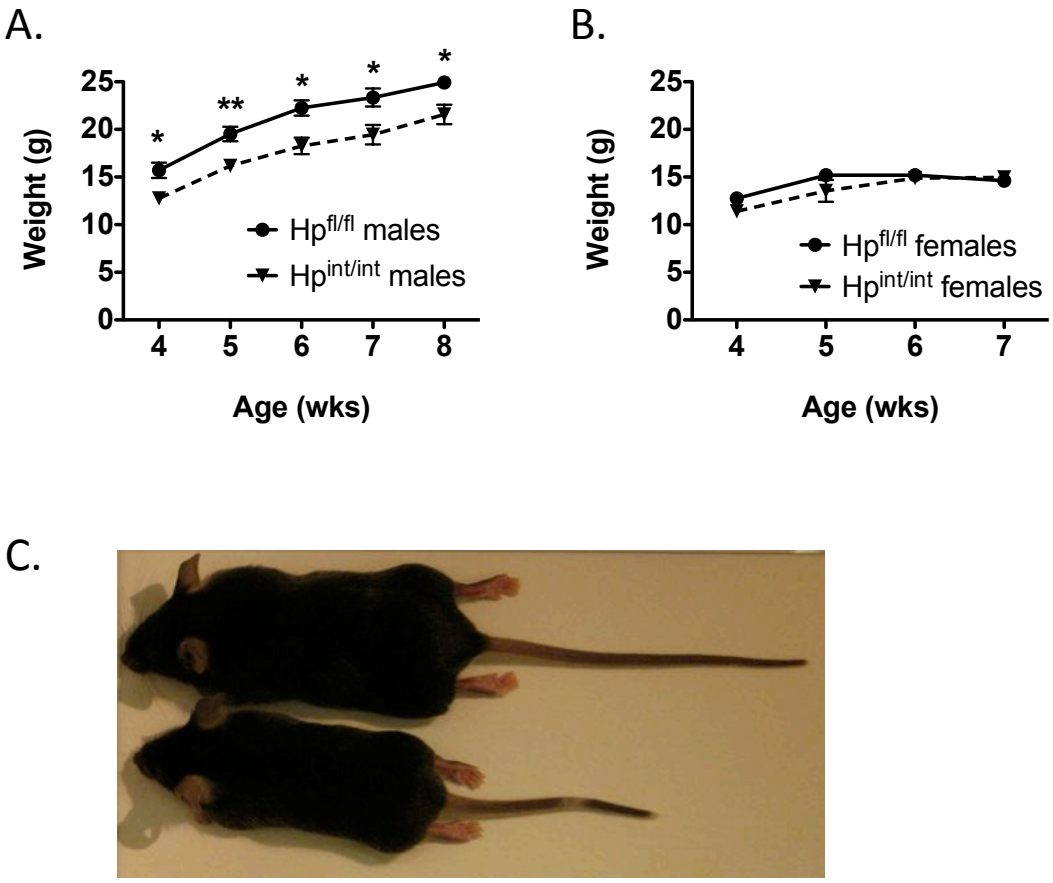

Figure 2.7. Weights of $Hp^{int/int}$ and $Hp^{fl/fl}$ littermates at UCB. A. Weight timecourse for male $Hp^{int/int}$ and $Hp^{fl/fl}$ littermates, N = 4-8 mice per age per genotype. **B.** Weight timecourse for female $Hp^{int/int}$ and $Hp^{fl/fl}$ littermates, N = 3-7 mice per age per genotype. Mice in A and B were on the AIN-93G diet. Mean ± SEM. Significance was determined by t-test using GraphPad Prism. * $P \leq 0.05$, ** $P \leq 0.01$. **C.** Photograph showing the small size, short tail, and hip dysplasia phenotype (mouse on bottom, littermate on top) found in some mice of this strain that appears to be independent of HP intestinal knockout status.

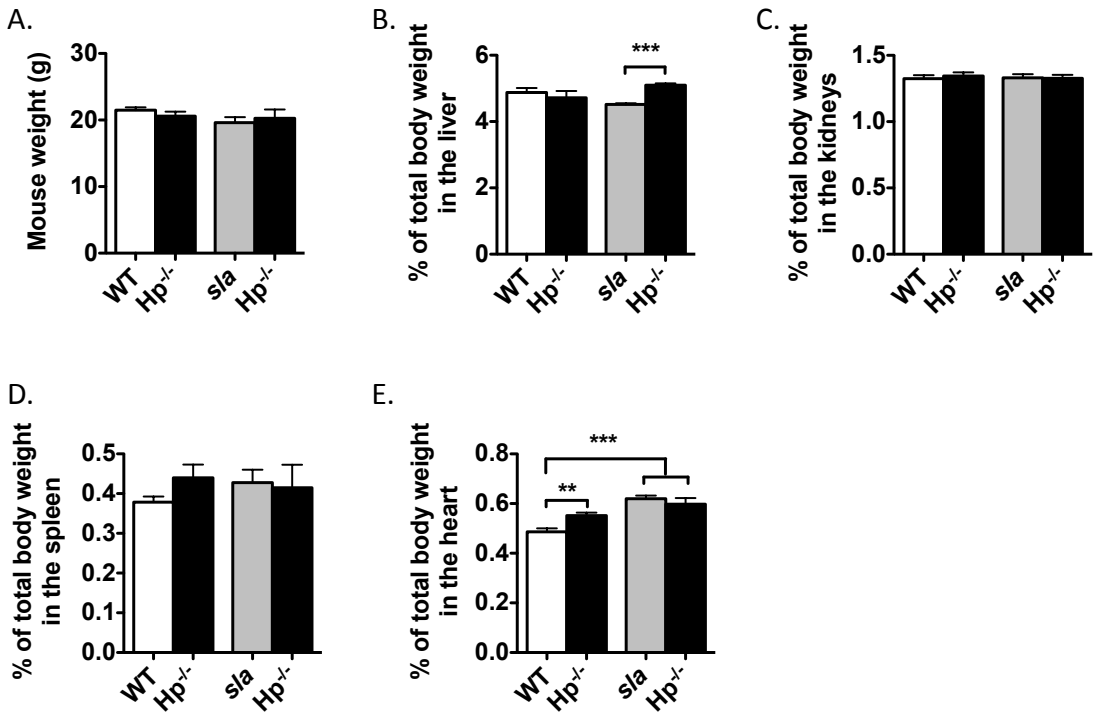

Figure 2.8. Weights and relative tissue weights of 6-7 week old male WT and Hp$^{-/-}$ littermates, and *sla* and Hp$^{-/-}$ littermates, at QIMR. A. The average mouse weight. **B-E.** The percent of total body weight in various tissues. Bars showing littermate data are paired. WT (N = 8) and Hp$^{-/-}$ (N = 10) littermates, and *sla* (N = 4) and Hp$^{-/-}$ (N = 4) littermates. Mean ± SEM. Significance was determined by t-test between littermate pairs as well as by one-way ANOVA across all groups using GraphPad Prism. ** P ≤ 0.01, *** P ≤ 0.001.

4. Hematology and serum iron

Young Hp$^{-/-}$ mice have a hypochromic, microcytic anemia, but the anemia resolves as the animals age (Figure 2.9). At 6-7 weeks of age, male Hp$^{-/-}$ mice maintained on a chow diet had approximately the same number of red cells as WT littermates, but they showed classic symptoms of iron-deficiency anemia: their cells were significantly smaller and made up a smaller fraction of the total blood volume (lower hematocrit). Hp$^{-/-}$ mouse blood contained significantly less hemoglobin overall, and less per red cell than WT mice. The average concentration of hemoglobin in the cells was also low. Hp$^{-/-}$ mice had nearly twice the number of reticulocytes as WT littermates, suggesting that these mice were able to produce new red cells and were beginning to recover from the anemia. No significant differences were seen in the number of platelets. By early adulthood (10-15 weeks of age), male Hp$^{-/-}$ mice were no longer anemic but still showed signs of recovery from iron deficiency. Hp$^{-/-}$ mice had significantly more red cells, but the red cells were just as small as at 6-7 weeks of age and they still

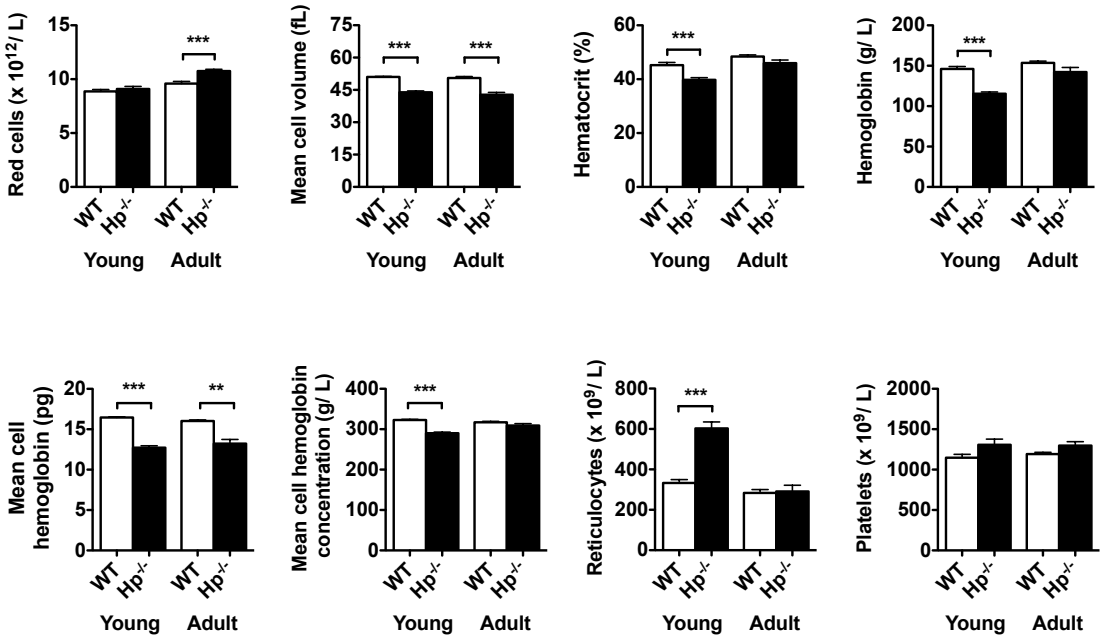

Figure 2.9. Hematology of young (6-7 week old) and adult (9-15 week old) WT and $Hp^{-/-}$ male littermates born to $Hp^{+/-}$ mothers at QIMR and maintained on a chow diet. N = 8 young WT, 10 young $Hp^{-/-}$, 7 adult WT, and 7 adult $Hp^{-/-}$ mice except for reticulocytes, which were counted in an independent experiment, where N = 7, 7, 8, and 6, respectively. Mean ± SEM. Littermate comparisons by t-test in GraphPad Prism. ** P ≤ 0.01, *** P ≤ 0.001.

contained less hemoglobin than the red cells of WT littermates. The average concentration of hemoglobin per red cell, however, no longer differed from that of WT mice and neither the hematocrit nor the total amount of hemoglobin in the blood were lower in adult $Hp^{-/-}$ mice than in WT littermates.

$Hp^{-/-}$ and *sla* littermates born to $Hp^{sla/-}$ mothers were indistinguishable hematologically at 6-7 weeks of age (Figure 2.10). Furthermore, when hematology data for $Hp^{-/-}$ and *sla* littermates born to $Hp^{sla/-}$ mothers were compared to $Hp^{-/-}$ mice born to $Hp^{+/-}$ mothers (see Figure 2.9 for reference), no parameters were significantly different except for mean cell volume, which was lower in pups born to the $Hp^{sla/-}$ mothers. This is presumed to be due to the likely lower iron status of $Hp^{sla/-}$ mothers than the $Hp^{+/-}$ mothers, resulting in pups born to the former beginning postnatal life with lower iron stores than pups born to the latter. At 10-11 weeks of age, $Hp^{-/-}$ and *sla* littermates still had signs of iron deficiency. *Sla* mice had slightly but significantly higher hematocrit and hemoglobin levels than their $Hp^{-/-}$ littermates, but were not different in any other hematological parameters.

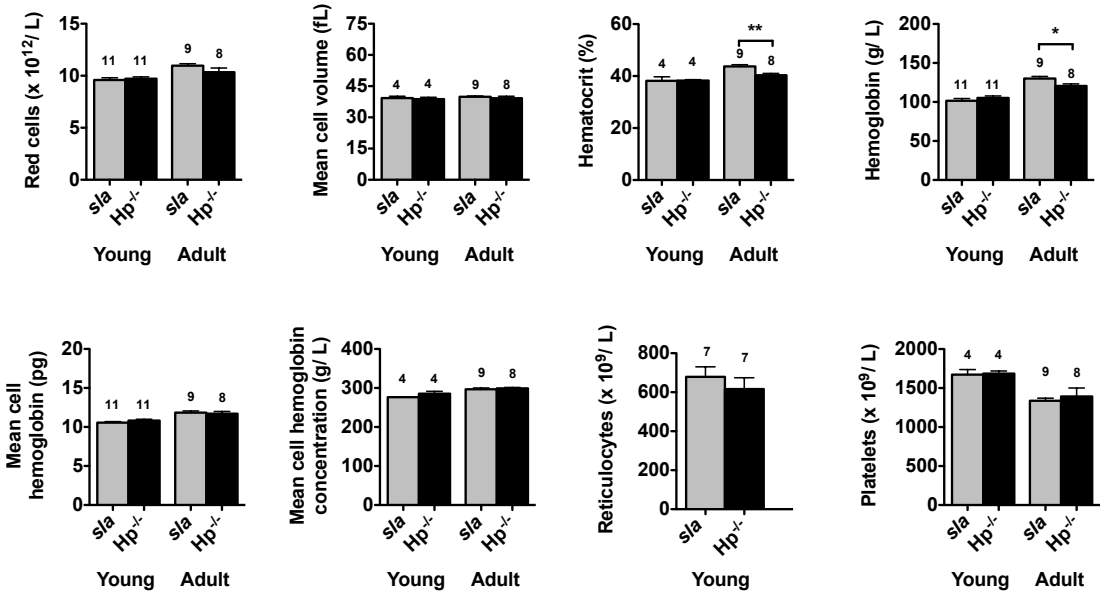

Figure 2.10. Hematology of young (6-7 week old) and adult (10-11 week old) *sla* and Hp$^{-/-}$ male littermates born to Hp$^{sla/-}$ mothers at QIMR and maintained on a chow diet. The number of mice per group is listed above each column. Data for young mice came from two independent experiments with equal numbers of each genotype per experiment. A different instrument was used to measure blood parameters in one of these experiments (N = 7 per group), which had non-veterinary calibrations for measuring cell size. Thus only values for red cells, hemoglobin, and mean cell hemoglobin could be reliably pooled. Bars showing littermate data are paired. Mean ± SEM. Littermate comparisons by t-test in GraphPad Prism. * P ≤ 0.05, ** P ≤ 0.01.

The hematology of young (6-7 week old) Hp$^{int/int}$ mice and Hp$^{fl/fl}$ littermates was only studied at UCB, so results from those animals cannot be directly compared with that of young Hp$^{-/-}$ mice at QIMR. However, the same general trends emerged. Hp$^{int/int}$ male mice 6-7 weeks old born to Hp$^{fl/fl}$ mothers and maintained on a chow diet exhibited a hypochromic, microcytic anemia with similar characteristics to those of Hp$^{-/-}$ mice at QIMR (Figure 2.11). Maintenance of mice from this same cross on a different diet, the AIN-93G purified diet, resulted in improved hematological parameters, although these mice still had smaller red cells containing less hemoglobin than Hp$^{fl/fl}$ littermates (Figure 2.12). No differences in hematological parameters were seen between Hp$^{fl/fl}$ control mice on either diet except in mean cell volume, which was lower in mice fed the chow diet. Interestingly, 6-7 week old Hp$^{int/int}$ mice born to Hp$^{int/int}$ mothers were clearly more anemic than Hp$^{int/int}$ mice born to Hp$^{fl/fl}$ mothers (Figure 2.13, as compared to Figure 2.12).

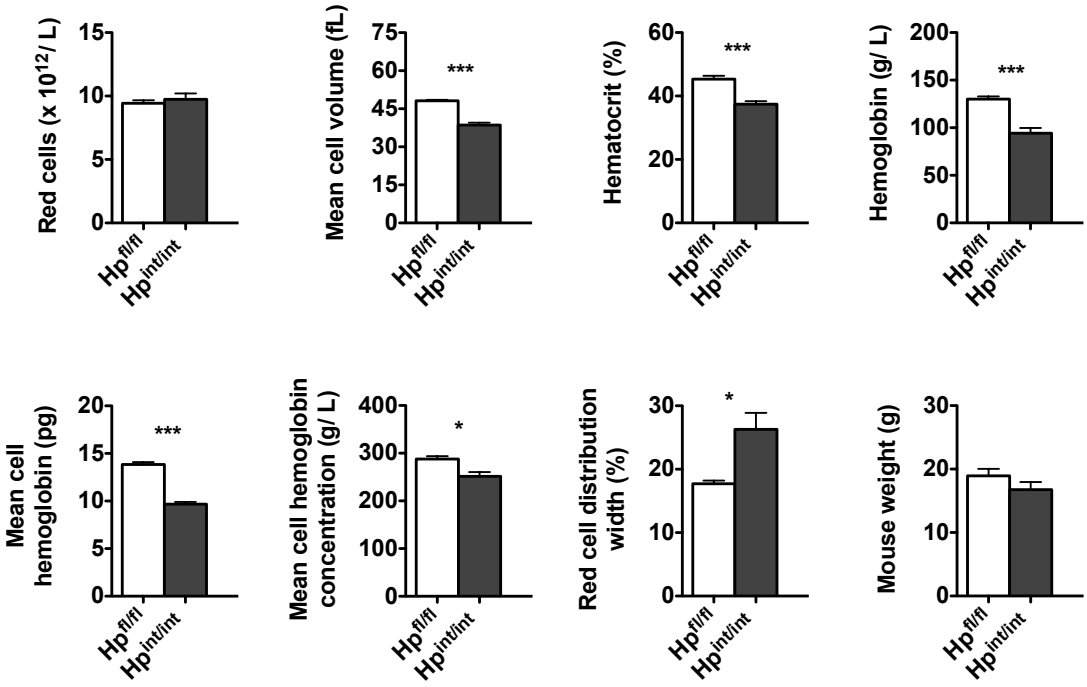

Figure 2.11. Hematology and weights of young (6-7 week old) male $Hp^{int/int}$ and $Hp^{fl/fl}$ littermates born to $Hp^{fl/fl}$ mothers at UCB and maintained on a chow diet. N = five per genotype. Mean ± SEM. Littermate comparisons by t-test in GraphPad Prism. * P ≤ 0.05, *** P ≤ 0.001.

By 13-14 weeks of age, all $Hp^{int/int}$ mice had recovered from their anemia and their blood parameters were generally not significantly different from $Hp^{fl/fl}$ littermates, although the $Hp^{int/int}$ mice born to $Hp^{int/int}$ mothers exhibited significantly less hemoglobin per cell and also an increased red cell distribution width than $Hp^{fl/fl}$ littermates. An increased red cell distribution width was also seen in adult $Hp^{int/int}$ mice born to $Hp^{fl/fl}$ mothers (Figure 2.12). $Hp^{int/int}$ male mice born to $Hp^{fl/fl}$ mothers at 10-12 weeks of age were also studied at QIMR and found to have similar parameters to $Hp^{fl/fl}$ littermates, with the exception of having smaller red cells with less hemoglobin per cell (Figure 2.14).

Serum iron and TIBC were examined in 6-7 week old $Hp^{int/int}$ and $Hp^{fl/fl}$ littermates born to $Hp^{fl/fl}$ mothers and $Hp^{-/-}$ and WT littermates at QIMR (Figure 2.15). Serum iron was significantly lower in the $Hp^{-/-}$ mice compared to littermate controls. Serum iron levels in $Hp^{int/int}$ mice and controls, however, were similar. TIBC is an indirect measurement of the amount of TF protein in the serum, and serum levels of TF typically increase in response to iron deficiency. TIBC was significantly greater in both $Hp^{int/int}$ and $Hp^{-/-}$ mice compared to controls. A pilot assay with Hp^{-}

$^{/-}$ and WT serum samples to separate and detect the different species of TF by urea-PAGE and immunoblotting confirmed the serum iron results, indicating that a larger proportion of TF is in the apo (iron-free) form in $Hp^{-/-}$ mice than in controls.

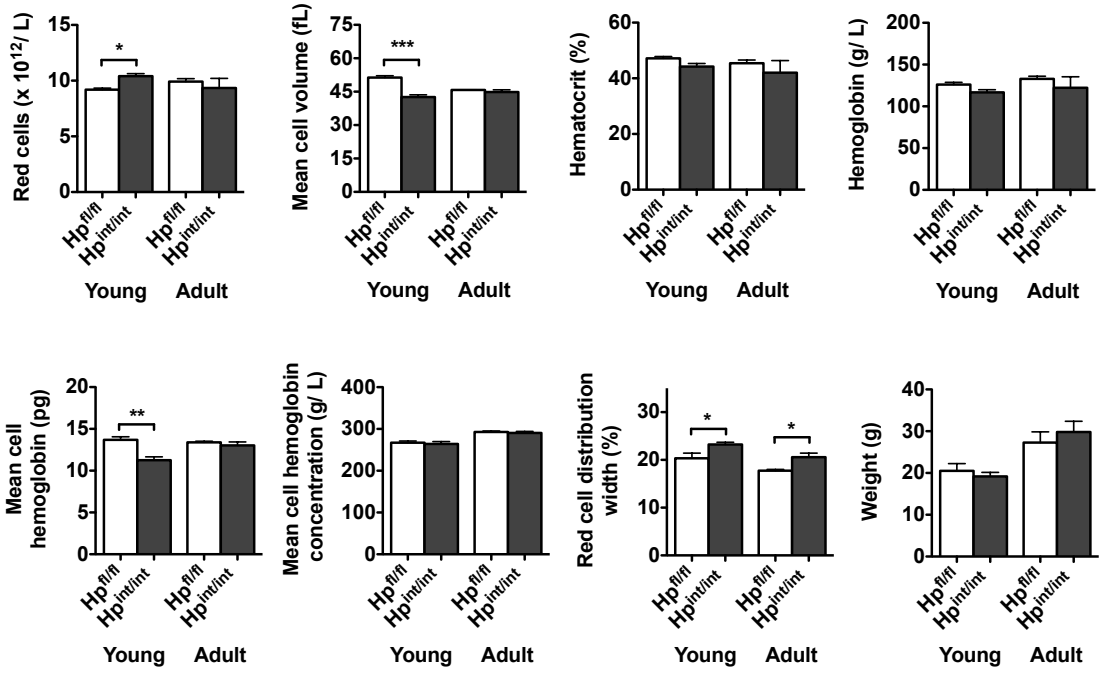

Figure 2.12. Hematology of young (6-7 week old) and adult (12-14 week old) male $Hp^{int/int}$ and $Hp^{fl/fl}$ littermates born to $Hp^{fl/fl}$ mothers at UCB and maintained on an AIN-93G diet. N = 7 $Hp^{int/int}$ and N = 4 $Hp^{fl/fl}$ young littermates, and N = 4 $Hp^{int/int}$ and N = 4 $Hp^{fl/fl}$ adult littermates. Mean ± SEM. Littermate comparisons by t-test in GraphPad Prism. * $P \leq 0.05$, ** $P \leq 0.01$, *** $P \leq 0.001$.

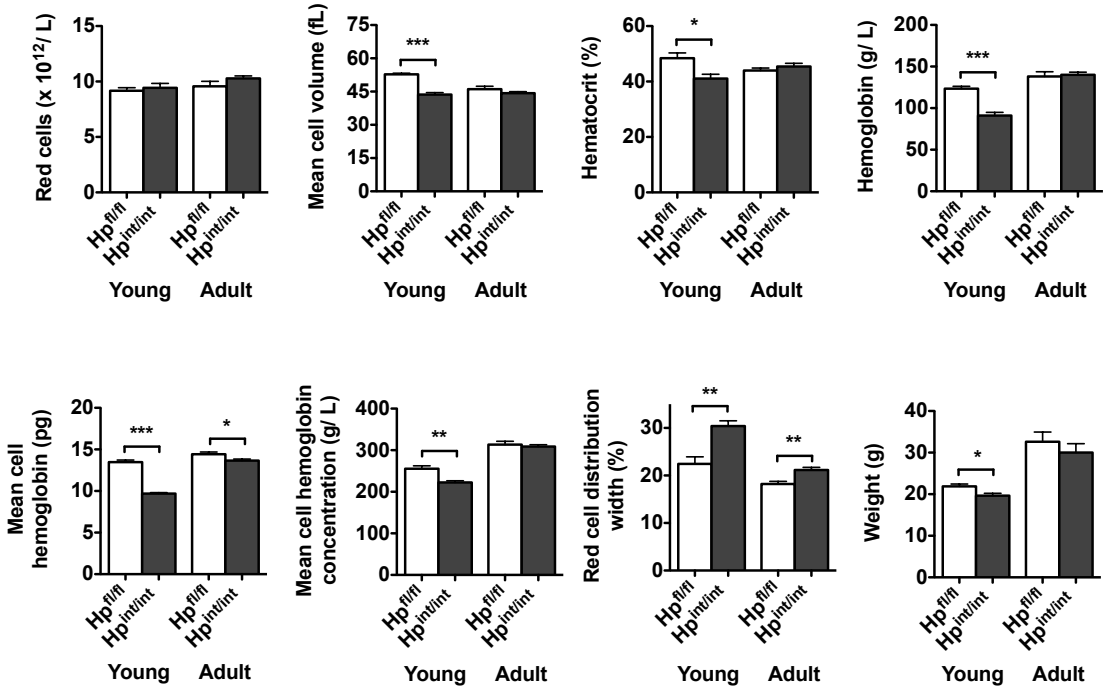

Figure 2.13. Hematology and weights of young (6-7 week old) and adult (13-14 week old) male $Hp^{int/int}$ and $Hp^{fl/fl}$ littermates born to $Hp^{int/int}$ mothers at UCB and maintained on an AIN-93G diet. N = 6 $Hp^{int/int}$ and N = 4 $Hp^{fl/fl}$ young littermates, and N = 7 $Hp^{int/int}$ and N = 4 $Hp^{fl/fl}$ adult littermates. Mean ± SEM. Littermate comparisons by t-test in GraphPad Prism. * $P \leq 0.05$, ** $P \leq 0.01$, *** $P \leq 0.001$.

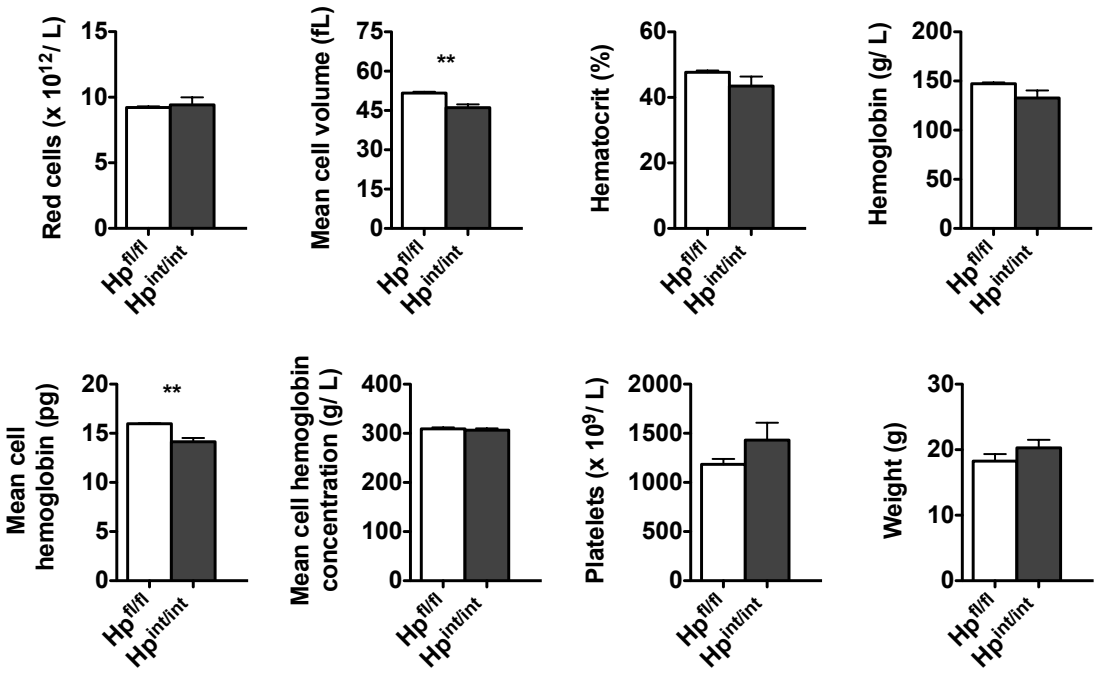

Figure 2.14. Hematology and weights of adult (10-12 week old) male $Hp^{int/int}$ and $Hp^{fl/fl}$ littermates born to $Hp^{fl/fl}$ mothers at QIMR and maintained on a chow diet. N = 5 $Hp^{int/int}$ and N = 6 $Hp^{fl/fl}$. Mean ± SEM. ** P ≤ 0.01 by t-test in GraphPad Prism.

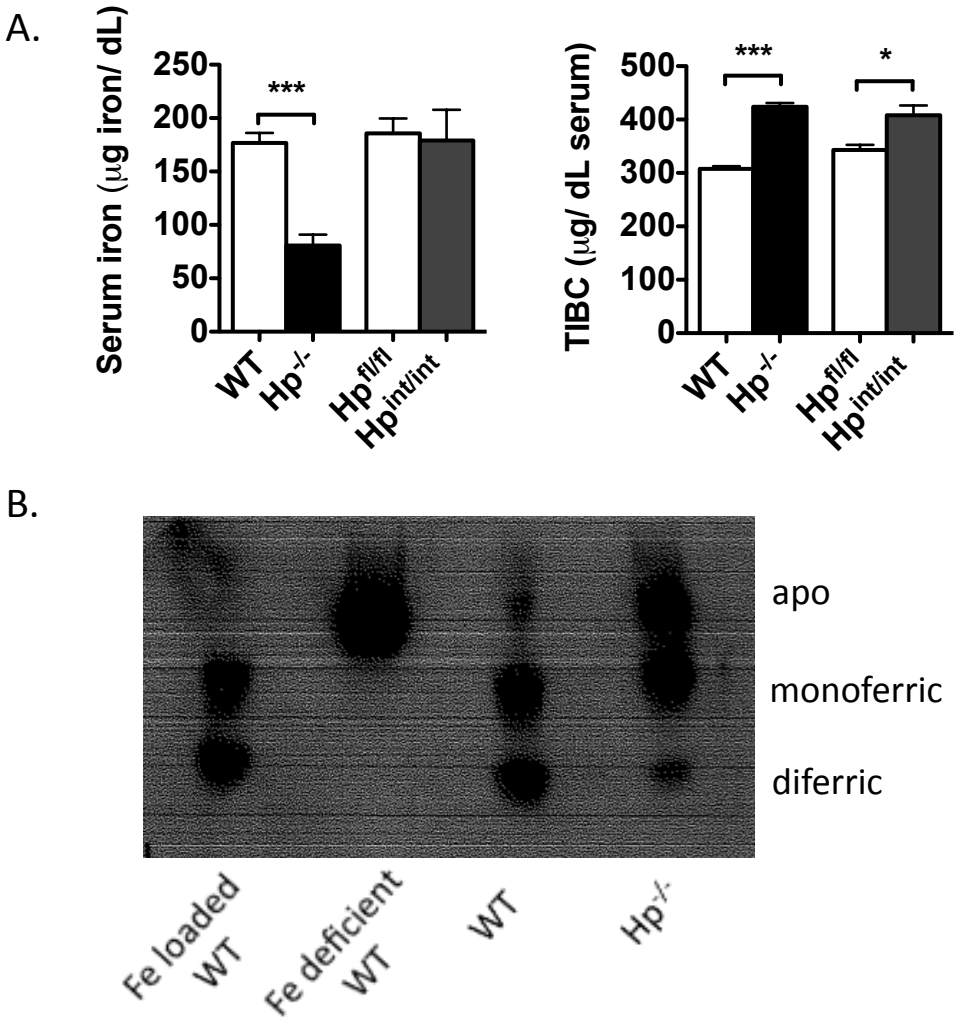

Figure 2.15. Serum iron and transferrin in young male mice. A. Serum iron and total iron binding capacity (TIBC) was measured in 6-7 week old male $Hp^{int/int}$ (N = 6) and $Hp^{fl/fl}$ (N = 5) littermates born to $Hp^{fl/fl}$ mothers, as well as male $Hp^{-/-}$ (N = 7) mice and WT (N = 7) littermates. Bars showing littermate data are paired. Mean ± SEM. Littermate comparisons by t-test in GraphPad Prism. * $P \leq 0.05$, *** $P \leq 0.001$. **B.** Urea-PAGE assay immunoblot showing transferrin speciation in serum. Data from WT mice fed a high or low iron diet as well as results from one $Hp^{-/-}$ mouse and a WT littermate maintained on chow are shown.

5. Tissue iron

Perls' Prussian blue staining for ferric iron in the duodenum of $Hp^{int/int}$, $Hp^{-/-}$, *sla*, and control WT and $Hp^{fl/fl}$ mice for an least four mice per genotype revealed strong iron deposits in the supranuclear region of enterocytes in the $Hp^{int/int}$, $Hp^{-/-}$, and *sla* mutant models but not in controls (Figure 2.16). In the $Hp^{int/int}$, $Hp^{-/-}$, and *sla* mutant models, the iron deposits were not present in every enterocyte, but enterocytes containing iron deposits were typically clustered together. Enterocytes near the villus tips, which are the oldest population of enterocytes, showed strong staining. These patterns are consistent with progressive iron accumulation in enterocytes over their 3-4 day lifespan and/or increased dietary iron uptake by mature enterocytes. Enterocytes showing iron loading in $Hp^{-/-}$ mice overall had a more bluish tint, which could be due to leaching from the major supranuclear deposits. This can occur with this staining method when iron levels are particularly high. Little variation was seen in the overall degree of staining of mice of the same genotype in WT, $Hp^{fl/fl}$, *sla*, and $Hp^{-/-}$ mice. Some variation, however, was observed in the intensity of staining in sections from $Hp^{int/int}$ mice, but staining was in general similar to that in *sla* and $Hp^{-/-}$ enterocytes. A larger sample size would be required to accurately estimate the degree of variation between the mice. In addition to the duodenum, a panel of tissues (jejunum, ileum, liver, spleen, pancreas, lung, gonad, heart, kidney, brown fat, and white fat) from 9-11 week old $Hp^{-/-}$ and WT littermates (N = 4 per group) was also examined by Perls' stain (data not shown). No staining was seen in either genotype in the jejunum, ileum, pancreas, lung, testes, heart, kidney, skin, brown fat, or white fat. Punctate staining was observed in the white pulp of the WT spleen and to a lesser extent in the $Hp^{-/-}$ spleen. WT mice showed a mild blue blush in the liver in some areas near the portal tract, but little to no staining was observed in $Hp^{-/-}$ livers.

Liver non-heme iron concentration was significantly lower in male $Hp^{-/-}$ mice than in WT littermate controls, as well as in $Hp^{int/int}$ mice versus $Hp^{fl/fl}$ controls, at both 6-7 and 9-11 weeks of age (Figure 2.17). No differences were detected in the liver non-heme iron concentrations of $Hp^{-/-}$ and *sla* littermates at 6-7 or 9-11 weeks of age, and both genotypes had iron levels that were not significantly different from levels in the livers of $Hp^{-/-}$ mice born to $Hp^{+/-}$ mothers. The levels in all $Hp^{-/-}$ and *sla* mice examined at 6-7 weeks of age were, however, at the lower limit of detection for this assay so differences below this threshold could potentially exist. For both age groups, there were no significant differences in non-heme liver iron when WT and $Hp^{fl/fl}$ mice were compared. Adult WT mice that had been maintained on iron-deficient or iron-loaded diets for six weeks or more were also included as controls for the assay and gave expected results. Iron levels in kidney and spleen were also tested in 6-7 week old $Hp^{-/-}$ and WT littermates and were significantly lower in $Hp^{-/-}$ mice. Heart iron levels were not significantly different (Figure 2.18).

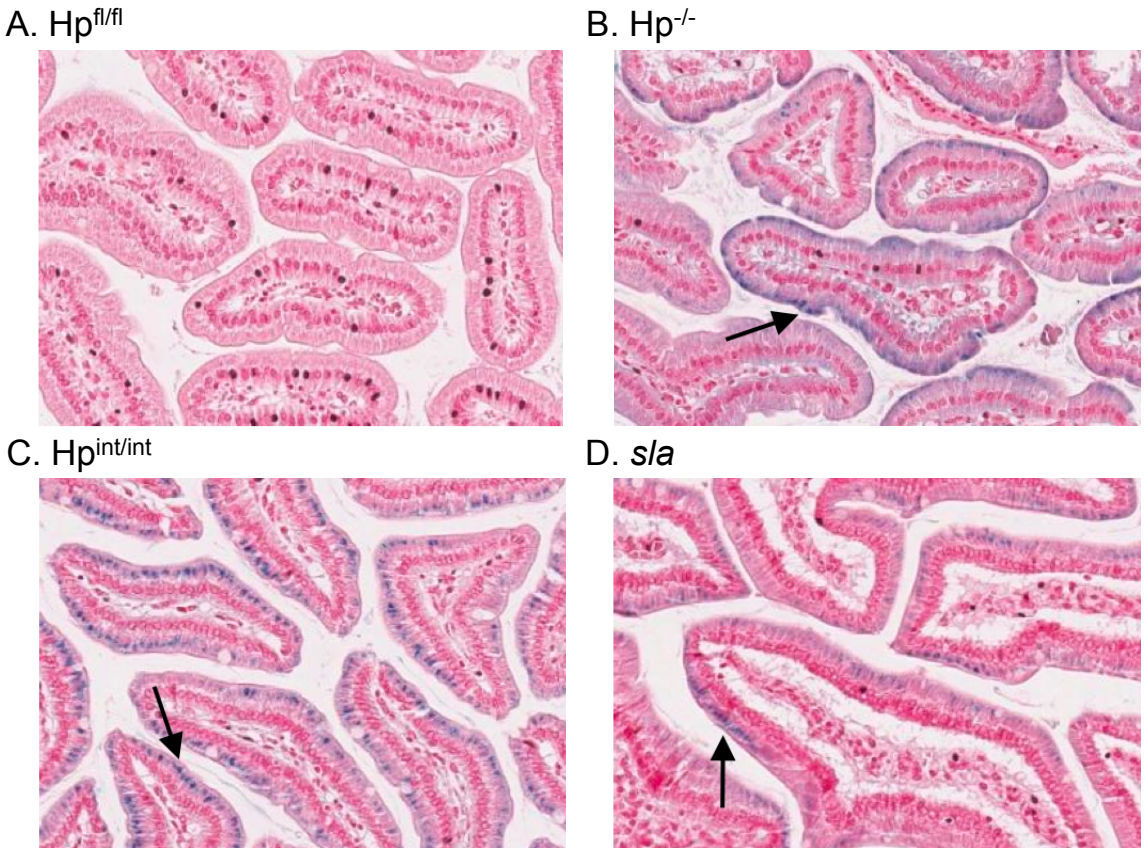

Figure 2.16. Representative Perls' Prussian blue stained duodenal sections from 6-7 week old male mice maintained on a chow diet. $Hp^{fl/fl}$ and $Hp^{int/int}$ mice are littermates. Aperio Scanscope XT. 20x magnification. Non-heme iron stains blue**.**

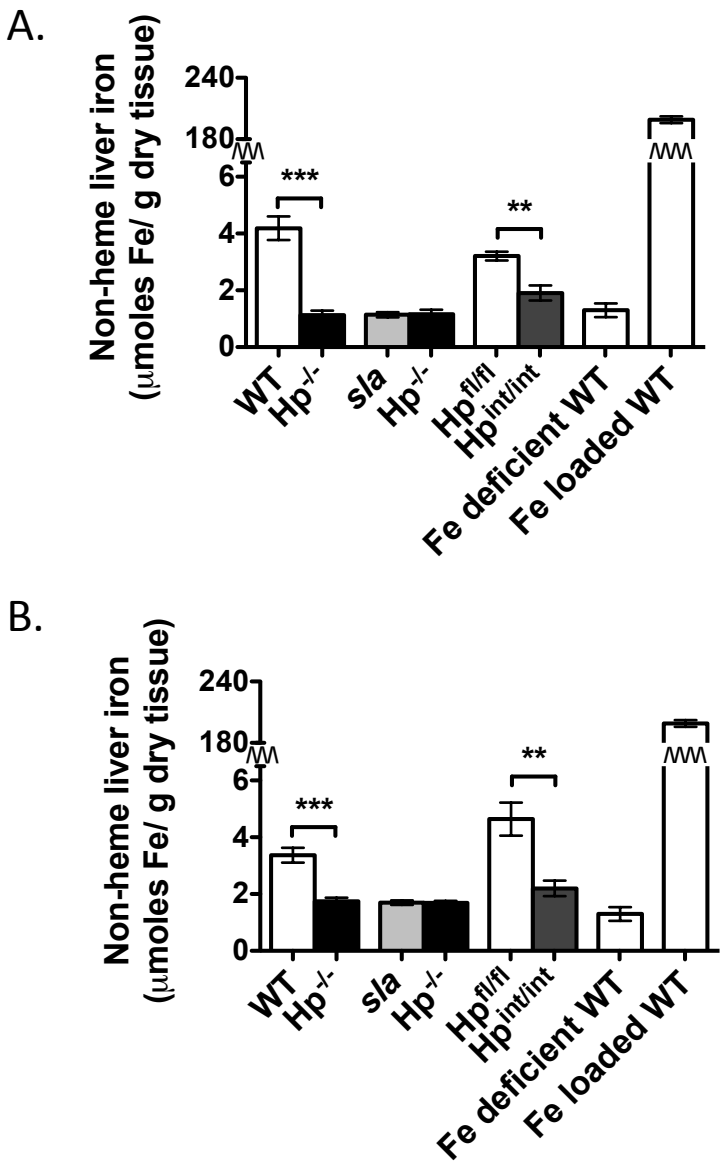

Figure 2.17. Non-heme iron in the liver of young and adult male mice. Iron in dried tissue was measured by a colorimetric assay that only detects non-heme iron. Non-heme iron in livers from **A.** 6-7 week old $Hp^{int/int}$ (N = 6) and $Hp^{fl/fl}$ (N = 5) littermates born to $Hp^{fl/fl}$ mothers, $Hp^{-/-}$ (N = 7) and WT (N = 7) littermates, and *sla* (N = 7) and $Hp^{-/-}$ (N = 7) littermates. **B.** 9-11 week old $Hp^{int/int}$ (N = 6) and $Hp^{fl/fl}$ (N = 6) littermates born to $Hp^{fl/fl}$ mothers, $Hp^{-/-}$ (N = 6) and WT (N = 8) littermates, and *sla* (N = 9) and $Hp^{-/-}$ (N = 8) littermates. Data from livers of adult WT mice fed an iron deficient (N = 3) or iron loaded diet (N = 2) are also shown. Bars showing littermate data are paired. Mean ± SEM. Littermate comparisons by t-test in GraphPad Prism. ** $P \leq 0.01$ *** $P \leq 0.001$.

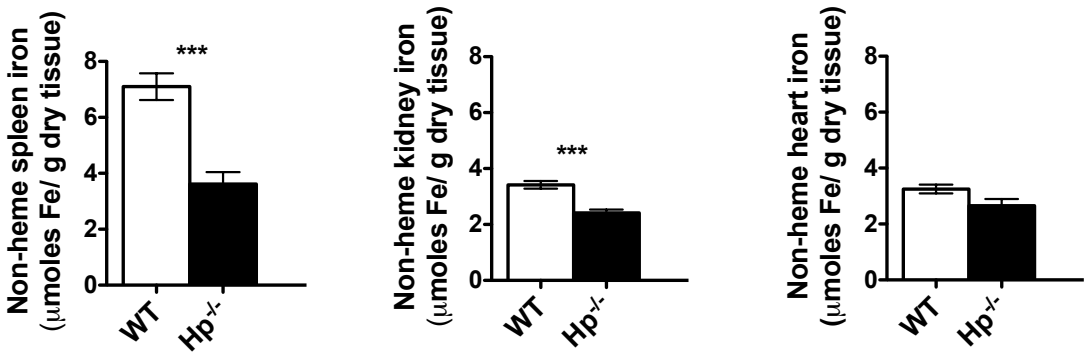

Figure 2.18. Non-heme iron in the spleen, kidney, and heart of young 6-7 week old male Hp$^{-/-}$ (N = 7) and WT (N = 7) littermates. Bars showing littermate data are paired. Mean ± SEM. Littermate comparisons by t-test in GraphPad Prism. *** P ≤ 0.001.

6. Expression of genes related to iron acquisition and status

Liver mRNA expression of several genes was tested in 6-7 week old Hp$^{int/int}$, Hp$^{-/-}$, and control mice (Figure 2.19). Total *Hamp* and *Hamp1* mRNA levels were significantly lower in 6-7 week old Hp$^{-/-}$ mice versus WT littermates, consistent with iron deficiency in Hp$^{-/-}$ mice. Expression of *Tfrc*, which inversely correlates with tissue iron levels, was significantly greater in Hp$^{-/-}$ mice than in controls. Both *Hif2*α and *Dmt1* mRNA levels were significantly higher in Hp$^{-/-}$ livers than in controls, but the difference represented less than a two-fold change and thus is likely not of biological significance (data not shown). No significant differences were observed in the expression of any genes tested when Hp$^{int/int}$ mice and littermate controls were compared. However, there was a high degree of variation among the Hp$^{int/int}$ mice, with some showing levels of *Hamp1* similar to Hp$^{-/-}$ mice and others showing levels similar to controls. No differences were detected in the mRNA levels of liver *App*, *Hif1*α, *Hfe*, and *Tmprss6* between any groups (only *App* results are shown). Liver *Cp* mRNA expression was examined in a different group of male Hp$^{-/-}$ and littermates at 9-10 weeks of age and no differences were observed (data not shown).

No significant differences were found in iron importer *Dmt1* mRNA expression in 9-11 week old Hp$^{-/-}$ and WT enterocytes, whereas WT mice made iron-deficient by an iron-deficient diet had greatly increased *Dmt1* expression (Figure 2.20). *Dmt1* expression in enterocytes is increased in iron deficiency but is controlled at

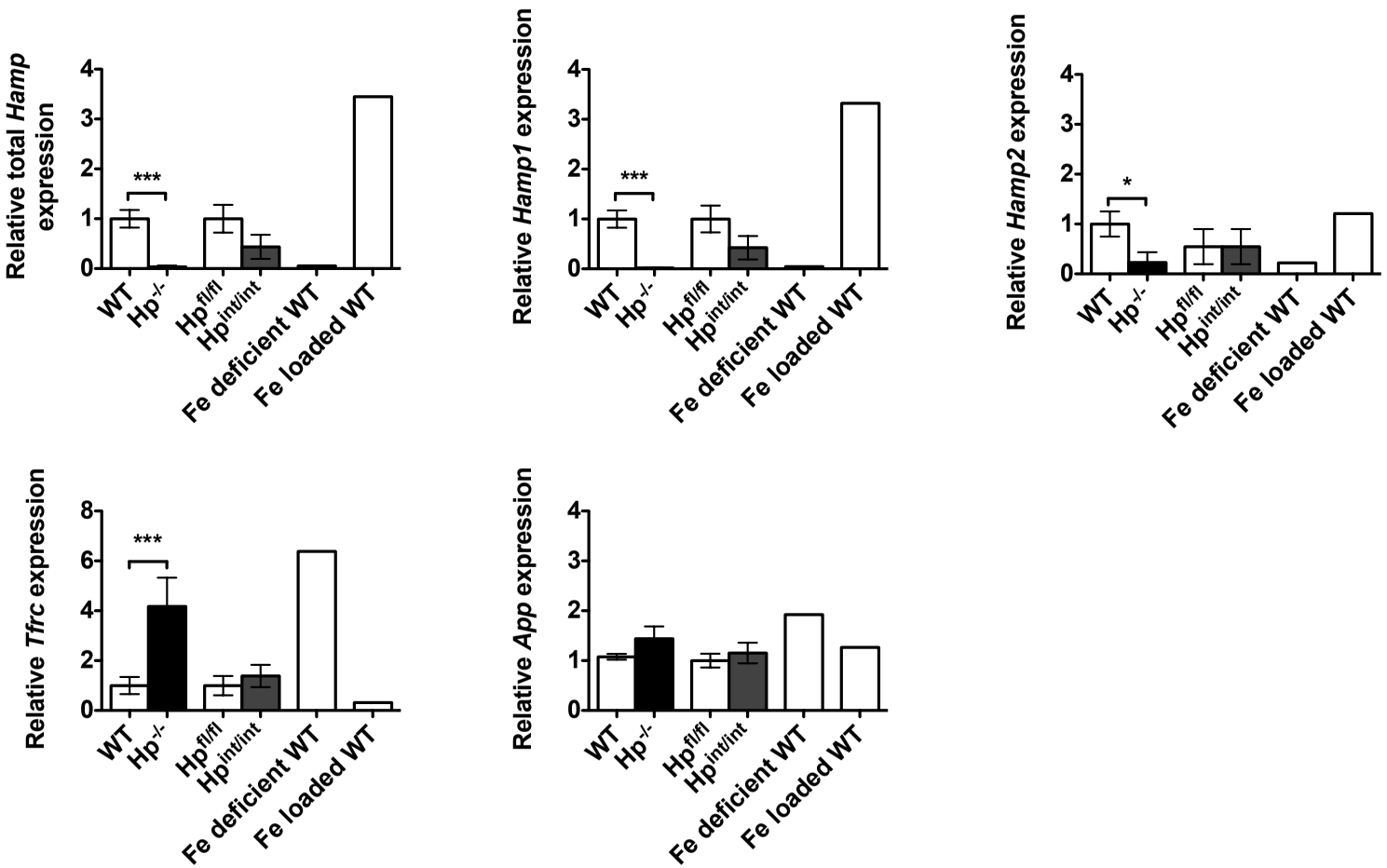

Figure 2.19. mRNA expression in the livers of young male mice. The expression of selected genes involved in iron metabolism was measured by RT-qPCR in livers from 6-7 week old male $Hp^{int/int}$ (N = 5) and $Hp^{fl/fl}$ (N = 5) littermates born to $Hp^{fl/fl}$ mothers, and male $Hp^{-/-}$ (N = 7) and WT (N = 7) littermates. Data from single adult mice fed an iron-deficient or iron-loaded diet are also shown. The expression results were normalized to expression of the *Hprt* housekeeping gene, and then normalized to expression in the controls. Bars showing littermate data are paired. Mean ± SEM. Littermate comparisons by t-test in GraphPad Prism. * $P \leq 0.05$, *** $P \leq 0.001$.

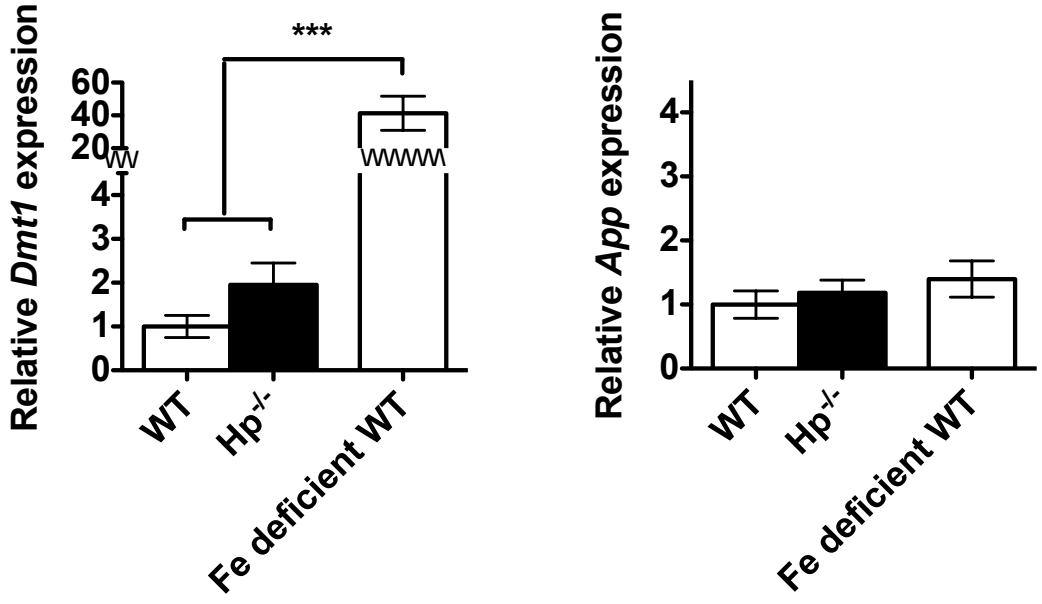

Figure 2.20. mRNA expression in isolated duodenal enterocytes of adult male mice. The expression of *Dmt1* and *App* mRNA was measured by RT-qPCR in enterocytes from 9-11 week old male $Hp^{-/-}$ (N = 4) and WT (N = 4) littermates. Data from four adult WT mice fed an iron-deficient diet are also shown. The expression results were normalized to the expression of the *Hprt* housekeeping gene, and then normalized to expression in the WT littermate controls. Mean ± SEM. Littermate comparisons by t-test and one-way ANOVA across all groups in GraphPad Prism. *** $P \leq 0.001$.

the cellular level, thus the expression of *Dmt1* only increases if iron levels in the enterocyte itself are low. A similar result to what was observed in $Hp^{-/-}$ enterocytes has previously been reported in *sla* mice and provides further support for iron loading in $Hp^{-/-}$ enterocytes (Chen, Su et al. 2003). No significant differences were observed in enterocyte *App* mRNA expression in 9-11 week old male mice, suggesting that upregulation of enterocyte *App* mRNA levels is not involved in compensating for the loss of HP.

FTN protein, a marker of iron stores, was examined by immunoblotting and levels were generally higher in $Hp^{-/-}$ enterocytes than WT controls in both young and adult mice, although differences were only statistically significant in 6-7 week old mice (Figure 2.21). FTN expression in $Hp^{int/int}$ mice was surprisingly not significantly different from controls in either young or adult mice (Figure 2.22).

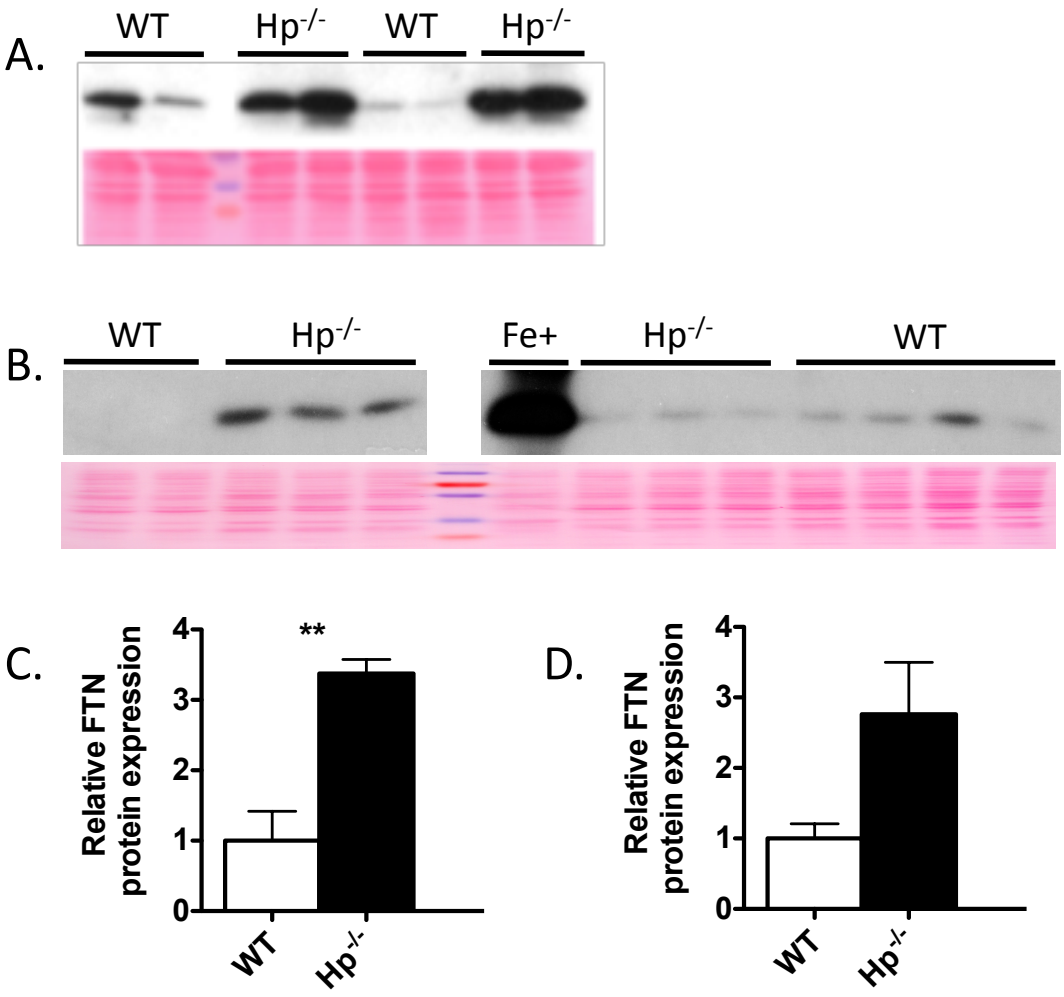

Figure 2.21. FTN protein expression in isolated duodenal enterocytes from $Hp^{-/-}$ and WT littermates. FTN protein expression (~21 kD) was visualized by immunoblot in both young (6-7 week old) and adult (10-15 week old) male littermate enterocytes. **A.** FTN immunoblot, with the Ponceau S stained membrane below, of enterocytes from young $Hp^{-/-}$ (N = 4 randomly pooled samples from 2-3 unique mice each) and WT (N = 4 randomly pooled samples from 2-3 unique mice each) littermates. **B.** FTN immunoblot, with the Ponceau S stained membrane below, of enterocytes from adult $Hp^{-/-}$ (N = 6) and WT (N = 6) littermates, as well as of a WT mouse maintained on an iron-loaded diet (Fe+). **C.** Densitometry for panel A is shown. **D.** Densitometry for panel B is shown. Densitometry data was determined by calculating the immunoblot band density and the corresponding Ponceau S protein stain density (full lane) with UN-SCAN IT software (Silk Scientific). The ratio of FTN to Ponceau S stained protein density for each lane was normalized to the average ratio for the WT controls on the same blot. The normalized values were then averaged. Mean ± SEM. Littermate comparisons by t-test in GraphPad Prism. ** $P \leq 0.01$. The data in this figure was collected by Yan Lu.

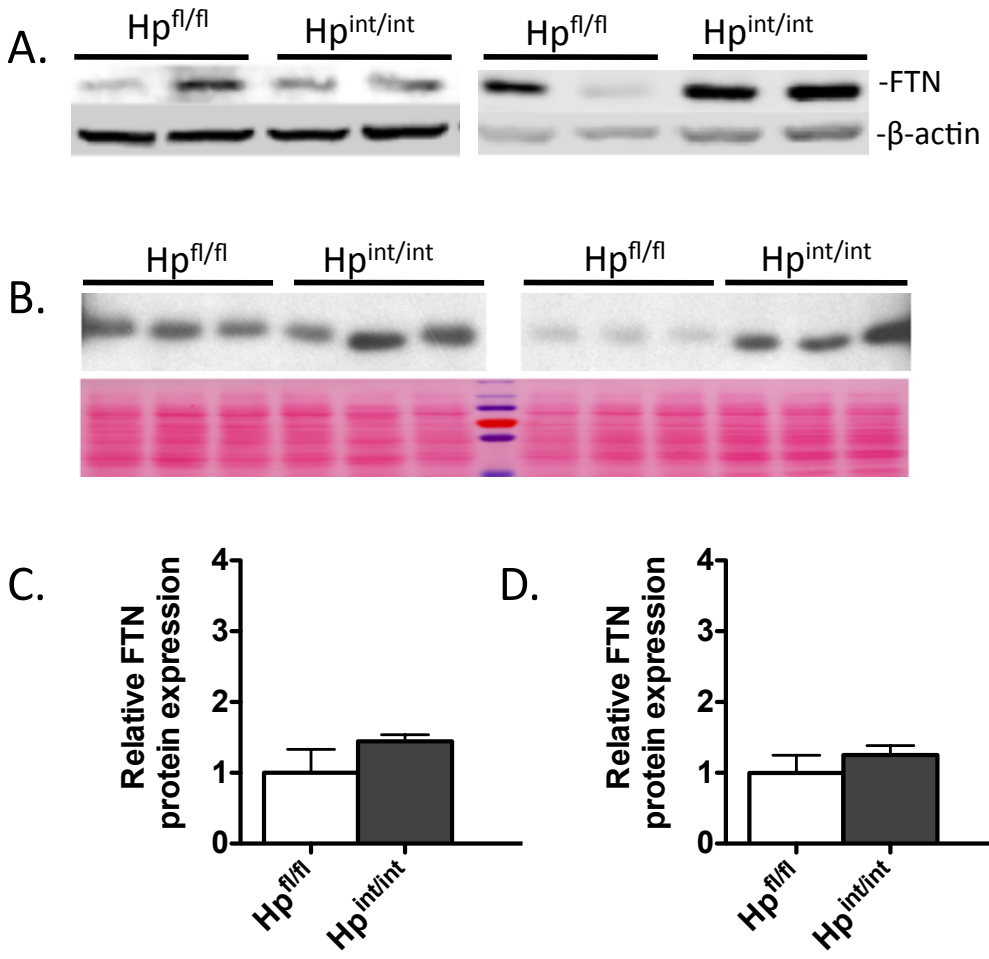

Figure 2.22. FTN protein expression in isolated duodenal enterocytes from $Hp^{int/int}$ and $Hp^{fl/fl}$ littermates. FTN protein expression (~21 kD) was visualized by immunoblot in both young (6-7 week old) and adult (10-15 week old) male littermate enterocytes. **A.** FTN immunoblot, with the β-actin (~42 kD) immunoblot loading control below, of enterocytes from young $Hp^{int/int}$ (N = 4) and $Hp^{fl/fl}$ (N = 4) littermates. **B.** FTN immunoblot, with the Ponceau S stained membrane below, of enterocytes from adult $Hp^{int/int}$ (N = 6) and $Hp^{fl/fl}$ (N = 6) littermates. **C.** Densitometry for panel A is shown. **D.** Densitometry for panel B is shown. Densitometry data for panel A was determined by calculating FTN immunoblot band density and the corresponding β-actin band density (panel A) with ImageJ software (NIH), or for panel B by calculating FTN immunoblot band density and Ponceau S protein stain density (full lane) with UN-SCAN IT software (Silk Scientific). The ratio of FTN to β-actin or Ponceau S stained protein density for each lane was normalized to the average ratio for the $Hp^{fl/fl}$ controls on the same blot. The normalized values were then averaged. Mean ± SEM. Littermate comparisons by t-test in GraphPad Prism. The data in panels B and D was collected by Yan Lu.

7. Ferroxidase activity

Ferroxidase activity was measured by a visiting collaborator (Yan Lu, University of Florida, James Collins laboratory) in a cuvette-based TF iron-loading assay in both membrane and cytosolic fractions of freshly isolated enterocytes. Ferroxidase activity was significantly lower in the cytosolic fraction of duodenal enterocytes from adult male $Hp^{-/-}$ mice versus WT littermates, but no significant differences were noted in the membrane fraction (Figure 2.23). When enterocytes from adult male $Hp^{int/int}$ mice and $Hp^{fl/fl}$ littermates were tested, ferroxidase activity was generally lower but not significantly different in the cytosolic or membrane fractions between the two groups of mice.

In addition, ferroxidase activity was detected using the in-gel ferrozine assay. A prominent clear band was observed in $Hp^{fl/fl}$ mouse enterocytes at the expected location, but a clear band of a similar size was not observed in $Hp^{int/int}$ enterocytes. Instead, a band with an apparent higher molecular weight was observed in the $Hp^{int/int}$ mouse enterocytes. More studies need to be done, but it is likely that the higher band is due to FTN ferroxidase activity, which is expected to increase in iron-loaded $Hp^{int/int}$ enterocytes. Purified FTN gives a high molecular weight clear band when tested in this assay (data not shown).

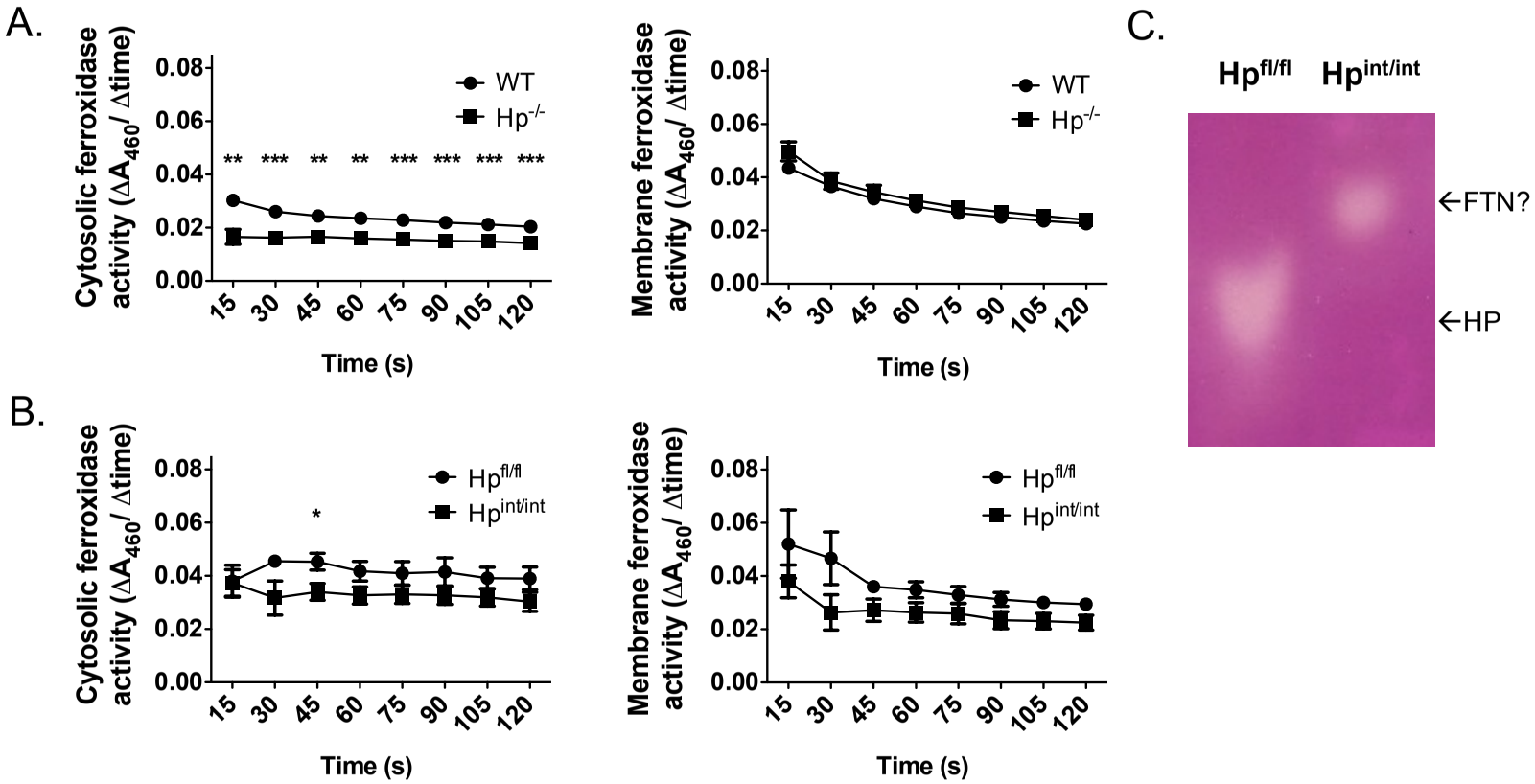

Figure 2.23. Ferroxidase activity in isolated duodenal enterocytes. Ferroxidase activity was measured by a TF iron-loading assay in cytosolic and membrane fractions from **A**. adult male $Hp^{-/-}$ (N = 7) and WT littermates (N = 7) and **B**. adult male $Hp^{int/int}$ (N = 6) and $Hp^{fl/fl}$ littermates (N = 4 cytosolic and N = 6 membrane). Mean ± SEM. Significant differences in ferroxidase activity in knockouts versus controls at each time point were determined by t-test in GraphPad Prism. * $P \leq 0.05$, ** $P \leq 0.01$, *** $P \leq 0.001$. The data in panels A and B were collected by Yan Lu. **C**. In-gel ferrozine ferroxidase assay with clarified lysates from an $Hp^{int/int}$ mouse and an $Hp^{fl/fl}$ littermate at ~6 weeks of age.

8. Iron absorption

Iron absorption was determined by whole body counting following gavage with a dose of radioactive iron. Iron absorption was uniformly low and not detectably different between $Hp^{-/-}$, $Hp^{int/int}$, and WT control adults on the QIMR chow diet (Figure 2.24). When adult male $Hp^{-/-}$ and WT littermates were put on an iron-deficient diet for one week prior to dosing with radioactive iron, $Hp^{-/-}$ mice absorbed significantly less iron than WT mice despite having liver non-heme iron stores only half that of WT mice. Very little radiolabeled iron was detected in the GI tract (stomach to anus) of any mice, and there were no differences between the level in WT and $Hp^{-/-}$ mice, indicating that the intestinal enterocytes had turned over as expected in the five day post-dose period. No differences were detected between $Hp^{-/-}$ and WT mice in the distribution of the absorbed radiolabeled iron when the intestinal tract, spleen, liver and remaining carcass were counted separately.

A trend toward decreased iron absorption was also seen in a small pilot study of four week old $Hp^{-/-}$ versus WT littermates that had been fed an iron-deficient diet since weaning (Figure 2.25). In addition, significantly more of the absorbed iron was in the liver of the four week old $Hp^{-/-}$ mice compared to WT animals, suggesting differences in iron distribution. Both $Hp^{-/-}$ and WT mice at 1.5 weeks of age absorbed nearly 100% of a gavaged dose (data not shown), suggesting that HP is not required for iron absorption, at least from the form of iron in the dose, at this age.

Strong stimulation of iron absorption induced by three weeks on an iron-deficient diet and injection of the hemolytic agent PHZ in $Hp^{int/int}$, $Hp^{fl/fl}$, and $Cp^{-/-}$ mice led to very high iron absorption in all mice, indicating that adult mice lacking HP are able to upregulate iron absorption appropriately when body demands are very high (Figure 2.26). An iron-deficient diet for six weeks (Figure 2.26) or five months (data not shown) also highly upregulated iron absorption in $Hp^{-/-}$, $Hp^{int/int}$, *sla*, and control mice. $Hp^{-/-}$ males however had a significantly lower level of iron absorption than controls in the six-week iron-deficient diet study.

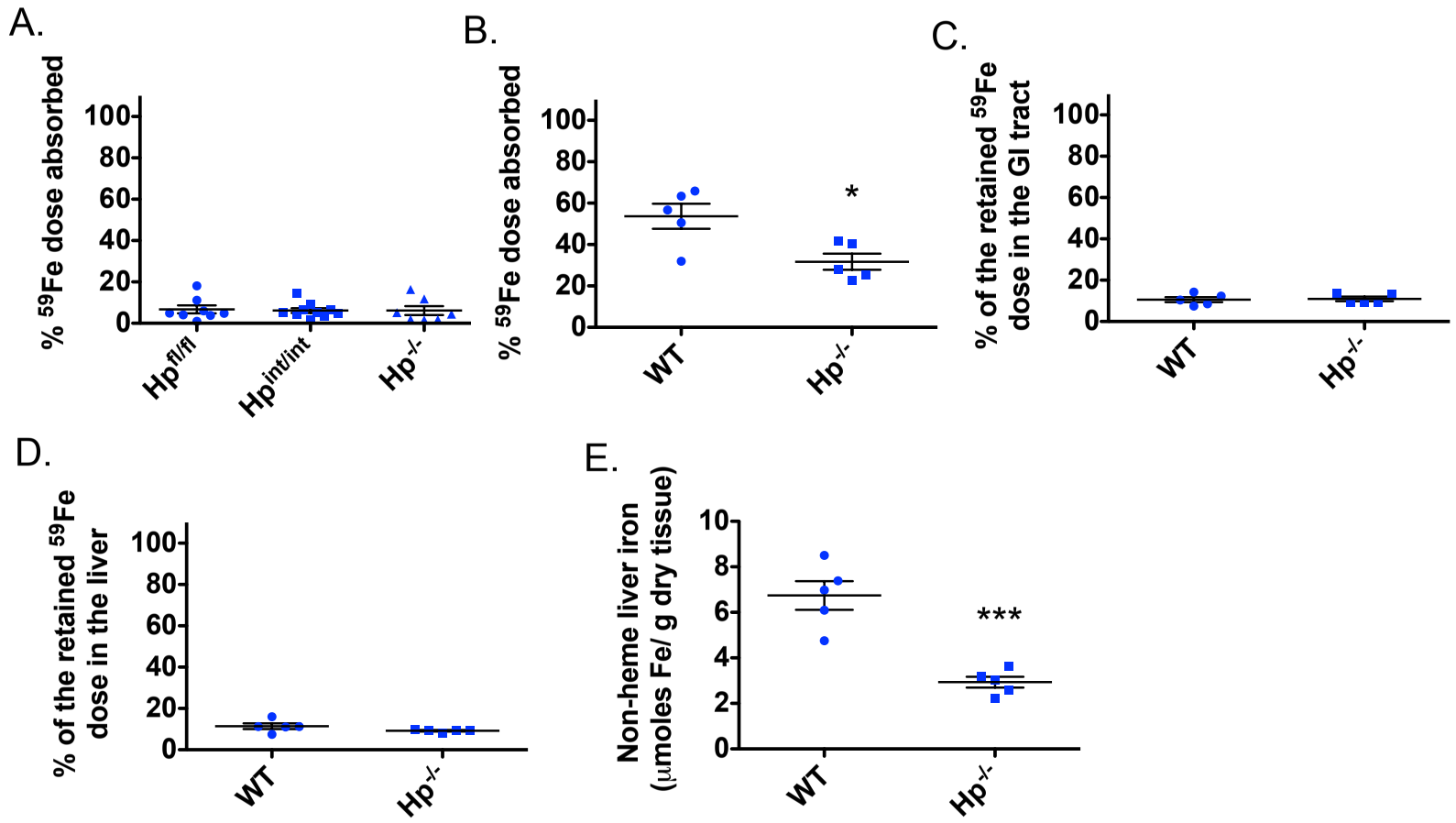

Figure 2.24. Iron absorption in adult mice. A. Whole body iron absorption in mice (8-9 weeks old at dose, both sexes) maintained on a chow diet. Mice were gavaged with ^{59}Fe and the % retained five days after dosing was determined. $Hp^{fl/fl}$ (N = 8), $Hp^{int/int}$ (N = 10), $Hp^{-/-}$ (N = 7). **B-D**. Male $Hp^{-/-}$ (N = 5) and WT littermates (N = 5) 9-16 weeks old were put on an iron-deficient diet for one week and then dosed by gavage with ^{59}Fe. The % dose retained five days after dosing was determined. **E**. Non-heme liver iron for the mice in B-D as measured by colorimetric assay. Mean ± SEM. T-test in GraphPad Prism, * $P \leq 0.05$, *** $P \leq 0.001$.

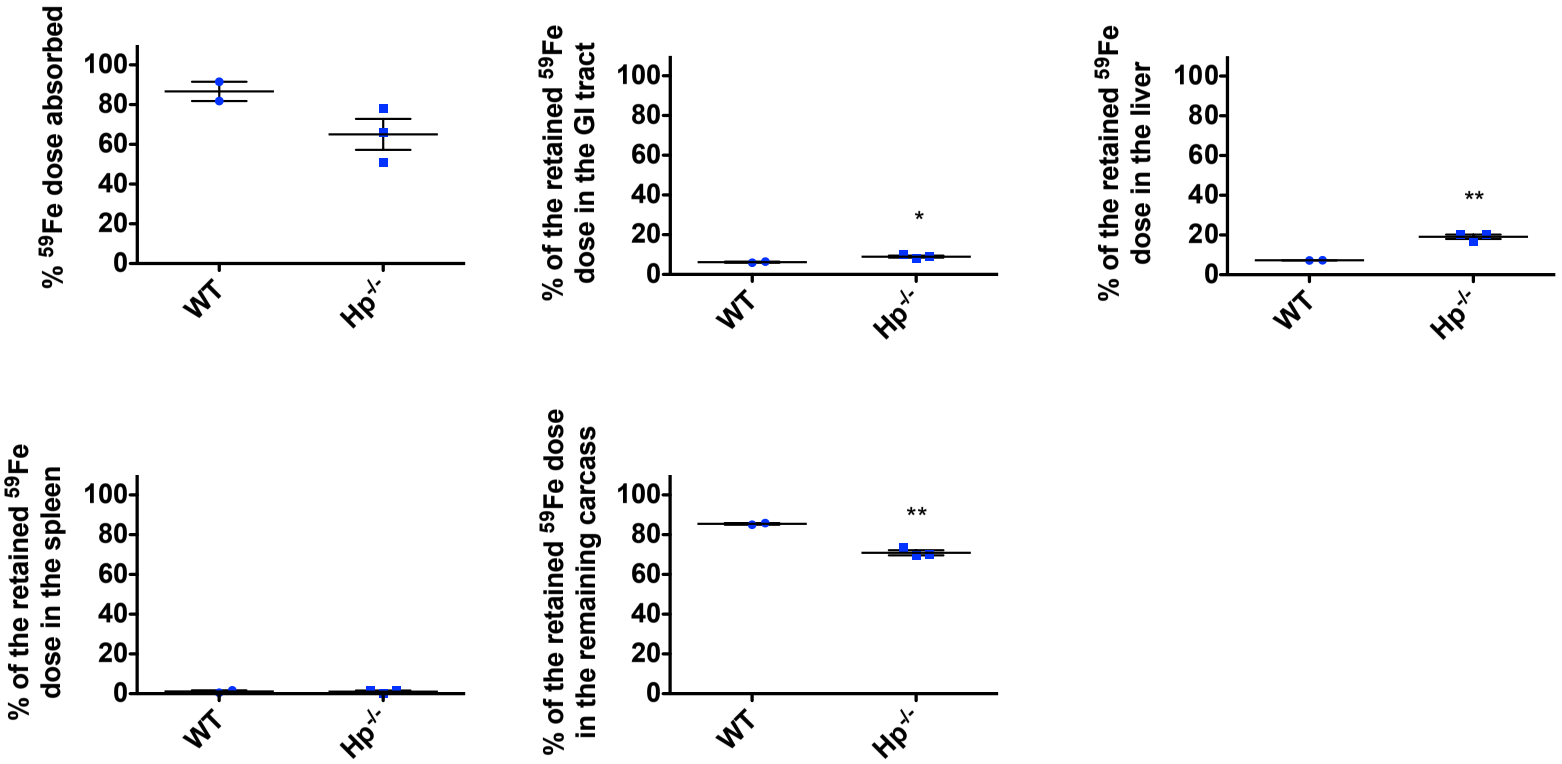

Figure 2.25. Pilot study of iron absorption and distribution in weanling mice. Male $Hp^{-/-}$ (N = 3) and WT littermates (N = 2) were put on an iron-deficient diet for one week at weaning (three weeks old) and then dosed by gavage with ^{59}Fe. The % dose retained five days after dosing in the whole animal and various tissues was determined. Gastrointestinal tract (GI tract) is from the esophagus just above the stomach to the anus, including contents. The "remaining carcass" in the last panel consists of everything except the liver, spleen, and GI tract. Mean ± SEM. T-test in GraphPad Prism, * $P \leq 0.05$, ** $P \leq 0.01$.

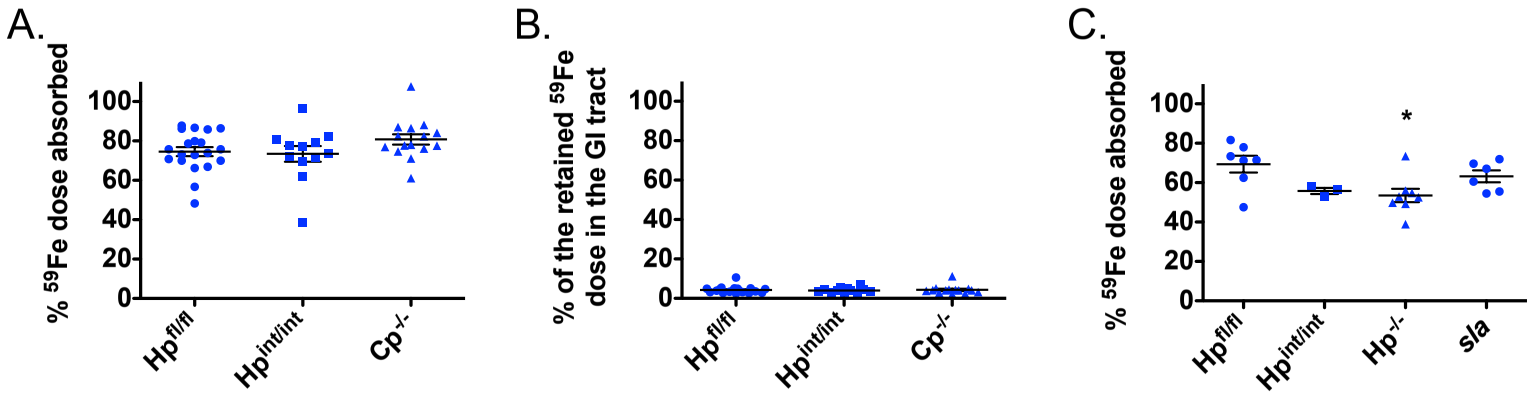

Figure 2.26. Iron absorption in mice following stimulation. Mice were gavaged with ^{59}Fe and the % retained in the whole animal five days after dosing was determined**. A.** Whole body iron absorption and **B.** the percentage of the retained dose in the gastrointestinal (GI) tract in mice following dietary and hemolysis-induced stimulation. Mice aged 4-6 weeks (both sexes) were switched to an iron-deficient diet and then given phenylhydrazine (PHZ) by intraperitoneal injection (100 mg/kg) after two weeks. Five days later mice were dosed with ^{59}Fe. $Hp^{fl/fl}$ (N = 20), $Hp^{int/int}$ (N = 12), $Cp^{-/-}$ (N = 14). **C.** Whole body iron absorption in mice following dietary-induced stimulation of absorption. Weanling male mice (three weeks old) were placed on a iron-deficient diet for six weeks prior to dosing with ^{59}Fe. $Hp^{fl/fl}$ (N = 7), $Hp^{int/int}$ (N = 3), $Hp^{-/-}$ (N = 8), *sla* (N = 6). The dose retained in the GI tract was negligible and not different between the groups (data not shown). Mean ± SEM. One-way ANOVA and Tukey's post test in GraphPad Prism, * $P \leq 0.05$.

IV. Discussion

The mechanisms by which dietary iron is absorbed and transferred from intestinal enterocytes to the blood are complex, and details are still emerging as to the identity and roles of proteins involved in this process. Our results demonstrate that HP is not essential for intestinal iron absorption, and indicate that another mechanism, MCF mediated or not, must exist. However, this alternative mechanism cannot fully compensate for the lack of HP, as knockout of HP in either the whole animal or the intestine alone led to significant iron deficiency.

Young $Hp^{-/-}$ and $Hp^{int/int}$ mice both exhibited a hypochromic, microcytic anemia that improved with age, characteristics similar to those reported previously for *sla* mice (Chen, Attieh et al. 2009). At 6-7 weeks of age, $Hp^{-/-}$ mice were significantly iron-deficient, as indicated by reduced liver *Hamp1* expression, low serum and tissue iron, and elevated *Tfrc* expression in the liver. The hearts of $Hp^{-/-}$ mice were also enlarged relative to WT littermates, likely as a response to their anemia (Jankowska and Ponikowski 2010). $Hp^{int/int}$ mice had a slightly milder and more variable phenotype than $Hp^{-/-}$ mice. The iron status of both $Hp^{-/-}$ and $Hp^{int/int}$ mice improved in adulthood but liver non-heme iron levels and red cell hemoglobin levels still remained lower in $Hp^{-/-}$ and $Hp^{int/int}$ mice versus littermate controls. The more severe iron deficiency phenotype observed in young relative to adult knockout mice is likely explained by the greater iron requirements during growth.

The iron deficiency phenotype of the $Hp^{-/-}$ and $Hp^{int/int}$ mice, coupled with the dramatic iron loading that was observed in the supranuclear region of $Hp^{-/-}$ and $Hp^{int/int}$ enterocytes by Perls' stain, suggested defects in iron absorption, as has been reported in *sla* mice (Sorbie, Hamilton et al. 1974). In order to confirm this, we performed several iron absorption studies. In experiments with adult mice maintained on a chow diet, iron absorption was very low and no differences could be detected between the amount of a radioactive iron dose absorbed by $Hp^{-/-}$ mice and controls. The percentage of the dose absorbed by the control group was expected to be low, given the iron replete status of these mice. However, $Hp^{-/-}$ mice also absorbed similarly low levels of iron despite their significantly lower iron status, indicating that the level of absorption was not appropriate in $Hp^{-/-}$ relative to their iron status. In order to better examine the defect in absorption in $Hp^{-/-}$ mice, $Hp^{-/-}$ mice and controls were tested with stimuli that normally augment iron absorption. After being challenged with an iron-deficient diet for one week, iron absorption in both adult $Hp^{-/-}$ and control groups increased; however, adult $Hp^{-/-}$ mice absorbed significantly less radioactive iron than controls. When mice were challenged with an iron-deficient diet for six weeks from weaning, both $Hp^{-/-}$ and $Hp^{int/int}$ mice absorbed less iron than controls, but the difference was not significant for the $Hp^{int/int}$ mice, likely due to the smaller number of these animals examined. This same trend was observed in young mice after one week on an

iron-deficient diet from weaning. These findings show that $Hp^{-/-}$ mice are able to upregulate iron absorption when stressed, but they are not able to upregulate it as effectively as WT mice.

Interestingly, when iron absorption was strongly stimulated with an iron-deficient diet coupled with injection of PHZ to lyse red cells and stimulate erythropoiesis, $Hp^{int/int}$ mice were able to increase their iron absorption to the same level as controls. Although $Hp^{-/-}$ mice were not tested in that particular assay, in another assay where mice were strongly stressed by an iron-deficient diet for 20 weeks, $Hp^{-/-}$ mice absorbed similarly high levels as controls (data not shown). Together these results indicate that while HP is important for adequate iron absorption, other mechanisms for iron absorption are upregulated in the face of increased iron needs. Under strong duress these alternative mechanisms may even override the detrimental effects of HP ablation on iron absorption. The $Hp^{-/-}$ mice will be particularly useful in characterizing and identifying these alternative mechanisms.

Because HP appears to be involved in efficient iron efflux from enterocytes, it might be expected that other cell types that rely on HP would show iron accumulation in the whole body knockout model. Currently HP is only known to play an important role in the intestine, eye, and brain, with cells in these tissues accumulating iron when HP expression is perturbed (Schulz, Vulpe et al. 2011; Wolkow, Song et al. 2012). With the exception of the duodenum, however, no dramatic increases in iron loading in any cell types were observed by Perls' stain in age-matched panels of tissues from $Hp^{-/-}$ versus control mice at 9-11, 23, and 76-79 weeks of age. The brain however was not studied. Because HP is also ablated in the intestine of $Hp^{-/-}$ mice, less iron is available to load other cells in the body, and thus any iron-loading phenotypes may not be readily apparent without administration of parenteral iron to bypass intestinal iron absorption. As has been shown in the eye, some cell types express other ferroxidases that could at least partially compensate for the lack of HP, so double knockout models may provide an even more sensitive means to determine the importance of HP in other cell types (Wolkow, Song et al. 2012).

The similar phenotypes of the $Hp^{-/-}$ and $Hp^{int/int}$ mice indicate that HP function in intestinal enterocytes alone is particularly important for maintaining systemic iron homeostasis. This is not surprising considering the critical role of these cells in body iron acquisition, as well as the high level of HP expression and lack of other MCFs in these cells. Despite the similar phenotypes overall, in several studies the $Hp^{-/-}$ mice were significantly different from controls whereas the $Hp^{int/int}$ mice were not, which could suggest that HP plays some extra-intestinal roles in iron metabolism. However, the major contributor to the reduced phenotypical significance in the $Hp^{int/int}$ mice was most likely variation in the degree of knockout in $Hp^{int/int}$ mice, which at the protein level generally was very high but there were some outliers. Screening of mice for the degree of knockout before

inclusion in any future analyses may help to resolve this issue. In addition, some $Hp^{fl/fl}$ and $Hp^{int/int}$ mice were observed to have a small body, short tail, and hip dysplasia. This may be the result of another mutation and could have added some variability to the studies.

Initial comparisons of liver iron levels, *Hamp* mRNA expression, and hematology between *sla* mice born to *sla* mothers and $Hp^{-/-}$ mice born to $Hp^{+/-}$ mothers at QIMR suggested the *sla* mice may have a less severe phenotype than the $Hp^{-/-}$ mice (data not shown). While both models were on a C57BL/6J background, there was some concern that the background of the *sla* mice may have diverged from that of the $Hp^{-/-}$ mice as the *sla* mice had been maintained in Australia for almost 20 years. A cross was therefore made between the $Hp^{-/-}$ and *sla* strains in order to generate $Hp^{sla/-}$ mothers that could be bred with $Hp^{-/-}$ males to generate $Hp^{-/-}$ and *sla* male littermates. This avoided the confounding effects of different maternal genotypes and backgrounds. No major differences were seen in the general phenotype of the progeny from this cross, and at 6-7 weeks of age the mice both exhibited similar degrees of iron deficiency as reflected by their hematology and non-heme liver iron levels. However, at 10-11 weeks of age the $Hp^{-/-}$ mice had slightly but significantly lower hemoglobin and hematocrit than their *sla* littermates. These results weakly suggest that the mutant *SLA* protein may retain some limited function, although more studies are clearly needed. Because the body first directs limited iron supplies to developing blood cells, differences in the iron content in other tissues not yet examined may be greater in $Hp^{-/-}$ and *sla* littermates than the differences in the hematology. Although the levels of non-heme iron in the livers of 6-7 week old $Hp^{-/-}$ and *sla* littermates were not significantly different, the levels were near the limit of detection for that assay, so differences may only become apparent if a more sensitive technique is used. If the *sla* protein is able to partially fulfill the roles of the wild-type HP protein, further comparisons between the $Hp^{-/-}$ and *sla* models could provide insight into the requirements for HP protein function.

Maternal HP appears to be particularly important in the growth and health of pups. Pups born to $Hp^{-/-}$ mothers exhibited delayed growth when compared to pups born to $Hp^{+/-}$ mothers. In addition, the hematological parameters of $Hp^{int/int}$ pups born to $Hp^{int/int}$ mothers indicated a more severe iron deficiency than in $Hp^{int/int}$ pups born to $Hp^{fl/fl}$ mothers. At UCB, all progeny born to $Hp^{-/-}$ and $Hp^{int/int}$ mothers, regardless of pup genotype (even $Hp^{fl/fl}$ pups), began to lose their truncal hair at about two weeks of age. A full recovery of hair typically occurred within 3-4 weeks after weaning. The degree of truncal hair loss was no greater in pups with knockout of HP, and thus the effect appeared to be due to a maternal factor. Several other genetic models of iron deficiency exhibit a similar phenotype, although in those models the phenotype has only been linked to the genotype of the affected mouse, not maternal genotype. These models include mice with tamoxifen-induced knockout of FPN1 before weaning, and mice with

disruption of *Tmprss6*, which leads to an overproduction of the iron absorption-blocking hormone hepcidin throughout life. In the latter strain, iron injections have been demonstrated to rescue the hair loss phenotype (Folgueras, de Lara et al. 2008). WT mice also can exhibit some mild hair loss when maintained for long periods on an iron-deficient diet. Together these data suggest that the hair loss in pups born to $Hp^{-/-}$ mothers is due to iron deficiency brought on by the inability of the mother to provide adequate iron for her pups. The mechanism by which iron deficiency leads to hair loss is unknown but may simply be due to a critical requirement for iron by the hair follicle that is not met in these models. The mechanism could also potentially involve inflammation, as the other few knockout mouse models reported to have a similar phenotype also had phenotypes related to inflammation. In one of these models, the phenotype was found to be reversed by topical application of aspirin (Wan, Saghatelian et al. 2007; Vanderford, Greer et al. 2010). Inflammation is known to affect iron metabolism so the relationship may be complex (Roy 2012).

Because the hair loss phenotype was seen in pups from both the $Hp^{-/-}$ and $Hp^{int/int}$ mothers, lack of HP expression specifically in the intestine of the mothers appears to be the major factor influencing this phenotype. The knockout mothers may provide inadequate iron to the fetus due to defects in their own ability to absorb iron from their intestine during pregnancy and/or nursing. There is some early evidence that the truncal hair loss is at least in part due to differences in the milk of $Hp^{-/-}$ versus WT mothers. In preliminary cross fostering studies performed by Erica Lachenauer and Julie Luong at UCB, WT and $Hp^{-/-}$ mothers were timed-mated with males with genotypes that matched the mother, and one half of the pups from each litter was switched to the other mother within three days of birth. All of the pups nursed by the WT mothers exhibited normal hair growth while all of the pups nursed by the $Hp^{-/-}$ mothers exhibited truncal hair loss.

Overall, fewer $Hp^{-/-}$ and $Hp^{int/int}$ mice were weaned than WT and $Hp^{fl/fl}$ littermate controls, but the difference was only significant in the $Hp^{int/int}$ mice. Mean lethality based on these results, and assuming no lethality in WT or $Hp^{fl/fl}$ littermates, was ~27% in both the $Hp^{int/int}$ mice (males and females) and $Hp^{-/-}$ males. There may not have been enough power in the $Hp^{-/-}$ mouse analyses to detect a difference in viability, as fewer mice were examined in these studies and female knockouts were compared with heterozygotes, which may have lower viability than WT females (not generated in this cross). Alternatively, it has been reported that global expression of Cre recombinase alone can cause embryonic anemia and lethality (Naiche and Papaloannou 2007). The villin-cre recombinase is expressed in intestinal progenitor cells and extraembryonic tissues during fetal development, but a survey of the literature found no reports that Cre recombinase expression alone in these tissues affects viability (el Marjou, Janssen et al. 2004). A recent study with controls expressing the villin-cre transgene did not find any evidence of lethality, but the total number of mice

examined was not reported (Zhong, Baker et al. 2012). Our breeding schemes did not generate littermates expressing Cre in the absence of *Heph* floxed alleles and Cre was not retained in any whole body knockout mice studied, so it is not possible to tell from our results if the expression of Cre itself, or Cre coupled with the effects of knockout of HP, explains the reduced viability. There also remains the remote possibility that ablation of HP during fetal development only in villin-expressing cells in $Hp^{int/int}$ mice, but not in all cells as in $Hp^{-/-}$ mice, could lead to increased lethality. The villin promoter has been shown to drive expression in extraembryonic tissues that could be important in the transfer of iron to the developing fetus, which is supported by the complete embryonic lethality observed in *Fpn1* floxed mice bearing the villin-cre recombinase transgene (el Marjou, Janssen et al. 2004; Donovan, Lima et al. 2005). It is not known whether HP plays a role at this stage. Iron trafficking in some tissues can involve multiple cell types, and disruption in only a subset could potentially affect iron flux in a more detrimental way than complete disruption.

A visiting collaborator, Yan Lu from Prof James Collins group at the University of Florida, examined the ferroxidase activity in $Hp^{-/-}$ enterocytes by a TF iron loading ferroxidase assay and found that levels in the cytosolic fraction were significantly lower than levels in WT littermates, but surprisingly no differences were seen in the activity in the membrane fraction. Although HP is detected by immunoblot in both fractions and appears to be of a similar molecular weight, HP is hypothesized to primarily exist in a membrane-bound form, and very little is known about the cytosolic form or how it is produced (Ranganathan, Lu et al. 2012; Ranganathan, Lu et al. 2012). The lack of a significant difference in ferroxidase activity in the membrane fraction could potentially be due to the harsher method used to prepare the membrane fraction than the cytosolic fraction. This could have destroyed the activity of HP in WT lysates. Studies are being performed currently to examine this. If the result is real, however, it suggests that another ferroxidase may make up the bulk of the activity on the membrane, or that another ferroxidase is induced in $Hp^{-/-}$ mice to levels that compensate for $Hp^{-/-}$. During the course of these investigations, APP was reported by another group to be a ferritin-like ferroxidase, and a literature search provided some evidence for expression of APP in enterocytes (Duce, Tsatsanis et al. 2010; Pallebage-Gamarallage, Galloway et al. 2012). APP exists in both a membrane bound form as well as a cytosolic form, and shows activity in TF iron loading ferroxidase assays. Studies are currently underway to measure the expression of APP in $Hp^{-/-}$ mice and controls and to determine if this protein is responsible for any of the ferroxidase activity in enterocytes. Because APP is also expressed in the liver and secreted into the serum like CP, we examined *App* and *Cp* mRNA levels in the liver and *App* mRNA levels in enterocytes by RT-qPCR in $Hp^{-/-}$ and control mice, but no significant differences were detected. Future studies at the protein and activity level are likely to be the most informative.

CHAPTER 3.

THE ROLE OF OTHER FERROXIDASES IN INTESTINAL IRON ABSORPTION AND METABOLISM

I. Rationale

The release of dietary iron from intestinal cells into the blood requires the iron transporter FPN1, as mice with postnatal ablation of FPN1 expression in the intestine alone are not able to absorb dietary iron and consequently develop very severe iron deficiency (Donovan, Lima et al. 2005). Several studies in other cell types have also indicated that FPN1 requires a ferroxidase in order to remain on the cell surface and properly export iron (Jeong and David 2003; De Domenico, Ward et al. 2007; Kono, Yoshida et al. 2010). As described in Chapter 2, however, knockout in mice of the only identified MCF expressed in intestinal enterocytes, HP, perturbed, but did not completely abolish, intestinal iron absorption. The survival and relatively mild phenotype of HP knockout mice indicates that another mechanism for iron absorption, ferroxidase mediated or not, must exist.

There are several known ferroxidases that could potentially be involved in intestinal iron absorption and that could partially compensate for the loss of HP in mice. The circulating MCF CP is a strong candidate as it has been shown to augment intestinal iron absorption in cases of extreme iron need (Cherukuri, Potla et al. 2005). CP also shares a high degree of sequence similarity with HP, co-immunoprecipitates with FPN1, and is known to play an iron release role in other cell types (Harris, Durley et al. 1999; Vulpe, Kuo et al. 1999; Jeong and David 2003). ZP, the only other known mammalian MCF besides HP and CP, is less likely to play a role in intestinal iron absorption than CP because no ZP expression has been detected in the small intestine or in serum (Chen, Attieh et al. 2010). Recently, APP has been reported to possess a ferritin-like ferroxidase activity and to interact with FPN1. Ablation of APP in neurons (which do not express CP or HP) led to reduced iron export. In addition, older APP knockout mice developed iron loading in tissues where APP is normally expressed (Duce, Tsatsanis et al. 2010). Because APP is present in the circulation and has been reported to be expressed in duodenal enterocytes, APP has the potential to play a role in intestinal iron absorption (Bush, Beyreuther et al. 1993; Zheng and Koo 2006; Pallebage-Gamarallage, Galloway et al. 2012).

To test the potential contribution of CP to intestinal iron absorption in mice lacking HP, we generated mice with genetic ablation of both ferroxidases ($Hp^{-/-}$ $Cp^{-/-}$ mice). A mouse model lacking CP and expressing only the *sla* mutant form of HP ($Hp^{sla/sla}$ $Cp^{-/-}$) was previously reported to be viable and to exhibit a tissue iron loading phenotype (Xu, Pin et al. 2004). However, no intestinal iron absorption studies were reported, and because the *sla* mutant may be a hypomorph and not equivalent to a null *Heph* allele, it was not possible to use that model to unequivocally determine if HP and CP together are required for intestinal iron absorption, or if not, the importance of the role of CP. In order to differentiate between phenotypes due to ablation in the intestine versus other tissues, we also generated a mouse model with whole body knockout of CP but knockout of HP only in the intestine ($Hp^{int/int}$ $Cp^{-/-}$). In addition, we generated mouse models with ablation of both HP and APP ($Hp^{-/-}$ $App^{-/-}$) and HP and ZP ($Hp^{-/-}$ $Zp^{-/-}$). Preliminary observations are reported here.

II. Methods

1. Generation of mouse models

$Hp^{-/-}$ $Cp^{-/-}$ mice were generated by crossing the $Hp^{-/-}$ mouse strain with the $Cp^{-/-}$ mouse strain (both described in Chapter 2) for several generations. $Hp^{int/int}$ $Cp^{-/-}$ mice were similarly created by crossing the $Hp^{int/int}$ mouse strain (described in Chapter 2) with the $Cp^{-/-}$ mouse strain. The $App^{-/-}$ $Hp^{-/-}$ and $App^{-/-}$ $Hp^{int/int}$ strains were created by crossing $App^{-/-}$ mice (from the colony of Professor Ashley Bush at the University of Melbourne, but originally obtained from The Jackson Laboratory, B6.129S7-App^{tm1Dbo}/J, stock #004133) with $Hp^{-/-}$ mice and $Hp^{int/int}$ mice, and then crossing the progeny.

As noted in Chapter 2, the gene encoding HP, *Heph*, is located on the X chromosome, and thus males only carry one *Heph* allele. For simplicity, all mice that are homozygous or hemizygous for a particular *Heph* allele, regardless of sex, are denoted here as "$Hp^{x/x}$", where "x" is the *Heph* allele they carry. For example, a male mouse with a knockout allele of *Heph* will be referred to as "$Hp^{-/-}$", as will a female with two *Heph* knockout alleles. The exceptions to this nomenclature, for simplicity, are wild-type mice, referred to as "WT", and mice homozygous or hemizygous for the *sla* allele of *Heph*, referred to as "*sla*". In addition, in some studies the littermates of mice with double knockout of two genes are referred to simply as "non-DKO".

Mice with a *Hephl1* floxed allele were commercially created for us by the UC Davis Mouse Biology Program. Exon 2 of the gene encoding ZP, *Hephl1*, was chosen for targeting because it is located near the start of the protein-coding region and encodes residues that make up the Type II Cu site required for ferroxidase activity. In addition, removal of exon 2 would lead to a frameshift that introduces an early stop codon. The targeting construct used to generate the

mice contained LoxP sites that flanked exon 2, a 11.5 kb 5' arm of homology (containing exon 1), a 11.2 kb 3' arm of homology (containing exons 3-6 and the 5' portion of exon 7), a Diphtheria Toxin A (DTA) cassette, and a Neomycin (neo) cassette flanked by FRT sites (Figure 3.1). C57BL/6N embryonic stem (ES) cells were microinjected with this targeting sequence and one clone was selected that successfully incorporated the targeting construct and had a high percentage of cells (88%) with the expected karyotype. The cells were injected into white BALB/c blastocysts and implanted into pseudo-pregnant females. Three high percentage chimeric males were generated (estimated 75-85% C57BL/6 cells based on coat color) and bred with wild-type C57BL/6 females. Black pups were genotyped and four females heterozygous for the *Hephl1* floxed allele and still bearing the FRT-flanked neo cassette ($Zp^{fl(neo)/+}$) were sent to QIMR.

In order to remove the neo cassette, the $Zp^{fl(neo)/+}$ females were crossed with a C57BL/6J mouse bearing the FlpE transgene ("FlpE" mouse, B6.Cg-Tg(ACTFLPe)9205Dym/J, The Jackson Laboratory) kindly provided by Dr. Ian Tonks at QIMR. When pups inherit a copy of the FlpE transgene, the FlpE recombinase protein is expressed and excises regions of DNA flanked by FRT sites, in this case the neo cassette. To make the *Hephl1* floxed strain, denoted as $Zp^{fl/fl}$, the $Zp^{fl/+}$ FlpE mice lacking neo were first bred with wild-type C57BL/6J mice, and then those containing a *Hephl1* floxed allele, but lacking the FlpE transgene ($Zp^{fl/+}$), were backcrossed onto the C57BL/6J strain for multiple generations until at least 97% C57BL/6J. These $Zp^{fl/+}$ mice were then bred together to generate $Zp^{fl/fl}$ mice.

To make a whole body ZP knockout strain, $Zp^{fl/fl}$ mice were bred with C57BL/6J mice bearing the Cre recombinase transgene driven by the eIIa promoter, which is ubiquitously active ("eIIa-cre" mice, B6.FVB-Tg(EIIa-cre)C5379Lmgd, The Jackson Laboratory). Expression of Cre recombinase leads to excision of the region in the DNA between the LoxP sites (exon 2 of *Hephl1*). Progeny containing both the eIIa-cre transgene and the *Hephl1* floxed allele ($Zp^{fl/+}$ EIIa) were then bred together and pups were selected for by genotyping that likely contained germline deletion of *Hephl1*. These mice were then backcrossed onto the C57BL/6J line to remove both the FlpE and eIIa-cre recombinase transgenes, and to generate mice at least 97% C57BL/6J and heterozygous for the Zp knockout allele ($Zp^{+/-}$). To generate ZP knockout mice ($Zp^{-/-}$), $Zp^{+/-}$ mice were then crossed. The Hp/Zp double knockout strain ($Hp^{-/-}$ $Zp^{-/-}$) was created by crossing the $Hp^{-/-}$ and $Zp^{-/-}$ strains and then crossing their progeny.

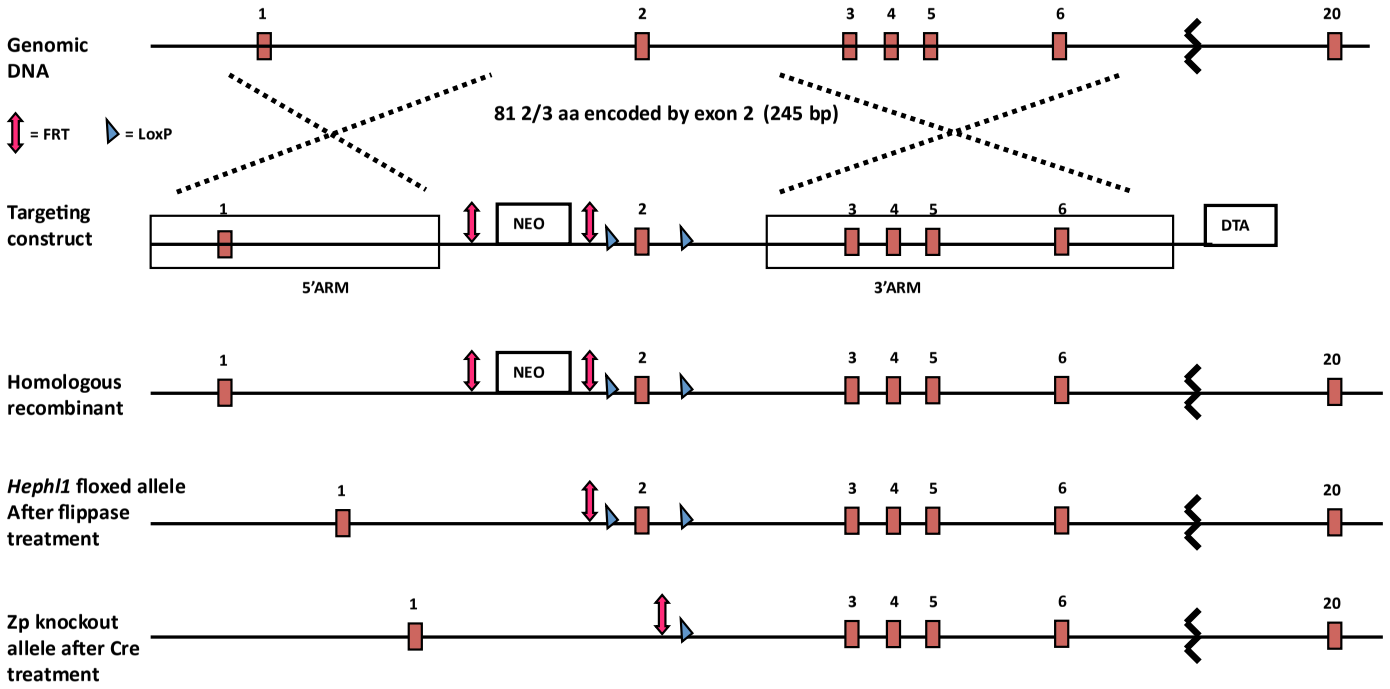

Figure 3.1. Generation of the floxed and knockout *Hephl1* alleles. The targeting construct contained LoxP sites that flanked exon 2, a 11.5 kb 5' arm of homology (containing exon 1), a 11.2 kb 3' arm of homology (containing exons 3-6 and 5'portion of exon 7), a Diphtheria Toxin A (DTA) cassette, and a Neomycin (neo) cassette flanked by FRT sites for selective deletion. The Neo element allowed for positive selection in ES cells, and the DTA element permitted negative selection in ES cells. After homologous recombination of the targeting construct to generate the *Hephl1* floxed allele in ES cells, chimeric mice were generated bearing the *Hephl1* floxed allele in their germline. Crossing a mouse with the *Hephl1* floxed allele with a mouse bearing the FlpE flippase transgene led to progeny with *Hephl1* floxed alleles lacking Neo. Deletion of exon 2 by breeding with mice bearing the ella-cre recombinase transgene created progeny with a frameshift in *Hephl1*, resulting in a premature stop and a predicted truncated protein of 71 amino acids, as compared to 1136 amino acids for WT, that should lead to gene inactivation. This inactivated *Hephl1* allele is called a Zp knockout allele. Adapted from a figure by the UC Davis Mouse Biology Program.

Tamoxifen-inducible FPN1 intestinal knockout mice ($Fpn^{fl/fl}$ vilERT2) were generated by Dr. Deepak Darshan at QIMR as previously described by crossing $Fpn^{fl/fl}$ mice (generated and kindly provided by Professor Nancy Andrew at Duke University in the US) with C56BL/6J mice bearing the vilERT2-cre recombinase transgene (Tg(Vil-cre/ERT2)23Syr) (Donovan, Lima et al. 2005). The vilERT2 mice were originally created by Dr. Sylvie Robine at the University Pasteur in France and were kindly provided to us by the laboratory of Professor Nicholas Davidson at Washington University in the US. The vilERT2-cre recombinase transgene produces a chimeric protein consisting of Cre recombinase fused to a modified estrogen receptor (ERT2) that is responsive to tamoxifen. The expression of this transgene is driven by the villin promoter and thus the chimeric protein is expressed constitutively in the intestine. However, the chimeric protein is retained in the cytosol due to the ERT2 domain. Administration of tamoxifen to a mouse with this transgene leads to translocation of the chimeric protein to the nucleus, where the Cre-recombinase portion can induce recombination of any floxed DNA, leading to targeted gene knockout (el Marjou, Janssen et al. 2004).

2. Animals

$Hp^{-/-}$ $Cp^{-/-}$ mice were studied at both the University of California, Berkeley (UCB) (Berkeley, California, USA) and at the Queensland Institute of Medical Research (QIMR) (Herston, Queensland, Australia). The $Hp^{int/int}$ $Cp^{-/-}$, $Zp^{-/-}$, $Hp^{-/-}$ $Zp^{-/-}$, $App^{-/-}$ $Hp^{int/int}$, and $App^{-/-}$ $Hp^{-/-}$ strains were generated and studied at QIMR. Unless otherwise noted, experimental results reported are from studies done at QIMR and with mice on a standard rodent chow diet containing ~160 ppm iron (Norco Stockfeeds, South Lismore, NSW, Australia). For studies done at UCB, mice were maintained on a standard rodent chow diet containing ~270 ppm iron (Harlan-Teklad, Indianapolis, IN). Iron-deficient or iron-loaded WT mice were used as assay controls in some experiments. Mice were iron overloaded by maintenance on an iron-loaded diet (1% carbonyl iron) for six weeks that was made in-house and described previously (Frazer, Vulpe et al. 2001). To make mice iron-deficient, mice were weaned onto an iron-deficient diet also made as described but without any iron. Mice were also put on an iron-deficient diet for one week prior to dosing in some iron absorption experiments as noted, and they were maintained on this diet until the end of the experiment. Mice fed the iron-deficient diet and/or dosed with ^{59}Fe were provided with iron-free deionized water and housed in grid-bottom cages designed to minimize coprophagia. All mice were allowed unlimited access to food and water. All mice were on the C57BL/6J background except the $Fpn^{fl/fl}$ vilERT2 mice, which were on a mixed background. For all experiments, littermate controls were used where possible, and, if not, age-matched controls or a mix of littermates and age matched controls were examined. All work performed was in accordance with NIH guidelines and with approval from the Office of Laboratory Animal Care at the University of California,

Berkeley and the Queensland Institute of Medical Research Animal Ethics Committee.

3. Tamoxifen-induced knockout of *Fpn1* in the intestine

Pups (~10-15 days old) resulting from crosses of a $Fpn^{fl/fl}$ female with a $Fpn^{fl/fl}$ vilERT2/+ male were injected once daily for four days with tamoxifen in order to induce intestinal knockout of *Fpn1* in the pups bearing the vilERT2 transgene (predicted to be 50% of all pups based on this cross). The tamoxifen solution was prepared fresh on the first day of injection by dissolving tamoxifen powder (Sigma, St. Louis, MO) in 100% ethanol to 50 mg/mL. The dissolved tamoxifen was then diluted to 8.3 mg/mL in sunflower seed oil (Sigma) to make the injection solution, and protected from light in a foil-wrapped tube. Mice were weighed and the injection site area on the upper back was wiped with 70% ethanol for sterilization. The tamoxifen solution was then injected subcutaneously at 0.075 mg tamoxifen/g body weight. The remaining tamoxifen solution was stored at 4°C, and then warmed by hand and vortexed to ensure solubilization prior to use on subsequent days. Mice were closely monitored for any adverse reactions.

4. Blood analyses

Blood collection was performed as described in Chapter 2. All blood was analyzed at the Pathology Department of the Royal Brisbane and Women's Hospital (Brisbane, Australia) using a Sysmex XE-5000 automated hematology analyzer (Roche Diagnostics, Castle Hill, NSW, Australia). The instrument used in these studies reports higher values overall for mean cell volume and platelets than the instruments used in Chapter 2, so these parameters and results derived from them (mean cell hemoglobin concentration) cannot be directly compared between the studies in the different chapters.

5. Iron absorption assays

Iron absorption was studied either by dosing by gavage, as described in Chapter 2, or by dosing via an isolated duodenal gut segment. The latter procedure has been previously described in experiments with rats (Frazer, Wilkins et al. 2003), and was modified slightly for mice. In brief, a mouse was placed in an induction chamber and anesthetized by inhalation of 2.5% isoflurane in oxygen, delivered at a flow rate of 2 L/min using a veterinary anesthetic machine (The Stinger™, Advanced Anaesthesia Specialists, Gladesville, NSW, Australia). The mouse was then removed from the chamber and placed ventral side up on a prewarmed (37°C) heating pad covered with two layers of benchcoat (one piece large enough to cover the whole heating pad, and another piece on top just larger than the mouse). The nose and mouth of the mouse were immediately placed inside a nose cone that was connected to a continuous flow of 1 L/min oxygen with 1.5% isoflurane anesthetic. Mice were monitored throughout the whole experiment to ensure adequate depth of anesthesia. After ensuring the mouse was

unresponsive to paw pinch, a midline incision was made in the abdomen. The duodenum was exposed and three loose ligatures were placed around it, with care taken to avoid positioning that could impair blood flow once the ligatures were tied. Two of the ligatures were placed approximately 0.5 cm distal to the pylorus and one at the ligament of Treitz. A small incision was made just proximal to the uppermost ligature, a cannula was inserted, and the upper ligature tied to secure the cannula. A second incision was then made just distal to the lowest ligature. The duodenal segment was flushed with 5 mL of saline solution (prewarmed to 37°C) via the cannula, and then the lower ligature was tightened. The duodenal segment was then infused with 100 µL of a freshly prepared solution containing 200 µM ferrous sulfate in 10 mM HCl and spiked with ~3 µCi ^{59}Fe radiolabeled iron (Perkin-Elmer, Waltham, MA, cat # NEZ037001MC) per dose. Next, the second ligature at the proximal end of the segment was tied off and the cannula removed. The abdomen of the animal was then covered with warm, damp gauze to prevent drying. Thirty minutes after the iron dose was administered, the duodenal segment was carefully excised and placed on a separate small piece of benchcoat (the benchcoat piece was checked later by counting to ensure that the duodenal gut segment had not leaked). The animal was then killed by cervical dislocation. The duodenal segment was cut open at both ends and washed extensively with 20 mL of saline. The wash solutions were recovered and saved for analysis. Any attached pancreas and mesentery were carefully trimmed from the exterior of the duodenal segment and placed on the benchcoat with the rest of the carcass. The duodenal segment was wrapped in a piece of foil. The whole liver was then excised from the carcass and wrapped in separate piece of foil. The rest of the carcass was then wrapped in the benchcoat piece under it and placed in a 50 mL tube. The radioactivity in the wash solution, the duodenal segment, the liver, and the remaining carcass was counted using a RAM DA Gamma Counter with a PM-11 tube at a distance of 10 cm, and background was subtracted. The total ^{59}Fe dose (total counts) was calculated as the sum of the counts in the wash, gut segment, liver, and remaining carcass. The percentage of the total dose retained in the gut segment was calculated by dividing the counts in the gut segment by the total counts and multiplying by 100. The transferred dose was defined as the total number of counts in the liver and remaining carcass, i.e. the iron that had been transferred out of the gut segment to the rest of the body. The percentage of the transferred dose in the liver was calculated by dividing the counts in the liver by the sum of the counts in the liver and the rest of the carcass, and then multiplying by 100.

6. Energy expenditure pilot study

Vertical and horizontal movement, oxygen consumption (Δ $\%O_2$), carbon dioxide production (Δ $\%CO_2$), and water consumption were measured over 24 hours using the Comprehensive Laboratory Animal Monitoring System (CLAMS;

Columbus). In brief, mice were weighed and then housed singly in individual airtight center-feeder style cages in a temperature-controlled room with a continuous 12 hour on, 12 hour off light/dark cycle beginning with lights on at 07:00. Vertical and horizontal movements were measured by the number of times the mouse interrupted invisible infrared beams. The differences in the percentage of oxygen and carbon dioxide in the input and output airflow were automatically calculated by the CLAMS OxyMax software. The water consumed and the heat (kilocalories/hour) generated by each mouse was also calculated by the software as described by the manufacturer (Columbus Instruments 2012). Water and food was provided ad libitum.

7. Other assays and statistical analyses

Tissue collection, PCR genotyping, mRNA analyses, tissue iron staining, quantitative tissue iron measurements, and statistical analyses were performed as described in Chapter 2.

III. Results

1. Viability and general phenotype of $Hp^{-/-}$ $Cp^{-/-}$ and $Hp^{int/int}$ $Cp^{-/-}$ mice

$Hp^{-/-}$ $Cp^{-/-}$ and $Hp^{int/int}$ $Cp^{-/-}$ mice were successfully generated and were viable, but more litters will need to be examined to determine if these pups are weaned at ratios that are statistically the same as expected. Males of both strains were fertile. The fertility of female $Hp^{-/-}$ $Cp^{-/-}$ and $Hp^{int/int}$ $Cp^{-/-}$ mice was not tested, but $Hp^{+/-}$ $Cp^{-/-}$ and $Hp^{-/-}$ $Cp^{+/-}$ females were fertile. The few $Hp^{-/-}$ $Cp^{-/-}$ mice generated but not sacrificed died unexpectedly between 23-30 weeks of age of unknown causes. Early lethality has also been reported in $Hp^{sla/sla}$ $Cp^{-/-}$ mice (Hahn, Qian et al. 2004). No abnormal lethality was observed in adult $Hp^{int/int}$ $Cp^{-/-}$ mice.

$Hp^{-/-}$ $Cp^{-/-}$ mice had overt visible signs of a severe anemia starting before weaning and could be easily distinguished by eye from littermates throughout their lifespan. The mice had pale skin, which was readily detectable by examining the paws and feet (Figure 3.2). The urine of the $Hp^{-/-}$ $Cp^{-/-}$ mice, like that of WT mice made severely iron-deficient by an iron-deficient diet, was clear instead of yellow. While WT, $Hp^{-/-}$, and $Cp^{-/-}$ littermates developed yellow to brown iron deposits on their teeth, the teeth of $Hp^{-/-}$ $Cp^{-/-}$ mice remained white. Unlike the $Hp^{-/-}$ $Cp^{-/-}$ mice, however, $Hp^{int/int}$ $Cp^{-/-}$ mice could not be reliably distinguished by eye from their littermates by examining their paws or teeth (although some were noted to have lighter teeth and paler paws than littermates), suggesting a milder phenotype (data not shown).

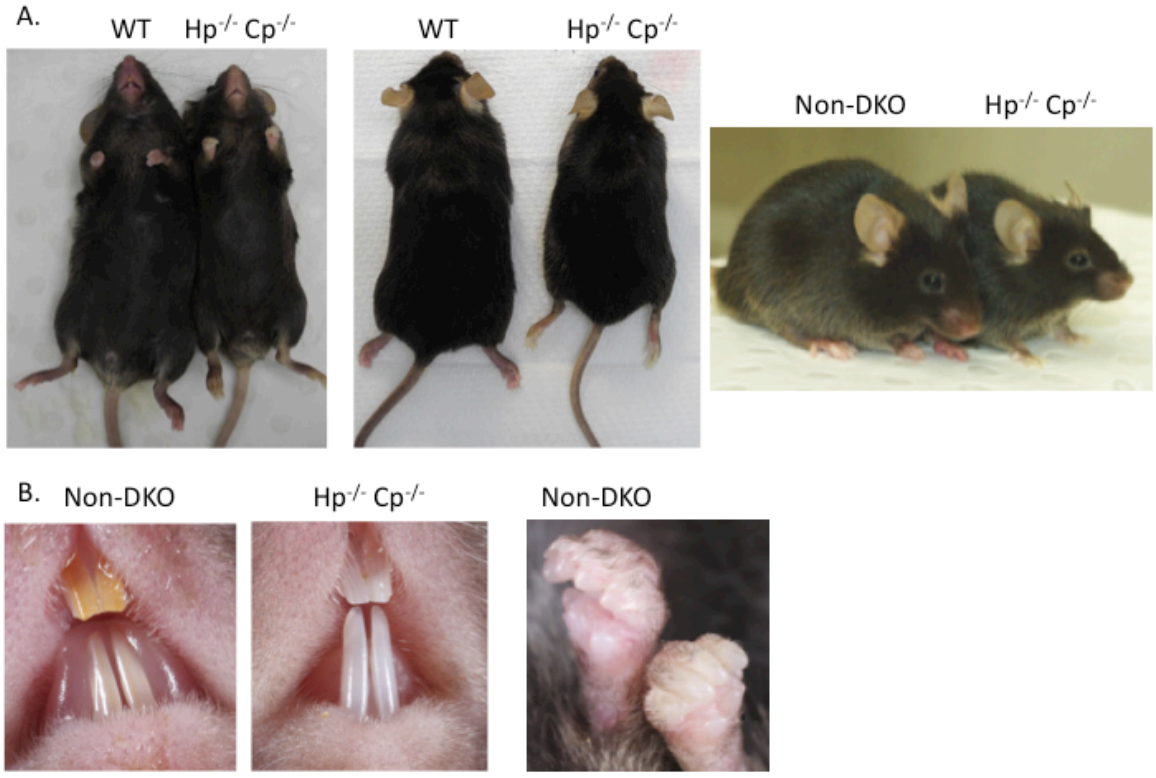

Figure 3.2. Comparative photographs of adult age and sex-matched pairs of $Hp^{-/-}$ $Cp^{-/-}$ mice and controls. **A.** Whole body comparisons, 17-20 week old males. **B.** Close-up of teeth and front paws of 9-11 week old female littermates.

Weights of male $Hp^{-/-}$ $Cp^{-/-}$ mice and non-DKO littermates were measured from 3-10 weeks of age, and $Hp^{-/-}$ $Cp^{-/-}$ mice weighed less than their non-DKO littermates, with the difference becoming significant at five weeks of age (Figure 3.3). The rate of growth of the male $Hp^{-/-}$ $Cp^{-/-}$ mice was slower than that of the male non-DKO littermates until approximately 8 weeks of age, when the rates became similar. Based on preliminary data with animals at ages up to 24 weeks, male $Hp^{-/-}$ $Cp^{-/-}$ mice never catch up in weight and can be generally distinguished by eye from their male non-DKO littermates by size, in addition to pallor (data not shown). The weights of age-matched $Hp^{-/-}$ $Cp^{-/-}$, $Hp^{int/int}$ $Cp^{-/-}$, and littermate non-DKO males and females at 9-11 weeks of age, as well as WT males that had been maintained on an iron-deficient diet since weaning, were also examined. For the males, no significant differences were detected in the weights of $Hp^{int/int}$ $Cp^{-/-}$ mice and controls, but $Hp^{-/-}$ $Cp^{-/-}$ mice weighed significantly less than non-DKO controls and were similar in weight to WT males with severe diet-induced iron deficiency. No significant differences were detected in average weight in any

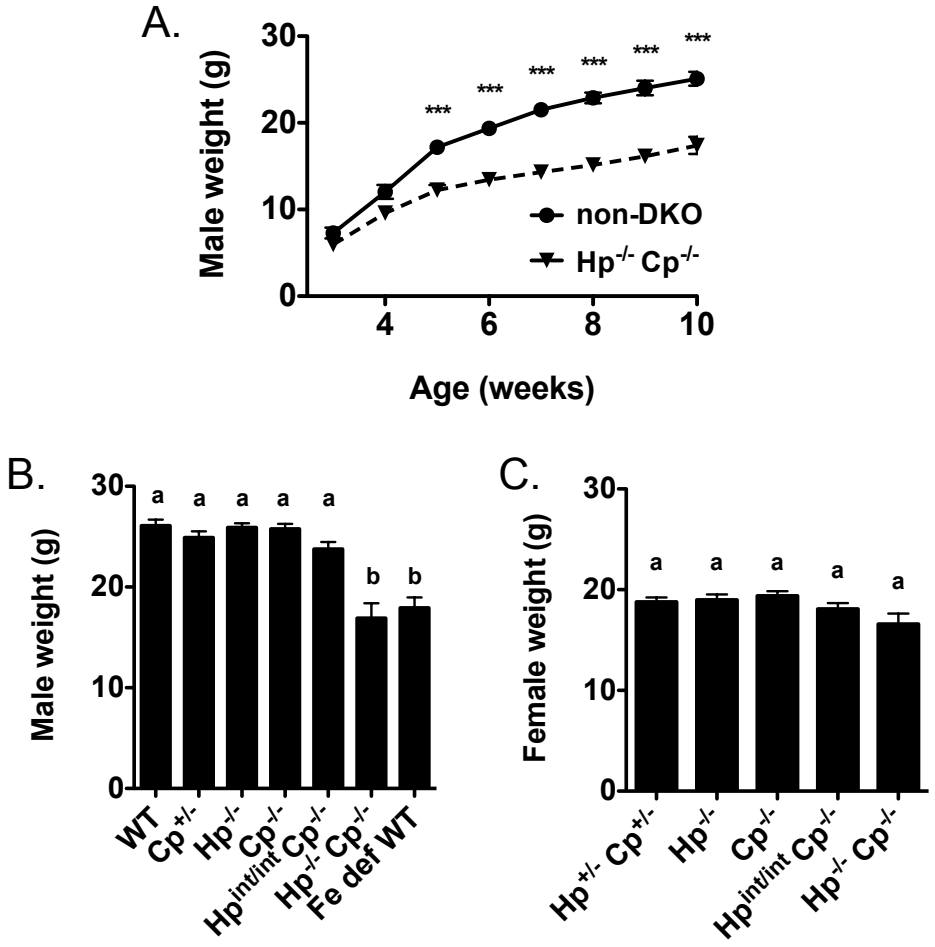

Figure 3.3. Weights of $Hp^{-/-}$ $Cp^{-/-}$, $Hp^{int/int}$ $Cp^{-/-}$, and littermate mice. A. Average weight timecourse for $Hp^{-/-}$ $Cp^{-/-}$ and non-DKO littermate male mice ($Hp^{-/-}$, WT, $Cp^{+/-}$, and $Cp^{-/-}$). N = 4-17 mice per age per group. **B.** Average weights of adult (9-11 week old) males measured at a single time point. N = 4-16 mice per genotype. **C.** Average weights of adult (9-11 week old) females measured at a single time point. N = 3-12 mice per genotype. All mice were maintained on a chow diet except for the Fe deficient WT mice (Fe def WT). Controls on the chow diet in panels B and C are a mix of littermates of the $Hp^{-/-}$ $Cp^{-/-}$ and $Hp^{int/int}$ $Cp^{-/-}$ mice, with floxed alleles considered as WT. Mean ± SEM. Significance was determined by t-test (panel A, *** $P \leq 0.001$) and by one-way ANOVA followed by Tukey's post test (panels B and C; groups with shared letters are not significantly different) using GraphPad Prism.

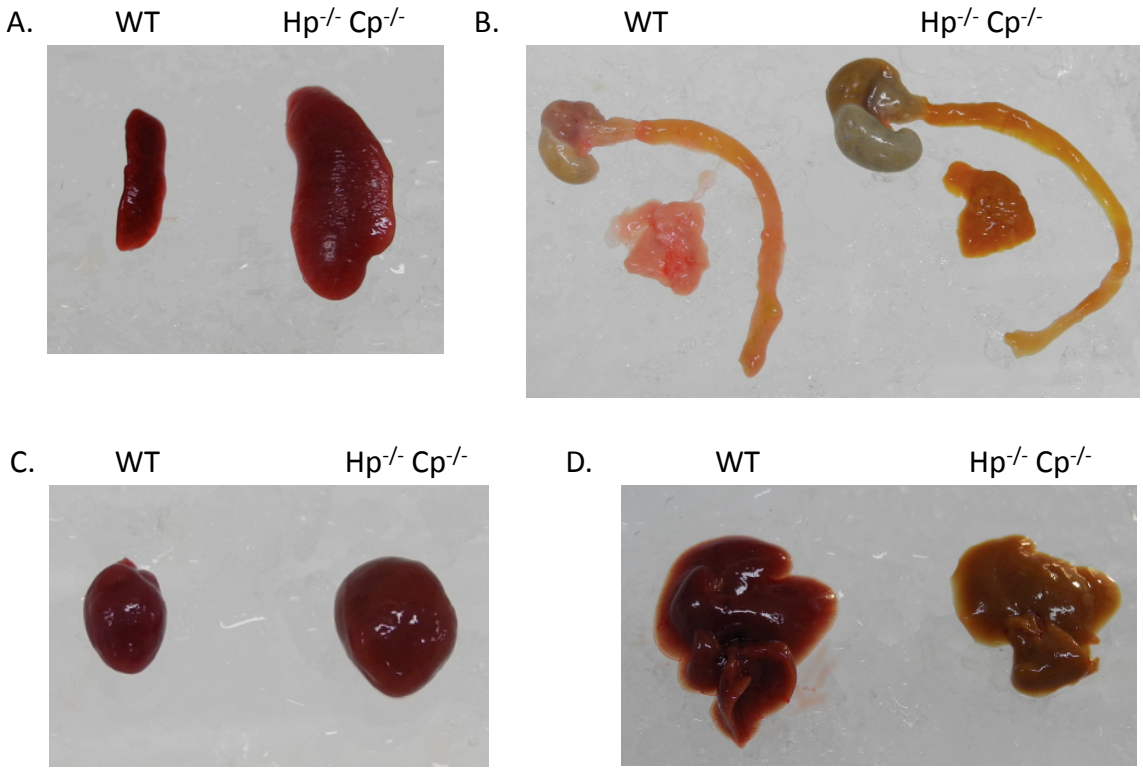

Figure 3.4. Comparative photographs of male 20-23 week old WT (left) and $Hp^{-/-}$ $Cp^{-/-}$ (right) mouse tissues. **A.** Spleen. **B.** Stomach, duodenum, and pancreas. **C.** Heart. **D.** Liver.

female genotypes, however, although the sample size of female $Hp^{-/-}$ $Cp^{-/-}$ mice (N = 3) was low.

All $Hp^{-/-}$ $Cp^{-/-}$ mice examined at 9-11 and 20-23 weeks of age had pale blood and pale, grossly enlarged hearts and spleens, similar to what was observed in mice with diet-induced iron-deficiency and consistent with severe anemia (Figure 3.4). The pancreatic tissue of the mice was a marked bronze color, in clear contrast to the light tan color observed in WT, $Hp^{-/-}$, and $Cp^{-/-}$ controls, and similar to the color in diet-induced iron-overloaded mice (data not shown). Some $Hp^{-/-}$ $Cp^{-/-}$ mice at 20-23 weeks of age appeared to have gastromegaly, although cleaned stomach weights were not measured and this could have been simply due to more food in the stomach. There were no marked differences in the size of the hearts and spleens of $Hp^{int/int}$ $Cp^{-/-}$ mice compared to controls, and no obvious differences in the color of the blood or pancreas (data not shown). Of note, two of the 11 adult $Hp^{-/-}$ $Cp^{-/-}$ mice sacrificed, and one of the 11 adult $Hp^{int/int}$ $Cp^{-/-}$ mice sacrificed, had one necrotic, fluid-filled kidney. This had not been observed in any other mice in our colony.

2. Hematology

Blood parameters were examined in both male and female $Hp^{-/-}$ $Cp^{-/-}$ and $Hp^{int/int}$ $Cp^{-/-}$ and littermate controls at 9-11 weeks of age (Figures 3.5 and 3.6) and male mice at 20-23 weeks of age (Figure 3.7). Male mice made iron-deficient by dietary means were also included for comparison, but these were not littermates. $Hp^{int/int}$ littermate controls were not generated in the crosses made and thus were not available for comparison. At both ages examined, $Hp^{-/-}$ $Cp^{-/-}$ mice had a very severe hypochromic, microcytic anemia similar to that of the severely iron-deficient WT mice. They had less than half the number of red cells and the cells were significantly smaller than all littermate controls, leading to a greatly reduced hematocrit. Total hemoglobin levels were less than a third of that of controls. Due to the much smaller size of the red cells, the average concentration of hemoglobin in each cell was not significantly different than that of controls at 9-11 weeks of age. However, by 20-23 weeks of age, mean cell hemoglobin concentration had dropped to levels significantly lower than controls. No reticulocytes were detected in any $Hp^{-/-}$ $Cp^{-/-}$ mice examined, indicating that the mice possessed little capacity to generate new red cells. Platelet levels were, on average, over 10 times that of controls. The serum of $Hp^{-/-}$ $Cp^{-/-}$ mice was also noted to be a clear yellow, in contrast to the clear but lighter straw-colored serum of $Cp^{-/-}$, $Hp^{-/-}$, WT and iron-deficient controls. $Hp^{int/int}$ $Cp^{-/-}$ mice were anemic at 9-11 weeks, but the anemia was much less severe than in the $Hp^{-/-}$ $Cp^{-/-}$ mice. Although $Hp^{int/int}$ $Cp^{-/-}$ mice had significantly smaller and fewer red cells, a lower hematocrit, and less hemoglobin than WT controls, only female mice were significantly different in any parameters from their $Cp^{-/-}$ littermates, which have been reported previously to exhibit a mild anemia (Cherukuri, Tripoulas et al. 2004). Plasma iron levels were also analyzed by a visiting collaborator, Pavle Matak, in adult $Hp^{-/-}$ $Cp^{-/-}$ mice (N = 7) and WT controls (N = 5) and found to be approximately three times lower in the $Hp^{-/-}$ $Cp^{-/-}$ mice. Plasma iron levels were 4.8 ± 0.8 µmol/L in $Hp^{-/-}$ $Cp^{-/-}$ mice and 15.8 ± 1.2 µmol/L in controls.

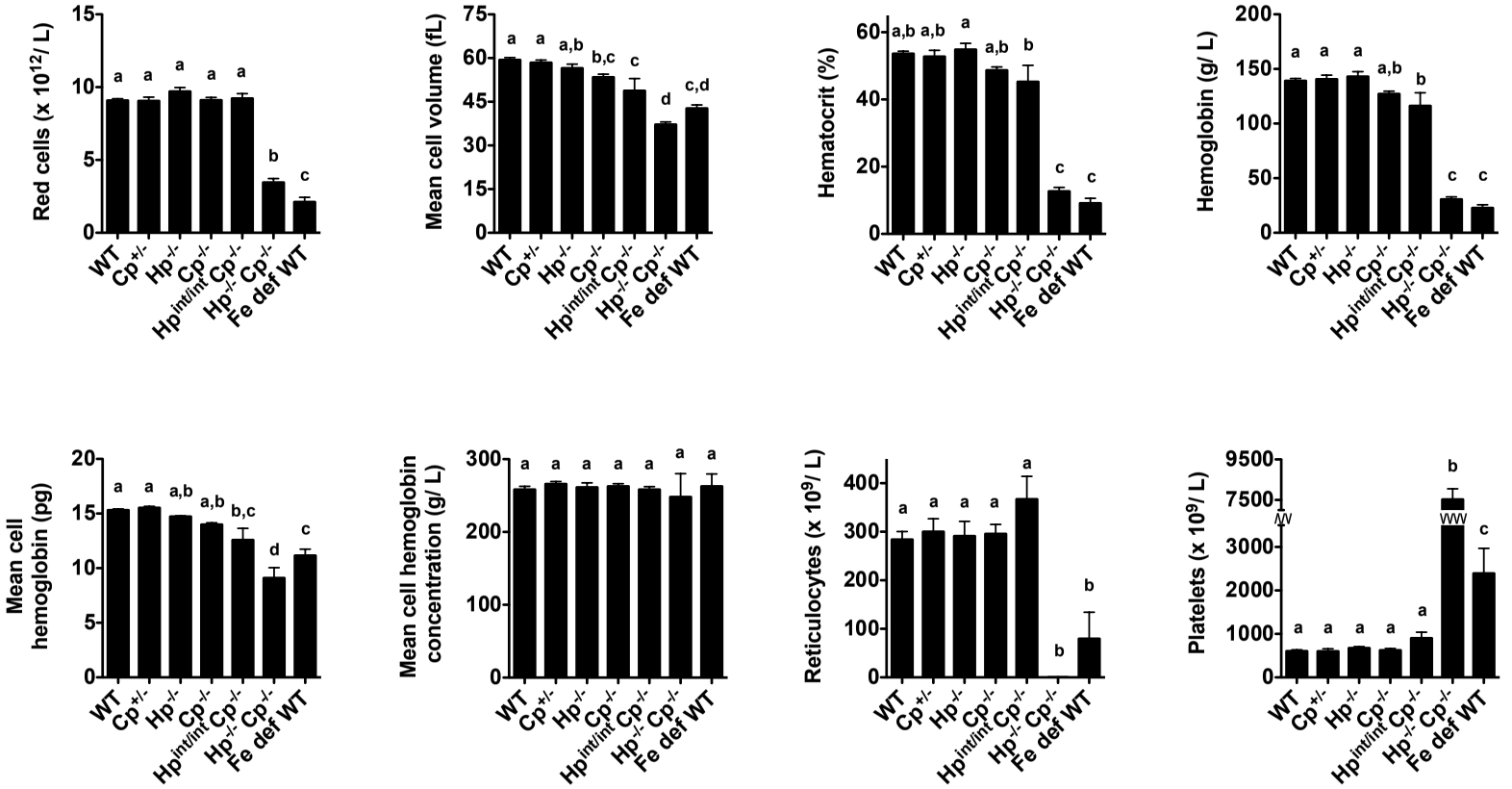

Figure 3.5. Hematology of 9-11 week old male littermates on a chow diet, and 16-17 week old WT mice fed an iron-deficient diet since wean (Fe def WT). Mean ± SEM. WT (N = 8), $Hp^{-/-}$ (N = 6), $Cp^{-/-}$ (N = 12), $Hp^{int/int}$ $Cp^{-/-}$ (N = 4), $Cp^{+/-}$ (N = 9), $Hp^{-/-}$ $Cp^{-/-}$ (N = 6), Fe def WT (N = 7). Groups with shared letters are not significantly different as determined by one-way ANOVA followed by Tukey's post test using GraphPad Prism.

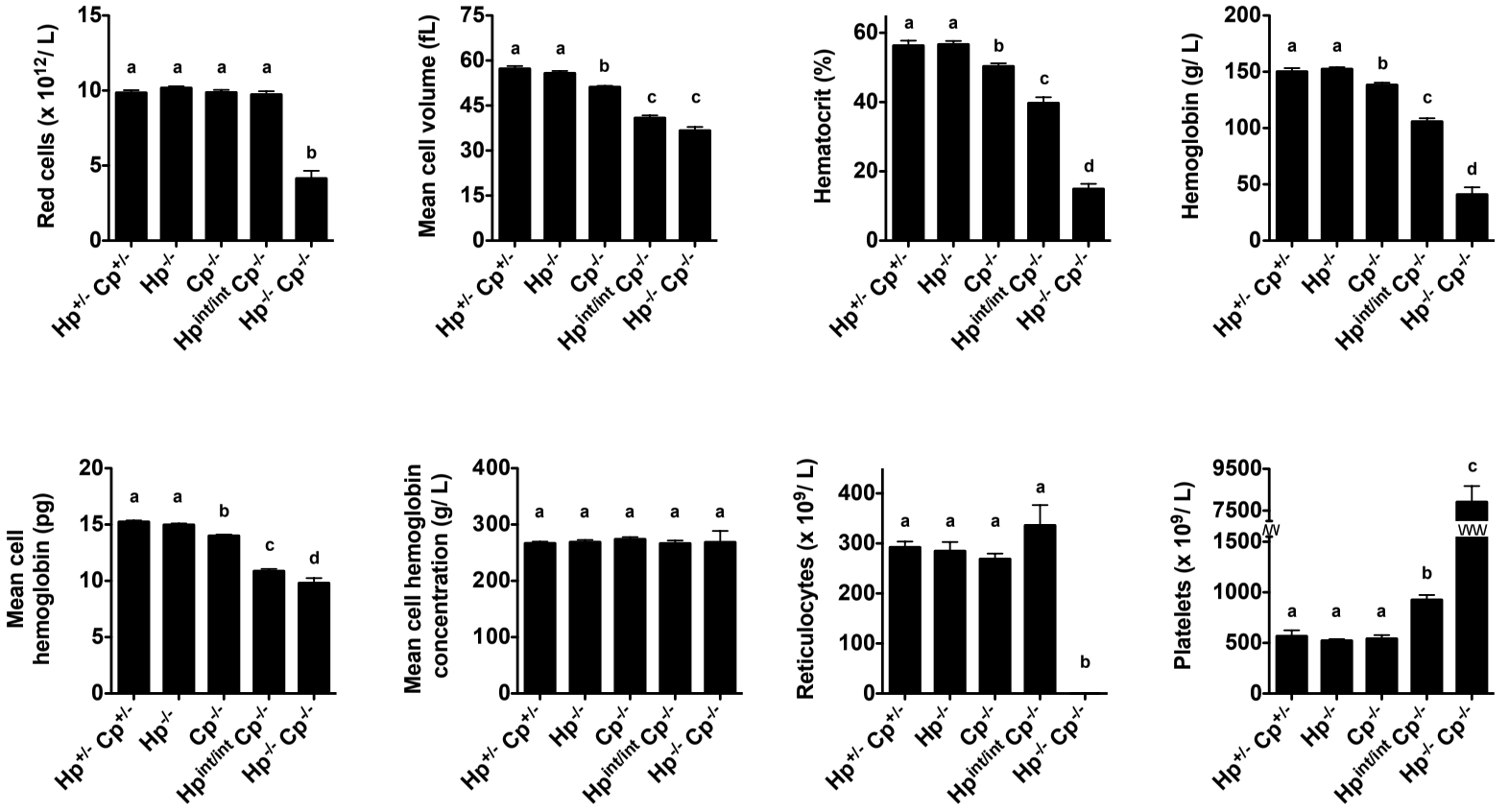

Figure 3.6. Hematology of 9-11 week old female littermates on a chow diet. Mean ± SEM. $Hp^{+/-}$ $Cp^{+/-}$ (N = 12), $Hp^{-/-}$ (N = 9), $Cp^{-/-}$ (N = 6), $Hp^{int/int}$ $Cp^{-/-}$ (N = 7), and $Hp^{-/-}$ $Cp^{-/-}$ (N = 3). Groups with shared letters are not significantly different as determined by one-way ANOVA followed by Tukey's post test using GraphPad Prism.

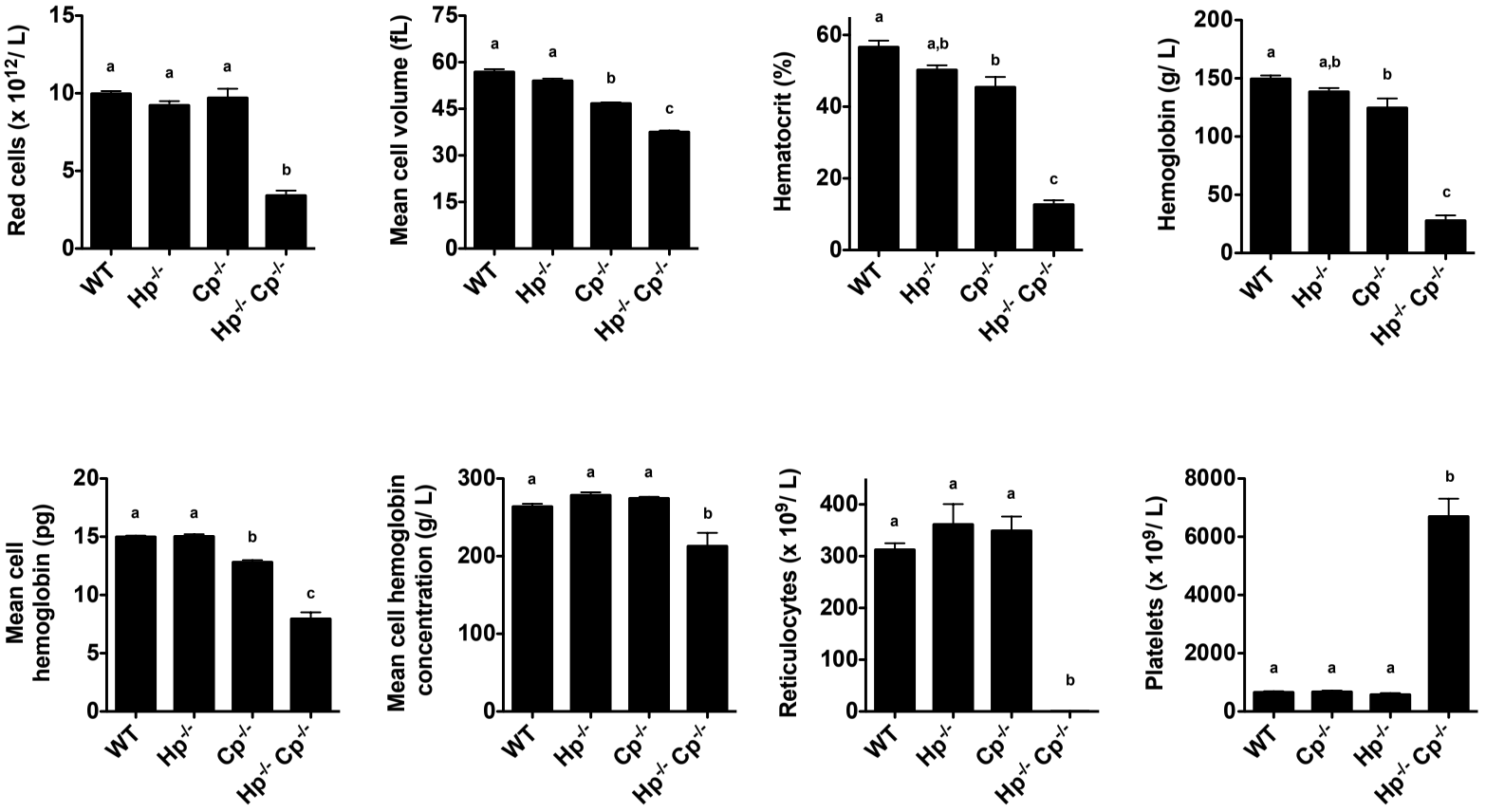

Figure 3.7. Hematology of 20-23 week old male littermates and age-matched controls on a chow diet. Mean ± SEM. WT (N = 8), $Hp^{-/-}$ (N = 4), $Cp^{-/-}$ (N = 7), and $Hp^{-/-}$ $Cp^{-/-}$ (N = 6). Groups with shared letters are not significantly different as determined by one-way ANOVA followed by Tukey's post test using GraphPad Prism.

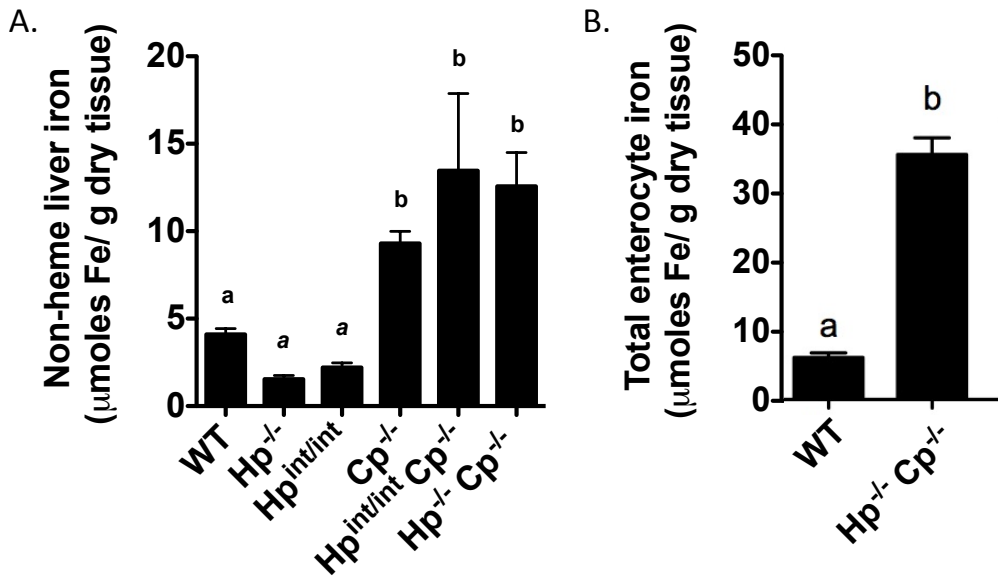

Figure 3.8. Liver and duodenal enterocyte iron in adult male mice. **A.** Non-heme iron in dried liver tissue was measured by a colorimetric assay. Mice were age-matched adult (9-11 weeks old) male WT (WT: N = 11, pooled with $Hp^{fl/fl}$: N = 6), $Hp^{-/-}$ (N = 10), $Hp^{int/int}$ (N = 6), $Cp^{-/-}$ (N = 16), $Hp^{int/int}$ $Cp^{-/-}$ (N = 4), and $Hp^{-/-}$ $Cp^{-/-}$ (N = 6) littermates. **B**. Total iron in dried duodenal enterocytes was measured by atomic absorption spectroscopy. Mice were age-matched adult male WT (N = 6) and $Hp^{-/-}$ $Cp^{-/-}$ littermates (N = 6). Data for enterocytes was collected by Pavle Matak. Mean ± SEM. Groups with shared letters are not significantly different as determined by one-way ANOVA followed by Tukey's post test (panel A) and by t-test (panel B) using GraphPad Prism. Groups with letters in italics (panel A) are significantly different than groups with the same letter without italics ($P \leq 0.01$) when examined by t-test; the one-way ANOVA analysis has less power due to the smaller number of mice in the $Hp^{int/int}$ $Cp^{-/-}$ group.

3. Tissue iron

Non-heme liver iron in 9-11 week old males, as measured by colorimetric assay, was significantly greater in all mice with knockout of CP, relative to WT, $Hp^{-/-}$, and $Hp^{int/int}$ littermate controls. No significant differences were seen between the liver iron levels in $Cp^{-/-}$, $Hp^{int/int}$ $Cp^{-/-}$ and $Hp^{-/-}$ $Cp^{-/-}$ mice (Figure 3.8). Females at this age with knockout of CP were noted to have approximately twice the amount of liver iron as males (data not shown), potentially because females are smaller and do not have to utilize as much of their iron stores for growth. Pavle Matak measured total iron by atomic absorption spectroscopy in adult $Hp^{-/-}$ $Cp^{-/-}$ and WT duodenal enterocytes and found that levels were greater in $Hp^{-/-}$ $Cp^{-/-}$ enterocytes than controls (Figure 3.8).

A panel of tissues (duodenum, jejunum, ileum, liver, spleen, pancreas, lung, gonad, heart, kidney, brown fat, white fat, adrenal gland) was collected, paraffin

processed, and stained for ferric iron by the Perls' Prussian Blue method, which is semi-quantitative. Tissues were examined from at least four mice (littermates and age matched) at 9-11 weeks of age per genotype per sex. As reported in Chapter 2, strong iron loading was observed in duodenal enterocytes of $Hp^{-/-}$ mice, especially at the villus tips. Little to no staining was observed in WT controls and $Cp^{-/-}$ enterocytes, but strong staining was seen in all $Hp^{int/int}$ $Cp^{-/-}$ and $Hp^{-/-}$ $Cp^{-/-}$ samples (Figure 3.9), consistent with HP ablation in enterocytes in these mice. In the liver, the staining results were generally in agreement with the non-heme liver iron assay findings, with WT and $Hp^{-/-}$ mice showing the lowest levels of staining, and $Cp^{-/-}$, $Hp^{int/int}$ $Cp^{-/-}$, and $Hp^{-/-}$ $Cp^{-/-}$ mice showing greater staining, although staining appeared more intense in most $Hp^{int/int}$ $Cp^{-/-}$ and $Hp^{-/-}$ $Cp^{-/-}$ livers as compared to $Cp^{-/-}$ livers (Figure 3.10). A pilot study with DAB-enhanced Perls' staining revealed some finer detail (Figure 3.11). Staining appeared to be primarily localized in the regions proximal to the portal tract, with some evidence of Kuppfer cell iron loading in the $Cp^{-/-}$ mice. In summary, all mice with HP knockout in the intestine showed iron loading in that tissue, and all mice with CP knockout (global) showed iron loading in the liver.

In the spleen, punctate iron deposits were seen in the white pulp in WT and $Cp^{-/-}$ mice, and to a lesser extent in $Hp^{-/-}$ mice. Strong iron deposits were also seen in 12-week old control WT mice that had been maintained on an iron-loaded diet (1% carbonyl iron) for six weeks. However, no iron staining was apparent in the spleens of any $Hp^{int/int}$ $Cp^{-/-}$ mice or $Hp^{-/-}$ $Cp^{-/-}$ mice (Figure 3.12). The $Hp^{-/-}$ $Cp^{-/-}$ mice, but no other mice, showed iron deposits in the heart, exocrine pancreas, and kidney. Some, but not all (likely due to the cut orientation) $Hp^{-/-}$ $Cp^{-/-}$ mice had a defined ring of iron loading in the adrenal gland as well (Figures 3.13-3.16). No iron staining was observed in mice from any groups at 9-11 weeks of age in the skin, jejunum, ileum, lung, gonad, brown fat, or white fat (data not shown). In addition, skin, tongue, colon, cecum, stomach, and skeletal muscle were also examined in two $Hp^{-/-}$ $Cp^{-/-}$ mice and no staining was observed. Females showed similar overall staining patterns to males (data not shown). A small study of tissues (liver, pancreas, brown fat, duodenum, jejunum, ileum, lungs, spleen, and heart) from 20-23 week old WT, $Hp^{-/-}$, $Cp^{-/-}$, and $Hp^{-/-}$ $Cp^{-/-}$ males showed similar results as seen in the 9-11 week old mice, although the iron loading in the exocrine pancreas of the $Hp^{-/-}$ $Cp^{-/-}$ mice was much more pronounced at this age (Figure 3.17).

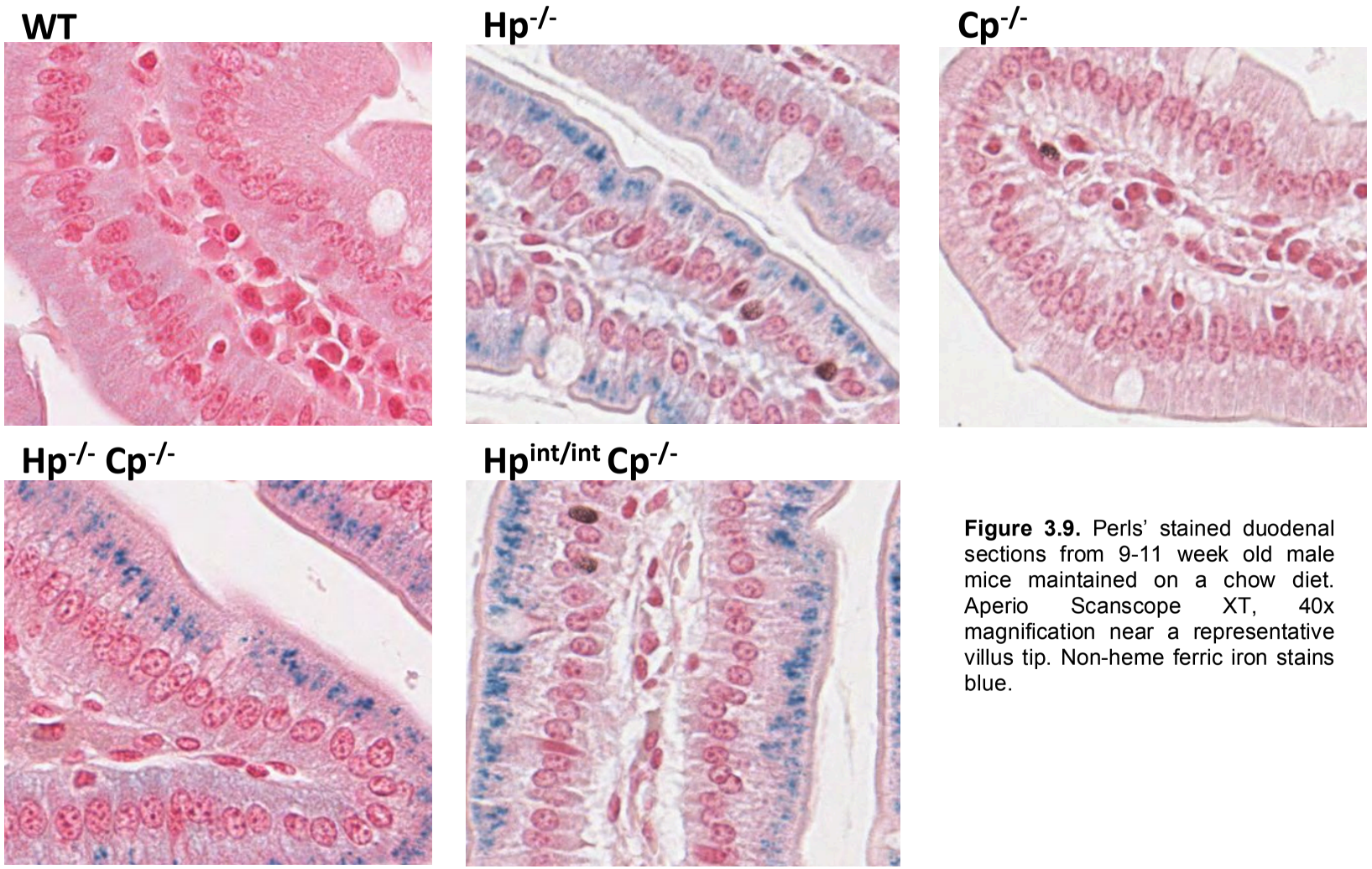

Figure 3.9. Perls' stained duodenal sections from 9-11 week old male mice maintained on a chow diet. Aperio Scanscope XT, 40x magnification near a representative villus tip. Non-heme ferric iron stains blue.

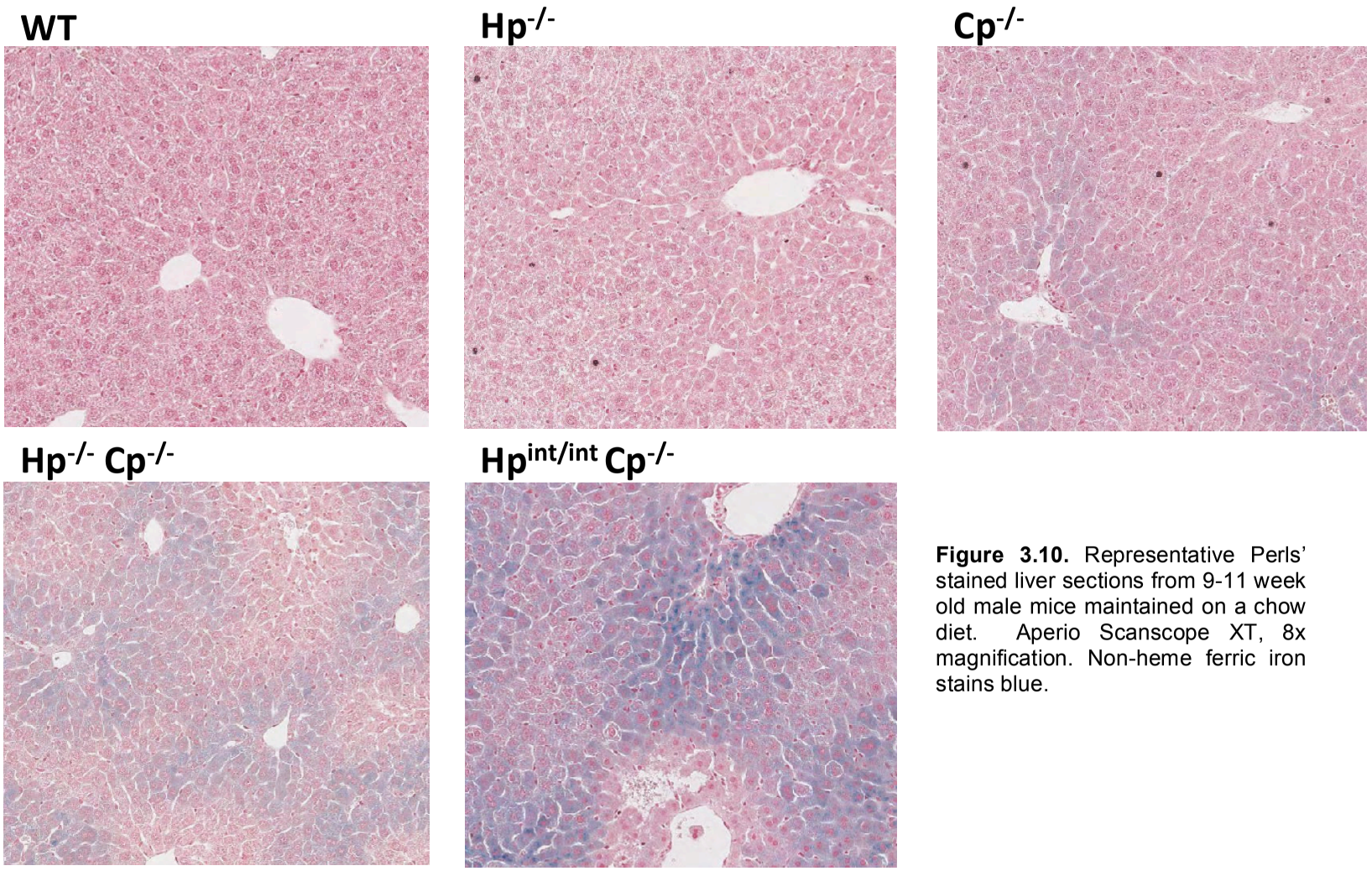

Figure 3.10. Representative Perls' stained liver sections from 9-11 week old male mice maintained on a chow diet. Aperio Scanscope XT, 8x magnification. Non-heme ferric iron stains blue.

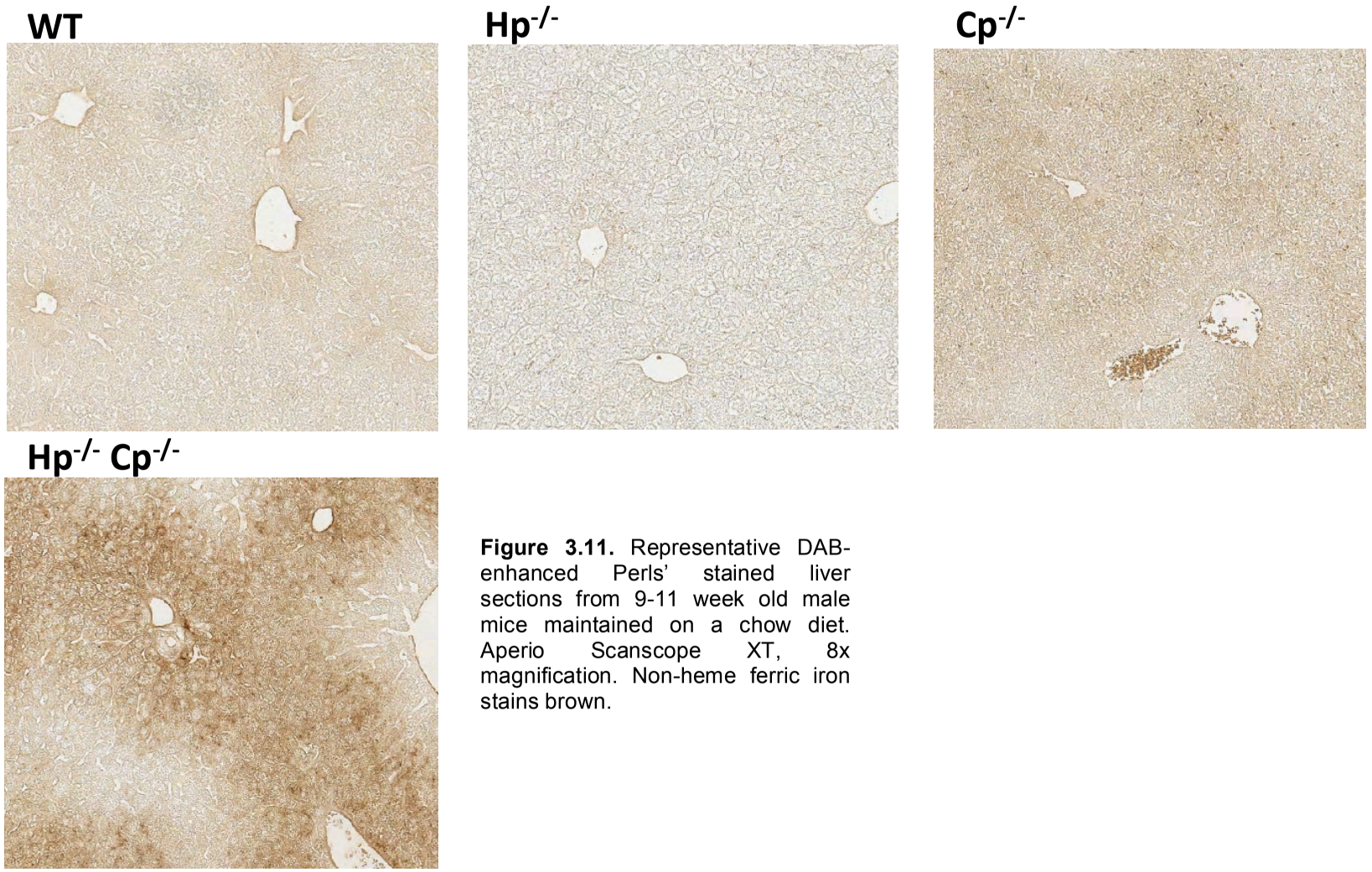

Figure 3.11. Representative DAB-enhanced Perls' stained liver sections from 9-11 week old male mice maintained on a chow diet. Aperio Scanscope XT, 8x magnification. Non-heme ferric iron stains brown.

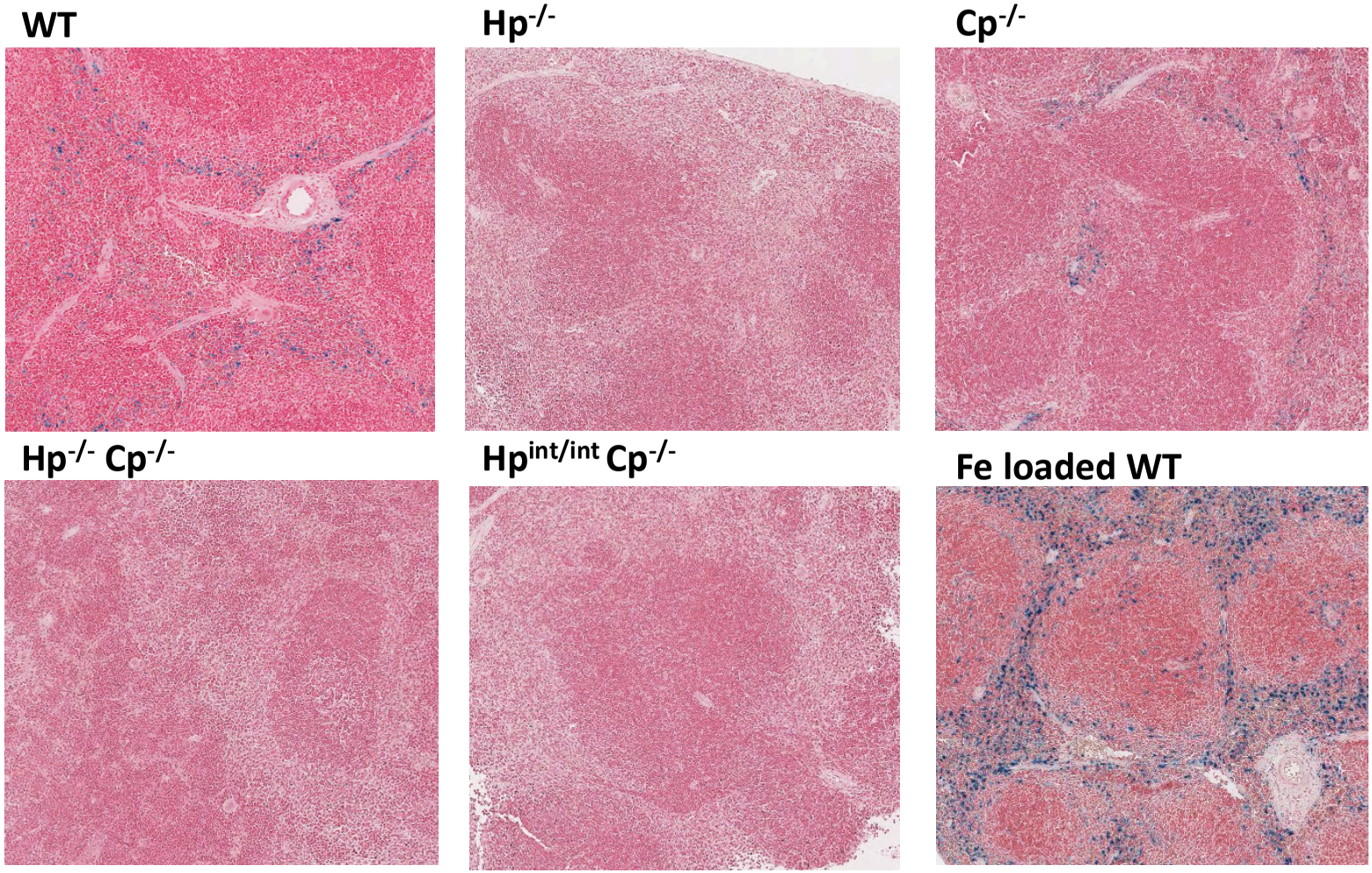

Figure 3.12. Representative Perls' stained spleen sections from 9-11 week old male mice maintained on a chow diet, as well as a 12 week old WT male mouse maintained on an iron-loaded (1% carbonyl) diet for six weeks (Fe loaded WT). Aperio Scanscope XT, 5x magnification. Non-heme ferric iron stains blue.

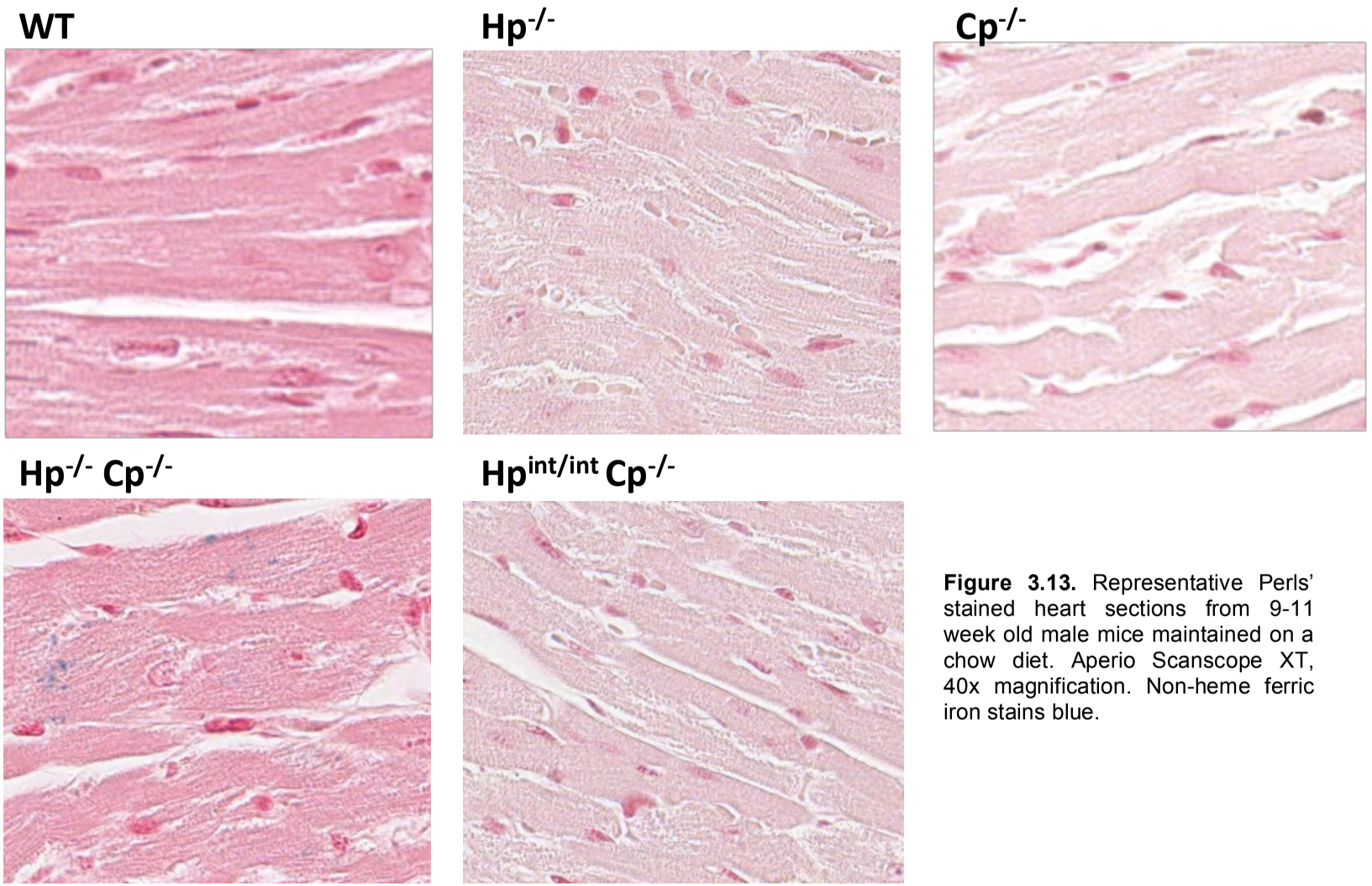

Figure 3.13. Representative Perls' stained heart sections from 9-11 week old male mice maintained on a chow diet. Aperio Scanscope XT, 40x magnification. Non-heme ferric iron stains blue.

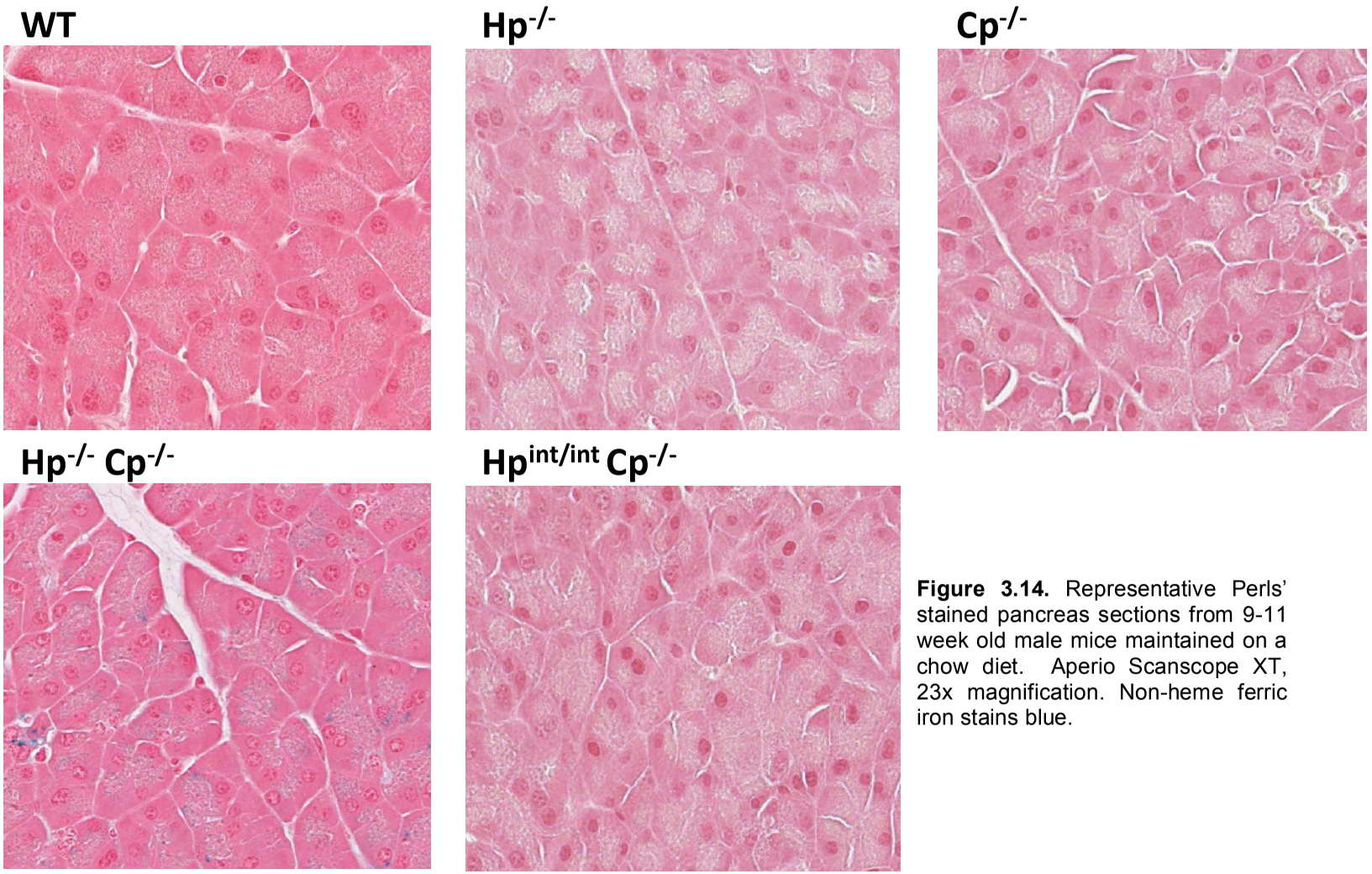

Figure 3.14. Representative Perls' stained pancreas sections from 9-11 week old male mice maintained on a chow diet. Aperio Scanscope XT, 23x magnification. Non-heme ferric iron stains blue.

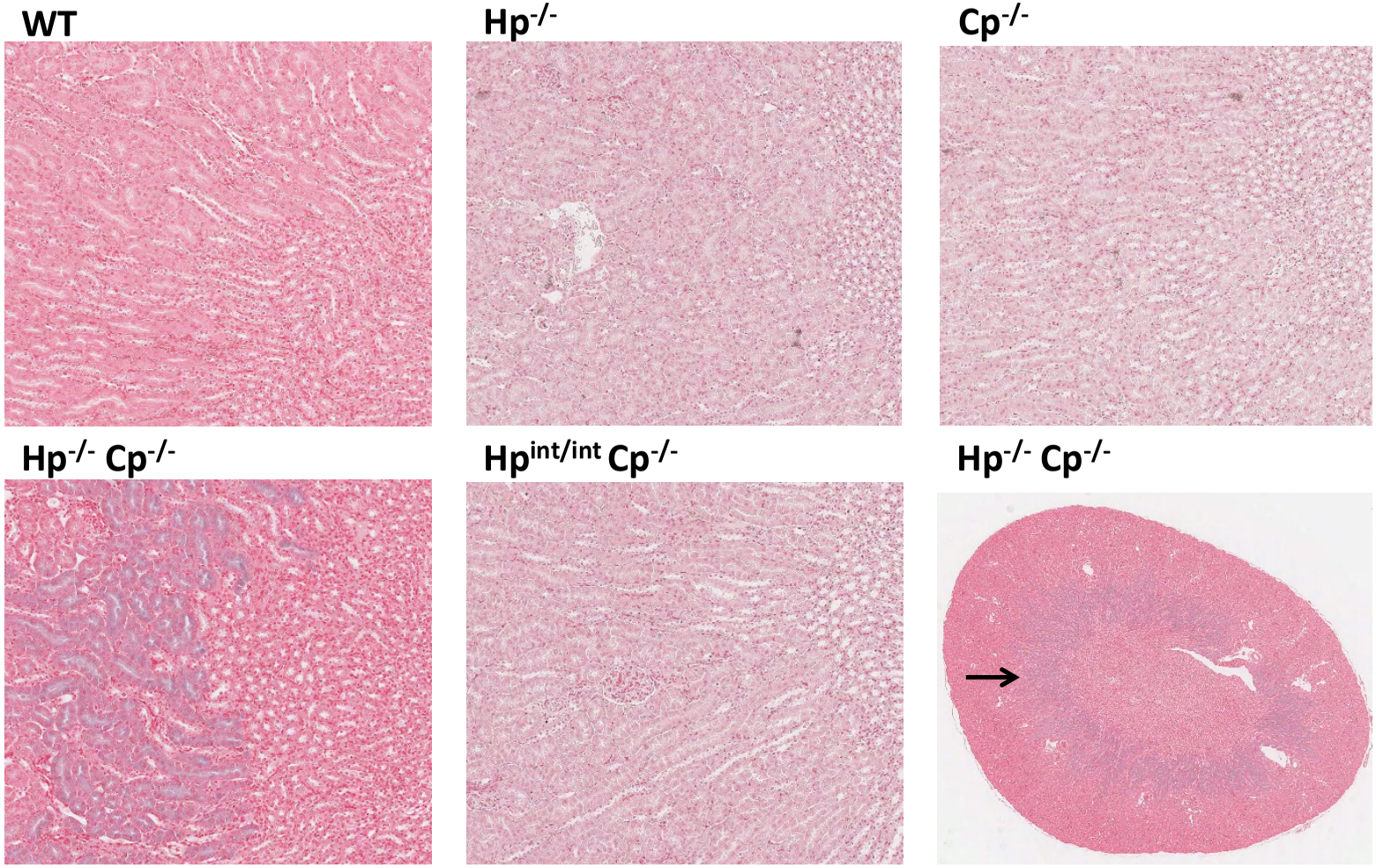

Figure 3.15. Representative Perls' stained kidney sections from 9-11 week old male mice maintained on a chow diet. Aperio Scanscope XT, 5x magnification, and one 1x image (bottom right) showing the ringed region of iron-loading in the $Hp^{-/-}$ $Cp^{-/-}$ kidney. Non-heme ferric iron stains blue.

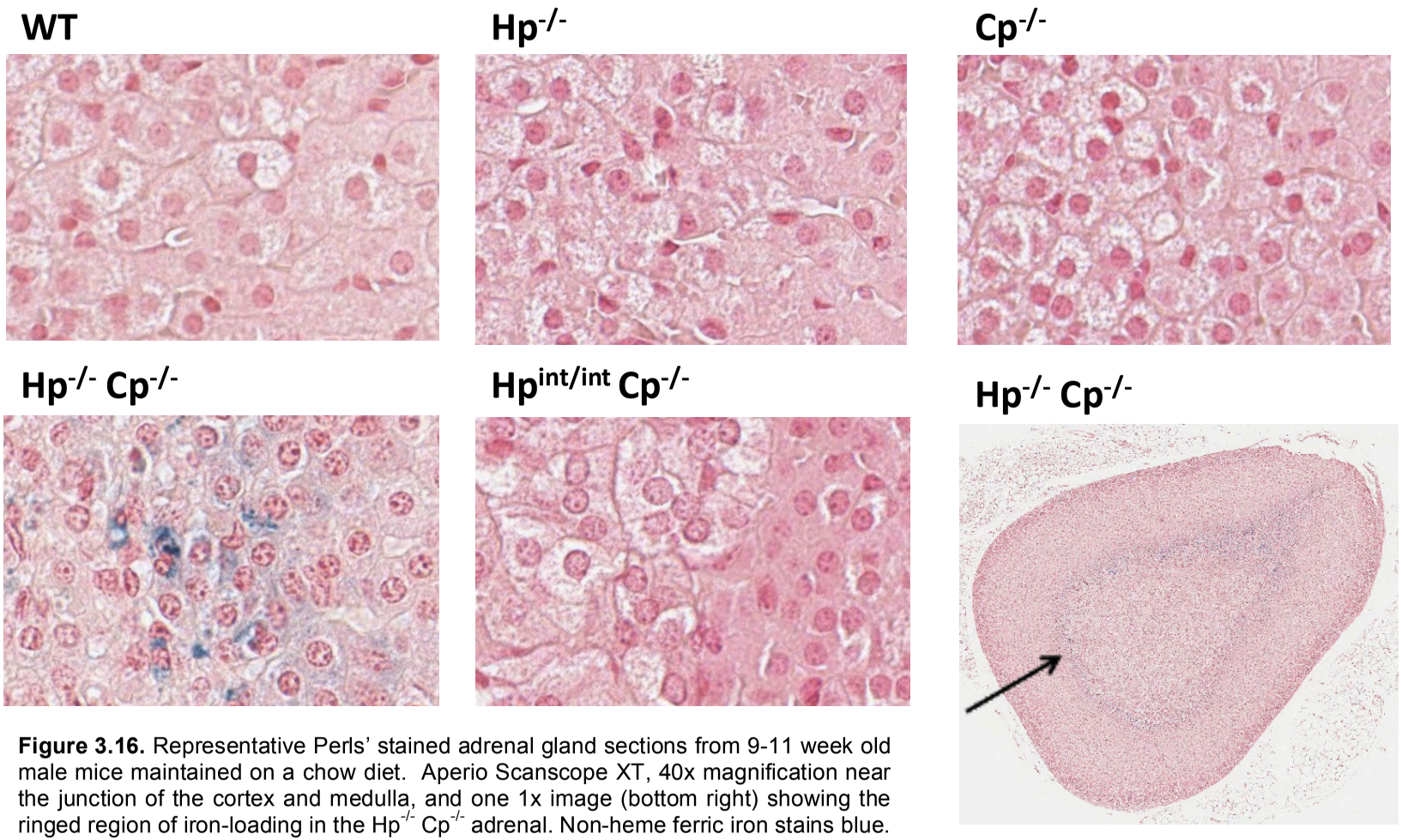

Figure 3.16. Representative Perls' stained adrenal gland sections from 9-11 week old male mice maintained on a chow diet. Aperio Scanscope XT, 40x magnification near the junction of the cortex and medulla, and one 1x image (bottom right) showing the ringed region of iron-loading in the $Hp^{-/-}$ $Cp^{-/-}$ adrenal. Non-heme ferric iron stains blue.

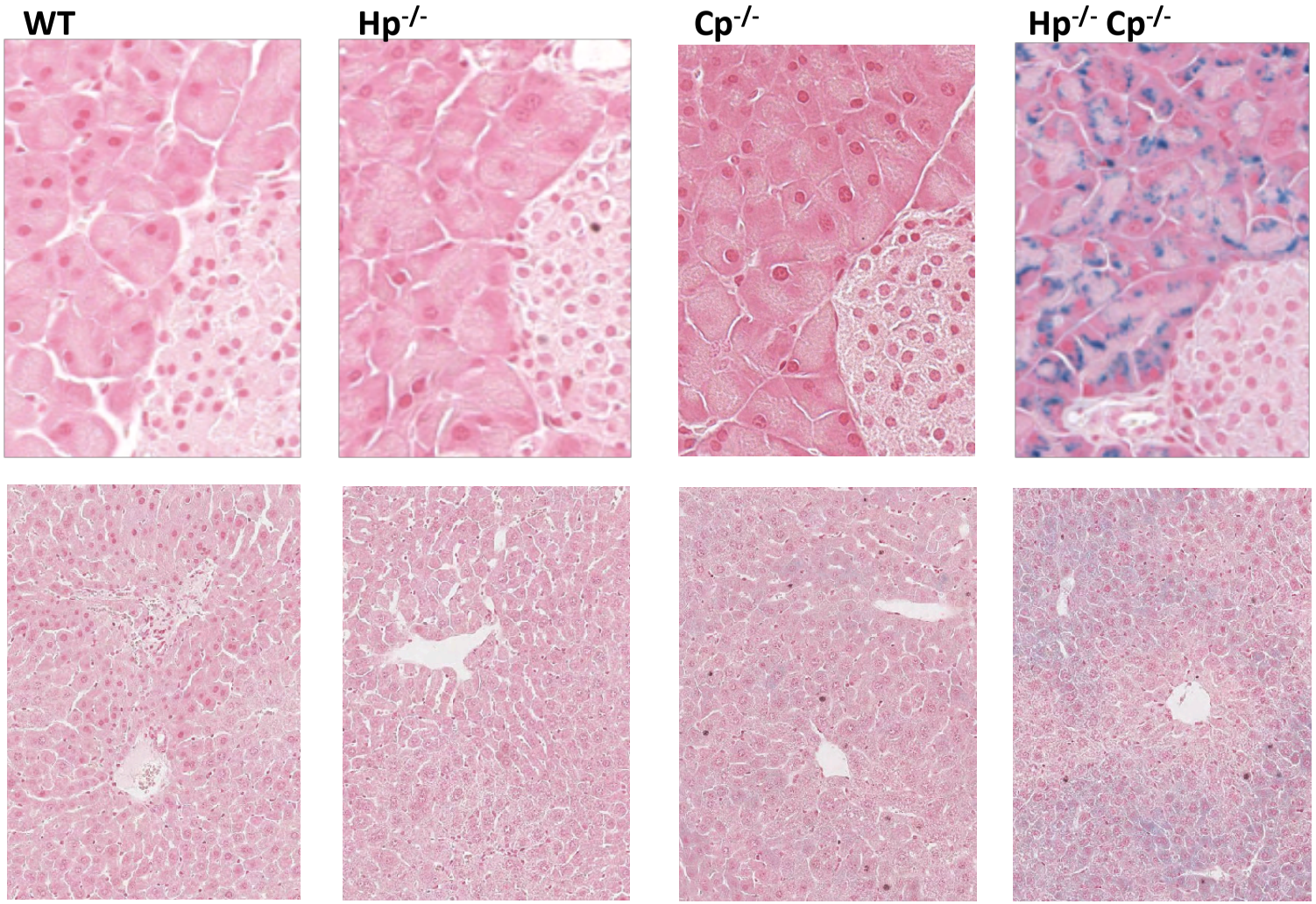

Figure 3.17. Representative Perls' stained pancreas (40x magnification, top row, exocrine tissue at left and islet at bottom right) and liver (8x magnification, bottom row) sections from 23 week old male mice maintained on a chow diet. Aperio Scanscope XT. Non-heme ferric iron stains blue.

Pavle Matak also measured liver *Hamp1* and *Tfrc* mRNA expression in $Hp^{-/-}$ $Cp^{-/-}$ mice and WT controls. *Hamp1* levels were virtually undetectable, indicative of the severe anemia in these mice, while *Tfrc* levels were similar to WT, consistent with the liver not being iron-deficient (data not shown). However, liver *Tfrc* mRNA expression has been reported previously to be decreased in iron-overloaded mice, so it is possible that expression in the $Hp^{-/-}$ $Cp^{-/-}$ mice is greater than would be expected given that their livers are iron-loaded compared to WT (Chua, Herbison et al. 2008).

4. Iron absorption and distribution

The absorption of a radiolabeled dose of iron and the distribution of the dose retained were examined in young $Hp^{-/-}$ $Cp^{-/-}$ and $Hp^{int/int}$ $Cp^{-/-}$ mice of both sexes, and littermate controls (Figure 3.18). Mice at five weeks of age were put on an iron-deficient diet for one week and then dosed by gavage with ^{59}Fe. Body radioactive iron was measured by whole body counting just after the gavage and then again five days later. The mice were then sacrificed and the percentage of the retained dose in the GI tract (esophagus just above the stomach to the anus, plus the pancreas, attached mesentery, and intestinal contents), liver, 200 µL of blood, and in the rest of the carcass (referred to as “carcass” in this experiment) was determined. No significant differences between the groups were found in the percentage of the total dose retained in the whole body, including the GI tract, when analyzed by one-way ANOVA, with the exception of the $Cp^{-/-}$ and $Hp^{-/-}$ $Cp^{-/-}$ mice, which retained significantly more of the dose than WT mice. When each group was individually compared to WT by t-test, again, only absorption by $Cp^{-/-}$ and $Hp^{-/-}$ $Cp^{-/-}$ mice was significantly different.

Differences, however, in the distribution of the absorbed iron were found (Figure 3.18). First of all, of the ^{59}Fe retained in the whole animal, significantly more iron was in the GI tract in the $Hp^{-/-}$ $Cp^{-/-}$ mice (19% ± 1%, mean ± SEM) than any of the other groups (WT: 7.9% ± 0.8%; $Cp^{-/-}$: 6.3% ± 0.3%; $Hp^{-/-}$: 8% ± 1%; $Hp^{int/int}$: 7.4% ± 0.3%; and $Hp^{int/int}$ $Cp^{-/-}$: 8.7% ± 0.7%). To determine the approximate distribution of the iron in the GI tract in the $Hp^{-/-}$ $Cp^{-/-}$ mice, different regions were separated and the radiation in each region counted. The small intestine was divided into three segments of equal length with the upper segment denoted as proximal, the middle segment as central, and the lower segment as distal small intestine. Any food or waste in the GI tract was left inside. Mesentery and pancreatic tissue were trimmed and pooled together. Significantly more radiolabeled iron (36% ± 4%) was found in the proximal small intestine than in any of the other regions of the GI tract (stomach: 10.8% ± 0.9%; central small intestine: 13% ± 1%; distal small intestine: 8% ± 1%; cecum: 16.3% ± 0.9%; colon/rectum: 11% ± 2%; and pancreas/mesentery: 5% ± 3%).

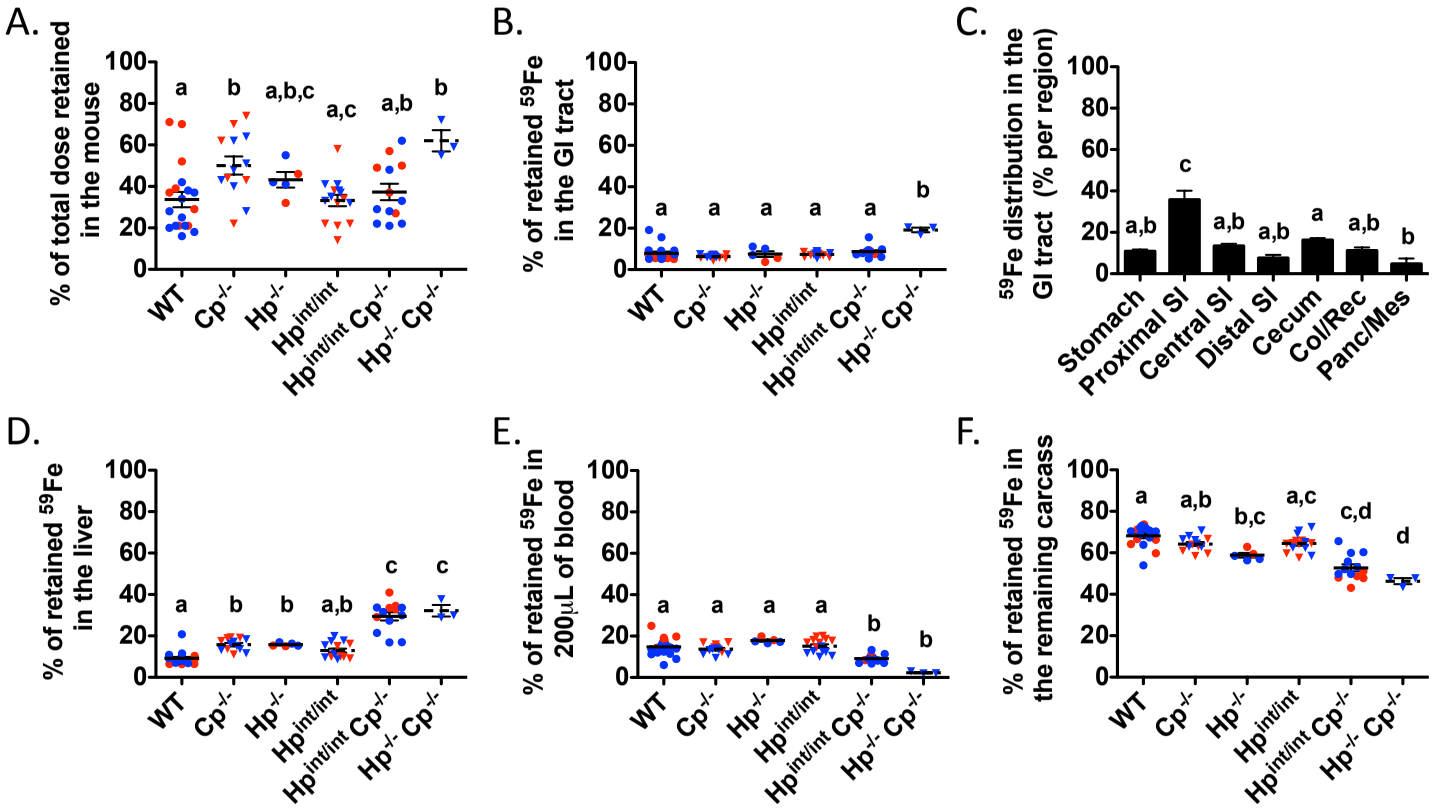

Figure 3.18. Absorption and distribution of a gavaged radiolabeled iron dose in young mice. $Hp^{int/int}$ $Cp^{-/-}$ (8M, 5F), $Hp^{-/-}$ $Cp^{-/-}$ (3M) and littermate WT (11M, 8F), $Cp^{-/-}$ (7M, 6F), $Hp^{-/-}$ (3M, 2F), and $Hp^{int/int}$ (7M, 8F) mice were put on an iron-deficient diet for one week at five weeks of age and then dosed by gavage with ^{59}Fe. The % dose retained five days after dosing and the distribution in selected tissues was determined. WT and $Cp^{-/-}$ controls are a pool of littermate mice with WT or floxed Hp alleles. **A.** The percentage of the ^{59}Fe dose retained in the body, including the GI tract (Mean ± SEM). **B, D-F.** The percentage of the retained ^{59}Fe in different tissues. Males (M, blue), females (F, red). Mean ± SEM. **C.** The distribution of ^{59}Fe in the GI tract (displayed is the percentage of the total ^{59}Fe in the GI tract in each region, mean ± SEM). SI = small intestine; Col/Rec = colon/rectum; Panc/Mes = pancreas/mesentery. For all data, significant differences were determined by one-way ANOVA followed by Tukey's post test in GraphPad Prism. Groups with shared letters are not significantly different.

Of the ^{59}Fe retained by the animal, a significantly greater percentage was found in the livers of $Cp^{-/-}$ and $Hp^{-/-}$ mice (15.8% ± 0.8% and 15.8% ± 0.4%) compared to the livers of WT mice (9.2% ± 0.7%). The amount of ^{59}Fe in $Hp^{int/int}$ mouse livers (13% ± 1%), however, was not significantly different from WT by one-way ANOVA followed by Tukey's post test (limited in power due to the lower number of $Hp^{-/-}$ $Cp^{-/-}$ mice in this experiment) but was significantly different in a direct comparison by t-test. The fraction of radioactive iron in the liver in both the $Hp^{int/int}$ $Cp^{-/-}$ (29% ± 2%) and $Hp^{-/-}$ $Cp^{-/-}$ (32% ± 3%) mice was significantly greater than that in any of the other genotypes.

Equal small volumes of whole blood were taken from each mouse in order to determine if any differences existed in the percentage of radiolabeled iron in this tissue per unit volume. No significant differences (as determined by one-way ANOVA and Tukey's post test or by t-test as compared to WT) were detected in the percentage of the total retained dose in 200 µL of whole blood from WT (15% ± 1%), $Cp^{-/-}$ (13.7% ± 0.6%), $Hp^{-/-}$ (17.8% ± 0.6%), or $Hp^{int/int}$ (15.2% ± 0.9%) mice, but significantly less was present in the blood of $Hp^{int/int}$ $Cp^{-/-}$ (9.1% ± 0.5%) and $Hp^{-/-}$ $Cp^{-/-}$ (2.3% ± 0.3%) mice. By t-test, significantly less radioactive iron was present in the $Hp^{-/-}$ $Cp^{-/-}$ mice than in the $Hp^{int/int}$ $Cp^{-/-}$ mice. The 200 µL whole blood samples were centrifuged to pellet the red cells and serum was removed to a new tube (no hemolysis was observed). No radiation could be detected in the serum fraction in any mice, indicating that most, if not all, of the radioactive iron in the blood was likely already incorporated into cells. The percentage of the retained iron dose remaining in the rest of the carcass (not including the liver, GI tract, or the 200 µL blood sample) was similar in WT (68% ± 1%), $Cp^{-/-}$ (64% ± 1%), and $Hp^{int/int}$ (65% ± 1%) mice, but significantly lower than WT in the $Hp^{-/-}$ (59% ± 1%), $Hp^{int/int}$ $Cp^{-/-}$ (53% ± 2%), and $Hp^{-/-}$ $Cp^{-/-}$ (46% ± 1%) mice as determined by one-way ANOVA followed by Tukey's post test.

Because $Hp^{-/-}$ $Cp^{-/-}$ mice could be readily distinguished from their non-DKO littermates before weaning, this suggested impairments in iron absorption and/or proper distribution in neonates, as had been seen in older mice. Iron absorption was thus measured in 15 day old neonatal littermates four days after gavage of a radiolabeled iron dose (Figure 3.19). The $Hp^{-/-}$ $Cp^{-/-}$ mice (N = 4) were identified by their pale color, and although not genotyped, the non-DKO littermates (N = 8) were expected to contain a mix of HP knockout, CP knockout, and WT alleles. The mice were returned to their mother after dosing. In this experiment, there was large variation in the amount of iron retained in the $Hp^{-/-}$ $Cp^{-/-}$ mice, and the amount retained (60% ± 14%) was not significantly different from littermate non-DKO controls (84% ± 4%). However, $Hp^{-/-}$ $Cp^{-/-}$ neonates had significant differences in the distribution of the retained iron. Of the dose retained in $Hp^{-/-}$ $Cp^{-/-}$ mice after four days, 23 ± 3% was in the GI tract, 38 ± 3% was in the liver, 1.7 ± 0.2% was in the spleen, and 37 ± 1% was in the rest of the carcass. Of note, the spleens in the $Hp^{-/-}$ $Cp^{-/-}$ mice were grossly enlarged (likely due to the severe

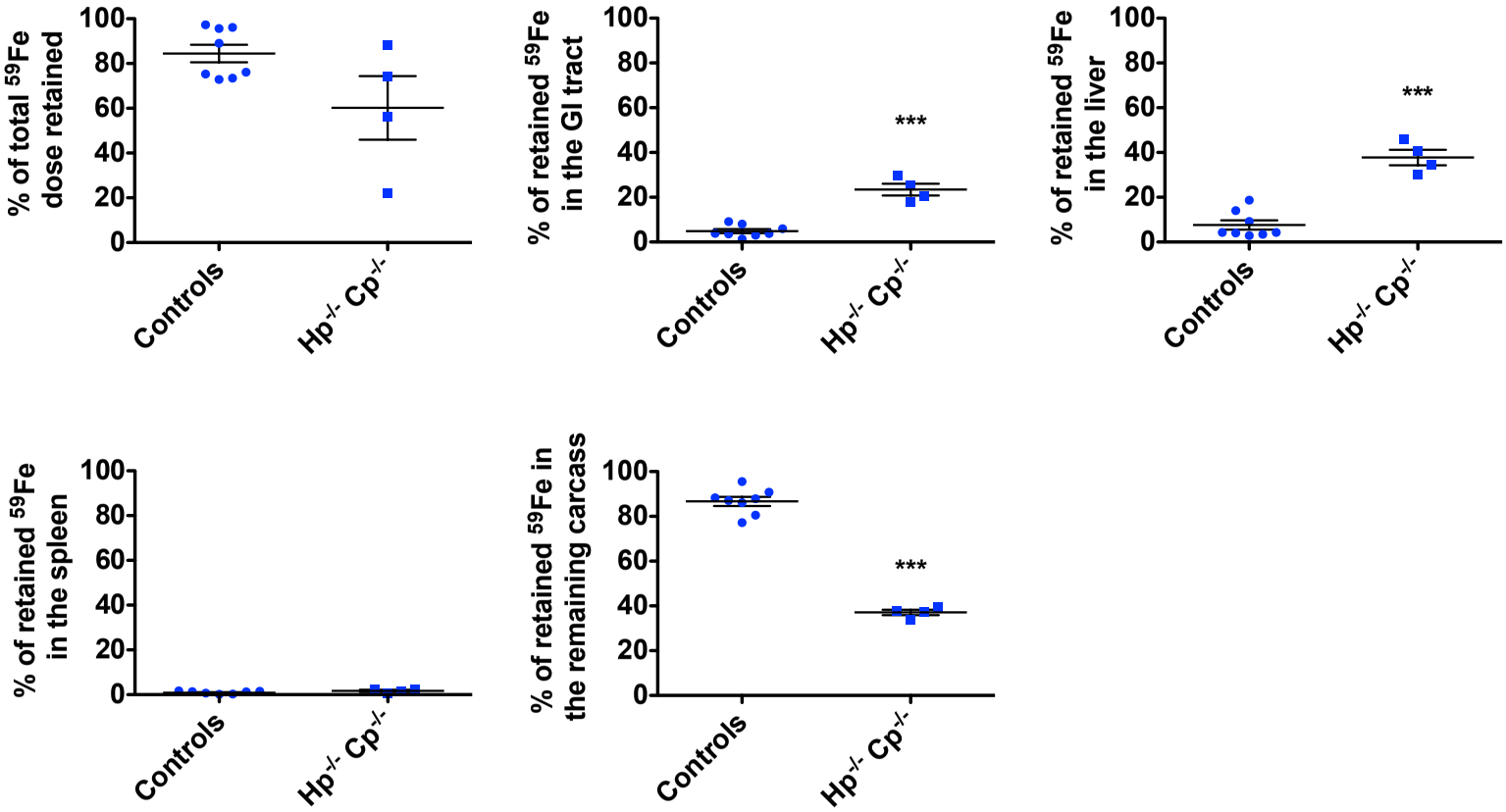

Figure 3.19. Absorption and distribution of a gavaged radiolabeled iron dose in neonate mice. Nursing 15 day old neonate $Hp^{-/-}$ $Cp^{-/-}$ (N = 4) and non-DKO littermate controls (N = 8) were dosed by gavage with ^{59}Fe. The % dose retained four days after dosing and the distribution in selected tissues was determined. **A.** The percentage of the ^{59}Fe dose retained in the body. **B**. The percentage of the retained ^{59}Fe in the GI tract. **C**. The percentage of the retained ^{59}Fe in the liver. **D**. The percentage of the retained ^{59}Fe in the spleen. **E**. The percentage of the retained ^{59}Fe in the rest of the carcass. Mean ± SEM. Significant differences were determined by t-test in GraphPad Prism. *** $P \leq 0.001$.

anemia). Of the dose retained in the non-DKO littermates, however, 4.9 ± 0.9% was in the GI tract, 8 ± 2% was in the liver, 0.9 ± 0.3% was in the spleen, and 87 ± 2% was in the rest of the carcass. Together, these results suggest impaired transfer of iron from the intestine of the $Hp^{-/-}$ $Cp^{-/-}$ neonates to the body, as well as an abnormal retention of the transferred iron in the liver.

A small experiment was performed to examine radiolabeled iron absorption from ligated duodenal gut segments. By this technique, the amount of iron taken up and transferred specifically by the duodenum, as well as the distribution of this iron in a shorter period post-transfer, can be determined. In this experiment, a dose of radioactive iron was administered for 30 minutes via a ligated duodenal gut segment (as described in the Methods section) in anesthetized 8 week old WT, $Hp^{-/-}$, and $Hp^{-/-}$ $Cp^{-/-}$ mice (N = 3 per group) five days after they had been put on an iron-deficient diet. The ligated gut segment was then excised, opened, and washed, and the radioactive iron remaining in the gut segment, the wash solutions, the liver, and the rest of the carcass were counted. No significant differences between any of the groups were observed in the fraction of the total dose retained in the washed duodenal gut segment (Figure 3.20). In addition, no significant differences were found in the percentage of the total dose transferred from the gut segment to the rest of the body (liver and rest of the carcass combined). However, $Hp^{-/-}$ $Cp^{-/-}$ mice had a significantly greater fraction of this transferred iron in the liver (59% ± 7%) than WT mice (5% ± 2%). Although the percentage of transferred iron in the liver was greater in all individual $Hp^{-/-}$ mice (mean ± SEM = 28% ± 11%) than WT mice, there was a large amount of variation and the difference was not statistically significant. In a separate control experiment performed in the same way, iron absorption was compared in 8 week old $Fpn^{int/int}$ mice (FPN1 was ablated by tamoxifen injection prior to weaning, N = 3) and WT littermates (N = 3). The $Fpn^{int/int}$ mice were severely anemic based on their similar appearance to additional littermates whose hematology was examined (data not shown). FPN1 is the only known iron exporter in the intestine and thus if the ligated gut experimental procedure is performed correctly iron absorption into the body is expected to be extremely low. As expected, the percentage of the total dose transferred from the gut segment to the rest of the body was very low (4 ± 2%) and significantly lower than that of WT controls (25% ± 2%).

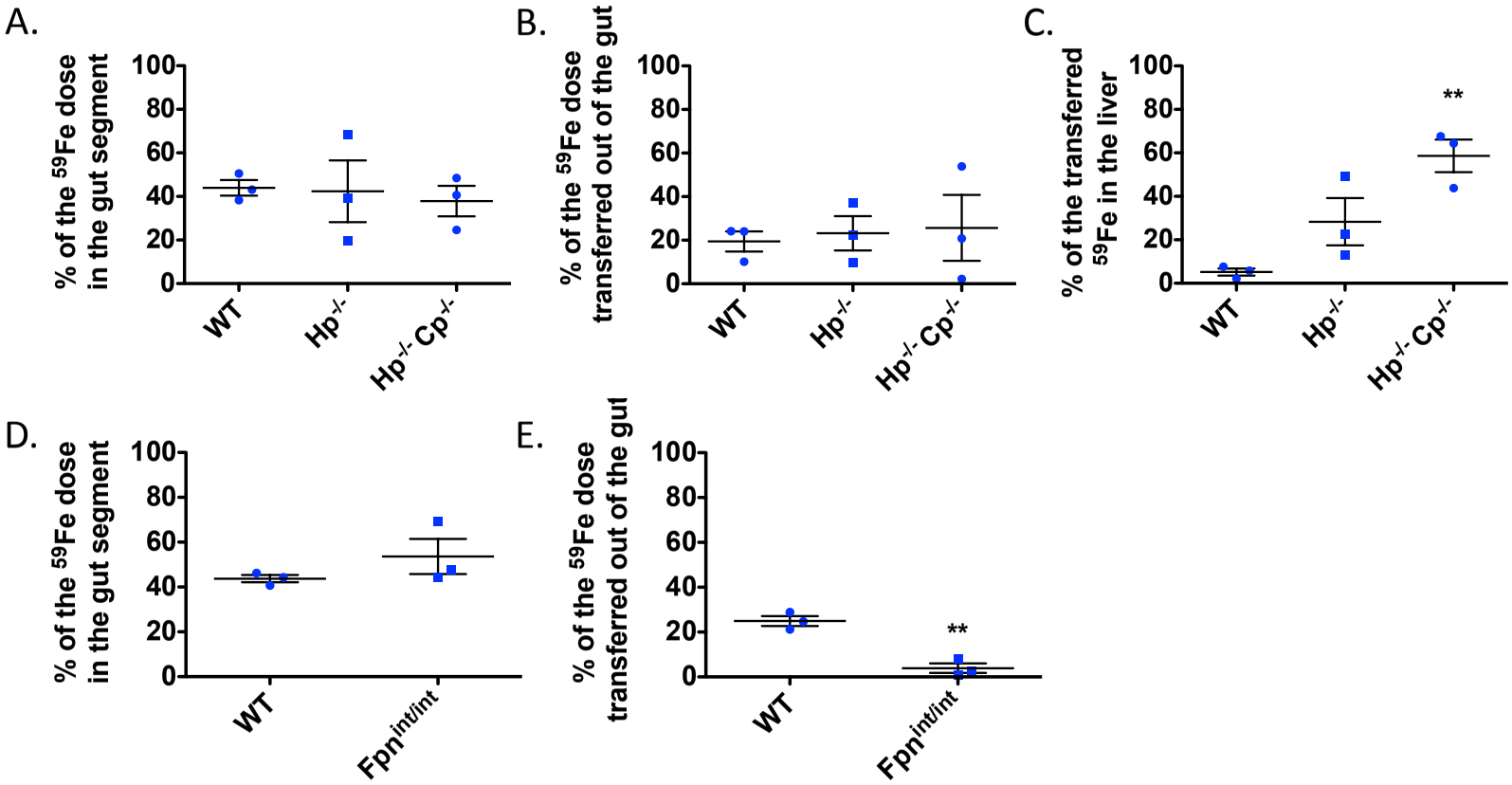

Figure 3.20. Absorption and distribution of a radiolabeled iron dose, administered via a ligated duodenal gut segment, in adult mice. A dose of ^{59}Fe was administered via a ligated duodenal gut segment (Methods) for thirty minutes to anesthetized 8 week old WT, $Hp^{-/-}$, and $Hp^{-/-}$ $Cp^{-/-}$ mice (N = 3 per group) five days after they had been put on an iron-deficient diet. In a separate control experiment performed in the same way, iron absorption was examined in 8 week old WT (N = 3) and $Fpn^{int/int}$ (N = 3) littermates. Thirty minutes after dosing, the ligated gut segment was excised, opened, and washed, and the radioactive iron remaining in the segment, the wash solutions, the liver, and the rest of the carcass was counted. **A and D.** Percentage of the total ^{59}Fe dose retained in the washed duodenal segment. **B and E**. Percentage of the total ^{59}Fe dose transferred from the gut segment to the body. **C.** Percentage of the transferred ^{59}Fe dose in the liver. Mean ± SEM. Significant differences were determined by one-way ANOVA followed by Tukey's post test and by t-test in GraphPad Prism. ** $P \leq 0.01$.

5. Energy expenditure in $Hp^{-/-}$ $Cp^{-/-}$ mice

In a pilot experiment, 24 hour energy expenditure data were collected simultaneously for two adult (17 weeks old) $Hp^{-/-}$ $Cp^{-/-}$ mice and two non-DKO littermate controls at UCB (Figure 3.21). Total locomotor activity, oxygen consumption, and CO_2 production were greatly decreased in the $Hp^{-/-}$ $Cp^{-/-}$ mice versus controls throughout the whole experiment. While the controls were more active during the dark cycle, the $Hp^{-/-}$ $Cp^{-/-}$ mice showed little evidence of any circadian rhythm in their activity. Despite being smaller and generating less heat, the $Hp^{-/-}$ $Cp^{-/-}$ mice drank more water than the controls, amounting to 3-4 times more per gram of body weight.

6. Generation and preliminary results from additional ferroxidase knockout models: $App^{-/-}$ $Hp^{-/-}$, $App^{-/-}$ $Hp^{int/int}$, $Zp^{-/-}$, and $Hp^{-/-}$ $Zp^{-/-}$

Additional double knockout mouse models with HP were created for two newly-discovered ferroxidases, APP and ZP, in order to determine how these genes may impact intestinal and whole body iron metabolism. Neither of these double knockout models have yet been well studied, but their viability and general phenotype indicate that these ferroxidases are not essential in mice lacking HP.

Mice with whole body ablation of both HP and APP ($App^{-/-}$ $Hp^{-/-}$) were created by crossing the two single knockout strains as described (Methods). If APP plays an important role intestinal iron absorption analogous to that of HP, we would expect to see a more severe iron-deficiency phenotype in $App^{-/-}$ $Hp^{-/-}$ mice. We successfully created $App^{-/-}$ $Hp^{-/-}$ mice, but there were no overt differences between these mice and their $Hp^{-/-}$ and $App^{-/-}$ littermates in appearance. $App^{-/-}$ $Hp^{-/-}$ male and female mice were fertile. $App^{-/-}$ $Hp^{int/int}$ mice were also created and did not exhibit any obvious phenotypes that were distinct from the single knockout strains.

We also generated mice with whole body ablation of ZP ($Zp^{-/-}$), and mice with whole body ablation of both HP and ZP ($Hp^{-/-}$ $Zp^{-/-}$). Both strains were viable and bred successfully, and the genotype ratios in the progeny were consistent with no perinatal mortality. Surprisingly, all mice with ablation of ZP were found to exhibit short, curled whiskers (vibrissae) throughout life (Figure 3.22). Mice heterozygous for the ZP knockout allele did not exhibit this phenotype, indicating that it is recessive. The coats of mice with ZP knockout also generally appeared less sleek. Tissues from one adult $Zp^{-/-}$ male were collected and no striking abnormalities were noted. The tissues were stained for iron by Perls' stain and for copper by Howell's copper stain, but no differences were noted from WT controls. Hematology also appeared normal. Further studies are needed to determine if APP and ZP ablation affect intestinal iron absorption and metabolism.

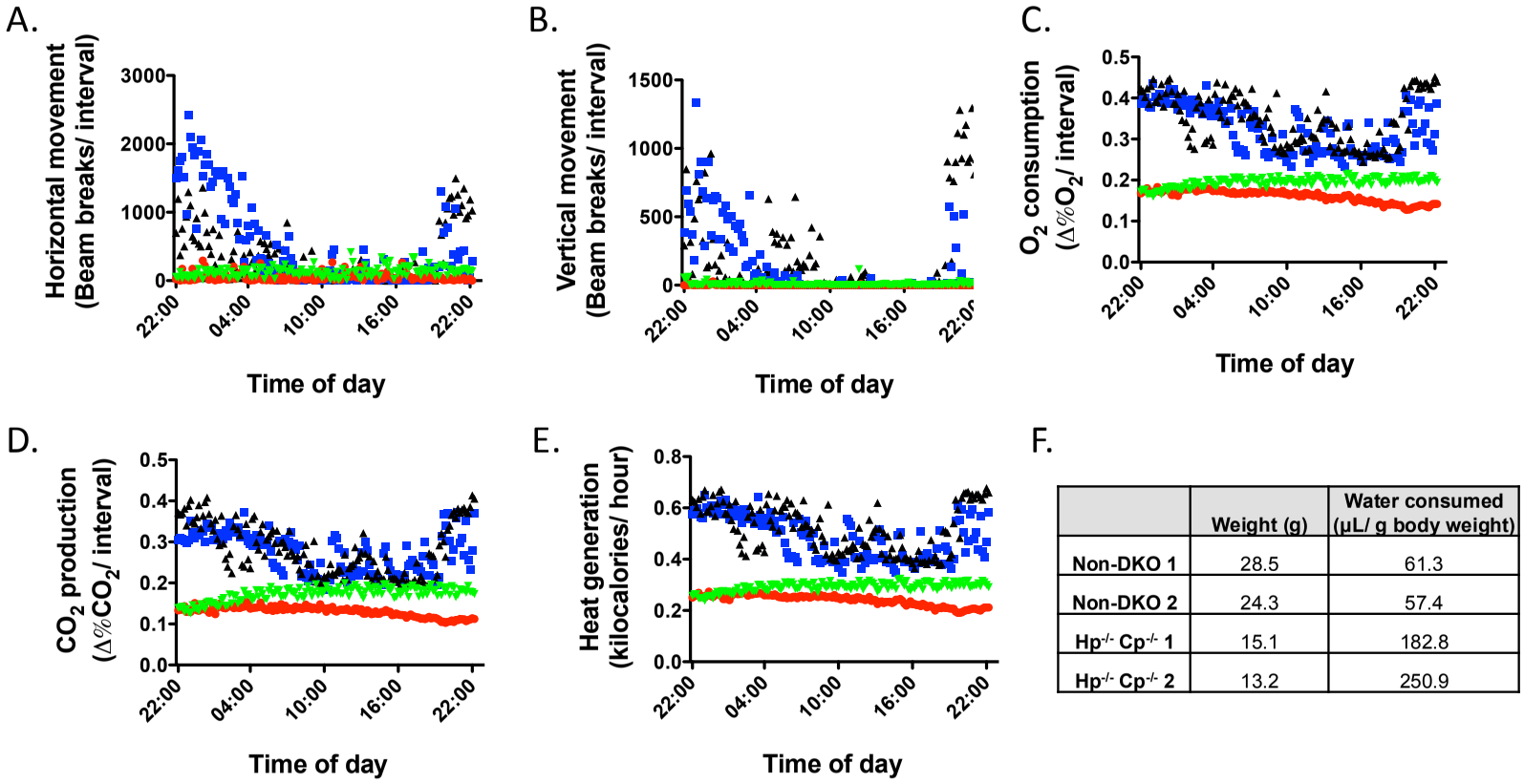

F.

	Weight (g)	Water consumed (µL/ g body weight)
Non-DKO 1	28.5	61.3
Non-DKO 2	24.3	57.4
$Hp^{-/-}$ $Cp^{-/-}$ 1	15.1	182.8
$Hp^{-/-}$ $Cp^{-/-}$ 2	13.2	250.9

Figure 3.21. 24 hour energy expenditure data was collected simultaneously for two 17 week old male $Hp^{-/-}$ $Cp^{-/-}$ (red circles = mouse 1; green triangles = mouse 2) and two non-DKO (black triangles = mouse 1; blue squares = mouse 2) littermates using a Columbus Instruments Oxymax Lab Animal Monitoring system (CLAMS) with four center-feeder style cages at UCB. Water and food were provided ad libitum; measurement interval 10 minutes. **A.** Horizontal and **B.** vertical movement as quantified by the number of infrared beam breaks. **C.** Oxygen consumption **D.** Carbon dioxide production. **E.** Heat generation. **F.** Body weight and water consumption. Results reported for A-E were calculated automatically by the CLAMS software (Methods).

A.

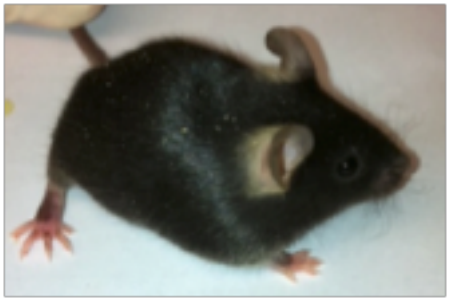

B.

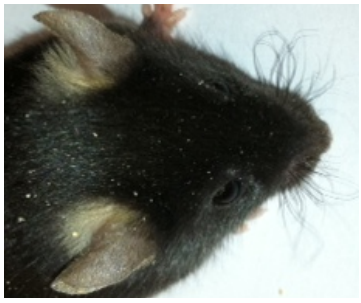

C.

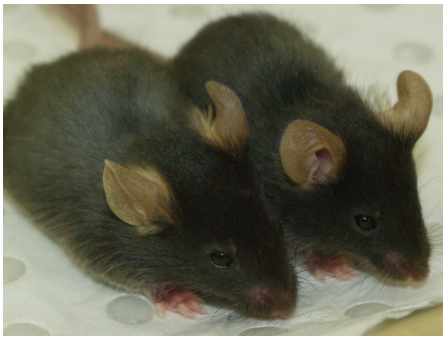

Figure 3.22. Photographs of representative mice with knockout of ZP. **A and B.** A young $Zp^{-/-}$ mouse showing the curly whisker phenotype. **C.** A young $Hp^{-/-}$ $Zp^{-/-}$ mouse (bottom left) next to a non-DKO littermate (bottom right).

IV. Discussion

Both $Hp^{-/-}$ $Cp^{-/-}$ and $Hp^{int/int}$ $Cp^{-/-}$ mice were viable and able to absorb dietary iron, demonstrating that these two MCFs are not absolutely required for iron release from intestinal enterocytes. Study of these models revealed, however, that HP and CP together are critical for maintaining normal iron homeostasis in both the intestine and other tissues.

While $Hp^{-/-}$ $Cp^{-/-}$ and $Hp^{int/int}$ $Cp^{-/-}$ mice survived, both double knockout strains had a more severe phenotype than single knockout models of HP or CP (Table 3.1). As described in Chapter 2, $Hp^{-/-}$ and $Hp^{int/int}$ mice exhibited iron loading in duodenal enterocytes throughout life, inappropriately low iron absorption (except when severely stressed), and an anemia when young that improved with age. Iron levels in the tissues of $Hp^{-/-}$ and $Hp^{int/int}$ mice (with the exception of duodenal enterocytes) were also low. $Cp^{-/-}$ mice, on the other hand, exhibited iron loading in the liver and reticuloendothelial macrophages and had a mild anemia that persisted throughout life (Harris, Durley et al. 1999; Cherukuri, Tripoulas et al. 2004). In addition, but not studied here, both the HP mutant strain *sla* and as well as $Cp^{-/-}$ mice, have been reported to have subtle but significant neurological abnormalities that become apparent in older mice, likely mostly due to a role for

Table 3.1. Overall summary of tissue iron levels and distribution in adult mice

Mouse	Anemia?	Liver iron*	Enterocyte iron*	Spleen iron*	Iron in heart, pancreas, adrenal, kidney*	Fraction of retained ^{59}Fe dose in the liver**	Fraction of retained ^{59}Fe dose in the GI tract**	Fraction of retained ^{59}Fe dose in the blood**
WT	None	Mild periportal stain	Little to no staining	Moderate staining in red pulp	No staining	Low	Low	High
Hp$^{-/-}$	Mild to none	↓	↑↑↑	↓	No staining	↑	Low	High
Hp$^{int/int}$	Mild to none	↓	↑↑↑	↓	No staining	↑	Low	High
Cp$^{-/-}$	Mild	↑	Little to no staining	Moderate staining in red pulp	No staining	↑	Low	High
Hp$^{int/int}$ Cp$^{-/-}$	Moderate	↑↑	↑↑↑	↓	No staining	↑↑	Low	↓
Hp$^{-/-}$ Cp$^{-/-}$	Severe	↑↑	↑↑↑	↓	↑↑ in some but not all cell types	↑↑	↑	↓

*Summary of data from Perls' staining as well as other methods of measurement (when performed) as described in Methods.
**Summary of data from ^{59}Fe iron absorption/distribution studies. Gray arrows indicate that results are suggestive in some studies, but more mice will need to be examined.

both of these proteins in the brain (Patel, Dunn et al. 2002; Schulz, Vulpe et al. 2011). The general phenotype of $Hp^{int/int}$ $Cp^{-/-}$ mice is consistent with a cumulative mild intestinal iron absorption defect due to intestinal ablation of HP contributing to the anemia brought on by defects in iron turnover and liver iron accumulation resulting from ablation of CP. Similarly to $Hp^{-/-}$ and $Hp^{int/int}$ mice, $Hp^{int/int}$ $Cp^{-/-}$ mice had iron loading in the absorptive epithelial cells of the duodenum and very little observable iron in the spleen by Perls' stain, suggesting defects in iron absorption. However, unlike $Hp^{int/int}$ and $Hp^{-/-}$ mice but consistent with $Cp^{-/-}$ mice, liver non-heme iron levels were significantly greater in $Hp^{int/int}$ $Cp^{-/-}$ mice than WT controls. The hematological parameters of $Hp^{int/int}$ $Cp^{-/-}$ mice suggested that they generally had less iron available for erythropoiesis than $Hp^{-/-}$, $Cp^{-/-}$ and WT control littermates. $Hp^{int/int}$ mice were not available for comparison in these hematology studies, but as reported in Chapter 2, the hematology of $Hp^{int/int}$ mice was similar to that of $Hp^{-/-}$ mice. Female $Hp^{int/int}$ $Cp^{-/-}$ mice had significantly lower mean cell volume, hematocrit, hemoglobin, and mean cell hemoglobin levels, and higher platelet levels, than $Hp^{-/-}$, $Cp^{-/-}$, and WT control mice. Male $Hp^{int/int}$ $Cp^{-/-}$ mice were not statistically different from $Cp^{-/-}$ mice in any blood parameters, but they showed a trend toward a more severe phenotype than $Cp^{-/-}$ mice that would likely have become significant with a larger number of mice.

$Hp^{-/-}$ $Cp^{-/-}$ mice had a much more severe phenotype than $Hp^{int/int}$ $Cp^{-/-}$ mice that was more complex than could be explained by the simple additive effect of the phenotypes of $Hp^{-/-}$ and $Cp^{-/-}$ mice. In a simple additive model based on the phenotypes of the single knockout mice, $Hp^{-/-}$ $Cp^{-/-}$ mice would be expected to have a similar phenotype as the $Hp^{int/int}$ $Cp^{-/-}$ mice, but with the potential for a more severe neurological phenotype, as whole-body HP ablation would also affect the brain, where HP has been shown to play a role in *sla* mice (Schulz, Vulpe et al. 2011). However, in addition to phenotypes observed in the $Hp^{int/int}$ $Cp^{-/-}$ mice, including iron loading in duodenal absorptive epithelial cells and the liver, and lack of iron deposits in the spleen, $Hp^{-/-}$ $Cp^{-/-}$ mice also exhibited a very severe anemia and marked iron loading in the peripheral tissues including the pancreas, heart, kidney, adrenal glands, and, as reported by a collaborator, the eye (Wolkow, Song et al. 2012). The iron loading in the peripheral tissues appeared to increase with age when examined by Perls' stain, but the anemia did not improve, suggesting that $Hp^{-/-}$ $Cp^{-/-}$ mice were still able to obtain some iron from the diet but that it was inappropriately distributed. These mice also died prematurely of unknown causes. Mice carrying the *sla* mutation in HP on a CP knockout background ($Hp^{sla/sla}$ $Cp^{-/-}$) have also been reported to have a general phenotype similar to $Hp^{-/-}$ $Cp^{-/-}$ mice, including increased levels of pancreatic, heart, liver, and brain iron at 24 weeks of age, and the development of symptoms of neurological abnormalities at 20-36 weeks of age, including weakness, poor grooming, and gait changes (Xu, Pin et al. 2004). These mice also developed iron loading in the eye and symptoms of macular degeneration, although the iron loading in the eye was not as severe as in $Hp^{-/-}$ $Cp^{-/-}$ mice, suggesting that the

$Hp^{-/-}$ $Cp^{-/-}$ phenotype may in general be more severe (Hahn, Qian et al. 2004; Hadziahmetovic, Dentchev et al. 2008; Wolkow, Song et al. 2012).

In iron absorption experiments where six week old mice were gavaged with a dose of radiolabeled iron and whole body retention (including any iron remaining in the GI tract) was measured five days later, $Hp^{-/-}$ $Cp^{-/-}$ mice surprisingly retained similar or higher levels of iron than controls. Greater than 20% of this iron remained in the GI tract, however, with the greatest fraction in the proximal small intestine. This result was unanticipated given that the average total lifespan of duodenal enterocytes, including the period before complete enterocyte differentiation when dietary iron absorption by these cells is low, is generally reported to be less than five days in adult mice (Johnson, Ghishan et al. 2012). Our findings suggest that enterocyte turnover may be decreased in $Hp^{-/-}$ $Cp^{-/-}$ mice. A similar result was obtained when whole body and intestinal iron in neonate mice were measured four days after dosing, but the finding was less surprising because neonate mice are known to have a longer enterocyte turnover time than weaned mice (Schmidt, Winton et al. 1988). Taking into account the retention in the GI tract, the amount of iron that was transferred from the intestine to the body of both neonate and six week old $Hp^{-/-}$ $Cp^{-/-}$ mice was inappropriately low given the severe anemia in these mice, and this indicates a defect in iron absorption. The absorption defect appears to be greater than that of $Hp^{-/-}$ and $Hp^{int/int}$ mice made similarly severely anemic either by an iron-deficient diet coupled with red cell lysis or by being maintained since weaning for months on an iron-deficient diet. As reported in Chapter 2, these mice were able to absorb iron at levels similar to WT. Comparison between these studies, however, must be treated with caution considering that the experiments were not identical and thus the iron status and stimuli for absorption may not have been the same.

$Hp^{int/int}$ $Cp^{-/-}$ and $Hp^{-/-}$ $Cp^{-/-}$ mice also exhibited perturbed systemic distribution of a radiolabeled iron dose in intestinal iron absorption experiments. In both models, a significantly larger proportion of the absorbed dose was found in the liver, and significantly less was incorporated into red cells, than WT controls five days after dosing. This alone is not surprising given that CP is known to be required for normal rates of iron release from the liver, and $Cp^{-/-}$ mice also had a greater proportion of the iron dose in the liver than WT mice in this gavage study (Lee, Nacht et al. 1968). However, the $Hp^{-/-}$ $Cp^{-/-}$ mice, and even more interestingly, the $Hp^{int/int}$ $Cp^{-/-}$ mice, had statistically greater retention of the absorbed iron dose in the liver than $Cp^{-/-}$ mice, suggesting that ablation of HP in the intestine can also affect dietary iron retention by the liver. In support of this, a greater proportion of the retained iron dose was in the liver of $Hp^{-/-}$ mice than WT controls in most but not all studies of radiolabeled iron absorption (see Chapter 2 experiments as well). Iron distribution in $Hp^{int/int}$ mice has so far only been examined in one study, and these mice generally retained more iron in the liver that WT mice, although the difference was not significant. Distribution defects were also observed in a

short-term experiment with $Hp^{-/-}$, $Hp^{-/-}$ $Cp^{-/-}$, and WT control mice. In this 30 minute duodenal gut loop absorption experiment, a significantly greater proportion of the iron dose absorbed was found in the livers of $Hp^{-/-}$ $Cp^{-/-}$ mice than in the livers of WT controls. $Hp^{-/-}$ mice also had a greater fraction of the absorbed iron dose in the liver in this experiment than WT mice, but the difference was not statistically significant likely due to the small number of mice examined. These findings suggest that there is increased iron uptake and/or decreased rates of iron release from the livers of mice with ablation of HP and/or CP compared to controls. Of note, steady state non-heme iron levels in the livers of $Hp^{-/-}$ and $Hp^{int/int}$ mice, as measured by colorimetric assay, were significantly lower than in WT controls, making it likely that any extra iron absorbed or retained by the liver in these mice is ultimately redistributed to the rest of the body on a longer time scale than examined in the gavage and gut loop experiments. In contrast, $Cp^{-/-}$, $Hp^{int/int}$ $Cp^{-/-}$, and $Hp^{-/-}$ $Cp^{-/-}$ mice had higher steady state levels of liver non-heme iron than WT mice as would be expected due to the known role of CP in iron release from the liver (Lee, Nacht et al. 1968).

One potential explanation for these observations is that ablation of HP in duodenal enterocytes may prevent all or at least a fraction of the iron exported from the intestine from binding to TF. As a result, this iron would enter the circulation as NTBI. Because the duodenal circulation travels first to the liver before joining the general circulation, this iron would be rapidly taken up by the liver, which has a particularly high affinity for NTBI, as demonstrated in studies of intestinal iron absorption in mice either lacking TF or with fully-saturated TF, where all newly absorbed iron is released from the intestine as NTBI (Craven, Alexander et al. 1987). Eventually, however, this iron would be released from the liver bound to TF to be redistributed by the circulation. In mice with ablation of CP as well, the rate of iron release from the liver would be decreased, leading to increased clearance times for iron and increased steady-state levels of liver iron.

Why then do $Hp^{-/-}$ $Cp^{-/-}$ mice but not $Hp^{int/int}$ $Cp^{-/-}$ mice exhibit progressive and marked iron loading in other peripheral tissues such as the pancreas and heart, and also exhibit a much more severe anemia? In the studies with $Hp^{int/int}$ mice described in Chapter 2, some variation was seen from mouse to mouse in the severity of the phenotype, with some mice exhibiting parameters similar to that of $Hp^{-/-}$ mice and some expressing a milder phenotype, suggesting that in some mice knockout of HP by the villin-cre recombinase was not complete. It is thus possible that there was some variation in the degree of knockout in the $Hp^{int/int}$ $Cp^{-/-}$ mice, and that even a small degree of residual HP expression could have "rescued" these mice from the much more severe phenotype seen in the $Hp^{-/-}$ $Cp^{-/-}$ mice, which have germline ablation of HP. Notably, however, all $Hp^{int/int}$ $Cp^{-/-}$ mice examined showed strong iron loading in the duodenum by Perls' stain, but none exhibited any of the distinguishable phenotypes of the global $Hp^{-/-}$ $Cp^{-/-}$ mice, such as loading of iron in peripheral tissues, a marked anemia,

distinguishable pallor, or premature death. The unique phenotype of the $Hp^{-/-}$ $Cp^{-/-}$ mice can therefore best be explained by a role for HP in iron metabolism in extra-intestinal tissues that becomes especially critical when CP is ablated. In some cell types, HP may contribute to normal rates of iron efflux. As has been reported for CP, HP may maintain the rate of iron efflux from cells by decreasing FPN1 turnover (De Domenico, Ward et al. 2007). Alternatively, HP may play a critical role in ensuring that iron exported from cells is bound to TF. These possibilities are not mutually exclusive and may depend on the cell type and circumstance.

In support of a role for HP and CP in the proper binding of iron to TF, the patterns of iron loading in the $Hp^{-/-}$ $Cp^{-/-}$ mice, as revealed by Perls' staining, were very similar to those in the hypotransferrinemic (*trf-hpx*) mouse as reported by Trenor et al. The *trf-hpx* mouse produces little to no functional TF due to a mutation in an mRNA splice donor site, and as a result all iron in the plasma is NTBI. NTBI is not effectively utilized by developing red cells and instead is rapidly cleared from the circulation by the liver and other peripheral tissues. The *trf-hpx* mouse thus exhibits a severe anemia, but the liver and peripheral tissues become severely iron-overloaded. The spleen, however, is spared (Trenor, Campagna et al. 2000). As most iron circulating in the bloodstream generally originates from reticuloendothelial macrophages after being recycled, the widespread peripheral iron loading and anemia in $Hp^{-/-}$ $Cp^{-/-}$ mice is not inconsistent with abnormal release of NTBI from these cells when HP and CP are ablated. Unlike iron absorbed from the intestine, iron released by reticuloendothelial macrophages throughout the body does not necessarily make a first pass through the liver before encountering peripheral tissues. CP and HP have been reported to be expressed in some macrophage types (Zhang, Xiong et al. 2004). Clearly many more studies are needed in order to decipher the cause of the severe anemia and tissue iron-loading in the $Hp^{-/-}$ $Cp^{-/-}$ mice and to determine which cell types are involved.

In addition to the striking iron distribution phenotype observed in $Hp^{-/-}$ $Cp^{-/-}$ mice, a pilot energy expenditure experiment with 17 week old mice suggested that these mice have dramatically reduced locomotor activity compared to controls, as well as potential disturbances in circadian rhythm. Reduced activity was also observed in $Hp^{-/-}$ $Cp^{-/-}$ mice at all ages when they were being weighed, but this was not quantitated. These findings are not surprising given the severe iron deficiency in these mice. Anemia is often associated with fatigue, and there are multiple reports of iron deficiency in rodents and humans resulting in reduced activity (Williamson and Ng 1980; Pinero, Jones et al. 2001; Crouter, DellaValle et al. 2012). In addition, some (but not all) studies have noted disruption of normal circadian rhythm in iron deficiency (Hunt, Zito et al. 1994). Ablation of CP, however, which is capable of metabolizing biogenic amines, including the neurotransmitters dopamine and serotonin, as well as the stress hormones

epinephrine and norepinephrine, may also further exacerbate these phenotypes (Lindley 2001). Biogenic amines are involved in regulating activity and circadian rhythm, and impact on how well an organism can handle stress (Brodal 2010). HP may also metabolize these compounds, although a study performed *in vitro* with recombinant HP expressed in yeast suggested this may not be the case (Vashchenko, Bleackley et al. 2011). The reduced activity could also be due to pathology in the CNS of these mice. Iron loading in certain regions of the brain has been reported in both *sla* and $Hp^{sla/sla}$ $Cp^{-/-}$ mice, and the loading correlated with motor defects in these animals (Schulz, Vulpe et al. 2011). In addition, the $Hp^{sla/sla}$ $Cp^{-/-}$ and $Hp^{-/-}$ $Cp^{-/-}$ mice die prematurely, and it has been suggested that in the former model this is due to CNS dysfunction (Xu, Pin et al. 2004). Dementia and motor defects are also observed in adult human patients with aceruloplasminemia (Morita, Ikeda et al. 1995). In 23 week old $Hp^{-/-}$ $Cp^{-/-}$ mice, surprisingly little pathology was observed by gross histological examination of the pancreas, liver, and other markedly iron-loaded tissues, and the anemia did not appear to worsen with age when compared with that of 9-11 week old mice, suggesting that failure of those tissues was not responsible for their premature deaths at 23-30 weeks of age. The brain however has not yet been examined for pathology.

$Hp^{-/-}$ $Cp^{-/-}$ mice drank more water than controls in the pilot energy expenditure experiment, despite being less active. Because human patients with aceruloplasminemia develop diabetes as adults (typically by 40 years of age but diabetes has also been described in a teenage case), presumably due to massive iron accumulation in the pancreas, the findings on water consumption tentatively suggest that these mice may have diabetes (Hatanaka, Okano et al. 2003). No studies have yet been performed to test this, however, and there are other possible explanations for the increased water intake of the $Hp^{-/-}$ $Cp^{-/-}$ mice that can only be ruled out with more experiments. However, given that diabetes is typically the first symptom in patients with the only human MCF disease currently known, this preliminary finding merits some discussion. In humans with aceruloplasminemia, as well as in $Hp^{-/-}$ $Cp^{-/-}$ mice, most pancreatic iron loading is in the exocrine pancreas, and the islets where insulin is produced show no signs of degeneration or necrosis. A reduction in the number of insulin-positive cells in the islets of aceruloplasminemia patients has been reported, however, despite no change in overall islet cell number (Kato, Daimon et al. 1997). It is thus unclear whether the iron loading itself causes or contributes to the progression of diabetes, or if the cause is due to another defect resulting from CP ablation. Of note, we did not see any evidence of iron loading (by Perls' staining) in the pancreas of $Cp^{-/-}$ mice, even in mice 76-79 weeks old (data not shown), and diabetes has not been observed in this model (Harris, Durley et al. 1999). This suggests that HP or other proteins may play a more protective role in the mouse than in humans in this tissue, or alternatively, that the longer lifespan of humans may result in phenotypes that do not have time to manifest in the lifespan of a

$Cp^{-/-}$ laboratory mouse. Rodent beta cells also appear to have a higher turnover rate than human beta cells, which could also potentially be protective (Cnop, Hughes et al. 2010; Carlotti, Zaldumbide et al. 2011).

The generation of the $Hp^{-/-}$ $Cp^{-/-}$ and $Hp^{int/int}$ $Cp^{-/-}$ models confirmed that FPN1 in enterocytes must be able to function to some extent without a ferroxidase, or alternatively, another ferroxidase must be present. We thus have begun studies to determine if other known ferroxidases could be involved in intestinal iron absorption. Mice generated with double knockout of both APP and HP were viable and did not appear to have a more severe phenotype than $Hp^{-/-}$ littermates, either by eye or in very preliminary hematology analyses (data not shown), suggesting that APP does not play a critical role in the release of iron from intestinal enterocytes. However, it is still possible that lack of APP could affect the loading of absorbed dietary iron onto TF, and more detailed studies are needed to examine this possibility. Mice were also generated with ablation of the only other known mammalian MCF, ZP. Like the $App^{-/-}$ $Hp^{-/-}$ mice, few studies have been performed with this model, but in preliminary observations the mice do not appear to have any overt defects in iron acquisition. Similarly, $Hp^{-/-}$ $Zp^{-/-}$ mice were viable and appeared generally similar to $Hp^{-/-}$ controls. ZP Is not known to be expressed in the intestine, so this protein is not as likely as APP to play a role in intestinal iron absorption (Chen, Attieh et al. 2010). The curly whisker phenotype of these mice, similar to what is observed in mice with a defective ATP7A copper transporter, interestingly suggests however that ZP may be important in copper metabolism (Wang, Zhu et al. 2012). Further study of these new ferroxidase knockout mouse models may also reveal additional roles for APP, ZP, and HP in other tissues as well.

Finally, collaborative studies with Yan Lu (from the laboratory of Professor James Collins at the University of Florida) have confirmed that ferroxidase activity still exists in $Hp^{-/-}$, $Hp^{-/-}$ $Cp^{-/-}$, and $App^{-/-}$ $Hp^{-/-}$ mouse enterocytes (Ranganathan, Lu et al. 2012). The origin of this activity is unknown and it is unclear if it is important for intestinal iron absorption. Xanthine oxidase, another ferroxidase expressed in intestinal enterocytes and present in the serum, is one potential candidate that can be tested. The mouse models developed here will thus be valuable tools in future experiments to characterize the ferroxidase activity remaining when APP, CP, and HP are ablated, and to hopefully identify any alternative ferroxidases involved in intestinal iron absorption as well as in iron metabolism in other cell types.

REFERENCES

Abboud, S. and D. J. Haile (2000). "A novel mammalian iron-regulated protein involved in intracellular iron metabolism." J Biol Chem **275**(26): 19906-19912.

Aisen, P., C. Enns, et al. (2001). "Chemistry and biology of eukaryotic iron metabolism." Int J Biochem Cell Biol **33**(10): 940-959.

Anderson, G. J. (2001). "Ironing out disease: inherited disorders of iron homeostasis." IUBMB Life **51**(1): 11-17.

Anderson, G. J., D. M. Frazer, et al. (2002). "Relationship between intestinal iron-transporter expression, hepatic hepcidin levels and the control of iron absorption." Biochem Soc Trans **30**(4): 724-726.

Anderson, G. J. and C. D. Vulpe (2009). "Mammalian iron transport." Cell Mol Life Sci **66**(20): 3241-3261.

Andriopoulos, B., Jr., E. Corradini, et al. (2009). "BMP6 is a key endogenous regulator of hepcidin expression and iron metabolism." Nat Genet **41**(4): 482-487.

ARC Australia. (2012). "Animal Resources Centre Biological Data." Retrieved July 2012, from http://www.arc.wa.gov.au/reference.php?to=biological_data.

Armah, C. N., P. Sharp, et al. (2008). "L-alpha-glycerophosphocholine contributes to meat's enhancement of nonheme iron absorption." Journal of Nutrition **138**(5): 873-877.

Bakhautdin, B., M. Febbraio, et al. (2012). "Protective role of macrophage-derived ceruloplasmin in inflammatory bowel disease." Gut.

Barbeau, K., E. L. Rue, et al. (2001). "Photochemical cycling of iron in the surface ocean mediated by microbial iron(III)-binding ligands." Nature **413**(6854): 409-413.

Bartnikas, T. B., D. R. Campagna, et al. (2010). "Characterization of mitochondrial ferritin-deficient mice." Am J Hematol **85**(12): 958-960.

Bates, G. W., E. F. Workman, Jr., et al. (1973). "Does transferrin exhibit ferroxidase activity?" Biochem Biophys Res Commun **50**(1): 84-90.

Behrenfeld, M. J. and Z. S. Kolber (1999). "Widespread iron limitation of phytoplankton in the south pacific ocean." Science **283**(5403): 840-843.

Bencze, K. Z., K. C. Kondapalli, et al. (2006). "The structure and function of frataxin." Crit Rev Biochem Mol Biol **41**(5): 269-291.

Bento, I., C. Peixoto, et al. (2007). "Ceruloplasmin revisited: structural and functional roles of various metal cation-binding sites." Acta Crystallogr D Biol Crystallogr **63**(Pt 2): 240-248.

Berman, H. M., J. Westbrook, et al. (2000). "The Protein Data Bank." Nucleic Acids Res **28**(1): 235-242.

Boelaert, J. R., S. J. Vandecasteele, et al. (2007). "The effect of the host's iron status on tuberculosis." J Infect Dis. **195**(12): 1745-1753.
Bothwell, T. H., R. W. Charlton, et al. (1979). Iron Metabolism in Man. Oxford, Blackwell Scientific.
Bou-Abdallah, F., P. Santambrogio, et al. (2005). "Unique iron binding and oxidation properties of human mitochondrial ferritin: a comparative analysis with Human H-chain ferritin." J Mol Biol **347**(3): 543-554.
Breuer, W., C. Hershko, et al. (2000). "The importance of non-transferrin bound iron in disorders of iron metabolism." Transfus Sci **23**(3): 185-192.
Brodal, P. (2010). The central nervous system : structure and function. New York, Oxford University Press.
Bush, A. I., K. Beyreuther, et al. (1993). "The beta A4 amyloid protein precursor in human circulation." Ann N Y Acad Sci **695**: 175-182.
Buys, S. S., C. B. Martin, et al. (1991). "Iron absorption in hypotransferrinemic mice." Blood **78**(12): 3288-3290.
Carlotti, F., A. Zaldumbide, et al. (2011). "beta-Cell Generation: Can Rodent Studies Be Translated to Humans?" J Transplant **2011**: 892453.
Casellas, J. and J. F. Medrano (2008). "Within-generation mutation variance for litter size in inbred mice." Genetics **179**(4): 2147-2155.
Cha, M. K. and I. H. Kim (1999). "Ceruloplasmin has a distinct active site for the catalyzing glutathione-dependent reduction of alkyl hydroperoxide." Biochemistry **38**(37): 12104-12110.
Chasteen, N. D. and P. M. Harrison (1999). "Mineralization in ferritin: an efficient means of iron storage." J Struct Biol **126**(3): 182-194.
Chen, H., Z. K. Attieh, et al. (2009). "Decreased hephaestin expression and activity leads to decreased iron efflux from differentiated Caco2 cells." J Cell Biochem **107**(4): 803-808.
Chen, H., Z. K. Attieh, et al. (2009). "Age-related changes in iron homeostasis in mouse ferroxidase mutants." Biometals **22**(5): 827-834.
Chen, H., Z. K. Attieh, et al. (2004). "Hephaestin is a ferroxidase that maintains partial activity in sex-linked anemia mice." Blood **103**(10): 3933-3939.
Chen, H., Z. K. Attieh, et al. (2010). "Identification of zyklopen, a new member of the vertebrate multicopper ferroxidase family, and characterization in rodents and human cells." J Nutr **140**(10): 1728-1735.
Chen, H., T. Su, et al. (2003). "Systemic regulation of Hephaestin and Ireg1 revealed in studies of genetic and nutritional iron deficiency." Blood **102**(5): 1893-1899.
Cherukuri, S., R. Potla, et al. (2005). "Unexpected role of ceruloplasmin in intestinal iron absorption." Cell Metab **2**(5): 309-319.
Cherukuri, S., N. A. Tripoulas, et al. (2004). "Anemia and impaired stress-induced erythropoiesis in aceruloplasminemic mice." Blood Cells Mol Dis **33**(3): 346-355.
Chua, A. C., C. E. Herbison, et al. (2008). "The role of Hfe in transferrin-bound iron uptake by hepatocytes." Hepatology **47**(5): 1737-1744.

Cnop, M., S. J. Hughes, et al. (2010). "The long lifespan and low turnover of human islet beta cells estimated by mathematical modelling of lipofuscin accumulation." Diabetologia **53**(2): 321-330.
Collins, H. L. (2003). "The role of iron in infections with intracellular bacteria." Immunol Lett **85**(2): 193-195.
Collins, J. F. and G. J. Anderson (2012). Molecular Mechanisms of Intestinal Iron Transport. Physiology of the Gastrointestinal Tract. L. R. Johnson. Oxford, Academic Press. **1:** 1921-1948.
Collins, J. F., M. Wessling-Resnick, et al. (2008). "Hepcidin regulation of iron transport." J Nutr **138**(11): 2284-2288.
Columbus Instruments. (2012). "Equations." Retrieved November 2012, 2012, from http://colinst.com/equations.pdf.
Conrad, M. E. and J. C. Barton (1981). "Factors affecting iron balance." Am J Hematol **10**(2): 199-225.
Conrad, M. E., S. Cortell, et al. (1966). "Polymerization and intraluminal factors in the absorption of hemoglobin-iron." J Lab Clin Med **68**(4): 659-668.
Conrad, M. E., L. R. Weintraub, et al. (1966). "Absorption of hemoglobin iron." Am J Physiol **211**(5): 1123-1130.
Craven, C. M., J. Alexander, et al. (1987). "Tissue distribution and clearance kinetics of non-transferrin-bound iron in the hypotransferrinemic mouse: a rodent model for hemochromatosis." Proc Natl Acad Sci U S A **84**(10): 3457-3461.
Crichton, R. R. (2001). Inorganic Biochemistry of Iron Metabolism From Molecular Mechanisms to Clinical Consequences. Chichester, New York, Wiley.
Crichton, R. R. and J. P. Declercq (2010). "X-ray structures of ferritins and related proteins." Biochim Biophys Acta **1800**(8): 706-718.
Crouter, S. E., D. M. DellaValle, et al. (2012). "Relationship between physical activity, physical performance, and iron status in adult women." Appl Physiol Nutr Metab **37**(4): 697-705.
Dahms, S. O., I. Konnig, et al. (2012). "Metal binding dictates conformation and function of the amyloid precursor protein (APP) E2 domain." J Mol Biol **416**(3): 438-452.
Darshan, D., D. M. Frazer, et al. (2010). "Molecular basis of iron-loading disorders." Expert Rev Mol Med **12**: e36.
Darshan, D., D. M. Frazer, et al. (2010). "Severe iron deficiency blunts the response of the iron regulatory gene Hamp and pro-inflammatory cytokines to lipopolysaccharide." Haematologica **95**(10): 1660-1667.
Darshan, D., L. Vanoaica, et al. (2009). "Conditional deletion of ferritin H in mice induces loss of iron storage and liver damage." Hepatology **50**(3): 852-860.
Das, D., N. Tapryal, et al. (2007). "Regulation of ceruloplasmin in human hepatic cells by redox active copper: identification of a novel AP-1 site in the ceruloplasmin gene." Biochem J **402**(1): 135-141.

David, S. and B. N. Patel (2000). Ceruloplasmin: Structure and function of an essential ferroxidase Advances in Structural Biology. S. K. Malhotra. Stamford, JAI PRESS INC. **6:** 211-237.
de Benoist, B., E. McLean, et al., Eds. (2008). Worldwide prevalence of anaemia 1993-2005: WHO Global Database on Anaemia. Geneva, World Health Organization.
De Domenico, I., M. B. Vaughn, et al. (2006). "Ferroportin-mediated mobilization of ferritin iron precedes ferritin degradation by the proteasome." EMBO J **25**(22): 5396-5404.
De Domenico, I., D. M. Ward, et al. (2007). "Ferroxidase activity is required for the stability of cell surface ferroportin in cells expressing GPI-ceruloplasmin." EMBO J **26**(12): 2823-2831.
De Domenico, I., D. M. Ward, et al. (2009). "Specific iron chelators determine the route of ferritin degradation." Blood **114**(20): 4546-4551.
De Domenico, I., D. M. Ward, et al. (2005). "The molecular basis of ferroportin-linked hemochromatosis." Proc Natl Acad Sci U S A **102**(25): 8955-8960.
De Luca, N. G. and P. M. Wood (2000). "Iron uptake by fungi: contrasted mechanisms with internal or external reduction." Adv Microb Physiol **43**: 39-74.
de Silva, D., S. Davis-Kaplan, et al. (1997). "Purification and characterization of Fet3 protein, a yeast homologue of ceruloplasmin." J Biol Chem **272**(22): 14208-14213.
Dhakshinamoorthy, S., A. K. Jain, et al. (2005). "Bach1 competes with Nrf2 leading to negative regulation of the antioxidant response element (ARE)-mediated NAD(P)H:quinone oxidoreductase 1 gene expression and induction in response to antioxidants." J Biol Chem **280**(17): 16891-16900.
Donovan, A., A. Brownlie, et al. (2000). "Positional cloning of zebrafish ferroportin1 identifies a conserved vertebrate iron exporter." Nature **403**(6771): 776-781.
Donovan, A., C. A. Lima, et al. (2005). "The iron exporter ferroportin/Slc40a1 is essential for iron homeostasis." Cell Metab **1**(3): 191-200.
Dostalikova-Cimburova, M., K. Kratka, et al. (2012). "Duodenal expression of iron transport molecules in patients with hereditary hemochromatosis or iron deficiency." J Cell Mol Med **16**(8): 1816-1826.
Drakesmith, H. and A. Prentice (2008). "Viral infection and iron metabolism." Nat Rev Microbiol **6**(7): 541-552.
Du, X., E. She, et al. (2008). "The serine protease TMPRSS6 is required to sense iron deficiency." Science **320**(5879): 1088-1092.
Duce, J. A., A. Tsatsanis, et al. (2010). "Iron-export ferroxidase activity of beta-amyloid precursor protein is inhibited by zinc in Alzheimer's disease." Cell **142**(6): 857-867.
Ebrahimi, K. H., P. L. Hagedoorn, et al. (2012). "A synthetic peptide with the putative iron binding motif of amyloid precursor protein (APP) does not catalytically oxidize iron." PLoS One **7**(8): e40287.

el Marjou, F., K. P. Janssen, et al. (2004). "Tissue-specific and inducible Cre-mediated recombination in the gut epithelium." Genesis **39**(3): 186-193.
Ferreira, C., D. Bucchini, et al. (2000). "Early embryonic lethality of H ferritin gene deletion in mice." J Biol Chem **275**(5): 3021-3024.
Finberg, K. E., R. L. Whittlesey, et al. (2010). "Down-regulation of Bmp/Smad signaling by Tmprss6 is required for maintenance of systemic iron homeostasis." Blood **115**(18): 3817-3826.
Flicek, P., M. R. Amode, et al. (2012). "Ensembl 2012." Nucleic Acids Res **40**(Database issue): D84-90.
Folgueras, A. R., F. M. de Lara, et al. (2008). "Membrane-bound serine protease matriptase-2 (Tmprss6) is an essential regulator of iron homeostasis." Blood **112**(6): 2539-2545.
Fortna, R. R., H. A. Watson, et al. (1999). "Glycosyl phosphatidylinositol-anchored ceruloplasmin is expressed by rat Sertoli cells and is concentrated in detergent-insoluble membrane fractions." Biol Reprod **61**(4): 1042-1049.
Frazer, D. M., C. D. Vulpe, et al. (2001). "Cloning and gastrointestinal expression of rat hephaestin: relationship to other iron transport proteins." Am J Physiol Gastrointest Liver Physiol **281**(4): G931-939.
Frazer, D. M., S. J. Wilkins, et al. (2003). "A rapid decrease in the expression of DMT1 and Dcytb but not Ireg1 or hephaestin explains the mucosal block phenomenon of iron absorption." Gut **52**(3): 340-346.
Galloway, S., L. Jian, et al. (2007). "beta-Amyloid or its precursor protein is found in epithelial cells of the small intestine and is stimulated by high-fat feeding." The Journal of Nutritional Biochemistry **18**: 279-284.
Gao, J., J. Chen, et al. (2009). "Interaction of the hereditary hemochromatosis protein HFE with transferrin receptor 2 is required for transferrin-induced hepcidin expression." Cell Metab **9**(3): 217-227.
Goswami, T. and N. C. Andrews (2006). "Hereditary hemochromatosis protein, HFE, interaction with transferrin receptor 2 suggests a molecular mechanism for mammalian iron sensing." J Biol Chem **281**(39): 28494-28498.
Grewal, M. S. (1962). "A sex-linked anaemia in the mouse." Genetics Research **3**: 238-247.
Gunshin, H., Y. Fujiwara, et al. (2005). "Slc11a2 is required for intestinal iron absorption and erythropoiesis but dispensable in placenta and liver." J Clin Invest **115**(5): 1258-1266.
Gunshin, H., B. Mackenzie, et al. (1997). "Cloning and characterization of a mammalian proton-coupled metal-ion transporter." Nature **388**(6641): 482-488.
Gutierrez, J. A., J. Yu, et al. (1997). "Functional expression cloning and characterization of SFT, a stimulator of Fe transport." J Cell Biol **139**(4): 895-905.

Ha-Duong, N. T., C. Eid, et al. (2010). "In vitro interaction between ceruloplasmin and human serum transferrin." Biochemistry **49**(48): 10261-10263.
Hadziahmetovic, M., T. Dentchev, et al. (2008). "Ceruloplasmin/hephaestin knockout mice model morphologic and molecular features of AMD." Invest Ophthalmol Vis Sci **49**(6): 2728-2736.
Hahn, P., Y. Qian, et al. (2004). "Disruption of ceruloplasmin and hephaestin in mice causes retinal iron overload and retinal degeneration with features of age-related macular degeneration." Proc Natl Acad Sci U S A **101**(38): 13850-13855.
Hall-Sizemore, A., J. J. Joseph, et al. (1994). "Xanthine oxidase: an efficient promoter of the iron loading of apoferritin." Biochem Mol Biol Int **33**(2): 393-403.
Han, O. and E. Y. Kim (2007). "Colocalization of ferroportin-1 with hephaestin on the basolateral membrane of human intestinal absorptive cells." J Cell Biochem **101**(4): 1000-1010.
Harding, K. B. and L. M. Neufeld (2012). "Iron deficiency and anemia control for infants and young children in malaria-endemic areas: a call to action and consensus among the research community." Adv Nutr **3**(4): 551-554.
Harris, D. C. and P. Aisen (1973). "Facilitation of Fe(II) autoxidation by Fe(3) complexing agents." Biochim Biophys Acta **329**(1): 156-158.
Harris, Z. L., A. P. Durley, et al. (1999). "Targeted gene disruption reveals an essential role for ceruloplasmin in cellular iron efflux." Proc Natl Acad Sci U S A **96**(19): 10812-10817.
Harrison, P. M. and P. Arosio (1996). "The ferritins: molecular properties, iron storage function and cellular regulation." Biochim Biophys Acta **1275**(3): 161-203.
Hatanaka, Y., T. Okano, et al. (2003). "Aceruloplasminemia with juvenile-onset diabetes mellitus caused by exon skipping in the ceruloplasmin gene." Intern Med **42**(7): 599-604.
Healy, J. and K. Tipton (2007). "Ceruloplasmin and what it might do." J Neural Transm **114**(6): 777-781.
Hellman, N. E. and J. D. Gitlin (2002). "Ceruloplasmin metabolism and function." Annu Rev Nutr **22**: 439-458.
Hempstead, P. D., S. J. Yewdall, et al. (1997). "Comparison of the three-dimensional structures of recombinant human H and horse L ferritins at high resolution." J Mol Biol **268**(2): 424-448.
Hinoi, T., G. Gesina, et al. (2005). "CDX2-regulated expression of iron transport protein hephaestin in intestinal and colonic epithelium." Gastroenterology **128**(4): 946-961.
Hintze, K. J., Y. Katoh, et al. (2007). "Bach1 repression of ferritin and thioredoxin reductase1 is heme-sensitive in cells and in vitro and coordinates expression with heme oxygenase1, beta-globin, and NADP(H) quinone (oxido) reductase1." J Biol Chem **282**(47): 34365-34371.

Hintze, K. J. and E. C. Theil (2005). "DNA and mRNA elements with complementary responses to hemin, antioxidant inducers, and iron control ferritin-L expression." Proc Natl Acad Sci U S A **102**(42): 15048-15052.
Hintze, K. J. and E. C. Theil (2006). "Cellular regulation and molecular interactions of the ferritins." Cell Mol Life Sci **63**(5): 591-600.
Hornbeck, P. V., J. M. Kornhauser, et al. (2012). "PhosphoSitePlus: a comprehensive resource for investigating the structure and function of experimentally determined post-translational modifications in man and mouse." Nucleic Acids Res **40**(Database issue): D261-270.
Horton, S. and J. Ross (2003). "The economics of iron deficiency." Food Policy **28**(1): 51-75.
Hubel, C. A., L. M. Bodnar, et al. (2004). "Nonglycosylated ferritin predominates in the circulation of women with preeclampsia but not intrauterine growth restriction." Clin Chem **50**(5): 948-951.
Hudson, D. M., S. B. Curtis, et al. (2009). "Human hephaestin expression is not limited to enterocytes of the GI tract but is also found in the antrum, the enteric nervous system and pancreatic {beta}-cells." Am J Physiol Gastrointest Liver Physiol.
Hudson, D. M., M. J. Krisinger, et al. (2008). "Neither human hephaestin nor ceruloplasmin forms a stable complex with transferrin." J Cell Biochem **103**(6): 1849-1855.
Hunt, J. R., C. A. Zito, et al. (1994). "Severe or marginal iron deficiency affects spontaneous physical activity in rats." Am J Clin Nutr **59**(2): 413-418.
Hurrell, R. F., R. M. B., et al. (2006). "Meat protein fractions enhance nonheme iron absorption in humans." Journal of Nutrition **136**(11): 2808-2812.
Ichida, K., Y. Amaya, et al. (1997). "Identification of two mutations in human xanthine dehydrogenase gene responsible for classical type I xanthinuria." J Clin Invest **99**(10): 2391-2397.
Ilbert, M. and V. Bonnefoy (2012). "Insight into the evolution of the iron oxidation pathways." Biochim Biophys Acta.
Imhoff-Kunsch, B. and V. Briggs (2012). "Antihelminthics in pregnancy and maternal, newborn and child health." Paediatr Perinat Epidemiol **26 Suppl 1**: 223-238.
Jankowska, E. A. and P. Ponikowski (2010). "Molecular changes in myocardium in the course of anemia or iron deficiency." Heart Fail Clin **6**(3): 295-304.
Jeong, J. a. G., M. L. (2009). "Homing in on iron homeostasis in plants." Trends in Plant Science **14**(5): 280-285.
Jeong, S. Y. and S. David (2003). "Glycosylphosphatidylinositol-anchored ceruloplasmin is required for iron efflux from cells in the central nervous system." J Biol Chem **278**(29): 27144-27148.
Jin, W., H. Takagi, et al. (2001). ""Opening" the ferritin pore for iron release by mutation of conserved amino acids at interhelix and loop sites." Biochemistry **40**(25): 7525-7532.

Johnson, L. R., F. K. Ghishan, et al. (2012). Physiology of the Gastrointestinal Tract. Set. San Diego, Academic Press Imprint

Elsevier Science & Technology Books.

Kalgaonkar, S. and B. Lonnerdal (2009). "Receptor-mediated uptake of ferritin-bound iron by human intestinal Caco-2 cells." J Nutr Biochem **20**(4): 304-311.

Kato, J., K. Fujikawa, et al. (2001). "A mutation, in the iron-responsive element of H ferritin mRNA, causing autosomal dominant iron overload." Am J Hum Genet **69**(1): 191-197.

Kato, T., M. Daimon, et al. (1997). "Islet changes in hereditary ceruloplasmin deficiency." Hum Pathol **28**(4): 499-502.

Kelley, M. K. and N. K. Amy (1984). "Effect of molybdenum-deficient and low iron diets on xanthine oxidase activity and iron status in rats." J Nutr **114**(9): 1652-1659.

Khalifa, N. B., J. Van Hees, et al. (2010). "What is the role of amyloid precursor protein dimerization?" Cell Adh Migr **4**(2): 268-272.

Komeili, A., Z. Li, et al. (2006). "Magnetosomes are cell membrane invaginations organized by the actin-like protein MamK." Science **311**(5758): 242-245.

Kono, S., K. Yoshida, et al. (2010). "Biological effects of mutant ceruloplasmin on hepcidin-mediated internalization of ferroportin." Biochim Biophys Acta **1802**(11): 968-975.

Kosman, D. J. (2010). "Multicopper oxidases: a workshop on copper coordination chemistry, electron transfer, and metallophysiology." J Biol Inorg Chem **15**(1): 15-28.

Kosman, D. J. (2010). "Redox cycling in iron uptake, efflux, and trafficking." J Biol Chem **285**(35): 26729-26735.

Kratz, A., M. Ferraro, et al. (2004). " Case records of the Massachusetts General Hospital. Weekly clinicopathological exercises. Laboratory reference values." The New England Journal of Medicine **351**(15): 1548-1563.

Kroger, A., E. B. Bachli, et al. (2011). "Hyperferritinemia without iron overload in patients with bilateral cataracts: a case series." J Med Case Rep **5**: 471.

Kuo, Y. M., T. Su, et al. (2004). "Mislocalisation of hephaestin, a multicopper ferroxidase involved in basolateral intestinal iron transport, in the sex linked anaemia mouse." Gut **53**(2): 201-206.

Kwok, E. Y., S. Severance, et al. (2006). "Evidence for iron channeling in the Fet3p-Ftr1p high-affinity iron uptake complex in the yeast plasma membrane." Biochemistry **45**(20): 6317-6327.

Lakhan, S. E., M. Avramut, et al. (2012). "Structural and Functional Neuroimaging in Migraine: Insights From 3 Decades of Research." Headache.

Langlois d'Estaintot, B., P. Santambrogio, et al. (2004). "Crystal structure and biochemical properties of the human mitochondrial ferritin and its mutant Ser144Ala." J Mol Biol **340**(2): 277-293.

Lee, G. R., S. Nacht, et al. (1968). "Iron metabolism in copper-deficient swine." J Clin Invest **47**(9): 2058-2069.
Lee, S., Y. Xue, et al. (2011). "The E2 domains of APP and APLP1 share a conserved mode of dimerization." Biochemistry **50**(24): 5453-5464.
Lee, S. M., Z. K. Attieh, et al. (2012). "Iron repletion relocalizes hephaestin to a proximal basolateral compartment in polarized MDCK and Caco2 cells." Biochem Biophys Res Commun **421**(3): 449-455.
Lei, P., S. Ayton, et al. (2012). "Tau deficiency induces parkinsonism with dementia by impairing APP-mediated iron export." Nat Med **18**(2): 291-295.
Levi, S., B. Corsi, et al. (2001). "A human mitochondrial ferritin encoded by an intronless gene." J Biol Chem **276**(27): 24437-24440.
Linder, N., J. Rapola, et al. (1999). "Cellular expression of xanthine oxidoreductase protein in normal human tissues." Lab Invest **79**(8): 967-974.
Lindley, P. F. (2001). Ceruloplasmin. Handbook of Metalloproteins. A. Messerschmidt, R. Huber, T. Poulos and K. Weighardt. Chichester, John Wiley and Sons**:** 1369-1380.
Lipkin, M. (1985). "Growth and development of gastrointestinal cells." Annual Review of Physiology **47**(1): 175-197.
Lonnerdal, B. (2009). "Soybean ferritin: implications for iron status of vegetarians." Am J Clin Nutr **89**(5): 1680S-1685S.
Luscieti, S., P. Santambrogio, et al. (2010). "Mutant ferritin L-chains that cause neurodegeneration act in a dominant-negative manner to reduce ferritin iron incorporation." J Biol Chem **285**(16): 11948-11957.
Lutsenko, S., N. L. Barnes, et al. (2007). "Function and regulation of human copper-transporting ATPases." Physiol Rev **87**(3): 1011-1046.
Ma, Y., M. Yeh, et al. (2006). "Iron Imports. V. Transport of iron through the intestinal epithelium." Am J Physiol Gastrointest Liver Physiol **290**(3): G417-422.
Macdougall, I. C. (2011). "Iron supplementation in nephrology and oncology: what do we have in common?" Oncologist **16 Suppl 3**: 25-34.
MacPyMOL (2006). The PyMOL Molecular Graphics System, Version 1.5.0.4 Schrödinger, LLC.
Maher, B. H., R. A. Lea, et al. (2012). "An x chromosome association scan of the Norfolk Island genetic isolate provides evidence for a novel migraine susceptibility locus at Xq12." PLoS One **7**(5): e37903.
Marques, L., A. Auriac, et al. (2012). "Immune cells and hepatocytes express glycosylphosphatidylinositol-anchored ceruloplasmin at their cell surface." Blood Cells Mol Dis **48**(2): 110-120.
Martin, F., T. Linden, et al. (2005). "Copper-dependent activation of hypoxia-inducible factor (HIF)-1: implications for ceruloplasmin regulation." Blood **105**(12): 4613-4619.

Mastrogiannaki, M., P. Matak, et al. (2009). "HIF-2alpha, but not HIF-1alpha, promotes iron absorption in mice." J Clin Invest **119**(5): 1159-1166.
McDermid, J. M., M. F. van der Loeff, et al. (2009). "Mortality in HIV infection is independently predicted by host iron status and SLC11A1 and HP genotypes, with new evidence of a gene-nutrient interaction." Am J Clin Nutr. **90**(1): 225-233.
McKie, A. (2008). "The role of Dcytb in iron metabolism: an update." Biochemical Society Transactions **36**(Pt 6): 1239-1241.
McKie, A. T., P. Marciani, et al. (2000). "A novel duodenal iron-regulated transporter, IREG1, implicated in the basolateral transfer of iron to the circulation." Mol Cell **5**(2): 299-309.
Meyer, L. A., A. P. Durley, et al. (2001). "Copper transport and metabolism are normal in aceruloplasminemic mice." J Biol Chem **276**(39): 36857-36861.
Meynard, D., L. Kautz, et al. (2009). "Lack of the bone morphogenetic protein BMP6 induces massive iron overload." Nat Genet **41**(4): 478-481.
Millard, K. N., D. M. Frazer, et al. (2004). "Changes in the expression of intestinal iron transport and hepatic regulatory molecules explain the enhanced iron absorption associated with pregnancy in the rat." Gut **53**(5): 655-660.
Morita, H., S. Ikeda, et al. (1995). "Hereditary ceruloplasmin deficiency with hemosiderosis: a clinicopathological study of a Japanese family." Ann Neurol **37**(5): 646-656.
Mukhopadhyay, C. K., B. Mazumder, et al. (2000). "Role of hypoxia-inducible factor-1 in transcriptional activation of ceruloplasmin by iron deficiency." J Biol Chem **275**(28): 21048-21054.
Naiche, L. A. and V. E. Papaloannou (2007). "Cre activity causes widespread apoptosis and lethal anemia during embryonic development." Genesis **45**(12): 768-775.
Nandal, A., J. C. Ruiz, et al. (2011). "Activation of the HIF prolyl hydroxylase by the iron chaperones PCBP1 and PCBP2." Cell Metabolism **14**(5): 647-657.
Nemeth, E. and T. Ganz (2009). "The role of hepcidin in iron metabolism." Acta Haematol **122**(2-3): 78-86.
Nemeth, E., S. Rivera, et al. (2004). "IL-6 mediates hypoferremia of inflammation by inducing the synthesis of the iron regulatory hormone hepcidin." J Clin Invest **113**(9): 1271-1276.
Nemeth, E., M. S. Tuttle, et al. (2004). "Hepcidin regulates cellular iron efflux by binding to ferroportin and inducing its internalization." Science **306**(5704): 2090-2093.
Nittis, T. and J. D. Gitlin (2004). "Role of copper in the proteosome-mediated degradation of the multicopper oxidase hephaestin." J Biol Chem **279**(24): 25696-25702.
O'Neill, H. A., O. Gakh, et al. (2005). "Assembly of human frataxin is a mechanism for detoxifying redox-active iron." Biochemistry **44**(2): 537-545.

O'Riordan, D. K., P. Sharp, et al. (1995). "Cellular mechanisms underlying the increased duodenal iron absorption in rats in response to phenylhydrazine-induced haemolytic anaemia." Eur J Clin Invest **25**(10): 722-727.
Ohgami, R. S., D. R. Campagna, et al. (2006). "The Steap proteins are metalloreductases." Blood **108**(4): 1388-1394.
Ohtsubo, T., Rovira, II, et al. (2004). "Xanthine oxidoreductase is an endogenous regulator of cyclooxygenase-2." Circ Res **95**(11): 1118-1124.
Osaki, S., D. A. Johnson, et al. (1966). "The possible significance of the ferrous oxidase activity of ceruloplasmin in normal human serum." Journal of Biological Chemistry **241**(12): 2746-2751.
Pallebage-Gamarallage, M. M., S. Galloway, et al. (2012). "Probucol suppresses enterocytic accumulation of amyloid-beta induced by saturated fat and cholesterol feeding." Lipids **47**(1): 27-34.
Park, S., O. Gakh, et al. (2002). "The ferroxidase activity of yeast frataxin." J Biol Chem **277**(41): 38589-38595.
Patel, B. N. and S. David (1997). "A novel glycosylphosphatidylinositol-anchored form of ceruloplasmin is expressed by mammalian astrocytes." J Biol Chem **272**(32): 20185-20190.
Patel, B. N., R. J. Dunn, et al. (2002). "Ceruloplasmin regulates iron levels in the CNS and prevents free radical injury." J Neurosci **22**(15): 6578-6586.
Perls, M. (1867). "Nachweis von Eisenoxyd in gewissen Pigmenten." Virchow's Arch Pathol Anat **39**: 42-48.
Pinero, D., B. Jones, et al. (2001). "Variations in dietary iron alter behavior in developing rats." J Nutr **131**(2): 311-318.
Piret, S. E., C. T. Esapa, et al. (2012). "A mouse model of early-onset renal failure due to a xanthine dehydrogenase nonsense mutation." PLoS One **7**(9): e45217.
Posey, J. E. and F. C. Gherardini (2000). "Lack of a role for iron in the Lyme disease pathogen." Science **288**(5471): 1651-1653.
Prohaska, J. R. (2011). "Impact of copper limitation on expression and function of multicopper oxidases (ferroxidases)." Adv Nutr **2**(2): 89-95.
Qian, Z. M., Y. Z. Chang, et al. (2007). "Expression of ferroportin1, hephaestin and ceruloplasmin in rat heart." Biochim Biophys Acta **1772**(5): 527-532.
Qiu, A., M. Jansen, et al. (2006). "Identification of an intestinal folate transporter and the molecular basis for hereditary folate malabsorption." Cell **127**(5): 917-928.
Raffin, S. B., C. H. Woo, et al. (1974). "Intestinal absorption of hemoglobin iron-heme cleavage by mucosal heme oxygenase." J Clin Invest **54**(6): 1344-1352.
Ramos, E., L. Kautz, et al. (2011). "Evidence for distinct pathways of hepcidin regulation by acute and chronic iron loading in mice." Hepatology **53**(4): 1333-1341.

Ranganathan, P. N., Y. Lu, et al. (2012). "Discovery of a cytosolic/soluble ferroxidase in rodent enterocytes." Proceedings of the National Academy of Sciences **109**(9): 3564-3569.
Ranganathan, P. N., Y. Lu, et al. (2012). "Discovery of a cytosolic/soluble ferroxidase in rodent enterocytes." Proc Natl Acad Sci U S A **109**(9): 3564-3569.
Ranganathan, P. N., Y. Lu, et al. (2012). "Immunoreactive Hephaestin and ferroxidase activity are present in the cytosolic fraction of rat enterocytes." Biometals **25**(4): 687-695.
Rogers, J. T., A. I. Bush, et al. (2008). "Iron and the translation of the amyloid precursor protein (APP) and ferritin mRNAs: riboregulation against neural oxidative damage in Alzheimer's disease." Biochem Soc Trans **36**(Pt 6): 1282-1287.
Rouault, T. A. (2012). Regulation of Iron Metabolism in Mammalian Cells. Iron Physiology and Pathophysiology in Humans. G. J. Anderson and G. D. McLaren. New York, Humana Press**:** 51-62.
Roy, C. N. (2012). The Anemia of Inflammation and Chronic Disease. Iron Physiology and Pathophysiology in Humans. G. J. Anderson and G. D. McLaren. New York, Humana Press**:** 303-320.
Rydén, L. (1984). Copper Proteins, Copper Enzymes. R. Lontie. Boca Raton, FL, CRC Press. **3:** 37-101.
Sabatucci, A., P. Vachette, et al. (2007). "Structural characterization of the ceruloplasmin: lactoferrin complex in solution." J Mol Biol **371**(4): 1038-1046.
San Martin, C. D., C. Garri, et al. (2008). "Caco-2 intestinal epithelial cells absorb soybean ferritin by mu2 (AP2)-dependent endocytosis." J Nutr **138**(4): 659-666.
Santambrogio, P., G. Biasiotto, et al. (2007). "Mitochondrial ferritin expression in adult mouse tissues." J Histochem Cytochem **55**(11): 1129-1137.
Sarkar, J., V. Seshadri, et al. (2003). "Role of ceruloplasmin in macrophage iron efflux during hypoxia." J Biol Chem **278**(45): 44018-44024.
Sazawal, S., R. E. Black, et al. (2006). "Effects of routine prophylactic supplementation with iron and folic acid on admission to hospital and mortality in preschool children in a high malaria transmission setting: community-based, randomised, placebo-controlled trial." Lancet **367**(9505): 133-143.
Schmidt, G. H., D. J. Winton, et al. (1988). "Development of the pattern of cell renewal in the crypt-villus unit of chimaeric mouse small intestine." Development **103**(4): 785-790.
Schmidt, P. J., P. T. Toran, et al. (2008). "The transferrin receptor modulates Hfe-dependent regulation of hepcidin expression." Cell Metab **7**(3): 205-214.

Schulz, K., C. D. Vulpe, et al. (2011). "Iron efflux from oligodendrocytes is differentially regulated in gray and white matter." J Neurosci **31**(37): 13301-13311.
Seelig, M. S. (1972). "Review: relationships of copper and molybdenum to iron metabolism." Am J Clin Nutr **25**(10): 1022-1037.
Shah, Y. M., T. Matsubara, et al. (2009). "Intestinal hypoxia-inducible transcription factors are essential for iron absorption following iron deficiency." Cell Metab **9**(2): 152-164.
Shamsian, B. S., N. Rezaei, et al. (2009). "Severe hypochromic microcytic anemia in a patient with congenital atransferrinemia." Pediatr Hematol Oncol **26**(5): 356-362.
Sharp, P. A. (2010). "Intestinal iron absorption: Regulation by dietary and systemic factors." International Journal for Vitamin and Nutrition Research **80**(4-5): 231-242.
Shaw, J. A., D. J. Macey, et al. (2010). "Tooth use and wear in three iron-biomineralizing mollusc species." Biol Bull **218**(2): 132-144.
Shaw, J. G. and J. F. Friedman (2011). "Iron deficiency anemia: focus on infectious diseases in lesser developed countries." Anemia **2011**: 260380.
Shayeghi, M., G. O. Latunde-Dada, et al. (2005). "Identification of an intestinal heme transporter." Cell **122**(5): 789-801.
Shi, H., K. Z. Bencze, et al. (2008). "A cytosolic iron chaperone that delivers iron to ferritin." Science **320**(5880): 1207-1210.
Shiva, S., X. Wang, et al. (2006). "Ceruloplasmin is a NO oxidase and nitrite synthase that determines endocrine NO homeostasis." Nat Chem Biol **2**(9): 486-493.
Skikne, B. S., S. R. Lynch, et al. (1981). "Role of gastric acid in food iron absorption." Gastroenterology **81**(6): 1068-1071.
Sonnweber, T., C. Ress, et al. (2012). "High-fat diet causes iron deficiency via hepcidin-independent reduction of duodenal iron absorption." J Nutr Biochem.
Sorbie, J., D. L. Hamilton, et al. (1974). "Effect of various factors on iron absorption in mice with X-linked anaemia." Br J Haematol **27**(4): 559-569.
Stoltzfus, R. J. (2008). "Research needed to strengthen science and programs for the control of iron deficiency and its consequences in young children." J Nutr **138**(12): 2542-2546.
Stoltzfus, R. J. (2011). "Iron interventions for women and children in low-income countries." J Nutr **141**(4): 756S-762S.
Stuart, K. A., G. J. Anderson, et al. (2004). "Increased duodenal expression of divalent metal transporter 1 and iron-regulated gene 1 in cirrhosis." Hepatology **39**(2): 492-499.
Stuart, K. A., G. J. Anderson, et al. (2003). "Duodenal expression of iron transport molecules in untreated haemochromatosis subjects." Gut **52**(7): 953-959.

Syed, B. A., N. J. Beaumont, et al. (2002). "Analysis of the human hephaestin gene and protein: comparative modelling of the N-terminus ecto-domain based upon ceruloplasmin." Protein Eng **15**(3): 205-214.
Taylor, M., A. Qu, et al. (2011). "Hypoxia-inducible factor-2α mediates the adaptive increase of intestinal ferroportin during iron deficiency in mice." Gastroenterology **140**(7): 2044-2055.
Terada, K., Y. Kawarada, et al. (1995). "Copper incorporation into ceruloplasmin in rat livers." Biochim Biophys Acta **1270**(1): 58-62.
Texel, S. J., S. Camandola, et al. (2012). "Ceruloplasmin deficiency results in an anxiety phenotype involving deficits in hippocampal iron, serotonin, and BDNF." J Neurochem **120**(1): 125-134.
The Jackson Laboratory (2009). Breeding Strategies for Maintaining Colonies of Laboratory Mice: A Jackson Laboratory Resource Manual, The Jackson Laboratory.
Theil, E. C. (2004). "Iron, ferritin, and nutrition." Annu Rev Nutr **24**: 327-343.
Theil, E. C. (2011). "Ferritin protein nanocages use ion channels, catalytic sites, and nucleation channels to manage iron/oxygen chemistry." Curr Opin Chem Biol **15**(2): 304-311.
Theil, E. C., H. Chen, et al. (2012). "Absorption of iron from ferritin is independent of heme iron and ferrous salts in women and rat intestinal segments." Journal of Nutrition **142**(3): 478-483.
Theil, E. C., M. Matzapetakis, et al. (2006). "Ferritins: iron/oxygen biominerals in protein nanocages." J Biol Inorg Chem **11**(7): 803-810.
Topham, R. W., M. R. Jackson, et al. (1986). "Studies of the ferroxidase activity of native and chemically modified xanthine oxidoreductase." Biochem J **235**(1): 39-44.
Torrance, J. D. and T. H. Bothwell (1968). "A simple technique for measuring storage iron concentrations in formalinised liver samples." S Afr J Med Sci **33**(1): 9-11.
Torti, F. M. and S. V. Torti (2002). "Regulation of ferritin genes and protein." Blood **99**(10): 3505-3516.
Trenor, C. C., 3rd, D. R. Campagna, et al. (2000). "The molecular defect in hypotransferrinemic mice." Blood **96**(3): 1113-1118.
Truett, G. E., P. Heeger, et al. (2000). "Preparation of PCR-quality mouse genomic DNA with hot sodium hydroxide and tris (HotSHOT)." Biotechniques **29**(1): 52, 54.
Umbreit, J. N., M. E. Conrad, et al. (2001). "The ferrireductase paraferritin contains divalent metal transporter as well as mobilferrin." American Journal of Physiology Gastrointestinal and Liver Physiology **282**(3): G534-539.
Untergasser, A., I. Cutcutache, et al. (2012). "Primer3--new capabilities and interfaces." Nucleic Acids Res **40**(15): e115.

Vanderford, D. A., P. K. Greer, et al. (2010). "Alopecia in IL-10-deficient mouse pups is c-kit-dependent and can be triggered by iron deficiency." Experimental Dermatology **19**(6): 518-526.
Vanoaica, L., D. Darshan, et al. (2010). "Intestinal ferritin H is required for an accurate control of iron absorption." Cell Metab **12**(3): 273-282.
Vashchenko, G., M. R. Bleackley, et al. (2011). "Oxidation of organic and biogenic amines by recombinant human hephaestin expressed in Pichia pastoris." Arch Biochem Biophys **514**(1-2): 50-56.
Verga Falzacappa, M. V., M. Vujic Spasic, et al. (2007). "STAT3 mediates hepatic hepcidin expression and its inflammatory stimulation." Blood **109**(1): 353-358.
Verley, F. A., D. Grahn, et al. (1967). "Sex ratio of mice as possible indicator of mutation rate for sex-linked lethals." The Journal of heredity **58**(6): 285-290.
Viatte, L. and S. Vaulont (2009). "Hepcidin, the iron watcher." Biochimie **91**(10): 1223-1228.
Vorbach, C., A. Scriven, et al. (2002). "The housekeeping gene xanthine oxidoreductase is necessary for milk fat droplet enveloping and secretion: gene sharing in the lactating mammary gland." Genes Dev **16**(24): 3223-3235.
Vujic Spasic, M., J. Kiss, et al. (2007). "Physiologic systemic iron metabolism in mice deficient for duodenal Hfe." Blood **109**(10): 4511-4517.
Vulpe, C. D., Y. M. Kuo, et al. (1999). "Hephaestin, a ceruloplasmin homologue implicated in intestinal iron transport, is defective in the sla mouse." Nat Genet **21**(2): 195-199.
Wallace, D. F., L. Summerville, et al. (2009). "Combined deletion of Hfe and transferrin receptor 2 in mice leads to marked dysregulation of hepcidin and iron overload." Hepatology **50**(6): 1992-2000.
Wan, Y., A. Saghatelian, et al. (2007). "Maternal PPAR gamma protects nursing neonates by suppressing the production of inflammatory milk." Genes and development **21**(15): 1895-1908.
Wang, W., M. A. Knovich, et al. (2010). "Serum ferritin: Past, present and future." Biochim Biophys Acta **1800**(8): 760-769.
Wang, Y., S. Zhu, et al. (2012). "Conditional knockout of the Menkes disease copper transporter demonstrates its critical role in embryogenesis." PLoS One **7**(8): e43039.
Wang, Z., C. Li, et al. (2006). "Structure of human ferritin L chain." Acta Crystallogr D Biol Crystallogr **62**(Pt 7): 800-806.
Weiss, G. and L. T. Goodnough (2005). "Anemia of chronic disease." N Engl J Med **352**(10): 1011-1023.
West, A. R. and P. S. Oates (2008). "Mechanisms of heme iron absorption: current questions and controversies." World J Gastroenterol **14**(26): 4101-4110.

Wheby, M. S. (1970). "Site of iron absorption in man." Scand J Haematol **7**(1): 56-62.
Wheby, M. S., G. E. Suttle, et al. (1970). "Intestinal absorption of hemoglobin iron." Gastroenterology **58**(5): 647-654.
Williamson, A. M. and K. T. Ng (1980). "Behavioral effects of iron deficiency in the adult rat." Physiol Behav **24**(3): 561-567.
Wolkow, N., D. Song, et al. (2012). "Ferroxidase hephaestin's cell-autonomous role in the retinal pigment epithelium." The American journal of pathology **180**(4): 1614-1624.
Worthington, M. T., S. M. Cohn, et al. (2001). "Characterization of a human plasma membrane heme transporter in intestinal and hepatocyte cell lines." Am J Physiol Gastrointest Liver Physiol **280**(6): G1172-1177.
Wrighting, D. M. and N. C. Andrews (2006). "Interleukin-6 induces hepcidin expression through STAT3." Blood **108**(9): 3204-3209.
Wyllie, J. C. and N. Kaufman (1982). "An electron microscopic study of heme uptake by rat duodenum." Lab Invest **47**(5): 471-476.
Xu, X., S. Pin, et al. (2004). "Aceruloplasminemia: an inherited neurodegenerative disease with impairment of iron homeostasis." Ann N Y Acad Sci **1012**: 299-305.
Yeh, K. Y., M. Yeh, et al. (2009). "Iron feeding induces ferroportin 1 and hephaestin migration and interaction in rat duodenal epithelium." Am J Physiol Gastrointest Liver Physiol **296**(1): G55-65.
Young, S. P., M. Fahmy, et al. (1997). "Ceruloplasmin, transferrin and apotransferrin facilitate iron release from human liver cells." FEBS Lett **411**(1): 93-96.
Zaitsev, V. N., I. Zaitseva, et al. (1999). "An X-ray crystallographic study of the binding sites of the azide inhibitor and organic substrates to ceruloplasmin, a multi-copper oxidase in the plasma." J Biol Inorg Chem **4**(5): 579-587.
Zhang, A. S., S. Xiong, et al. (2004). "Localization of iron metabolism-related mRNAs in rat liver indicate that HFE is expressed predominantly in hepatocytes." Blood **103**(4): 1509-1514.
Zhang, D. L., R. M. Hughes, et al. (2009). "A ferroportin transcript that lacks an iron-responsive element enables duodenal and erythroid precursor cells to evade translational repression." Cell Metab **9**(5): 461-473.
Zheng, H. and E. H. Koo (2006). "The amyloid precursor protein: beyond amyloid." Mol Neurodegener **1**: 5.
Zheng, S. J. (2010). "Iron homeostasis and iron acquisition in plants: maintenance, functions and consequences." Ann Bot **105**(5): 799-800.
Zhong, Z., J. J. Baker, et al. (2012). "Lrp5 and Lrp6 play compensatory roles in mouse intestinal development." J Cell Biochem **113**(1): 31-38.
Zoller, H., I. Theurl, et al. (2003). "Duodenal cytochrome b and hephaestin expression in patients with iron deficiency and hemochromatosis." Gastroenterology **125**(3): 746-754.

APPENDIX

Appendix 1.1. Genotyping protocol and primers

I. Protocol summary

DNA is prepared for genotyping from tail tips (1-2 mm long), ear punches, or a small aliquot (~5-10 µL) of homogenized tissue using either the QuickExtract™ DNA Extraction Solution (Epicentre®, cat #QE09050) per the manufacturer's instructions (but with only 50 µL extract solution per sample) at QIMR or the Hotshot Method at UCB (Truett, Heeger et al. 2000). For each genotyping reaction, 1 µL of prepared DNA is added to 11 µL of master mix. At QIMR, the MangoTaq™ DNA polymerase master mix (Bioline, cat #BIO-21083) is prepared per the manufacturer's instructions. At UCB, the GoTaq® Hotstart DNA Polymerase Master Mix (Promega, cat #M5122) is prepared as recommended by the manufacturer. Depending on the PCR machine used, the magnesium concentration may need to be increased, and glycerol may need to be added, for best results. The genotyping primers are stored frozen in 10 mM Tris-HCl, pH 8, at a concentration of 100 µM and thawed/refrozen for each use, and generally 0.125 µL are used per primer per reaction. PCR conditions are generally as follows: 95°C for 5 minutes, (95°C for 30 seconds, annealing temperature as noted below for 30 seconds, 72°C for 45 seconds) x 33 cycles, 72°C for 45 seconds, and then 4°C. The PCR products are then separated at 100V on 3% agarose gels made up with TAE buffer (50x TAE: 242 g Tris-base; 57.1 mL acetic acid; 18.6 g EDTA; complete to 1 L) and visualized with ethidium bromide.

II. Genotyping primers, annealing temperatures, and expected results

1. Hephaestin

A. Set 1: DL1 and DL2, 55°C annealing temperature

Primers:
DL1: 5'- GACCTAGGAAGGAGAATCATGAG -3'
DL2: 5'- TTTGCGAGCCGACCTTACACC -3'

Expected products:
240 bp = WT allele present
300 bp = Hp floxed allele present

Notes: Faint background doublet located between 240 and 300 bp seen in some $Hp^{-/-}$ samples.

B. Set 2. KO1, KO2, oIMR7338, oIMR7339, 55°C annealing temperature

Primers:
KO1: 5'- TGTCATTCAATTCCTGGAAAA -3'
KO2: 5'- CCAAGAAAATGGAGAAAGAGG -3'
oIMR7338: 5'- CTAGGCCACAGAATTGAAAGATCT -3'
oIMR7339: 5'- GTAGGTGGAAATTCTAGCATCATCC-3'

Expected products:
320 bp = genotyping reaction successful
230 bp = Hp knockout allele present

Notes: Primers oIMR17338 and oIMR7339, recommended by The Jackson Laboratory website, are internal controls that yield a 320 bp product in all mouse DNA samples if the reaction was successful.

C. Set 3. hephe9F1 and hephindelRC1, 55°C annealing temperature

Primers:
hephe9F1: 5'- TGCATGTTCCTAAACCAGGA -3'
hephindelRC1: 5'- CAGCCTTGCACACCAGTAGA -3'

Expected products:
370 bp = Hp WT (not *sla*) allele present

D. Set 4. hephe9F1 and hephslaRC1, 55°C annealing temperature

Primers:
hephe9F1: 5'- TGCATGTTCCTAAACCAGGA -3'
hephslaRC1: 5'- ATCTTGTTGCTCAGGCTGGT -3'

Expected products:
480 bp = *sla* allele present

2. Villin-cre recombinase

Primers, 64°C annealing temperature:
oIMR1878: 5'- GTGTGGGACAGAGAACAAACC -3'
oIMR1879: 5'- ACATCTTCAGGTTCTGCGGG -3'
oIMR0015: 5'- CAAATGTTGCTTGTCTGGTG -3'
oIMR0016: 5'- GTCAGTCGAGTGCACAGTTT -3'

Expected products:

200 bp = genotyping reaction was successful
1100 bp= villin cre allele present

Notes: Primers oIMR15 and oIMR16 are internal controls that yield a 200 bp product in all mouse DNA samples if the reaction was successful. Primers oIMR1878 and oIMR1879 amplify villin-cre. These primers sequences were obtained by The Jackson Laboratory website listing for the B6.SJL-Tg(Vil-cre)997Gum mouse strain.

2. Ceruloplasmin

A. Set 1: oIMR17 and oIMR18, 58°C annealing temperature

Primers:
oIMR1117: 5'- CATACTCTGAACACCCTGAGAAAG -3'
oIMR1118: 5'- CATCAGATACCAGTTGACTTCATC -3'

Expected product:
500 bp band = Cp WT allele present

B. Set 2: oIMR17 and oIMR19, 64°C annealing temperature

Primers:
oIMR1117: 5'- CATACTCTGAACACCCTGAGAAAG -3'
oIMR1119: 5'- CCCGTGATATTGCTGAAGAGCTTG -3'

Expected product:
1000 bp band = Cp knockout allele present

Notes: oIMR17, oIMR18, and oIMR19 primer sequences were obtained from The Jackson Laboratory website listing for the B6-Cp^{tm1Hrs} mouse strain.

4. Zyklopen

A. Set 1: Zp-comF and Zp-loxR, 64°C annealing temperature

Primers:
Zp-comF: 5'- CCTTATGACTACAGTGAACAGGGTTCTG -3'
Zp-loxR: 5'- GTGATAGAGCTGAGATGGCGCAA -3'

Expected product:
344 bp = Zp floxed allele present

B. Set 2: Zp-comF and Zp-wtR, 64°C annealing temperature

Primers:
Zp-comF: 5'- CCTTATGACTACAGTGAACAGGGTTCTG -3'
Zp-wtR: 5'- CTACTCTCTGGCCCTTGCTTTTGC -3'

Expected product:
515 bp = Zp WT allele present

C. Set 1: Zp-koF and Zp-loxR, 64°C annealing temperature

Primers:
Zp-koF: 5'- CGACGGCCAGTGAATTGTAATA -3'
Zp-loxR: 5'- GTGATAGAGCTGAGATGGCGCAA -3'

Expected product:
200 bp = Zp knockout allele present

5. Neomycin resistance cassette

Primers, 64°C annealing temperature:
Neo F: 5'- AGGATCTCCTGTCATCTCACCTTGCTCCTG -3'
Neo R: 5'- AAGAACTCGTCAAGAAGGCGATAGAAGGCG -3'

Expected product:
500 bp = Neo allele present

Notes: The band will be strong if a Neo allele is present. There is sometimes faint background that overlaps with the 500 bp region.

6. FlpE transgene

Primers, 64°C annealing temperature:
FlpE Sd41 F: 5'- GTGGATCGATCCTACCCCTTGC -3'
FlpE Sd42: 5'- GGTCCAACTGCAGCCCAAGCTT -3'

Expected product:
700 bp = FlpE transgene present

Notes: A strong 500 bp is often present in samples with no FlpE transgene.

7. EIIa-cre recombinase

Primers, 55°C annealing temperature:
oIMR1084: 5'- GCGGTCTGGCAGTAAAAACTATC -3'
oIMR1085: 5'- GTGAAACAGCATTGCTGTCACTT-3'

Expected product:
100 bp = EIIa-cre transgene present

Notes: oIMR11084 and oIMR1085 primers sequences were obtained from The Jackson Laboratory website listing for the B6.FVB-Tg(EIIa-cre)C5379Lmgd mouse strain.

8. vilERT2 cre recombinase

Primers, 55°C annealing temperature:
vERT2-Cre 198: 5'- CGCGAACATCTTCAGGTTCT -3'
vERT2-2kbseqS: 5'- CAAGCCTGGCTCGACGGCC -3'

Expected product:
260 bp = vilERT2 transgene present

9. Amyloid precursor protein

Primers, 58°C annealing temperature:
APP1: 5'- CTGCTGCAGGTGGCTCTGCA -3'
APP2: 5'- CAGCTCTATACAAGCAAACAAG- 3'
APP3: 5'- CCATTGCTCAGCGGTGCTG -3'

Expected products:
470 bp = App knockout allele present
250 bp = App WT allele present

Appendix 1.2. Real-time quantitative PCR primers

Primers were generally designed using the NCBI Primer–BLAST tool (Untergasser, Cutcutache et al. 2012) by members of the Iron Metabolism Laboratory at QIMR.

Primers for unmodified regions of *Heph* mRNA
mHpBF1 F 5'- CATGCAATCAATGGGTTTGTCT -3'
mHpBF1 R 5'- TTTGCAACATCAGTGTGGTGTC -3'
mHpBF2 F 5'- CCCCAAGGCAAAGTAAGGACACC -3'
mHpBF2 R 5'- ACCCTCAGCCTGGAAGGAGTGA -3'
mHpBF3 F 5'- AGCATTGATGGGCCGCTGACA -3'
mHpBF3 R 5'- GGACCCTCAGCCTGGAAGGAGT -3'
mHpBF5 F 5'- TGCACTGCCATGTGACTGACCA -3'
mHpBF5 R 5'- TGCCCAGCATCTTCACATTGTCACC -3'
mHpBF7 F 5'- GGACCAGAGGAGCACTTGGGAA -3'
mHpBF7 R 5'- AGTGCTCCAACTCACCAGGCTCAG -3'

Primers for knockout regions of *Heph* mRNA
mHpBF8 F 5'- TGCAGTGGAACTATGCTCCCAAAGG -3'

mHpBF8 R 5'- GGAAGCCCAACCAGGCAGGCT -3’
mHpBF9 F 5'- TTGCGAGCCGACCTTACACC -3’
mHpBF9 R 5'- TGCCTCAGTGGGGGCATGACT -3’

Primers for other genes
Hamp1 F 5'- AGAGCTGCAGCCTTTGCAC -3'
Hamp1 R 5'- ACACTGGGAATTGTTACAGCATTTA -3'
Hamp2 F 5'- AGAGCTGCAGCCTTTGCAC -3'
Hamp2 R 5'- GGAGGGTTTGTTACAGCACTG -3'
Total *Hamp* F 5'- AGAGCTGCAGCCTTTGCAC -3'
Total *Hamp* R 5'- GAGGTCAGGATGTGGCTCTA -3'
Hprt F 5'- GGACTGATTATGGACAGGA -3'
Hprt R 5'- GAGGGCCACAATGTGATG -3'
Tmprss6 F 5'- ACTCTCCCAGTACCCACTGCTC -3'
Tmprss6 R 5'- GTCGGTTGTACTTCTGCCTCCT -3'
mTfrc F 5'- GGTGTTGCGGCGAAGTCCAGT -3’
mTfrc R 5'- ACTCAGTGGCACCAACAG CTC C -3'
App F 5'- CGTTGTCATAGCAACCGTGATT -3'
App R 5'- TCATATCCGTTCTGCTGCATCT -3'
Cp F 5'- CACAATGCACGTGAAAGATGAA -3'
Cp R 5'- ATGTTCCAGGGAAAAGGTCAAA -3'
Dmt1 F 5'- CCCAGGAAACATCGAATC -3'
Dmt1 R 5'- CCAGAGCAGCTTAAATCC -3'
Hfe F 5'- AGACCTATCAAGGCTGGCTGAC -3'
Hfe R 5'- CAACCAAGAAGATGGCACAGAC -3'
Hif1α F 5'- GAGCCTTAACCTGTCTGCCACT -3'
Hif1α R 5'- GAAAAAGGGAGCCATCATGTTC -3'

Appendix 1.3. Urea-PAGE (UPAGE) transferrin iron-loading assay

This procedure reveals the fraction of transferrin in the apo, monoferric, and diferric forms in serum.

I. UPAGE solutions and gel

1. 20x UPAGE buffer stock
(for making gels and 1x UPAGE TBE)

2 M Tris-base
0.2 M boric acid

For 500 mL dissolve 121.1 g Tris-base and 6.18 g boric acid in milliQ water, pH to 8.4 with HCl (a lot is required), then make up to 500 mL with milliQ water. Store at room temperature.

2. 1x UPAGE TBE
(for running buffer and sample prep)

0.1 M	Tris-base
0.01 M	boric acid
0.0016 M	EDTA

For 1 L, combine 50 mL 20x UPAGE buffer and 3.2 mL 0.5 M EDTA and complete up to 1 L with milliQ water. pH should be 8. Store at room temperature.

3. Urea solution, 7.5 M
(for making gels)

Dissolve completely (can take time) 22.5 g urea in a final volume of 50 mL water. Store at room temperature.

Removing metals:

Add ~5 g of Chelex-100 (Bio-Rad) per 100 mL of the above solutions. It generally works best to make up larger stock volumes of the solutions above but treat smaller amounts with Chelex so they can fit on an inversion mixer. Add the Chelex and then mix by inversion at room temperature for 1.5 hours. Then spin down at 1000 rpm for 10 minutes to pellet the Chelex.

4. UPAGE gel

For 20 mL, mix the following in order:

3 mL	40% acrylamide, 37:5:1 (Astral Scientific)
1 mL	20x UPAGE buffer, Chelex-treated
16 mL	7.5 M urea solution, Chelex-treated
20 µL	25% fresh ammonium persulfate (125 mg/ 500 µL milliQ water)
20 µL	TEMED

We use a 1.5 mm, 10-well comb, no stacking gel needed. Let the gel set for 1 hour at room temperature. Pre-run the gel at 4°C at 40V in 1x UPAGE TBE buffer for 50 minutes.

II. Preparation of samples and PAGE

Mouse or human serum samples (ideally fresh or only thawed once) are treated with rivanol to precipitate albumin. It is important to run on each gel control serum from an iron-loaded and an iron-deficient mouse for reference.

Rivanol precipitation buffer, 5 mL
18.75 mg rivanol
500 µL glycerol
4.5 mL 1x UPAGE TBE

Add 5 µL of serum to 400 µL of rivanol precipitation buffer in a 1.5 mL Eppendorf tube, vortex, and then let sit at room temperature for 10 minutes. Spin at maximum speed in a microfuge for one minute to pellet precipitate. Load 5 µL of the supernatant evenly at the base of the prerun gel wells. Run at 4°C at 40V overnight (~24 mAmps over 17 hours). Note that the rivanol (bright yellow) is cationic and will run in the opposite direction as the transferrin.

III. Immunoblotting

1. Transfer buffer
3.05 g Tris-base
14.4 g glycine

Make up to 850 mL with milliQ water. Add 150 mL methanol.

2. Tris-buffered saline (TBS), pH 7.6, 4x concentrate
9.68 g Tris-base
32 g NaCl

Dissolve in approximately 950 mL milliQ water and adjust to pH 7.6 with 10 M HCl, and then bring up to 1 L final volume with milliQ water.

Procedure:

Soak the UPAGE gel for 10 minutes in transfer buffer after PAGE, and transfer to a pre-wet (15 seconds in methanol, 2 minutes in water, 5 minutes in transfer buffer) PVDF membrane for 1 hr at 100V at 4ºC. Block 1 hour at room temperature in fresh blotto [10% nonfat milk powder in 0.1% TBS-T (1x TBS with 0.1% Tween-20)]. Incubate the membrane in primary antibody (1:1000 dilution of sheep anti-human TF, Silenus, cat #EC068) for 1 hour at room temperature in blotto. Wash three times for 10 minutes each in 0.1 % TBS-T. Incubate with secondary antibody (1:5000 dilution donkey anti-sheep HRP, Chemicon) for 1 hour at room temperature in blotto. Wash three times for 10 minutes each in 0.1 % TBS-T. Wash 5 minutes in TBS. Add the desired ECL reagent (Western lightning plus-ECL, Perkin-Elmer, cat# NEL104001EA; mix stock solutions 1:1 just before use, 2 mL per blot) and expose to film.

IV. Expected results

Apo-transferrin runs slower than monoferric transferrin, and diferric transferrin runs the fastest (lowest). Iron-loaded controls should have little apo-transferrin and iron-deficient controls should only have apo-transferrin.